

KUVEMPU



UNIVERSITY

“Studies on transition metal complexes of substituted benzimidazole; Synthesis, Characterization and biological activity”

Thesis Submitted to the Faculty of Science, Kuvempu University for the award of the Degree of

**DOCTOR OF PHILOSOPHY
IN
INDUSTRIAL CHEMISTRY**

Submitted By

Mr. Manjuraj.T M.Sc

Research Scholar

Department of Industrial Chemistry,
Sahyadri Science College
Kuvempu University

Under the Guidance of

Dr. G. Krishnamurthy

Associate professor

Department of Chemistry & Industrial chemistry
Sahyadri Science College, Shivamogga

Co-Guide

Dr. Yadav D. Bodke

Professor

Department of Chemistry,
Jnana Sahyadri, Kuvempu University,
Shankaraghatta, Shivamogga,

2018

R/E
GGO
MAN

Lib 3 (a)

L- 3904

Kuvempu University Library
Jnanasahyadri, Shankaraghatta

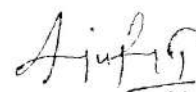
Declaration

I hereby declare that the research work presented in this thesis entitled **“Studies on transition metal complexes of substituted benzimidazole; Synthesis, Characterization and biological activity”** is entirely original and was carried out by me in the Department of Chemistry under the supervision of **Dr. G. Krishnamurthy**, Associate professor, Department of chemistry and Industrial chemistry, Sahyadri Science College, Shivamogga-577-203, Kuvempu University, Shankaraghatta - 577451.

I further declare that the results presented in the thesis or any part thereof has not been submitted elsewhere for any other degree, diploma of similar title in any other Universities.

Date: 23-03-2018

Place: Shivamogga



Mr. Manjuraj .T



KUVEMPUR UNIVERSITY



SAHYADRI SCIENCE COLLEGE (AUTONOMOUS)

(College with Potential for Excellence)

Dr. G. Krishnamurthy M.Sc., M.phil, Ph.D,

Associate professor,

Department of chemistry and Industrial chemistry,

Sahyadri Science College,

Shivamogga-577-203

e-mail: gkmnaiksahyadri@gmail.com

Mobile No: +91-9448774649

CERTIFICATE

This is to certify that the work reported in this thesis entitled
“Studies on transition metal complexes of substituted benzimidazole; Synthesis, Characterization and biological activity” submitted by **Mr. Manjuraj T** to the Faculty of Science, Kuvempu University, for the award of **Doctor of Philosophy in Industrial Chemistry** is a record of the bonafide and original research work carried out by him under my guidance and direct supervision. The work reported in this thesis has not formed the basis for the award of any degree or diploma or any other similar title.

Date: 23/3/18
Place: Shivamogga


23/3/18
Dr. G. Krishnamurthy

(Guide)

KUVEMPU



UNIVERSITY

Dr. Yadav D. Bodke M.Sc., Ph.D,

Professor,

Department of chemistry

Department of Chemistry,

Jnana Sahyadri, Kuvempu University,

Shankaraghatta, Shivamogga-577-203

Email: ydbodke@gmail.com

CERTIFICATE

This is to certify that the work reported in this thesis entitled **“Studies on transition metal complexes of substituted benzimidazole; Synthesis, Characterization and biological activity”** submitted by **Mr. Manjuraj T** to the Faculty of Science, Kuvempu University, for the award of **Doctor of Philosophy in Industrial Chemistry** is a record of the bonafide and original research work carried out by him under my guidance and direct supervision. The work reported in this thesis has not formed the basis for the award of any degree or diploma or any other similar title.

Date: 23/3/2018

Place: Shankaraghatta

Dr. Yadav D. Bodke

A handwritten signature in black ink, appearing to read 'Yadav'.

(Co-Guide)

23/3/18

ACKNOWLEDGEMENT

This work is the result of three and half years and the contributions of many people, without whose help it would have been very difficult to complete.

With deep regards and profound respect, I avail the opportunity to express my deep sense of gratitude and indebtedness to my research supervisor, **Dr. G. Krishnamurthy**, Associate Professor, Department of chemistry and Industrial chemistry, Sahyadri Science College, Shivamogga, for his valuable guidance, stimulating discussions, constant encouragement and giving solutions in every stage of this study. I greatly appreciate the patience shown by him during my entire research tenure under his supervision and also while dealing with my impatient behavior at times. I am deeply impressed by his continuous devotion to research, his sincerity and patience. I feel proud to be his student forever.

I place on records my sincere thanks to **Dr. Yadav D Bodke** Co-guide, Department of Industrial Chemistry, Kuvempu University, for his kindly support to carry out research work

I would like to thank **Prof. Jogan Shankar**, Honorable Vice Chancellor, Kuvempu University, for his support to carry out research work.

I also thank **Prof. H. S. Bhojya Naik**, Registrar, Kuvempu University, for his support to carry out research work.

I sincerely thank **Prof. Shashireka**, Principal, Sahyadri Science College, Shivamogga, for providing laboratory facilities during my research work.

It is my pleasant duty to express my sincere thanks to **Prof. Vasanthkumar Pai** Chairman, Department of Industrial Chemistry, Kuvempu University, for his kind co-operation during my research work. I also thank all faculty members of Department of Industrial Chemistry, Kuvempu University, **Dr. B.E Kumaraswamy**, other faculty members and also non-teaching staff of both the departments for their encouragement.

It is my pleasure to express my sincere thanks to **Dr. Vital Rao** Chairman and teaching and non-teaching staffs of department of chemistry, Sahyadri Science College, Shimoga.

It is to express my special gratitude to my seniors **Mr. Yuvaraj TCM**, **Dr. N. D. Shashikumar**, **Dr. N. D. Jayanna**, **Dr. Chidhanadha B.** and **Dr. Lokesh M R** for his help, everlasting support and their guidance.

I would also thank my research group **Mr. Mohamad Shafeulla**, **Sunil Kumar N**, **Jithendra Kumar K.S**, **Venugopal**, and **Mrs. Shewtha**

I remember with special love and gratitude, the pleasant moment I had with my research group, **Mr. Shreedhara S.H**, **Mr. Sarvajeeth M.S**, **Mr. Naveenaradhya**, **Mr. Pradeep (BHP)**, **Mr. Mutthu**, **Mr. pradeep**, **Dr. Ganesh S.D**, **Mr. Chetan Kuskur**, **Venugopal**, **Subbaraju A**, **Madhusudhan**, for their timely help, memorable moments spent with them and support throughout my course work.

I would also thank **Dr. M.C Prabhakar**, **Dr. Vishwanaath**, **Mr. Suresh**, **Dr. Arunkumar** and **Dr. Mahantesh** for their kindly support.

My deepest thanks to my friends **Mehaboob basha**, **Shambulingaswamy**, **Geetha N.R**, **Mallappa**, **Bitta**, **Kaleem**, **Ghazni**, **Shekharappa Sir**, **Purushothama Reddy** and **Satayappa Sir**, for their kindly support and love.

I would like to thank the Directors, Indian Institute of Science, Bangalore, SAIF, Cochin, and MIT Manipal for providing spectral data.

I take this occasion to express my profound gratitude to my parents **Shri Thippeswamy P.H and Smt. Gowramma** whose protective hands over my bowed head proved sustaining and enlivening. I would like to thank my brother **Muthuraj T**, and **Sister Lakshmi.T** for their instantaneous help, blessings and unending support.

Lastly, I wish to thank all those who helped me directly or indirectly to complete this research work

Mr. Manjuraj .T

CONTENTS

CHAPTER 1

INTRODUCTION

Title No.	Title	Page No.
1.1	Literature review	
1.2	Metal complexes of benzimidazole dithiocarbamate ligand	
1.3	Metal complexes of benzimidazole derived sulfonamide	
1.4	2-(4'-thiazolyl) benzimidazole derived metal complexes	
1.5	Metal complexes of 1,3-symmetrically and 1,3-unsymmetrically substituted imidazoles and benzimidazoles	1-11
1.6	2-(2-pyridyl) benzimidazole derived metal complexes	
1.7	Metal complexes of Quinoline-benzimidazole derivatives	
1.8	Mannich base reactions with benzimidazole	
1.9	2-mercaptobenzimidazole derivatives	
1.10	Bis-benzimidazole derivatives	
1.11	Biological activities of benzimidazoles	12-16
1.12	Metal complexes with substituted benzimidazole	17
1.13	Structural characterization tools	19-20
1.14	Molecular docking studies	21-23
1.15	Research Aim and Thesis Arrangement	24-25
	References	26-34

CHAPTER 2

Metal complexes of quinolin-8-yl [(5-methoxy-1H-benzimidazol-2-yl)sulfanyl] acetate: Spectral, XRD, thermal, DFT studies, cytotoxic, molecular docking and biological evaluation

Title No.	Title	Page No.
2.1	Introduction	
2.2	Experimental	
2.3	Results and discussion	
2.4	Procedures for biological evaluation	35-58
2.5	Results and discussion of biological evaluation	
2.6	Conclusion	
	References	59-64

CHAPTER 3

Co(II), Ni(II) and Cu(II) complexes of new mannich base of N'-(1H-benzimidazol-1-ylmethyl) pyridine-4-carbohydrazide: Spectral, XRD, DFT studies, molecular docking, antioxidant and antimicrobial studies.

Title No.	Title	Page No.
3.1	Introduction	
3.2	Experimental	
3.3	Results and discussion	
3.4	Procedures for biological evaluation	65-83
3.5	Results and discussion of biological evaluation	
3.6	Conclusion	
	References	84-88

CHAPTER 4

Synthesis, characterization, spectral, thermal, DFT, molecular docking and biological studies of benzimidazol-2-ylmethyl)-2-(pyridin-4-yl carbonyl)hydrazine carbothioamide and their Co(II), Ni(II) and Cu(II) complexes

Title No.	Title	Page No.
4.1	Introduction	
4.2	Experimental	
4.3	Results and discussion	
4.4	Procedures for biological evaluation	89-110
4.5	Results and discussion of biological evaluation	
4.6	Conclusion	
	References	111-115

CHAPTER 5

Studies on the synthesis, spectral, biological evaluation of 4-((1Z)-1-[2-(1H-benzimidazol-2-ylmethyl) hydrazinylidene] ethyl} phenol and 4-((1Z)-1-[2-(1H-benzimidazol-2-ylmethyl) hydrazinylidene]ethyl}aniline and their transition metal complexes

Title No.	Title	Page No.
5.1	Introduction	
5.2	Experimental	
5.3	Results and discussion	
5.4	Procedures for biological evaluation	116-138
5.5	Results and discussion of biological evaluation	
5.6	Conclusion	
	References	139-144

CHAPTER 6

Part A

Metal complexes of S-1H-benzimidazol-2-yl thiophene-2-carbothioate: Synthesis, spectral characterization, XRD, DFT, molecular docking and biological studies

Title No.	Title	Page No.
6.0	Introduction	
6.1	Experimental	
6.1.3	Results and discussion	
6.1.9	Procedures for biological evaluation	145-164
6.1.14	Results and discussion of biological evaluation	
6.1.19	Conclusion	

CHAPTER 6

Part B

The transition metal complexes of 2-[(thiophen-2-ylsulfanyl)methyl]-1H-benzimidazole : Synthesis, characterization, molecular docking and biological studies

Title No.	Title	Page No.
6.2	Experimental	
6.2.3	Results and discussion	
6.2.7	Results and discussion of biological evaluation	165-176
6.2.10	Conclusion	
	References	177-181

CHAPTER 7

Synthesis, Characterization, DFT and biological studies of mannich base N-(1H-benzimidazol-1-ylmethyl)-4-[(E)-phenyldiazenyl]aniline and their metal complexes

Title No.	Title	Page No.
7.2	Experimental	
7.3	Results and discussion	
7.4	Procedures for biological evaluation	181-196
7.5	Results and discussion of biological evaluation	
7.6	Conclusion	
	References	197-201

CHAPTER 8

Conclusion and Summary

Title No.	Title	Page No.
8.1	Conclusion and Summary	202-205

LIST OF FIGURES

Chapter 2

Figure No.	Figure caption	Page No.
2.1	Proposed structure of metal complexes [M=Co(II), Ni(II), Cu(II) and Zn(II)]	37
2.2	Optimized geometry of ligand QB	38
2.3	Standard bond lengths and bond angles of the ligand QB	39
2.4	HOMO LUMO frontier orbitals of the ligand QB	40
2.5	IR spectra of QB and its metal complexes	41
2.6	¹ H NMR spectrum of QB	42
2.7	¹ H NMR spectrum of [ZnCl ₂ (QB) ₂]	43
2.8	¹³ C NMR spectrum of QB	44
2.9	Mass spectrum of QB	44
2.10	Mass spectrum of [ZnCl ₂ (QB) ₂]	45
2.11	XRD Patterns of [CoCl ₂ (QB) ₂].2H ₂ O and [CuCl ₂ (QB) ₂] Complex	45
2.12	Electronic absorption spectra of QB and their metal complexes	47
2.13	TGA and DTA curves of [Co(QB) ₂ Cl ₂].2H ₂ O, [Ni(QB) ₂ Cl ₂].2H ₂ O and [Cu(QB) ₂ Cl ₂]	49
2.14	Linear fit graphs of [1] [Co(QB) ₂ Cl ₂].2H ₂ O, [2] [Ni(QB) ₂ Cl ₂].2H ₂ O and [3] [Cu(QB) ₂ Cl ₂]	50
2.15	Comparison of cytotoxic (%) inhibition of QB and their metal complexes	53
2.16	3D representation of (A) complex 1 (B) complex 2 and (C) complex 3 with epidermal growth factor receptor (EGFR) tyrosine kinase	55
2.17	DPPH scavenging activity of QB and their metal complexes	56

Chapter 3

Figure No.	Figure caption	Page No.
3.1	Proposed structure of metal complexes [M=Co(II), Ni(II) and Cu(II)]	66
3.2	Optimized geometry of ligand BI	67
3.3	Standard bond lengths and bond angles of the ligand BI	68
3.4	HOMO LUMO frontier orbitals of the ligand QB	69
3.5	¹ H NMR spectrum of the BI	70
3.6	¹ H NMR spectrum of the Zn(II) complex	70
3.7	Mass spectrum of the BI	71
3.8	Mass spectrum of the Zn(II) complex	71
3.9	IR Spectra of BI and Co(II) Complex	72
3.10	IR Spectra of Ni(II) and Cu(II) complexes	72

3.11	Uv-Visible spectra of the BI and their metal complexes	
3.12	XRD patterns of $[\text{CoCl}_2(\text{BI})_2]$	73
3.13	XRD patterns of $[\text{Ni}(\text{BI})_2]\text{Cl}_2 \cdot \text{H}_2\text{O}$	74
3.14	XRD pattern of $[\text{CuCl}_2(\text{BI})_2]$	
3.15	DPPH scavenging data of BI and their metal complexes	78
3.16	Ferric reducing scavenging data of BI and their metal complexes	79
3.17	Binding interaction of [A] Co(II), [B] Ni(II) and [C] Cu(II) complexes with 3MNG receptor	80
3.18	Graphical representations of antimicrobial studies	
3.19	Graphical representation of Minimal inhibitory concentration [MIC]	82

Chapter 4

Figure No.	Figure caption	Page No.
4.1	Proposed structure of metal complexes $[\text{M}=\text{Co}(\text{II}), \text{Ni}(\text{II}) \text{ and } \text{Cu}(\text{II})]$	91
4.2	Optimized geometry of the BPH	92
4.3	Standard bond lengths and bond angles of the BPH	94
4.4	HOMO LUMO frontier orbitals of the BPH	94
4.5	^1H NMR spectrum of the BPH	95
4.6	Mass spectrum of the BPH	95
4.7	^1H NMR spectrum of $[\text{NiCl}_2(\text{BPH})_2] \cdot 2\text{H}_2\text{O}$	96
4.8	Mass spectrum of $[\text{CuCl}_2(\text{BPH})_2] \cdot \text{H}_2\text{O}$	97
4.9	IR spectra of BPH and their metal complexes	97
4.10	Electronic absorption spectrum of BPH and their metal complexes	98
4.11	Thermogravimetric (TGA/DTG) curves of metal complexes	100
4.12	Linear fit graphs of $[\text{NiCl}_2(\text{BPH})_2] \cdot 2\text{H}_2\text{O}$	101
4.13	Linear fit graphs of $[\text{CuCl}_2(\text{BPH})_2] \cdot \text{H}_2\text{O}$	101
4.14	3-Dimensional (3D) interactions of BPH and their complexes (A) Tyrosinase enzyme (PDB ID: 3NM8) from Bacillus megaterium. (B) $[\text{CoCl}(\text{BPH})_2]\text{Cl} \cdot \text{H}_2\text{O}$ (C) $[\text{NiCl}_2(\text{BPH})_2] \cdot 2\text{H}_2\text{O}$ and (D) $[\text{CuCl}_2(\text{BPH})_2] \cdot \text{H}_2\text{O}$	105
4.15	Radical scavenging activities of the BPH and their complexes	106
4.16	Antibacterial activities of BPH and their metal complexes	107
4.17	Antifungal activities of BPH and their metal complexes	107
4.18	Graphical representation of anti-lipase assay	109

Chapter 5

Figure No.	Figure caption	Page No.
5.1	Proposed structure of metal complexes [M=Co(II), Ni(II) and Cu(II)]	118
5.2	¹ H NMR spectrum of LB	120
5.3	¹ H NMR spectrum of the BN	121
5.4	¹ H NMR spectrum of [Ni Cl ₂ (LB) ₂].2H ₂ O	121
5.5	¹ H NMR spectrum of [Ni Cl ₂ (BN) ₂].2H ₂ O	122
5.6	Mass spectrum of the LB	122
5.7	Mass spectrum of the BN	123
5.8	Mass spectrum of the [CoCl ₂ (LB) ₂].2H ₂ O	123
5.9	Mass spectrum of the [CoCl ₂ (BN) ₂].2H ₂ O	123
5.10	Electronic spectra of metal complexes	125
5.11	IR Spectra of LB and their metal complexes	125
5.12	IR spectra of BN and their metal complexes	126
5.13	TGA pattern of [Co(LB) ₂ Cl ₂] 2H ₂ O	126
5.14	TGA pattern of [Ni(LB) ₂ Cl ₂] 2H ₂ O	127
5.15	TGA pattern of [Cu(LB) ₂ Cl ₂]	127
5.16	X-ray diffraction pattern of [Ni(LB) ₂ Cl ₂] 2H ₂ O	128
5.17	X-ray diffraction pattern of [Cu(L) ₂ Cl ₂]	128
5.18	DPPH radical scavenging activity of LB and their metal complexes	131
5.19	DPPH radical scavenging activity of BN and their metal complexes	132
5.20	Anti-lipase assay of LB and their metal complexes	132
5.21	Anti-lipase assay of BN and their metal complexes	134
5.22	3D Interaction and hydrogen bonding of [Co(LB) ₂ Cl ₂].2H ₂ O with amino acids of receptor 2A91 and 2D interaction	134
5.23	3D Interaction and hydrogen bonding of [Cu(LB) ₂ Cl ₂]. H ₂ O with amino acids of receptor 2A91 and 2D interaction	135
5.24	Cytotoxicity activity (IC ₅₀ values) of LB and their metal complexes	137
5.25	Cytotoxicity activity (Inhibition %) of B and their metal complexes	137

Chapter 6

Part A

Figure No.	Figure caption	Page No.
6.1.1	Proposed structure of metal complexes [M=Co(II), Ni(II), Cu(II) and Zn(II)]	147
6.1.2	IR spectrum of BTC	148

6.1.3	IR spectrum of [Cu(BTC) ₂ Cl ₂]	
6.1.4	IR spectrum of [Ni(BTC) ₂ Cl ₂]	149
6.1.5	IR spectra of [CoCl ₂ (BTC) ₂]	
6.1.6	Uv-Visible spectrum of the BTC and their metal complexes	151
6.1.7	¹ H NMR spectrum of BTC	
6.1.8	¹ H NMR spectrum of [Zn(BTC) ₂ Cl ₂]	152
6.1.9	Mass spectrum of BTC	
6.1.10	Mass spectrum of [CoCl ₂ (BTC) ₂]	153
6.1.11	XRD pattern of [CoCl ₂ (BTC) ₂]	
6.1.12	XRD pattern of [NiCl ₂ (BTC) ₂]	154
6.1.13	XRD pattern of [CuCl ₂ (BTC) ₂]	
6.1.14	HOMO-LUMO frontier orbitals of BTC	155
6.1.15	HOMO-LUMO frontier orbitals of Co(II) complex	
6.1.16	Graphical representation of α -Amylase Inhibitory	158
6.1.17	Graphical representation of DPPH scavenging activity	160
6.1.18	Graphical representation of antifungal activity of the BTC and their metal complexes	161
6.1.19	3D interactions of [Cu(BTC) ₂ Cl ₂]	162
6.1.20	3D interactions of [CoCl ₂ (BTC) ₂]	
6.1.21	3D interactions of [Ni(BTC) ₂ Cl ₂]	163
6.1.22	3D interactions of [Zn(BTC) ₂ Cl ₂]	

Chapter 6

Part B

Figure No.	Figure caption	Page No.
6.2.1	Proposed structure of metal complexes [M=Co(II), Ni(II), Cu(II) and Zn(II)]	165
6.2.2	IR spectrum of BT	
6.2.3	IR spectrum of [CoCl ₂ (BT) ₂].H ₂ O	167
6.2.4	IR spectrum of [NiCl ₂ (BT) ₂].H ₂ O	
6.2.5	IR spectrum of [CuCl ₂ (BT) ₂]	168
6.2.6	¹ H NMR spectrum of BT	169
6.2.7	¹ H NMR spectrum of [ZnCl ₂ (BT) ₂]	
6.2.8	Mass spectrum of BT	170
6.2.9	Mass spectrum of [ZnCl ₂ (BT) ₂]	
6.2.10	Antioxidant activity of BT and its metal complexes	172
6.2.11	3D interactions of BT	173
6.2.12	3D interactions of [CoCl ₂ (BT) ₂].H ₂ O	
6.2.13	3D interactions of [NiCl ₂ (BT) ₂].H ₂ O	
6.2.14	3D interactions of [NiCl ₂ (BT) ₂].H ₂ O	174

Chapter 7

Figure No.	Figure caption	Page No.
7.1	Proposed structure of metal complexes [M=Co(II), Ni(II), Cu(II) and Zn(II)]	182
7.2	optimized geometry of BPA	183
7.3	Standard bond lengths and bond angles of BPA	184
7.4	HOMO LUMO frontier orbitals of BPA	185
7.5	HOMO LUMO frontier orbitals of the Co(II) complex	186
7.6	¹ H NMR spectrum of BPA	187
7.7	¹ H NMR spectrum of [NiCl ₂ (BPA) ₂]	187
7.8	Mass spectrum of BPA	
7.9	Mass spectrum of [ZnCl ₂ (BPA) ₂]	188
7.10	¹³ C NMR spectrum of BPA	
7.11	IR spectra of BPA and their metal complexes	189
7.12	XRD pattern of the BPA	
7.13	XRD pattern of [CoCl ₂ (BT) ₂]	191
7.14	XRD pattern of [CuCl ₂ (BT) ₂]	
7.15	Graphical representation of the anti-lipase assay	193
7.16	Graphical representation of nitric oxide method	194
7.17	Graphical representation of DPPH method	194
7.18	3D binding interactions of the ligand BPA	195
7.19	3D binding interactions of [CoCl ₂ (BT) ₂]	195
7.20	3D binding interactions of [NiCl ₂ (BT) ₂]	196

LIST OF TALBES

Chapter 2

Table No.	Table caption	Page No.
2.1	Analytical and physical properties of QB and their meta complexes	38
2.2	Selected structural parameters of ligand QB	39
2.3	FTIR spectral data (cm ⁻¹) of QB and its metal complexes	41
2.4	XRD data of [CoCl ₂ (QB) ₂] 2H ₂ O	45
2.5	XRD data of [CuCl ₂ (QB) ₂]	46
2.6	UV-Vis data of QB and its metal complexes	47
2.7	Thermal and Kinetic parameters of metal complexes	48
2.8	Cytotoxic potency (IC ₅₀ , μM) of the ligand and their metal complexes	53
2.9	Anti-lipase activity of ligand and their metal complexes	55
2.10	Antimicrobial activity data of QB and their metal complexes	57
2.11	MIC data of QB and metal their complexes	

Chapter 3

Table No.	Table Caption	Page No.
3.1	Analytical data and molar conductance values of BI and their metal complexes	67
3.2	Selected structural parameters of ligand BI	68
3.3	UV-Vis data of QB and its metal complexes	73
3.4	XRD data of [CoCl ₂ (BI) ₂] H ₂ O	75
3.5	XRD data of [Ni (BI) ₂ Cl ₂] H ₂ O	76
3.6	XRD data of [CuCl ₂ (BI) ₂]H ₂ O	81
3.7	Antimicrobial data – Zone inhibition	81
3.8	Antimicrobial data – minimal inhibitory concentration	82

Chapter 4

Table No.	Table caption	Page No.
4.1	Physical properties and analytical data of the metal complexes	91
4.2	Selected structural parameters of BPH	93
4.3	Characteristic IR bands of the ligand and its complexes	97
4.4	Thermogravimetric data of Co(II), Ni(II) and Cu(II) complexes.	99
4.5	Thermal and Kinetic parameters of Ni(II) and Cu(II) metal complexes	101
4.6	Docking study results of the BPH and their metal complexes	104
4.7	Antimicrobial results of BPH and their metal complexes	108
4.8	Antimicrobial results of BPH and their metal complexes	

Chapter 5

Table No.	Table caption	Page No.
5.1	Physical properties and analytical data of LB, BN and their metal complexes	119
5.2	The XRD data of the [Ni(LB) ₂ Cl ₂] 2H ₂ O	129
5.3	The XRD data of the [Cu(LB) ₂ Cl ₂]	133
5.4	Binding energy values of LB and their metal complexes	136
5.5	IC ₅₀ values of LB and its complexes on MCF-7 ^a and HeL ^b cancer cells.	136

Chapter 6

Part A

Table No.	Table caption	Page No.
6.1.1	Physical properties and analytical data of the metal complexes	147
6.1.2	IR spectral data of the ligand and their metal complexes	148
6.1.3	Uv-Visible data of the ligand and their metal complexes	150
6.1.4	Calculated quantum chemical parameters for BTC and Co(II) complex	156
6.1.5	α -Amylase inhibitory assay data of ligand and their metal complexes	159
6.1.6	DPPH Scavenging IC ₅₀ ($\mu\text{g}/\text{cm}^3$) data	160
6.1.7	Minimum inhibitory concentration data of the BTC and their metal complexes	162

Chapter 6

Part B

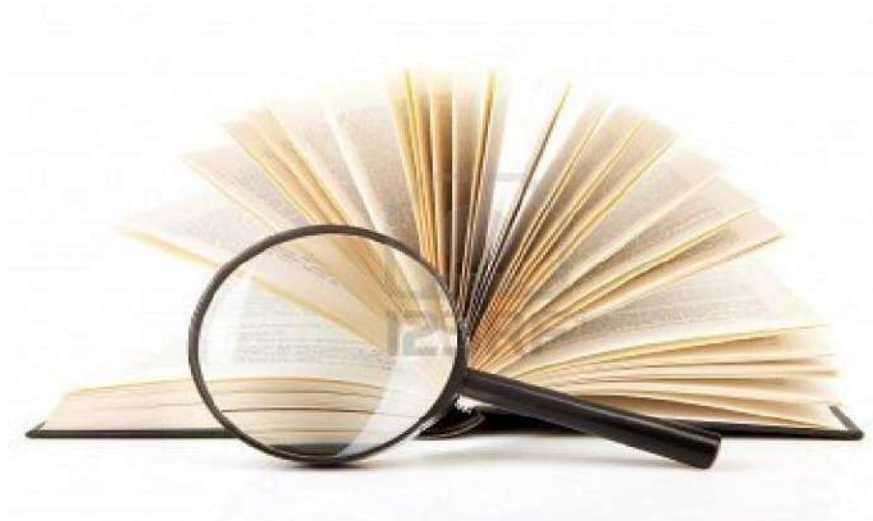
Table No.	Table caption	Page No.
6.2.1	Physical properties and analytical data of the metal complexes	166
6.2.2	Antimicrobial activity data of BT and its metal complexes	171
6.2.3	Minimum inhibitory concentration data of BT and its metal complexes	171

Chapter 7

Table No.	Table caption	Page No.
7.1	Physical properties and analytical data of BPA and their metal complexes	183
7.2	Selected structural parameters of BPA	184
7.3	Calculated quantum chemical parameters for BPA and Co(II) complex	186
7.4	Electronic spectral and magnetic moment data of metal complexes	190

Chapter – 1

**Background and general
introduction about
Benzimidazole derivatives
and their metal complexes**



Literature Review

INTRODUCTION

1.1 Literature review

In this chapter, the literature relating to the present research work is reviewed. Benzimidazoles of both natural and synthetic compounds are the key components of many bioactive compounds [1, 2]. The scaffold is a useful structural motif for the development of therapeutic agents/pharmaceutical preparations such as omeprazole (proton pump inhibitor), pimobendan (ionodilator) and mebendazole (anthelmintic) which is shown in (figure 1.1.). Benzimidazole moiety is a key component of vitamin B₁₂ which supports their effective use as therapeutics and their derivatives viz. antimicrobial, H₂ receptor blocker, antioxidant, anti-allergic, antihistamine and antitumor they are vastly in demand for use as precursors in metal-based drug systems [3, 4], sometimes called 1,2-dideazapurine and its derivatives can serve as model compounds for purine due to structural similarity.

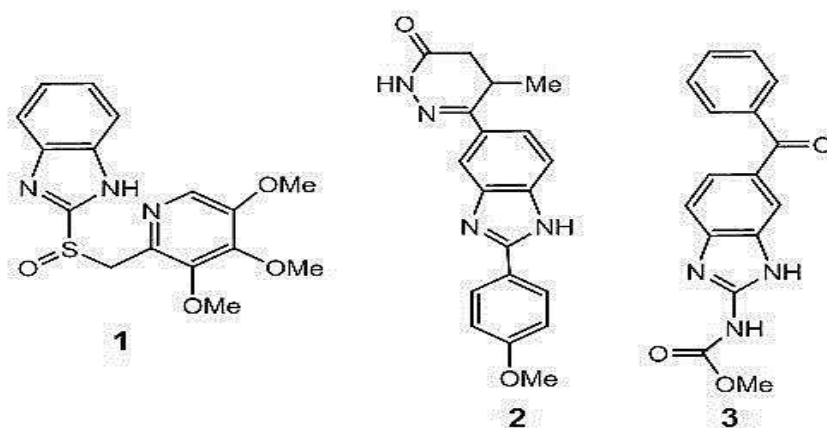


Figure 1.1 [1] Omeprazole [2] Pimobendan [3] Mebendazole

Benzimidazoles are very effective compounds with respect to their bacteria inhibitory activity [5]. Biochemical and pharmacological studies have showed that these molecules are effective against various strains of microorganisms. Some benzimidazole compounds inhibit the biosynthesis of ergosterol, required in the cell membrane of fungi and protozoa and a useful target for antifungal drugs. The result of many efforts to develop new molecules for effective antimicrobials reveals that the benzimidazoles are still one of the most versatile class of compounds against microbes.

Further the structure of imidazole engrossed much interest due to their usage in various applications such as in coordination, medicinal and supramolecular-chemistry. Because of having eminent thermal stability, good catalytic activity and superior optical properties, the metal complexes are significant with the much effective properties of imidazole scaffold which are due to (i) its hydrophobic nature, (ii) the planarity of benzimidazole moiety; (iii) delocalized π - electrons in the aromatic ring and (iv) hetero-atoms like nitrogen [6].

1.2 Metal complexes of benzimidazole dithiocarbamate ligand

G.G. Mohamed et al (2016) [7] reported that the magnetic and solid reflectance spectra of dithiocarbamate ligand and complexes, it was found that the geometrical structure of these complexes is octahedral (Figure 1.2). The thermal behavior of these chelates showed that the hydrated complexes loss water molecules of hydration in the first step followed immediately by decomposition of the anions and ligand molecules in the subsequent steps. Fungicidal activity of the prepared complexes and free ligand was evaluated against three soil borne fungi. Data obtained showed that the higher biological activity of the prepared complexes than the parent Schiff base ligand. Formulation of the most potent complex was carried out in the form of 25% WP. Fungicidal activity of the new formulation was evaluated and compared with the standard fungicide Pencycuron (Monceren 25% WP).

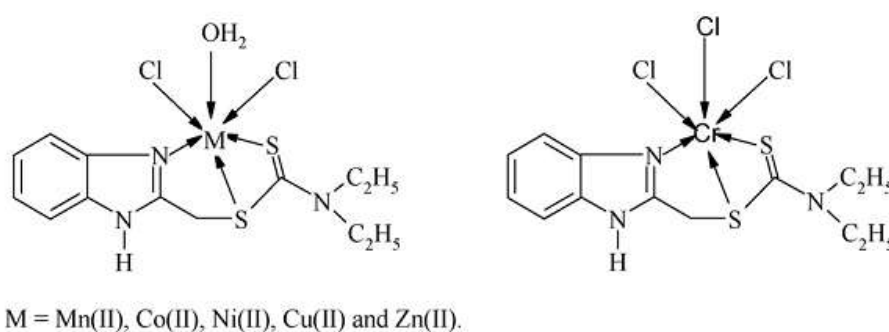


Figure 1.2

1.3 Metal complexes of benzimidazole derived sulfonamide

Adnan Ashraf et al (2016) [8], the benzimidazole and sulfonamide moieties are found in a number of pharmaceutically active molecules. By incorporating the

sulfonamide pharmacophore into the benzimidazole scaffold, we prepared 2-(*o*-sulfamoylphenyl)benzimidazole (Figure 1.3) was obtained from saccharin as a precursor. It was coordinated to the divalent transition metals Mn(II), Co(II), Ni(II), Cu(II) and Zn(II) to yield complexes of the general formula $[ML_2(H_2O)_n]$ ($n = 2$ for 2 and $n = 0$ for 3–6). All the compounds were characterized by elemental analysis, conductivity measurements, magnetic susceptibility, FT-IR and NMR spectroscopy. The molecular structures of ligand, Co(II) and Zn(II) were determined by X-ray diffraction analysis. In all metal complexes, the ligand behaved as a bidentate and chelating through the sulfonamidate nitrogen and the endocyclic nitrogen of benzimidazole. The molecular structure of Co(II) and Zn(II) is tetrahedral geometry. The molar conductivity data revealed that the metal complexes are non-electrolytes. The benzenesulfonamide derivative and its metal complexes were evaluated for their potential antimicrobial activity against a range of bacterial and fungal strains. $[Co(2-(o\text{-sulfamoylphenyl)benzimidazolate})_2]$ was identified as the most active antibacterial compound, while none of the compounds exhibited antifungal activity.

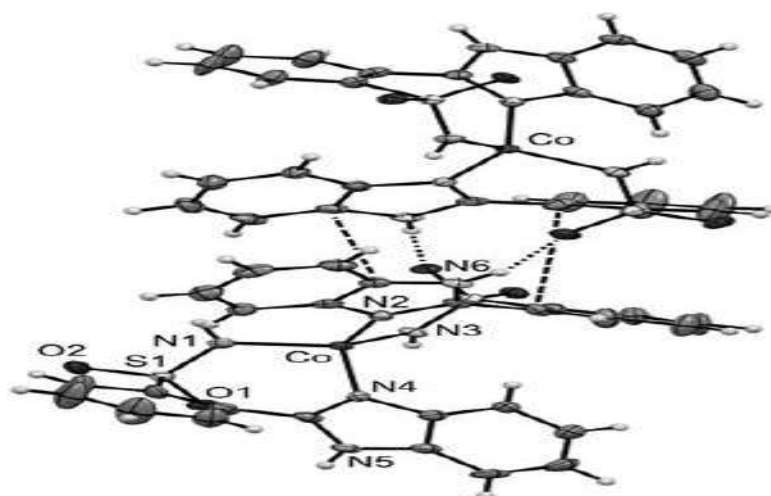


Figure 1.3

1.4 2-(4'-thiazolyl) benzimidazole derived metal complexes

Xia-Bing Fu et al, (2015), [9] Have synthesized, characterized and evaluated DNA binding and cleavage of two new Cu(II)–dipeptide complexes of 2-(4'-thiazolyl)benzimidazole, $[Cu(Gly-Gly)(TBZ)(Cl)] \cdot 4H_2O$ (1) and $[Cu(Gly-L-Leu)(TBZ)(Cl)] \cdot H_2O$ (2) (Gly-Gly = glycyl-glycine anion, Gly-L-Leu = glycyl-L-leucine anion and TBZ = 2-(4'-thiazolyl)benzimidazole) (Figure 1.4). The DNA

binding and cleavage properties of the complexes monitored by multispectroscopic techniques (UV absorption, fluorescence and circular dichroism), viscosity determination and agarose gel electrophoresis indicated that the complexes bound to calf thymus (CT)-DNA *via* a partial intercalative mode with considerable intrinsic binding constants ($K_b = 1.64 \times 10^5 \text{ M}^{-1}$ for 1 and $2.59 \times 10^5 \text{ M}^{-1}$ for 2) and cleaved pBR322 DNA efficiently in the mediation of ascorbic acid (AA), probably *via* an oxidative damage mechanism induced by $\bullet\text{OH}$. The antioxidant activities of the complexes have been evaluated by means of modified nitroblue tetrazolium (NBT) photo-reduction and cellular antioxidant activity (CAA) assays using HepG2 cells as a model, and it was found that IC_{50} values of 1 and 2 for dismutation of $\bullet\text{O}_2^-$ were 0.172 and 0.247 μM , respectively, and the CAA50 values were 10.57 and 10.74 μM . In addition, the complexes were subjected to *in vitro* cytotoxicity against three human carcinoma cell lines (HeLa, A549 and HepG2), which revealed that the complexes exhibited effective cytotoxicity (IC_{50} values varying from 33.17 to 100 μM) and selective inhibition toward HeLa cell lines. These findings indicate that the complexes have the potential to act as effective metalloproteinase chemotherapeutic agents.

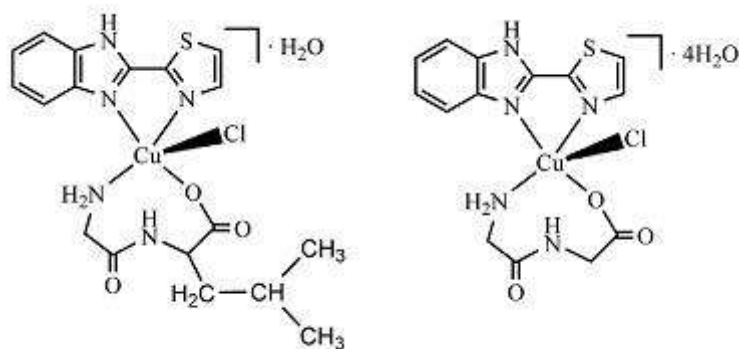


Figure 1.4

Benzimidazole/thioether Cu(II) complexes (Figure 1.5) interact with phospholipid bilayers as models of cell membranes and also with the membranes of live erythrocytes. N-methylation of the benzimidazole moiety confers a greater lipophilicity that results in enhanced cytotoxic activity, likely *via* passive diffusion through cell membranes.

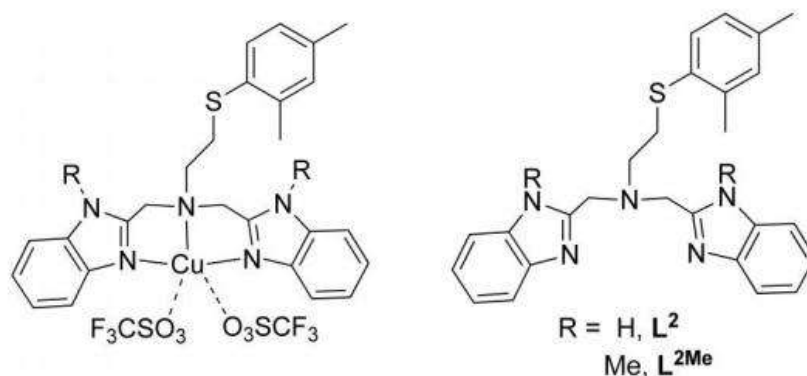


Figure 1.5

Mehdi Bouchouit et al., (2016), [10] described the coordination polyhedron around the metal center for all complexes may be described as a quasi-regular tetragonal geometry (Figure 1.6). The electronic structures indicated almost identical characteristics of neutral Co(II) on one hand and the Zn(II) on other hand, but the reduced Co(I) behave differently in accordance with the $-(\text{CH}_2)_2\text{-S-}$ bridge length and adopting different structures than those of the neutral ones and allowing a flexibility to the metal coordination sphere.

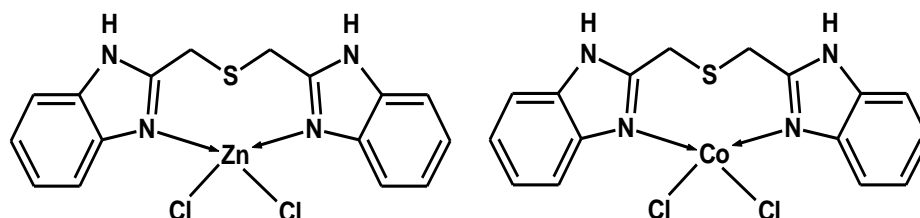


Figure 1.6

1.5 Metal complexes of 1,3-symmetrically and 1,3-unsymmetrically substituted imidazoles and benzimidazoles

Marika Marinelli et al (2016), [11] Novel zwitterionic N-heterocyclic carbenes (NHCs) precursors, 1,3-symmetrically substituted have been synthesized and used in the synthesis of multicharged silver(I)-NHC complexes (Figure 1.7). The N-heterocyclic carbene ligand precursor Him¹ and the intermediate HBzim^{PrSO₃} were also characterized by X-ray crystallography. Silver(I)-NHCs and the corresponding silver free ligands were assayed for their cytotoxic properties against a panel of human tumour cell lines including lung (A549), colon (HCT-15), breast

(MCF-7) and cervical (A431) cancers, along with melanoma (A375). Their anti-proliferative activity was further investigated on a human ovarian cell line pair which has been selected for sensitivity/resistance to *cisplatin*, i.e. 2008/C13* cancer cells. All complexes exhibited a similar cytotoxic profile both in *cisplatin*-sensitive and resistant cell lines, with resistance factors (R.F.) up to 9 times lower than that of *cisplatin*, attesting the ability of these derivatives to overcome acquired *cisplatin* resistance.

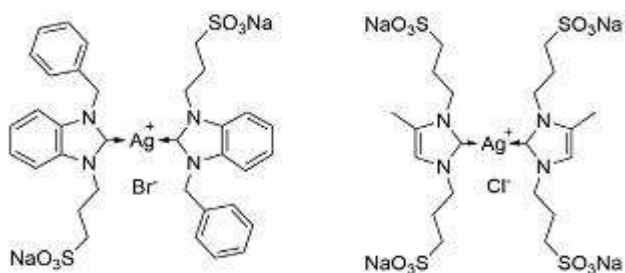


Figure 1.7

1.6 2-(2-pyridyl) benzimidazole derived metal complexes

Adam Lewis et al (2016), [12], 2-(2-pyridyl)benzimidazole (PyBIm) (Figure 1.8) are reported with the biological activity of these two complexes and a third Cu(II) complex containing 2-(2-pyridyl)benzothiazole (PyBTh), $[\text{Cu}(\text{PyBIm})(\text{NO}_3)(\text{H}_2\text{O})](\text{NO}_3)$, is a four coordinate, distorted square planar species with one ligand (N,N), nitrate and water bound to Cu(II). The $[\text{Cu}(\text{PyBIm})_3](\text{BF}_4)_2$ complex (2) has distorted octahedral geometry with a 3:1 Py(BIm) ligand to metal ratio. The distorted trigonal bi-pyramidal geometry of compound 3, $[\text{Cu}(\text{PyBTh})_2(\text{H}_2\text{O})](\text{BF}_4)_2$, is comprised of two PyBTh ligands and one water. Biological activity of 1–3 has been assessed by analyzing DNA interaction, nuclease ability, cytotoxic activity and antibacterial properties. Complex 3 exhibits potent concentration dependent SC-DNA cleavage forming single- and double-nicked DNA in contrast to the weak activity of complexes 1 and 2. Mechanistic studies indicate that all complexes utilize an oxidative mechanism however 1 and 2 employ O^{2-} as the principal reactive oxygen species while the highly active 3 utilizes 1O^2 . The interaction between 1–3 and DNA was investigated using fluorescence emission spectroscopy and revealed all complexes strongly intercalate DNA with K_{app} values of 2.65×10^6 , 1.85×10^6

and $2.72 \times 10^6 \text{ M}^{-1}$, respectively. Cytotoxic effects of 1–3 were examined using HeLa and K562 cells and show cell death in the micromolar range with the activity of 1 \approx 2 and were slightly higher than 3. Similar reactivity was observed in the antibacterial studies with *E. coli* and *S. aureus*. A detailed comparative analysis of the three complexes is presented.

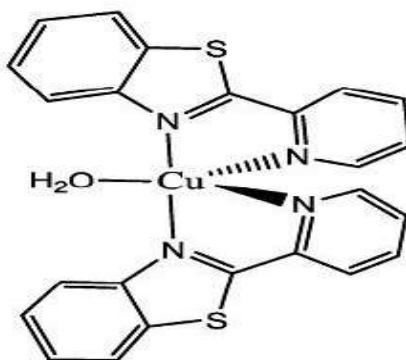


Figure 1.8

N-{2-[5-(2-Hydroxyphenylmethyleneamino)-1-alkylbenzimidazol-2-yl]phenyl}-4-methyl-benzenesulfamides (H_2L) and their zinc complexes Zn_2L_2 (Figure 1.9) were synthesized. The structure of the ligands and complexes was studied by IR, UV, ^1H NMR, X-ray absorption spectroscopy, and X-ray diffraction analysis. The complex show green photoluminescence ($\lambda_{\text{fl}} = 492 \text{ nm}$) with quantum yields $\phi = 0.07\text{--}0.17$.

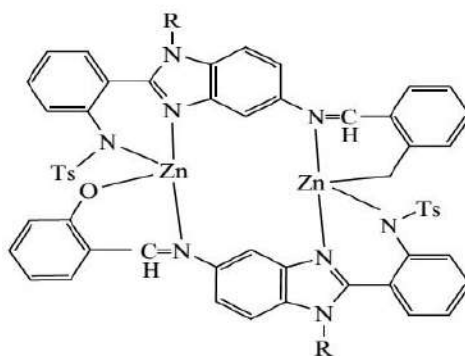


Figure 1.9

Babli Kumari et. al (2017) [13]. The benzimidazole derivative like 2-pyridylbenzimidazole (PBI) (Figure 1.10), viz. the Cu(II) complex, $[\text{Cu}(\text{PBI})_2(\text{NCS})]\text{ClO}_4$ (1) and a Co(II) complex, $[\text{Co}(\text{PBI})_2(\text{NCS})1.75\text{Cl}0.25]$ (2). The Cu(II) complex (1) shows catecholase like activity having $K_{\text{cat}} = 1.84 \times 10^4 \text{ h}^{-1}$.

Moreover, interactions of the complexes with hydrogen peroxide have been investigated using fluorescence spectroscopy. The interaction constant of 1 and 2 for H_2O_2 are $6.67 \times 10^2 \text{ M}^{-1}$ and $1.049 \times 10^3 \text{ M}^{-1}$ while their detection limits for H_2O_2 are $3.37 \times 10^{-7} \text{ M}$ and $2.46 \times 10^{-7} \text{ M}$ respectively.

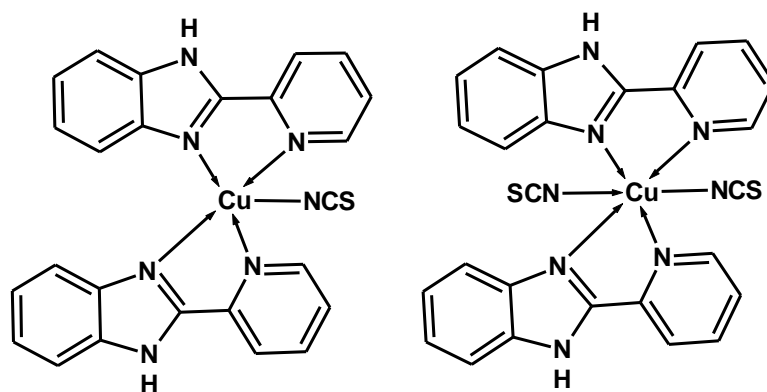


Figure 1.10

1.7 Metal complexes of Quinoline-benzimidazole derivatives

Quinoline-benzimidazole derivatives serves as good π -acceptor due to the presence of pyridine ring ends to stabilize metal ion acceptor center and the imidazole and its derivatives exhibit moderate π -donor properties [14]. Thus the steric and electronic properties around the metal center can be changed with benzimidazole type ligands.

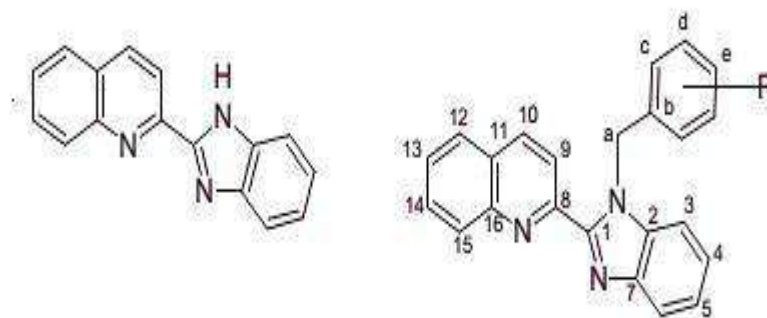


Figure 1.11

Metal complexes containing 2-(2'-quinolyl)benzimidazoles (Figure 1.11) are very rare but it displays excellent biological and pharmacological activity. 2-(2-(1H-benzo[d]imidazol-2-yl)quinolin-8-yloxy)acetate (Figure 1.12) based on quinoline derivative was designed and synthesized. Once combined with metal ion aqueous

solution, the forming quinoline-ligated complex displayed a rapid response with high selective and sensitive detection for sulfide anion [15].

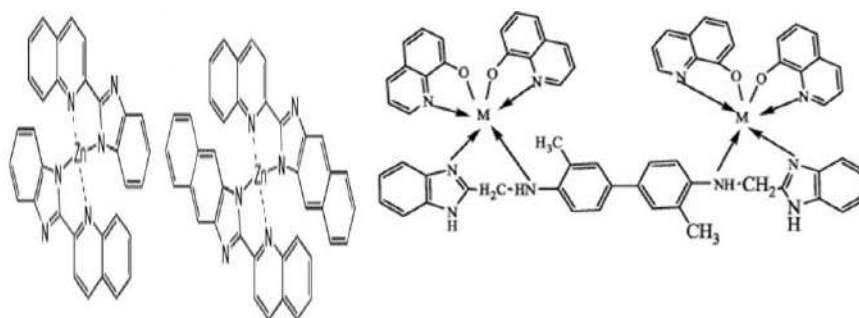


Figure 1.12

1.8 Mannich base reactions with benzimidazole

It is known that the compounds having least one reactive hydrogen atom react with formaldehyde and amines to form a mannich base. The mannich base reactions used for further development of research in the field of chemistry of new pharmacologically active compounds with different heterocyclic compounds, in benzimidazole chemistry, several synthetic strategies have been proposed for derivatives through 2-mercaptobenzimidazole, 2-aminobenzimidazole and 2-methoxybenzimidazole (Figure 1.13) with slight chemical modification with functions leading to a variety of compounds with broad spectrum of biological activities [16, 17].

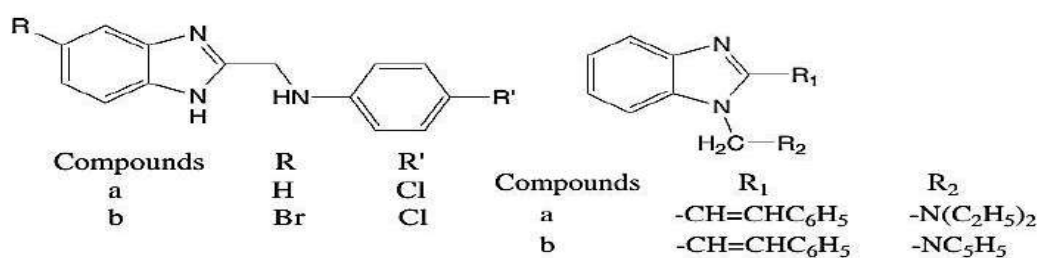


Figure 1.13

Mannich bases derived from 2-Substituted benzimidazoles by reacting 2-Substituted phenyl benzimidazoles, formaldehyde and secondary amine (Figure 1.14) [18].

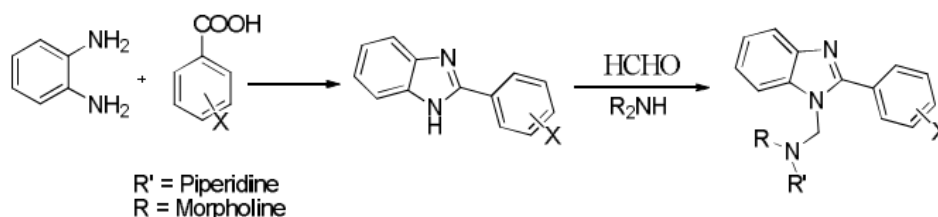


Figure 1.14

1, 2- Disubstituted Benzimidazole derived compounds using Mannich base reaction (Figure 1.15). The product prepared by 1st reacting diamine and glycine in acidified ethanol then substituted benzimidazole dissolved in secondary amine and formaldehyde [19].

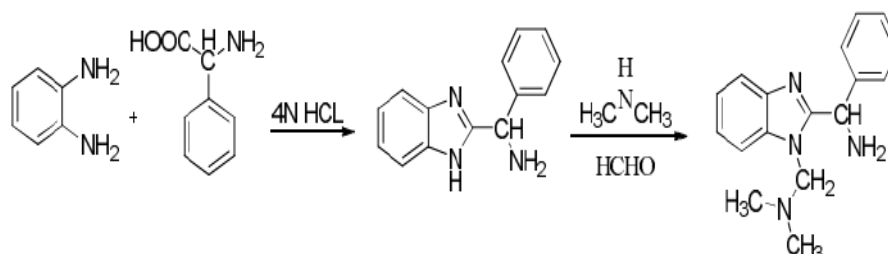


Figure 1.15

Benzimidazole through the cyclization reaction (Figure 1.16). All the compounds were seen for biological activities and some of the compounds showed moderate antibacterial and negligent antifungal activities [20].

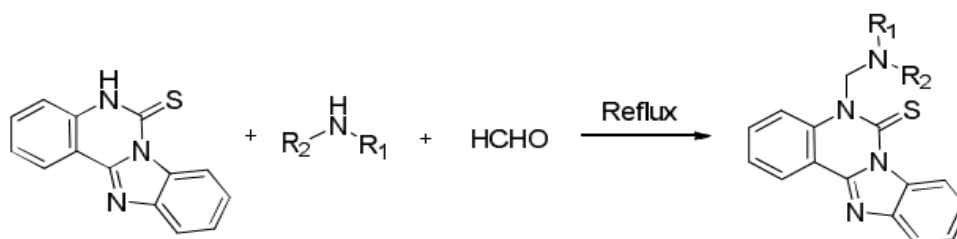


Figure 1.16

1.9 2-mercaptobenzimidazole derivatives

A novel series of 2-mercaptobenzimidazole is a class derivative imidazole moiety, the substitutions with 4-thiazolidinone and 1,3,4-oxadiazoles (Figure 1.17) derivatives were displays a vital role in the anticonvulsant *in vivo* activity by maximal electroshock (MES) model and antidiabetic activity using oral glucose tolerance test (OGTT). A series of mercapto compounds were studied for their

potential anticancer, antidiabetic, antitumour and antiasthmatic properties and antidiabetic activity [21].

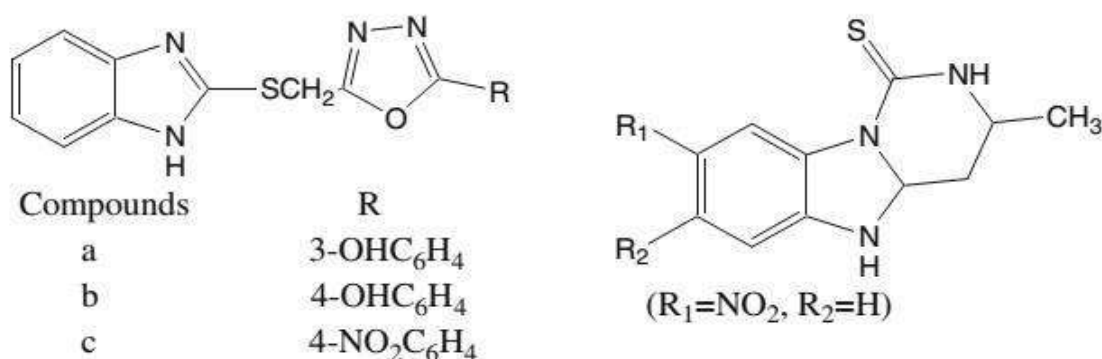


Figure 1.17

1.10 Bis-benzimidazole derivatives

G. Krishnamurthy et al., [22] synthesized bis(Benzimidazole) (Figure 1.18) coupled with flexible ligands on para, meta and orthoxylene as a bridging spacer moiety have been greatly used in crystal engineering and are of particular interest in coordination chemistry and also their thermal degradation studies have been done, since they are useful as bridging ligands. The nature of $-(\text{Ph}-\text{CH}_2)-$ spacers allows the ligand to bend and rotate when it coordinates to metal centers so as to conform to the coordination geometries of metal ions [23-25]. In contrast, the most exceptional compound of benzimidazole derivatives are 5,6-dimethyl-benzimidazole, which serves as an axial ligand for cobalt in vitamin B₁₂ [26-29] and 2,6-bis (Benzimidazole-2-yl) pyridine have been reported to display antimicrobial activity.

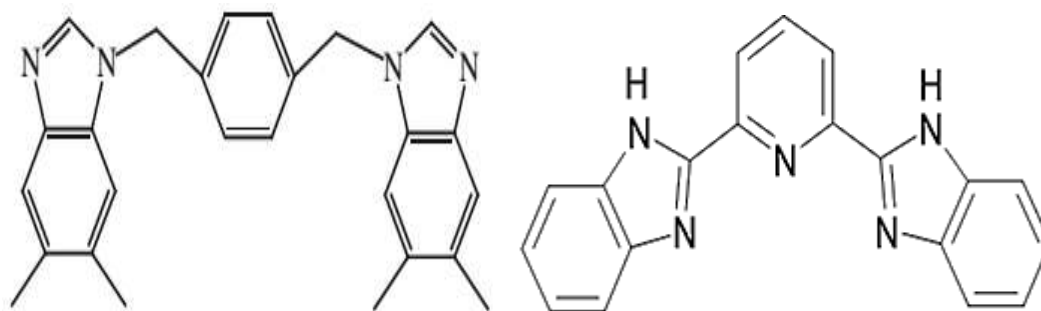


Figure 1.18

Most of the bis-Benzimidazole derived complexes are naturally specific groove binders, with Hoechst 33258 binding in a specific manner to the A–T sequence at pre-organized site of the minor groove of the DNA duplex [30]. Recently, many efficient Ru containing π -acceptor nitrogen-bearing ligands, especially N-hetero aromatic systems like pyridyl-based benzimidazolyl ligands have been widely studied. The pyridine ring as a good π -acceptor tends to stabilize the Ru(II) acceptor center and the imidazole and its derivatives exhibit moderate π -donor properties [31].

1.11 Biological activities of benzimidazoles

a. *Benzimidazole as antiviral agents*

Heterocyclic benzimidazole derivatives bearing amino substituents at C-5 of benzimidazole ring, by introducing various heterocyclic nuclei (pyridine, N-methyl pyrrole or imidazole) at C-2 and evaluated their antiviral activity towards coxacki-eyruses and echoviruses. Fairly strong activity was observed with 2-(1-methyl-1H-pyrrol-2-yl)-1H-benzimidazole-5-carboxamidehydrochloride, (**a-1**), and n-isopropyl-2-pyridin-2-yl-1H-benzimidazole-5-carboxamide, (**a-2**), towards adenovirus, which make them to be considered as leads against adenoviral replication [32].

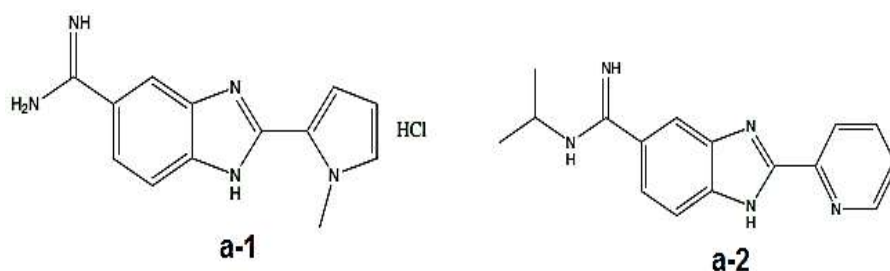


Figure a-1 and a-2

b. *Benzimidazole as anti-HIV agents*

Benzimidazole derivative involves HIV Type I integrase inhibitors using naphthamidines (**b-1**) and 2-aminobenzimidazoles (**b-2**) and found that A-201735, emerged as a potent integrate inhibitor [33].

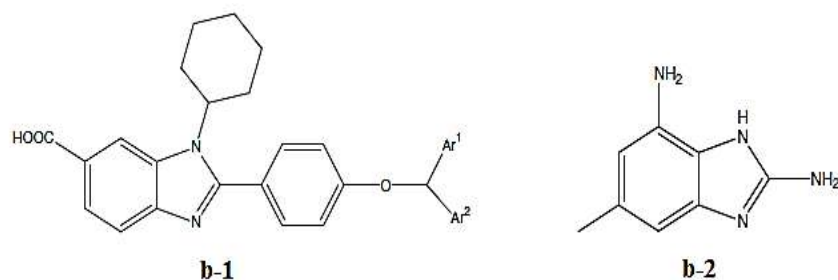


Figure b-1 and b-2

c. *Benzimidazole as antibacterial and antifungal agents*

Almost all the main classes of antibiotics have encountered resistance in clinical application. The emergence of bacterial resistance to β -lactam antibiotics, macrolides, quinolones and vancomycin is becoming a major worldwide health problem. Recent literature review revealed that benzimidazole derivatives have emerged as promising candidates for the development of antibacterial agents. The broad spectrum antimicrobial activity against various strains of microorganisms such as *Enterococcus*, *C. albicans* and *P. aeruginosa* [34]. From their study, they found that compound (**c-1**), N1-[4-(5,6-dichloro-2-piperidin-4-yl-benzoimidazol-1-ylmethyl)-benzyl]-ethane-1,2-diamine and 3,4-dichloro-substituted phenyl at position C-2 of N-bulky alkyl-substituted benzimidazole carboxamides, (**c-2**), exhibited the greatest activity with MIC values [35].

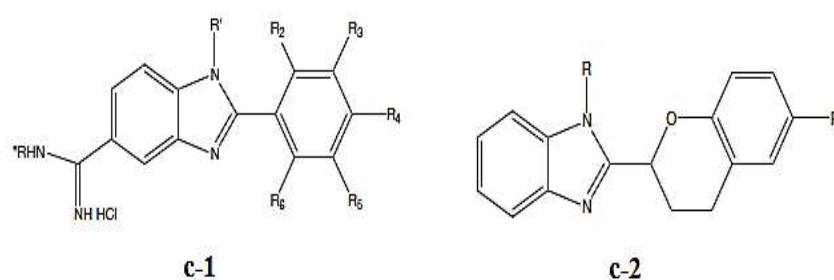


Figure c-1 and c-2

A series of 2-substituted phenyl-1H-(5-substituted) benzimidazole were prepared and evaluated *in vitro* against *Candida species*. The results of antimicrobial studies suggested that the cyano-substituted compounds (**c-3**) and (**c-4**) in particularly the compound 1-butyl-2-(4-fluoro-phenyl)-1H-benzimidazole-5-carbo

nitrile, (**c-5**, **c-6**) showed greatest activity with MIC value similar to that of fluconazole as antifungal agents [36].

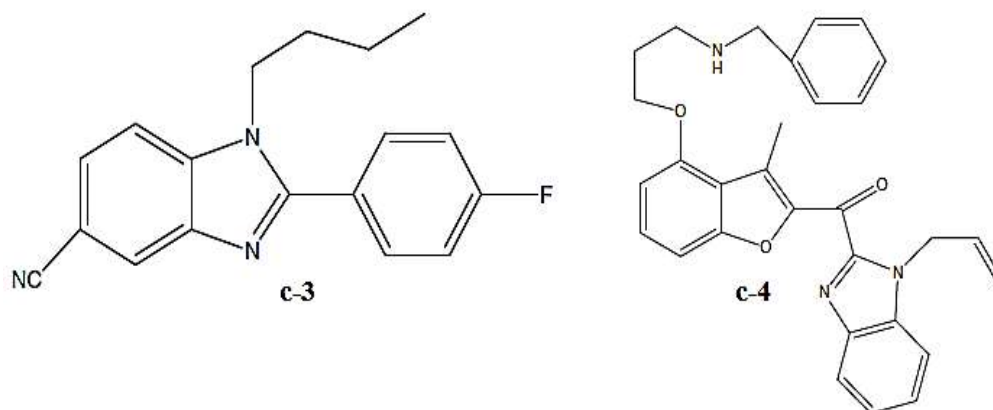


Figure c-1 and c-2

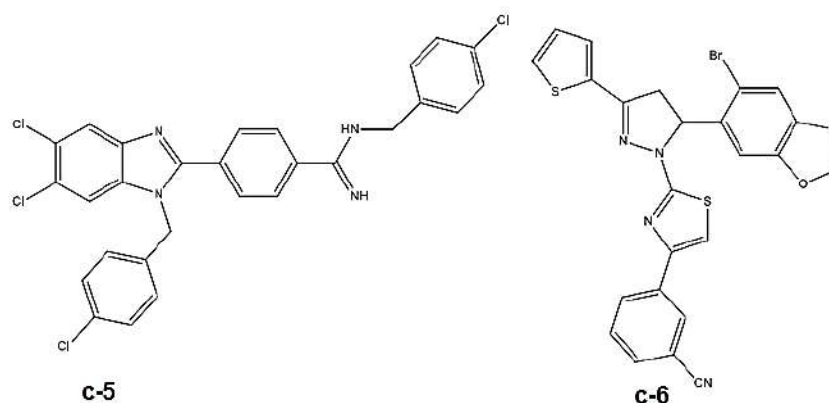


Figure c-3 and c-4

Plasma-bound ruthenium complexes (**c-7** and **c-8**) possess high affinity to cancer cells with transferrin receptors; this brings about diverse pharmacodynamics differences that exist between cancerous and healthy cells and forms the basis of higher cytotoxicity experienced with compounds respectively [37].

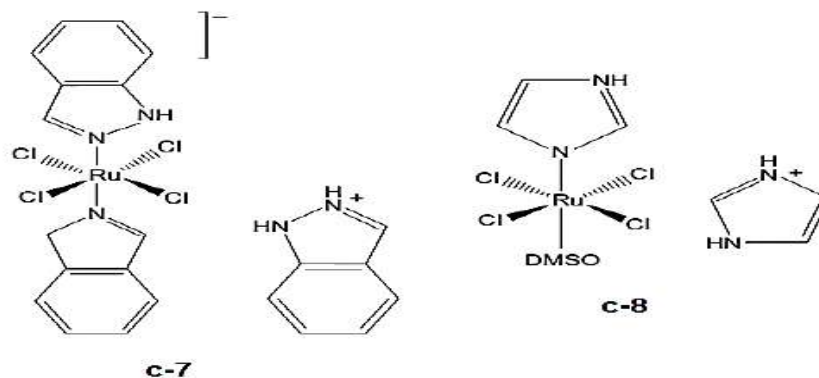


Figure c-7 and c-8

d. Benzimidazole as anticancer agents

Benzimidazole derivatives recently attracted medicinal chemists in exploring their potential as anticancer agents. Carbomethoxy-substituted benzimidazole derivatives of UK-1 [a *bis* (benzoxazole) natural product] isolated from a strain of *Streptomyces* and evaluated its cytotoxicity by Alamar Blue cytotoxicity assays against MCF-7, HL-60, HT-29 and PC-3 cell lines [38].

They found that the compound methyl 2-[2-(2-hydroxyphenyl)-1,3-benzoxazo 1-4-yl]-1H-benzimidazole-4-carboxylate, (**d-1** and **d-2**) exhibited cytotoxicity against the tested cell lines [39]. The benzimidazolium salts (IC_{50} is around 131 μM for 2 and 18 μM for 3), and silver complex (IC_{50} is around 12 μM for 4) showed increased potency to inhibit cancer cell growth compared to pyridine enhanced pre catalyst preparation stabilization and initiation (PEPPSI)Pd-NHC complexes against DLD-1 and MDA-MB-231 cancer cell lines (**d-9** to **d-5**) [41-43],

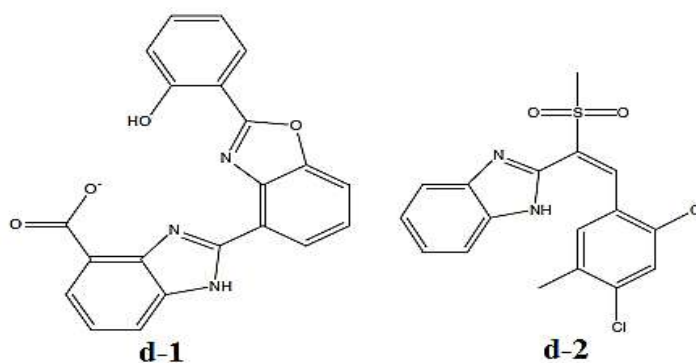


Figure d-1 and d-2

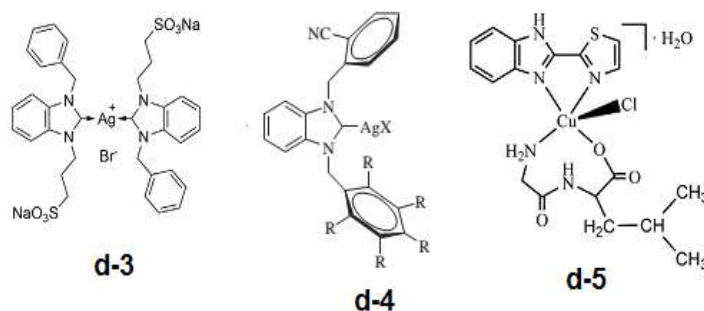


Figure d-3, d-4 and d-5

e. Benzimidazole as Anti-inflammatory and analgesic

Some 2-substituted benzimidazoles (**e-1** and **e-2**) have been synthesized by the condensation of o-phenylenediamine with 2-coumaranonyl acetic acid derivatives and indole 3-acid and evaluated their anti-inflammatory and analgesic activities [44]. The compounds were found to have significant anti-inflammatory activity at 50 mg/kg dose.

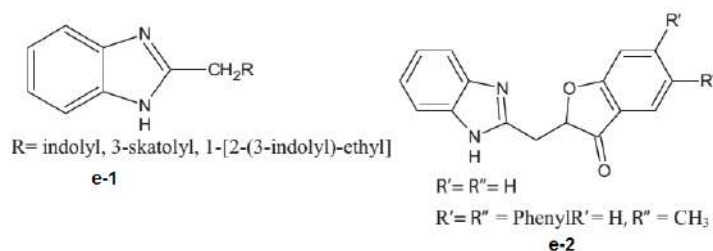


Figure e-1 and e-2

A new synthesis and their anti-inflammatory activity of a group of 1H-benzimidazole (**e-3**) were reported [45]. The compounds were assessed on rat adjuvant arthritis screen and indomethacin as standard compound. The result gave 30% or greater reduction in non-injected paw volume compared to control together with the result for indomethacin. Some imino sugars of methylbenzimidazole (**e-4**) have been prepared and anti-inflammatory activity of the compounds was studied by employing the cotton pellet granuloma bioassay in rats using indomethacin as reference standard. The granuloma % inhibition values were determined for each compound [46].

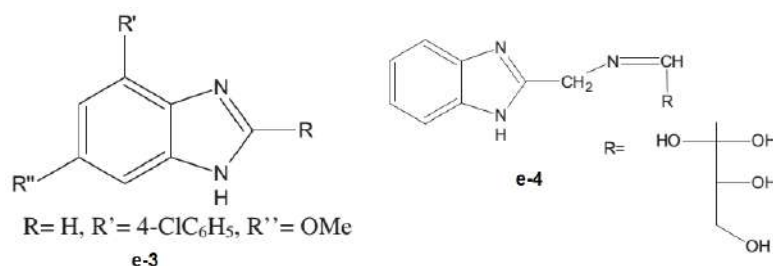


Figure e-3 and e-4

1-[2,3-(2-Phenylbenzimidazole)]2-methyl/phenyl-4-(3,4-disubstitutedbenzylidene)-5-oxoimidazoles (**e-5**) and novel 5-substituted-1-(phenylsulphonyl)-2-methylbenzimidazole derivatives (**e-6**) have been synthesized [47]. Compounds were evaluated for their anti-inflammatory and analgesic activities as well as gastric ulcerogenic effects by carrageenan-induced rat paw edema and acetic acid-induced writhing in mice using indomethacin as standard.

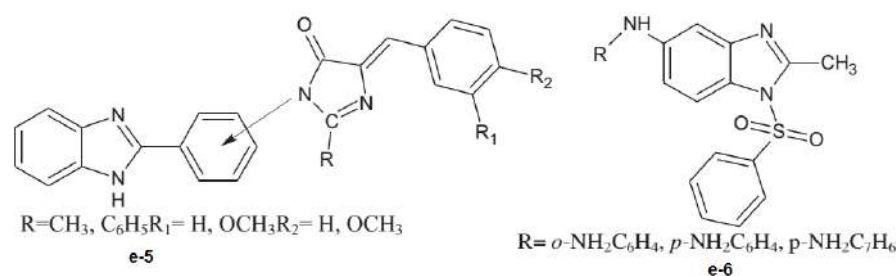


Figure e-5 and e-6

1.12 Metal complexes with substituted benzimidazole

The organometallics over the last few years has also triggered a gradually increasing number of studies in the field of medicinal chemistry, which take advantage of the fascinating chemical properties of these complexes. Since N-heterocyclic carbenes (NHCs) act as excellent σ -donor ligands, they can produce stable metal-NHCs with strong metal carbon bond. Functionalized imidazole-based NHCs have attracted special interest because they can be utilized to tune the environment and properties at the coordinated metal. In particular, water solubility has been a main attention in the development of metal-NHC complexes as therapeutic agents. Thus the steric and electronic properties around the metal center can be changed with benzimidazole type ligands [48, 49]. However, some

researchers show that their related Co, Ni, Cu, Ir, Re, Pd, Ti, Zn and Ru complexes have good optoelectronic and catalytic properties [50, 51].

The critical factors in the structure of metal ion complexes are the type of ligands and the oxidation state of the metal, which regulate the biological activity of the metal-based drugs. Moreover, oxidation state often dictates particular coordination geometry. In the recent years much effort has been made to increase the number of therapeutic metal complexes. Historically, metals and metal complexes have played a key role in the development of pharmacy and modern chemotherapy. However, they still remain a tiny minority of all therapeutics on the market today. Especially heavy metals, so called d-block metals have good cytotoxic potential [52]. There are many known and documented complexes that carry photochemical, anticancer or both of these activities.

1.13 Structural characterization tools

I. Estimation of carbon, nitrogen and oxygen

Elemental analysis of C, H and N were done on a Vario EL III CHN elemental analyzer at the SAIF, Cochin University and Kerala, INDIA.

II. IR spectroscopy

Infrared spectroscopy is the study of the interaction of infrared light with matter. The fundamental measurement obtained in infrared spectroscopy is an infrared spectrum, which is a plot of measured infrared intensity versus wavelength (or frequency) of light, the wavelengths found in infrared radiation are a little longer than those found in visible light. IR spectroscopy is useful for finding out what kinds of bonds are present in a molecule, and knowing what kinds of bonds. The fingerprint region (1500 to 500 cm^{-1}) is the region usually contains a very complicated series of absorptions. These are mainly due to all manner of bending vibrations within the molecule.

III. Electronic spectroscopy

Absorption of visible and ultraviolet (UV) radiation is associated with excitation of electrons, in both atoms and molecules, from lower to higher energy levels, Therefore in order to absorb light in the region from 200 - 800 nm (where spectra are measured), the molecule must contain either π bonds or atoms with non-bonding orbitals. A non-bonding orbital is a lone pair on, say, oxygen, nitrogen or a halogen and also molecules that contain conjugated systems, i.e. alternating single and double bonds, will have their electrons delocalised due to overlap of the p orbitals in the double bonds, Uv-visible spectrum are also involves in the absorption of transition metal complexes are also highly coloured, which is due to the splitting of the d orbitals when the ligands approach and bond to the central metal ion. Some of the d orbitals gain energy and some lose energy. The amount of splitting depends on the central metal ion and ligands. The difference in energy between the new levels affects how much energy will be absorbed when an electron is promoted to a higher level. The amount of energy will govern the colour of light which will be absorbed.

IV. NMR spectroscopy

Nuclear Magnetic Resonance (NMR) spectroscopy can be used in a large variety of experimental conditions (e.g., temperature, pH, ionic strength) to study the structure and behavior of transition metal complexes-based compounds in both the solution and the solid state. Even such a powerful method as the NMR spectroscopy definitely is, can be further enhanced when it is supported by theoretical quantum-chemical calculations. This approach combines the precision and accuracy of experiment and the predictive and explanatory power of quantum chemistry. It can provide an invaluable insight into the properties hidden in the measured quantities, like influence of the heavy atoms to the NMR chemical shifts of light atoms in its vicinity.

V. Thermogravimetric analysis (TGA)

Thermogravimetry is a technique in which the mass of the substance, in an environment heated or cooled at a controlled rate, is recorded as a function of temperature. The resulting mass change versus temperature curve give information concerning the thermal stability and composition of the initial sample, the thermal stability and composition of any intermediate compounds that may be formed and the composition of the initial sample and the compositions of the residue, if any. The analytical instrument used is a thermobalance with a furnace programmed for a linear rise of temperature with time. This technique can be used to study the kinetics of chemical reaction and determine basic kinetic constants such as the rate constant, activation energy, order of reaction, frequency factor etc.

VI. X-ray powder diffraction

X-ray powder diffraction (XRD) is a rapid analytical technique primarily used for phase identification of a crystalline material and can provide information on unit cell dimensions. The analyzed material is finely ground, homogenized, and average bulk composition is determined.

X-ray diffraction currently plays an important role in elucidating the structure of metal complexes. X-ray powder methods are based upon the fact that an X-ray diffraction is unique for each crystalline substance. It is the only analytical method that is providing qualitative and quantitative information about the

compounds present in a solid sample. For analytical diffraction studies the sample is ground to a fine homogeneous powder. When an X-ray beam traverses the material a significant number of the particle can be oriented in such a way to fulfill Bragg condition for reflection. Diffraction patterns are obtained by automatic scanning. The identification of a species from its diffraction patterns is based upon the position of lines and their relative intensities. The X-ray powder diffraction method is used now days to determine the lattice type of complexes.

VII. Molecular docking studies

Molecular docking is the study of how two or more molecular structures (e.g. drug and enzyme or protein) fit together [53]. In a simple definition, docking is a molecular modeling technique that is used to predict how a protein (enzyme) interacts with small molecules (ligands). The ability of a protein (enzyme) and nucleic acid to interact with small molecules to form a supramolecular complex plays a major role in the dynamics of the protein, which may enhance or inhibit its biological function. The behavior of small molecules in the binding pockets of target proteins can be described by molecular docking. The method aims to identify correct poses of ligands in the binding pocket of a protein and to predict the affinity between the ligand and the protein. Based on the types of ligand, docking can be classified as Protein–small molecule (ligand) docking, protein–nucleic acid docking, protein–protein docking.

Molecular docking analysis was performed to understand the binding efficiency of the FAD to the native and mutant proteins. The grid box was set around the active site residues THR94, TRP95, PRO97, HIS127, THR129, MET154, LEU156, ARG157, GLY158, ASP159, TYR174, ALA175, ALA195, TYR197, HIS201, ALA204, ASP210, HIS213, LYS217, ILE226, GLN228, and TYR321. When comparing the binding energy of FAD with the four protein molecules, the lowest binding energy was observed with native and the highest with A222V mutant complexes. When analyzing the native docked complex, FAD formed three hydrogen bonds with TYR197, ARG157, and GLY158. The A222V mutant protein did not show any hydrogen bond formation with FAD. E429A showed two-hydrogen bond formation with ASP159 and GLN228. An increase in

the number of hydrogen bonds formation was observed in R594Q. Four hydrogen bonds were formed with ASP159, THR94, and TYR197. This concludes that there is a loss of interaction in case of E429A and A222V mutations [54-56].

The application of docking in a targeted drug-delivery system is a huge benefit. One can study the size, shape, charge distribution, polarity, hydrogen bonding, and hydrophobic interactions of both ligand (drug) and receptor (target site).

- Molecular docking helps in the identification of target sites of the ligand and the receptor molecule.
- Docking also helps in understanding of different enzymes and their mechanism of action.
- The “scoring” feature in docking helps in selecting the best fit or the best drug from an array of options.
- Not everything can be proved experimentally as traditional experimental methods for drug discovery take a long time. Molecular docking helps in moving the process of computer-aided drug designing faster and also provides every conformation possible based on the receptor and ligand molecule.
- Docking has a huge advantage when it comes to the study of protein interactions.
- There are millions of compounds, ligands, drugs, and receptors, the 3D structure of which has been crystallized. Virtual screening of these compounds can be made.

HEX docking studies

Protein docking is the task of calculating the 3D structure of a protein complex from its unbound or model-built subunits. Although proteins are intrinsically flexible, many protein docking algorithms begin by assuming that the proteins are rigid and they use geometric hashing or fast Fourier transform (FFT) correlation techniques to find a relatively small number of putative docking

orientations which may be refined and re-scored using more sophisticated techniques [57-60].

Like the geometric hashing approach, the FFT-based approaches assume that the proteins to be docked are rigid, but they sample densely all possible rigid-body orientations in the 6D search space. However, because most FFT-based approaches use 3D Cartesian grid representations of the proteins, they can only compute translational correlations, and these must be repeated over multiple rotational samples in order to cover the 6D search space. Thus, despite the rigid-body assumption, Cartesian grid-based FFT docking algorithms are inherently computationally expensive. In order to address the main limitations of the Cartesian FFT approaches, the 'Hex' spherical polar Fourier (SPF) was developed using rotational correlations, and which reduces execution times by an order of magnitude. Nonetheless, Hex algorithm to obtain a further significant speed-up by exploiting the enormous computational power of modern graphics processor units (GPUs; in preparation) using the CUDA (Common Unified Device Architecture) development tools. For typical Hex docking calculations, a single high-performance GPU can evaluate ~170 million trial orientations/second. This corresponds to a speed-up of at least a factor of 45 compared to a contemporary central processor unit (CPU), and which are up to two orders of magnitude faster than conventional Cartesian grid-based FFT docking approaches. However, because high performance GPUs are relatively expensive, a Hex Server was developed, a web interface for Hex [61-63].

1.14 Research Aim and Thesis Arrangement

The contents of the current thesis have been divided into eight chapters.

Chapter 1: this chapter presents reviews of the literature concerning benzimidazole moiety and their derivatives, importance of benzimidazole based metal complexes, physical, analytical parameters, research aims and thesis arrangement.

Chapter 2: this Chapter illustrates the synthesis of imidazole-Quinoline based ligand and their metal complexes, characterization, physio-chemical analysis, DFT studies, cytotoxicity, molecular docking and other biological studies.

Chapter 3: In this chapter, the synthesis of new mannich base benzimidazole derived ligand and their Co(II), Ni(II) and Cu(II) metal complexes have been discussed. Further, of the compounds structure characterized by various spectroscopic techniques and DFT studies. The investigation of different biological activities and docking studies were performed.

Chapter 4: this chapter describes, the new isoniazid and imidazole based ligand and their metal complexes. Both the ligand and metal complexes were thoroughly characterized by various spectroscopic tools like NMR, IR, XRD, TGA studies and DFT studies, The screening of anti-lipase activity and other biological studies was discussed.

Chapter 5: the two ligands based on derivative of 2-hydroxy/amino-acetophenone moieties with 2-methylchlorobenzimidazole were synthesized. The elemental analysis, spectral characterization of metal complexes of both the ligands was carried out, the comparison biological studies were discussed for both ligands and their metal complexes.

Chapter 6: In this chapter the synthesis of two ligands and their complexes have been presented. The synthesis procedures, the results and discussion have been divided into two parts, part-a and part-b. The 2-mercaptobenzimidazole and 2-methylmercaptobenzimidazole are the basic motifs coupled with thiophene derivatives, both the synthesized ligands and their metal complexes were spectrally characterized and their different biological studies was discussed.

Chapter 7: this chapter deals with synthesis of ligand based on benzimidazole and azo derivative. The Co(II), Ni(II),Cu(II) and Zn(II) metal complexes were prepared and thoroughly characterized with NMR, IR, Uv-vis, XRD studies and DFT studies, along with various biological activities and molecular docking studies was also discussed.

Chapter 8: It is the concluding chapter, which focuses on the summary and discussion of the present working chapters regarding the elemental analysis, spectral characterization, and all the pharmacological and biological studies.

References

- [1] X. Ma, X. Li, Y.E. Cha, L.P. Jin, Highly thermo-stable one-dimensional lanthanide(III) coordination polymers constructed from benzimidazole -5,6-dicarboxylic acid and 1,10-Phenanthroline: synthesis, structure, and tunable white-light emission, *Cryst. Growth Des.* 12, 2012, 5227-5232.
- [2] S. Samai, K. Biradha, Chemical and mechano responsive metal-organic gels of bis (benzimidazole)-based ligands with Cd(II) and Cu(II) halide salts: self-sustainability and gas and dye sorptions, *Chem. Mater* 24, 2012, 1165-1173.
- [3] V.C.O. Njar, A.M.H. Brodie, Discovery and development of galeterone (TOK-001 or VN/124-1) for the treatment of all stages of prostate cancer, *J. Med. Chem.* 58, 2015, 2077-2087.
- [4] Y. Bansal, O. Silakari, The therapeutic journey of benzimidazoles: a review, *Bioorgan Med. Chem.* 20, 2012, 6208-6236.
- [5] Y.L. Yao, Y.X. Che, J.M. Zheng, The coordination chemistry of benzimidazole- 5,6-dicarboxylic acid with Mn(II), Ni(II), and Ln(III) complexes (Ln $\frac{1}{4}$ Tb, Ho, Er, Lu), *Cryst. Growth Des.* 8, 2008, 2299-2306.
- [6] C.H. Chen, W.S. Huang, M.Y. Lai, W.C. Tsao, J.T. Lin, Y.H. Wu, T.H. Ke, L.Y. Chen, C.C. Wu, Versatile, benzimidazole/amine-based am-bipolar compounds for electroluminescent applications: single-layer, blue, fluorescent OLEDs, hosts for single-layer, phosphorescent OLEDs, *Adv. Funct. Mater* 19, 2009, 2661-2670.
- [7] G.G. Mohamed, Z.H. Abd El-Wahab, Salicylidene-2-aminobenzimidazole Schiff base complexes of Fe(III), Co(II), Ni(II), Cu(II), Zn(II) and Cd(II), *J. Therm. Anal. Calorim.* 73, 2003, 347-359.
- [8] Adnan Ashraf, M. Ebel, D. Rehder, Synthesis, characterization, reactivity, and catalytic potential of model vanadium (IV, V) complexes with benzimidazole-derived ONN donor ligands, *Inorganic. Chem.* 45, 2006, 5924-5937.

- [9] Xia-Bing Fu a, Jia-Jia Zhang a, Dan-Dan Liu, Cu(II)–dipeptide complexes of 2-(4'-thiazolyl)benzimidazole: Synthesis, DNA oxidative damage, antioxidant and in vitro antitumor activity, *Journal of Inorganic Biochemistry* 143, 2015, 77-87.
- [10] Mehdi Bouchouit, Said Mohamed Elhadi, Mounira Kara Ali, Sofiane Bouacida, Synthesis, X-ray structure, theoretical investigation, corrosion inhibition and antimicrobial activity of benzimidazole thioether and their metal complexes, *Polyhedron*, 2016, <http://dx.doi.org/10.1016/j.poly.2016.08.045>.
- [11] Marika Marinelli, Maura Pellei, Cristina Cimarrelli, H.V. Rasika Dias, Novel multicharged silver(I)NHC complexes derived from zwitterionic 1,3-symmetrically and 1,3-unsymmetrically substituted imidazoles and benzimidazoles: Synthesis and cytotoxic properties, *Journal of Organometallic Chemistry* 806, 2016, 45-53
- [12] Adam Lewis, Molly McDonald, Stephanie Scharbach, Stefan Hamaway, The chemical biology of Cu(II) complexes with imidazole or thiazole containing ligands: Synthesis, crystal structures and comparative biological activity, *Journal of Inorganic Biochemistry* 157, 2016, 52-61.
- [13] Babli Kumari, Sangita Adhikari, Jesus Sanmartín Matalobos, Debasis Das, Cu(II) and Co(II) complexes of benzimidazole derivative: Structures, catecholase like activities and interaction studies with hydrogen peroxide, *Journal of Molecular Structure*, 2017, 10.1016/j.molstruc.2017.09.031.
- [14] M.R. Maurya, M. Bisht, A. Kumar, M.L. Kuznetsov, F. Avecilla, J.C. Pessoa, Synthesis, characterization, reactivity and catalytic activity of oxidovanadium(IV), oxidovanadium(V) and dioxidovanadium(V) complexes of benzimidazole modified ligands, *Dalton T* 40, 2011, 6968-6983.
- [15] O. Dayan, S. Demirmen, N. Ozdemir, Heteroleptic ruthenium(II) complexes of 2-(2-pyridyl) benzimidazoles: a study of catalytic efficiency towards transfer hydrogenation of acetophenone, *Polyhedron* 85, 2015, 926-932.

- [16] G. Krishnamurthy, Synthesis and thermal degradation kinetics of some Cobalt(II) Complexes with 1,2-disubstituted benzimidazoles, *Journal. Teach. Resear*, 17(1), 2010, 38-43.
- [17] O. Dayan, N. Ozdemir, Z. Serbetci, M. Dincer, B. Cetinkaya, O. Buyukgungor, Synthesis and catalytic activity of ruthenium(II) complexes containing pyridine-based tridentate triamines ('NNN') and pyridine carboxylate ligands (NO), *Inorg. Chim. Acta* 392, 2012, 246-253.
- [18] O. Dayan, S. Dayan, I. Kani, B. Cetinkaya, Ruthenium(II) complexes bearing pyridine-based tridentate and bidentate ligands: catalytic activity for transfer hydrogenation of aryl ketones, *Appl. Organomet. Chem.* 26, 2012, 663-670.
- [19] N.M. Shavaleev, S.V. Eliseeva, R. Scopelliti, J.C.G. Bunzli, Designing simple tridentate ligands for highly luminescent europium complexes, *Chem-Eur J.* 15, 2009, 10790-10802.
- [20] G. Krishnamurthy, N. Shashikala, Synthesis of Ruthenium(II) Carbonyl Complexes with 2-Monosubstituted and 1,2-Diisubstituted Benzimidazoles, *Journal of Serb. Chem. Soc.*, 74(10), 2009, 1085-1096.
- [21] Q.Y. Yu, B.X. Lei, J.M. Liu, Y. Shen, L.M. Xiao, R.L. Qiu, D.B. Kuang, C.Y. Su, Ruthenium dyes with heteroleptic tridentate 2,6-bis(benzimidazol-2-yl)-pyridine for dye-sensitized solar cells: enhancement in performance through structural modifications, *Inorg. Chim. Acta* 392, 2012, 388-395.
- [22] G. Krishnamurthy Synthesis, molecular modeling and biological activity of zinc(II) salts with 1,4-bis(benzimidazol-2-yl)benzene, *Journal of Chemistry*, 41, 2013, 54-96.
- [23] A.K. Vannucci, J.F. Hull, Z. Chen, R.A. Binstead, J.J. Concepcion, T.J. Meyer, Water oxidation intermediates applied to catalysis: benzyl alcohol oxidation, *J. Am. Chem. Soc.* 134, 2012, 3972-3975.

- [24] J. Diez, J. Gimeno, A. Lledos, F.J. Suarez, C. Vicent, Imidazole based ruthenium(IV) complexes as highly efficient bifunctional catalysts for the redox isomerization of allylic alcohols in aqueous medium: water as cooperating ligand, *Acs Catal.* 2, 2012, 2087-2099.
- [25] W.J. Ye, M. Zhao, W.M. Du, Q.B. Jiang, K.K. Wu, P. Wu, Z.K. Yu, Highly active ruthenium(II) complex catalysts bearing an unsymmetrical NNN ligand in the (asymmetric) transfer hydrogenation of ketones, *Chem-Eur J.* 17, 2011, 4737-4741.
- [26] G. Krishnamurthy, Shashikala N. Narashhimiah, Complexes of zinc(II) with 1,2-disubstituted Benzimidazoles, *Journal of chemical Research*, 12, 2006, 766-768.
- [27] G. Krishnamurthy, Synthesis, Characterization of Ruthenium(III) chloride Complexes with Some 1,2-Disubstituted Benzimidazoles and their Catalytic Activity, *Synthesis and Reactivity in Inorganic, Metal-Organic, and Nano-Metal Chemistry*, 41(6), 2011, 590-597.
- [28] F. Arjmand, M. Muddassir, Chiral preference of L-tryptophan derived metal based antitumor agent of late 3d-metal ions (Co(II), Cu(II) and Zn(II)) in comparison to d- and dl-tryptophan analogues: their in vitro reactivity towards CT DNA, 50-GMP and 50-TMP, *Eur. J. Med. Chem.* 45, 2010, 3549–3557.
- [29] J.R. Lakowicz, G. Webber, Quenching of fluorescence by oxygen. Probe for structural fluctuations in macromolecules, *Biochemistry* 12, 1973, 4161-4170.
- [30] A. Wolfe, G.H. Shimer, T. Meehan, Polycyclic aromatic hydrocarbons physically intercalate into duplex regions of denatured DNA, *Biochemistry* 26, 1987, 6392-6396.
- [31] H.T.A. Mohsen, F.A.F. Ragab, M.M. Ramla, H.I.E. Diwani, Novel benzimidazole pyrimidine conjugates as potent anti-tumor agents, *Eur. J. Med. Chem.* 45, 2010, 2336-2344.

- [32] S. Demirayak, I. Kayagil, L. Yurttas, Microwave supported synthesis of some novel 13-diarylpyrazino[12-a]benzimidazole derivatives and investigation of their anticancer activities, *Eur. J. Med. Chem.* 46, 2011, 411-416.
- [33] S. Demirayak, A. Usama, A.C. Mohsen, K. Agri, Synthesis and anticancer and anti-HIV testing of some pyrazino[12-a]benzimidazole derivatives, *Eur. J. Med.Chem.* 37, 2002, 255-260.
- [34] A. Kamal, P. Praveen Kumar, K. Sreekanth, B.N. Seshadri, P. Ramulu, Synthesis of new benzimidazole linked pyrrolo [21-c][1,4] benzodiazepine conjugates with efficient DNA-binding affinity and potent cytotoxicity, *Bioorg. Med.Chem. Lett.* 18, 2008, 2594-2598.
- [35] E. Moriarty, M. Carr, S. Bonham, M.P. Carty, F. Aldabbagh, Synthesis and toxicity towards normal and cancer cell lines of benzimidazole quinines containing fused aromatic rings and 2-aromatic ring substituents, *Eur. J. Med. Chem.* 45, 2010, 3762-3769.
- [36] E.J. Hanan, B.K. Chan, A.A. Estrada, D.G. Shore, J.P. Lyssikatos, Mild and general one-pot reduction and cyclization of aromatic and heteroaromatic 2-nitroamines to bicyclic 2H-imidazoles, *Syn-lett* 18, 2010, 2759-2764.
- [37] D. Yang, D. Fokas, J. Li, L. Yu, C.M. Baldino, A versatile method for the synthesis of benzimidazoles from o-nitroanilines and aldehydes in one step via a reductive cyclization, *Synthesis* 1, 2005, 47-56.
- [38] D. Seenaiyah, P. Ramachandra Reddy, G. Mallikarjuna Reddy, A. Padmaja, V. Padmavathi, N. Siva krishna, Synthesis, antimicrobial and cytotoxic activities of pyrimidinyl benzoxazole, benzothiazole and benzimidazole, *Eur. J. Med. Chem.* 77, 2014 1-7.
- [39] Subba Poojari, P. Parameswar Naik, G. Krishnamurthy, One-pot synthesis of thieno [2,3-d] pyrimidin-4-ol derivatives mediated by polyphosphonic anhydride, *Tetrahedron Letters*, 53, 2012, 4639-4643.

- [40] R.V. Shingalapur, K.M. Hosamani, R.S. Keri, M.H. Hugar, Derivatives of benzimidazole pharmacophore: synthesis anticonvulsant antidiabetic and DNA cleavage studies, *Eur. J. Med. Chem.* 45, 2010, 1753-1759.
- [41] K. Achar, K.M. Hosamani, H.R. Seetharamareddy, In-vivo analgesic and antiinflammatory activities of newly synthesized benzimidazole derivatives, *Eur. J. Med. Chem.* 45, 2010, 2048-2054.
- [42] Subba Poojari, P. Parameswar Naik, G. Krishnamurthy, Synthesis of macrocycles containing 1,3,4-oxadiazole and pyridine moieties, *Tetrahedron Letters* 55, 2014, 305–309.
- [43] A.O. El-Nezhawy, A.R. Bioumy, F.S. Hassan, A.K. Ismaiel, H.A. Omar, Design synthesis and pharmacological evaluation of omeprazole-like agents with anti-inflammatory activity, *Bioorg. Med. Chem.* 21, 2013, 1661-1670.
- [44] M. Ishikawa, K. Nonoshita, Y. Ogino, Y. Nagae, D. Tsukahara, H. Hosaka, H. Hosaka, H. Maruki, S. Ohyama, R. Yoshimoto, K. Sasaki, Y. Nagata, T. Nishimura, Discovery of novel 2-(pyridine-2-yl)-1H-benzimidazole derivatives as potent glucokinase activators, *Bioorg. Med. Chem. Lett.* 19, 2009, 4450-4454.
- [45] H.J. Kwak, Y.M. Pyun, J.Y. Kim, H.S. Pagire, K.Y. Kim, K.R. Kim, S.D. Rhee, W.H. Jung, J.S. Song, M.A. Bae, D.H. Lee, J.H. Ahn, Synthesis and biological evaluation of aminobenzimidazole derivatives with a phenylcyclohexyl acetic acid group as anti-obesity and anti-diabetic agents, *Bioorg. Med. Chem. Lett.* 23, 2013, 4713-4718.
- [46] D. Valdez-Padilla, S. Rodríguez-Morales, A. Hernandez-Campos, F. Hern and Luis, L. Yopez-Mulia, A. Tapia-Contreras, R. Castillo, Synthesis and anti-protozoal activity of novel 1-methylbenzimidazole derivatives, *Bioorg. Med. Chem.* 17, 2009, 1724-1730.

- [47] Z.S. Saify, M.K. Azim, W. Ahmad, M. Nisa, D.E. Goldberg, S.A. Hussain, S. Akhtar, A. Akram, A. Arayne, A. Oksman, I.A. Khan, New benzimidazole derivatives as antiplasmodial agents and plasmepsin inhibitors: synthesis and analysis of structure-activity relationships, *Bioorg. Med. Chem. Lett.* 22, 2012, 1282-1286.
- [48] Bhimagouda S. Patil, Krishnamurthy G, Bhojya naik H.S, Prashanth R.L, Manjunath G, Synthesis, characterization and antimicrobial studies of 2-(4-methoxy-phenyl)-5-methyl-4-(2-arylsulfanyl-ethyl)-2,4-dihydro-[1,2,4]triazole-3-ones and their corresponding sulfones, *Eur. J. Med Chem*, 45, 2010, 3329-3334.
- [49] H.B. Mallesh, G.Krishnamurthy, N. Shashikala, Reactions of 1-p-dimethylaminobenzyl-2-p-dimethylaminophenyl benzimidazoles with cobalt(II), zinc(II) on cadmium(II) salts, *Asian Journal of Chemistry*, 16(4), 2004, 1439-1446.
- [50] M. Singh, V. Tandon, Synthesis and biological activity of novel inhibitors of topoisomerase I: 2-Aryl-substituted 2-bis-1H-benzimidazoles, *Eur. J. Med. Chem.* 46, 2011, 659-669.
- [51] B. Sreekanth, G. Krishnamurthy, H. S. Bhojya Naik & T. K. Vishnuvardhan, Cu(II) and Mn(II) Complexes Containing Macroacyclic Ligand: Synthesis, DNA Binding, and Cleavage Studies, *Nucleosides, Nucleotides and Nucleic Acids*, 31(1), 2012, 1-13.
- [52] R. Sawant, D. Kawade, Synthesis and biological evaluation of some novel 2-phenyl benzimidazole-1-acetamide derivatives as potential anthelmintic agents, *Acta Pharm.* 61, 2011, 353-361.
- [53] N.D Shashikumar, G. Krishnamurthy, H.S Bhojyanaik, M.R Lokesh, K.S. Jithendra kumara, Synthesis of new biphenyl-substituted quinoline derivatives, preliminary screening and docking studies *J. Chem. Sci.* 126, 1, 2014, 205–212.

- [54] Y.K. Yoon, M.A. Ali, T.S. Choon, R. Ismail, A.C. Wei, R.S. Kumar, H. Osman, F. Beevi, Antituberculosis: synthesis and antimycobacterial activity of novel benzimidazole derivatives, *Biomed. Res. Inter.* 6, 2013, Article ID 926309.
- [55] K. Gobis, H. Foks, K. Bojanowski, E. Augustynowicz-Kope c, A. Napiorkowska, Synthesis of novel 3-cyclohexylpropanoic acid-derived nitrogen heterocyclic compounds and their evaluation for tuberculostatic activity, *Bioorg. Med. Chem.* 20, 2012, 137-144.
- [56] B. Zhou, B. Li, W. Yi, X. Bu, L. Ma, Synthesis antioxidant and antimicrobial evaluation of some 2-arylbenzimidazole derivatives, *Bioorg. Med. Chem. Lett.* 23, 2013, 3759-3763.
- [57] S. Caron, B.P. Jones, L. Wei, Preparation of substituted benzimidazoles and imidazopyridines using 2,2,2-trichloroethyl imidates, *Synthesis*, 2012, 3049-3054.
- [58] K. Bahrami, M.M. Khodaei, F. Naali, Mild and highly efficient method for the synthesis of 2-arylbenzimidazoles and 2-arylbenzothiazoles, *J. Org. Chem.* 73, 2008, 6835-6837.
- [59] J. She, Z. Jiang, Y. Wang, One-pot synthesis of functionalized benzimidazoles and 1H-pyrimidines via cascade reactions of o-amino anilines or naphthalene-1,8-diamine with alkynes and p-tolylsulfonyl azide, *Synlett*, 2009, 2023-2027.
- [60] X. Lv, W. Bao, Copper-catalyzed cascade addition/cyclization: an efficient and versatile synthesis of N-substituted 2-heterobenzimidazoles, *J. Org. Chem.* 74, 2009, 5618-5621.
- [61] Y. Luo, J.P. Yao, L. Yang, C.L. Feng, W. Tang, G.F. Wang, W. Lu, Design and synthesis of novel benzimidazole derivatives as inhibitors of hepatitis B virus, *Bioorg. Med. Chem.* 18, 2010, 5048-5055.

- [62] Sreekanth B, Krishnamurthy G, Bhojya Naik H.S, Vishnuvardhana T.K, Prabhakar M.C, Fe(II) complexes containing bioactive ligands: synthesis, DNA binding and cleavage studies, *Synth. React. Inorg. Metal-Org. Nano-Metal chem*, 40, 2010, 955-962.
- [63] K.S. Gudmundsson, P.R. Sebahar, L.D. Richardson, J.F. Miller, E.M. Turner, J.G. Catalano, A. Spaltenstein, W. Lawrence, M. Thomson, S. Jenkinson, Amine substituted N-(1H-benzimidazol-2-ylmethyl)-5678-tetrahydro-8-quinoli namines as CXCR4 antago- nists with potent activity against HIV-1, *Bioorg. Med. Chem. Lett.* 19, 2009, 5048-5052.

Chapter – 2

Metal complexes of
quinolin-8-yl [(5-methoxy-
1H-benzimidazol-2-
yl)sulfanyl] acetate:
Spectral, XRD, thermal,
DFT studies, cytotoxic,
molecular docking and
biological evaluation



2.1 INTRODUCTION

Benzimidazole derivatives are exciting heterocycles for the reason that they are present in many naturally occurring products and various drugs. They are also essential pharmacophores in contemporary drug discovery and remain the most flexible class of compounds possessing specific pharmacological effects such as antitumor [1-3], antiulcer [4-6], antifungal and antibacterial [7-9], antihelmintic [10], anti-inflammatory [12-14], anticonvulsant [10], anti-tubercular [11], antidepressant [12], antihypertensive [13], anticoagulant [14] and antiviral [15]. Moreover, benzimidazole is of considerable interest as a ligand towards transition metal ions and its presence in a variety of biological molecules such as ion heme systems, vitamin B₁₂ and its derivatives, and numerous metalloproteins. In this context, the complexes of transition metal salts with benzimidazole derivatives were considerably studied as a model structure of some vital organic molecules. Metal complexes of these ligands are very often more active than the uncoordinated ligands [16]. It has been reported that the transition metal complexes with a ligand containing benzimidazole bearing trimethylsilylpropyl and quinoline exhibit high antitumor activity [17-18]. The metal-ligand interaction and the geometry of the transition metal complexes in ligand chelation environment serves as models to enzyme containing metal ion [19].

The present research work focuses on synthesise and characterization of Co(II), Ni(II), Cu(II) and Zn(II) metal complexes derived from 5-methoxy-2-mercaptobenzimidazole and 8-quinolinol(QB), and determination of the cytotoxicity effect with metal complexes on MCF-7 (estrogen receptor-positive human breast cancer) and HeLa(human cervical cancer cell line), in addition to this the molecular docking studies also been performed. The *in vitro* antioxidant scavenging activity and antimicrobial potentials of metal complexes and their uncoordinated ligand also been examined.

Materials and methods

The chemicals 5-methoxy-2-benzimidazolethiol and 8-quinolinol were obtained from Sigma-Aldrich Co. The chlorides of Co(II), Ni(II), Cu(II) and Zn(II) were of

S.R.L. grade. All other reagents and solvents were purchased from commercial sources and were of analytical grade

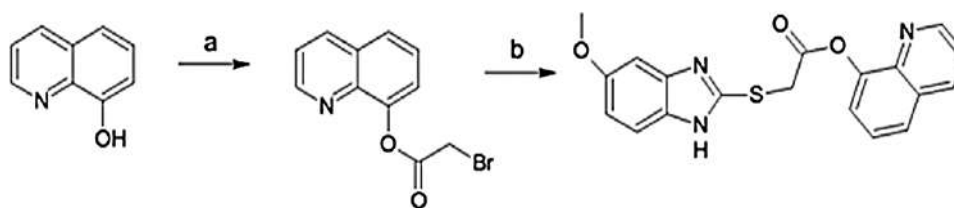
Physical measurements

Melting points had been recorded on an electro-thermal melting factor apparatus and are uncorrected. ^1H NMR spectra were recorded on Bruker four hundred MHz spectrometer at IISc, Bangalore, Karnataka, India. The chemical shifts have been proven in δ values (ppm) with tetramethylsilane(TMS) as an internal standard. LC-MS changed into acquired the usage of a C-18 column on Shimadzu, LCMS 2010A, Japan. The FT-IR spectra of the compounds were taken as KBr pellet (a hundred mg) the usage of Shimadzu Fourier Transform Infrared (FTIR) spectrometer. Magnetic susceptibility have been measured at 35 °C through the Gouy technique, Silica gel GF254 thin plates from Merck were used for TLC and spots were positioned either by UV or dipping in potassium permanganate solution. The powder X-ray studies was carried out by using Rigaku Mini-Flex instrument with $\text{Cu-K}\alpha$ radiation (wavelength 0.154nm), and The thermal gravimetric analysis of all metal complexes were taken by the Diamond TG/DT Analyzer (TG/DTA) at room temperature of 700 °C below heating pace of 20 °C min^{-1} .

2.2. Experimental

2.2.1 Synthesis of ligand Quinolin-8-yl [(5-methoxy-1H-benzimidazol-2-yl)sulfanyl]acetate (QB)

To a stirred solution of quinolin-8-ylbromoacetate (4.2 mmol) and 5-methoxy-2-benzimidazolethiol (4.2mmol) dissolved in anhydrous ethanol and anhydrous K_2CO_3 (30 mL) The mixture was refluxed for about 12 h, after completion of the reaction, the reaction mass was quenched to the cursed ice, the yellow coloured precipitate was collected by filtration and washed with ethanol and recrystallized with methanol by following the literature method [20].



Scheme 1 (a) Bromoacetyl bromide, DMF, TEA, RT 6 h (b) 5-methoxy-2-benzimidazolethiol, K_2CO_3 , EtOH reflux, 8 h.

2.2.2 General procedure for the synthesis of metal complexes $[M(QB)_2Cl_2] \cdot nH_2O$

A hot ethanolic solution of the 0.2 mmol QB was mixed with an ethanolic solution of 0.4 mmol of $MCl_2 \cdot 6H_2O$ ($M = Co, Ni, Cu$ and Zn metal salts). The mixture was stirred for 4 h then the colored solid precipitated was filtered off, washed with cold methanol, the obtained complexes were kept in a vacuum desiccator.

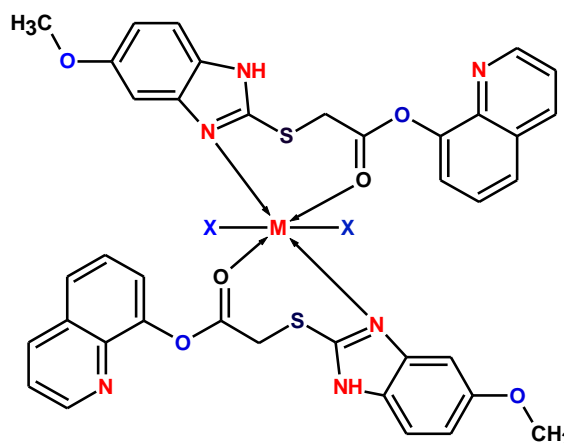


Figure 2.1 Proposed structure of metal complexes $[M = Co(II), Ni(II), Cu(II)$ and $Zn(II)]$

2.3. Results and discussion

The ligand QB was prepared from condensation of 5-methoxy-2-benzimidazolethiol and 8-quinolinol (Scheme 1). The ligand and its metal complexes (**1** to **4**) were found to be stable. The elemental analysis confirmed that all complexes **1** to **4** have 2:1 molar ratio between the ligand and the metal. The elemental analyses of the compounds **1**–**4** were consistent with the calculated results from the empirical formula of each compound represented in table 2.1. The molar

conductivities of 10^{-3} M of the complexes (dissolved in DMF) at room temperature were measured. The results are in the range $15\text{--}24 \text{ } \Omega^{-1}\text{mol}^{-1}\text{cm}^2$ for all the complexes. The slightly higher values observed may be due to partial dissociation of the complexes in DMF solvent [21].

Table 2.1 Analytical and physical properties of QB and their metal complexes

Compounds	Colour	Mol.Wt	Yield (%)	Calcd. (found) (%)			Molar conductance ($\text{ohm}^{-1}\text{cm}^2 \text{mol}^{-1}$)
				C	H	N	
$\text{C}_{19}\text{H}_{15}\text{N}_3\text{O}_3\text{S}$ (QB)	Light yellow	365	70	62.45 (62.52)	4.14 (4.24)	11.50 (11.32)	-
$[\text{CoCl}_2(\text{QB})_2] \cdot 2\text{H}_2\text{O}$ (1)	Dark green	858	65	53.15 (53.45)	3.29 (3.10)	9.79 (9.93)	22
$[\text{NiCl}_2(\text{QB})_2] \cdot 2\text{H}_2\text{O}$ (2)	Light blue	856	60	53.17 (53.30)	3.29 (3.09)	9.12 (8.98)	24
$[\text{CuCl}_2(\text{QB})_2]$ (3)	Light brown	861	63	52.87 (52.59)	3.27 (3.41)	9.74 (9.56)	21
$[\text{ZnCl}_2(\text{QB})_2]$ (4)	Cream	862	65	52.76 (52.96)	3.26 (3.02)	9.71 (9.49)	15

2.3.1 Computations investigation and frontier molecular orbital analysis

The computational calculations of ligand QB performed by Becke's three parameter hybrid exchange functional (B3LYP) with support of chemcraft 1.7 software [22] has been used for visualization of optimized structures (Figure 2.2), selected bond angles, bond length, dihedral angles (Figure 2.3 and table 2.2) and HOMO-LUMO of QB.

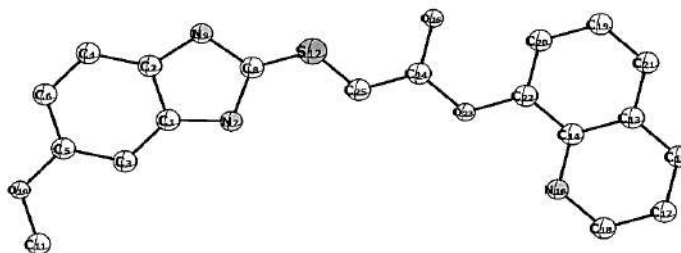


Figure 2.2 Optimized geometry of ligand QB

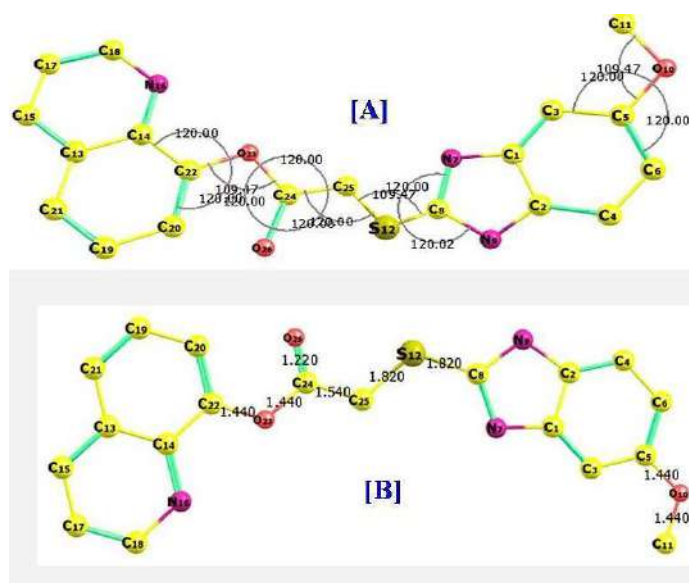


Figure 2.3 Standard bond lengths and bond angles of the ligand QB

Table 2.2 Selected structural parameters of ligand QB

Bond	Bond length (Å)	Angle (°)	(°)	Dihedral angle (°)	(°)
N(9)-H(39)	1.028	C(1)-N(7)-C(8)	104.000	C(1)-N(7)-C(8)	104.000
O(10)-C(11)	1.410	N(7)-C(8)-N(9)	109.421	N(7)-C(8)-N(9)	109.421
C(11)-H(27)	1.122	N(7)-C(8)-S(12)	125.288	N(7)-C(8)-S(12)	125.288
C(11)-H(28)	1.122	N(9)-C(8)-S(12)	125.288	N(9)-C(8)-S(12)	125.288
C(11)-H(29)	1.122	C(2)-N(9)-C(8)	85.177	C(2)-N(9)-C(8)	85.177
S(12)-C(25)	1.790	C(2)-N(9)-H(39)	137.408	C(2)-N(9)-H(39)	137.408
C(13)-C(14)	1.386	C(8)-N(9)-H(39)	137.408	C(8)-N(9)-H(39)	137.408

The HOMO-LUMO gap of organic molecules is important because they transmit to particular movements of electrons and may be most generous for single electron transfer. This is useful for a number of reactions and has vast effects in organic semiconductors, the field where this gap is most vital. It has been found that molecules with large HOMO-LUMO gap are highly stable and unreactive, while

those with small gaps are generally reactive [23]. By calculating the HOMO-LUMO energy gap, one can easily determine the excitation energy of an organic derivative at its ground state [24].

HOMO-LUMO gap of ligand QB are shown in figure 2.4, since in the ligand electronic transition from HOMO orbitals to the LUMO orbitals is $\pi \rightarrow \pi^*$ transitions. Energy separation between the HOMO and LUMO ($\Delta\varepsilon = \varepsilon_{\text{LUMO}} - \varepsilon_{\text{HOMO}}$) of QB is 7.109 eV, $f = 0.0229$, $\langle S^2 \rangle = 0.000$, $90 \rightarrow 92$, -0.11865 .

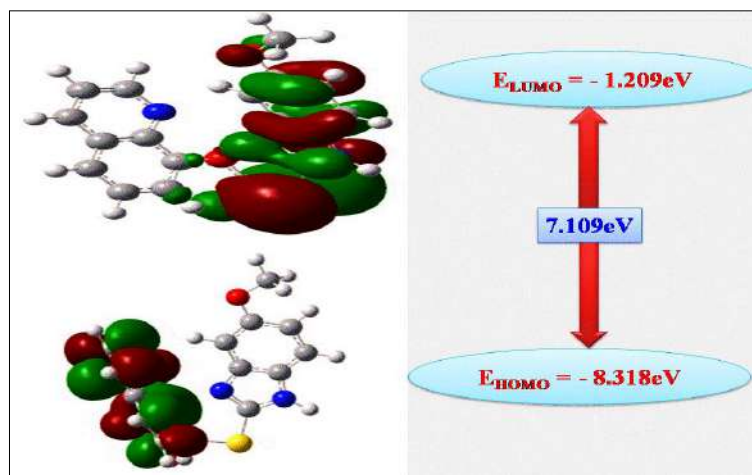


Figure 2.4 HOMO LUMO frontier orbitals of the ligand QB

2.3.2 FT-IR Spectra studies

The infrared spectral data of QB and its metal complexes are presented in Table 2.3. The broad band at the range of 3311 cm^{-1} assigned to $\nu(\text{N-H})$ vibration and $\nu(\text{Ar CH})$ vibrations appeared around 2890 cm^{-1} , and $(-\text{OCH}_3)$ stretching vibrations observed at 2823 cm^{-1} . The band at 1615 cm^{-1} was attributed to $\nu(\text{C=N})$. The ligand showed a sharp band at 1706 cm^{-1} for $\nu(\text{C=O})$ and the position of $\nu(\text{C=O})$ band is shifted to the lower frequencies by towards $1574\text{-}1570 \text{ cm}^{-1}$ in the spectra of the metal complexes, indicating that the coordination occurs through the oxygen atom to the metal ion [25]. The band $\nu(\text{C=N})$ stretching observed around 1578 cm^{-1} which is shifted to lower frequencies in the spectra of all the complexes in the range $1460\text{-}1497 \text{ cm}^{-1}$. Another small band appeared at 753 cm^{-1} , which is assigned to $\nu(\text{C-S-C})$ vibration, is probably due to the coordination properties of the ligand and suggesting the involvement of sulphur atoms in the bonding with the metal ions which is observed around 395 cm^{-1} , 400 cm^{-1} , 390 cm^{-1} and 405 cm^{-1} ,

for $\nu(\text{M-N})$ bonding and followed 545 cm^{-1} , 547 cm^{-1} , 522 cm^{-1} , and 531 cm^{-1} are assigned as $\nu(\text{M-O})$ mode of bonding [26, 27].

Table 2.3 FTIR spectral data (cm^{-1}) of QB and its metal complexes

Compounds	$\nu(\text{N-H})$	$\nu(\text{Ar CH})$	$\nu(\text{C=O})$	$\nu(\text{C=N})$	C-O	M-O	M-N
QB	3311	2890	1706	1578	1263	-	-
1	3343	2901	1573	1497	1266	395	545
2	3373	2895	1570	1460	1264	400	547
3	3376	2948	1574	1493	1270	390	522
4	3375	3050	1573	1497	1266	405	531

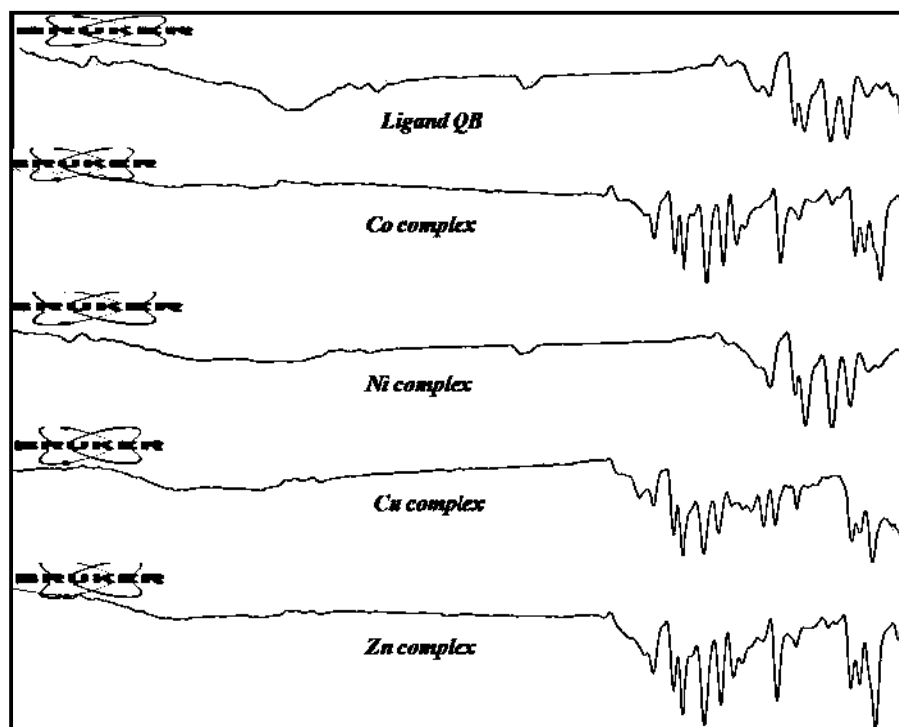


Figure 2.5 IR spectra of QB and its metal complexes

2.3.3 ^1H NMR and ^{13}C NMR Spectra

The ^1H NMR spectra of the compounds were obtained in DMSO-d_6 at room temperature using TMS as an internal standard. The ^1H NMR spectrum of the QB showed a singlet which is attributed to imidazole $-\text{NH}$ at 12.34 ppm , and a multiplet in the range 8.83 to 6.58 ppm for both imidazole and quinolines nuclei protons, the

resonance due to $-\text{CH}_2$ and $-\text{OCH}_3$ protons appeared as doublet and triplet peaks at 3.91 to 3.74 ppm and 3.32 to 2.50 ppm, which reveal the structure of QB and is represented in the figure 2.6. In comparison with QB, the ^1H NMR spectrum of Zn complex is illustrated in figure 2.7, showed that the methoxy and methyl protons signals are shifted to downfield. The aromatic protons resonance from 8.24 to 6.67 ppm as multiplet for imidazole and quinolinol are shifted to slight upper field due to the increased conjugation on coordination. The signal due to $-\text{NH}$ at 12.37 ppm shifted slightly indicating no participation of $-\text{NH}$ group in coordination with metal.

The ^{13}C NMR spectrum of the QB showed a signal at 184.4 ppm which is assigned to the $\text{C}=\text{O}$ and the signals at 115.8 to 138.9 ppm are due aromatic carbons. The peaks at 55.9 and 34.8 ppm are attributed to $-\text{OCH}_3$ and $-\text{CH}_2$ carbons respectively, and a characteristic signal at 156.2 ppm is assigned to the carbon of $\text{C}=\text{N}$ moiety which confirms the structure of the ligand and is represented in figure 2.8.

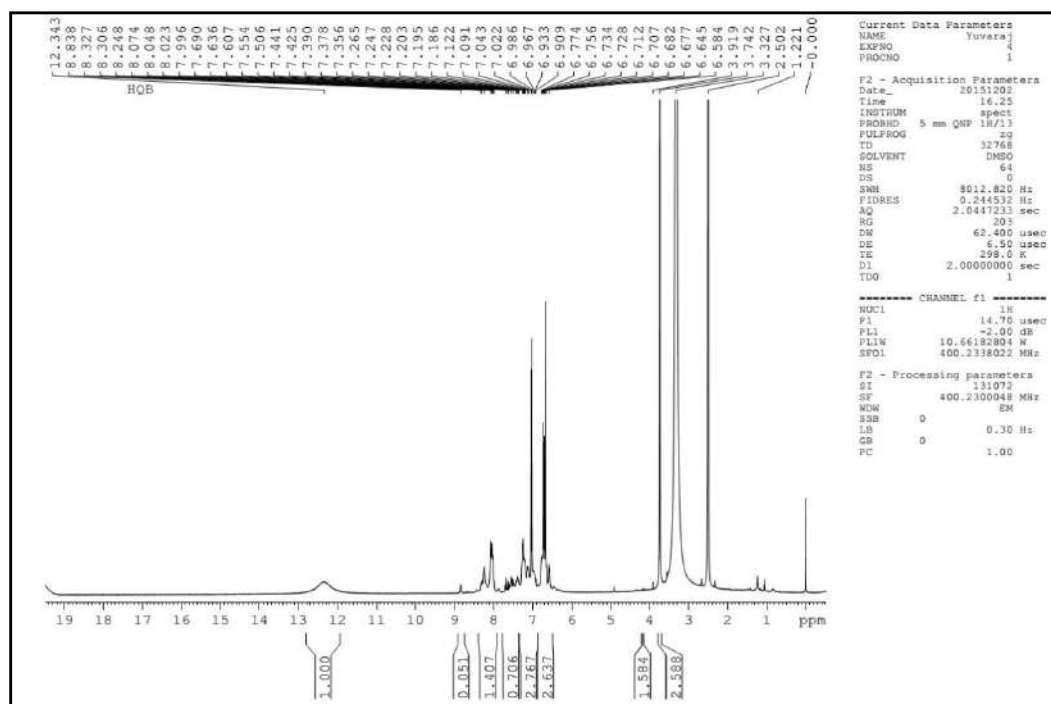
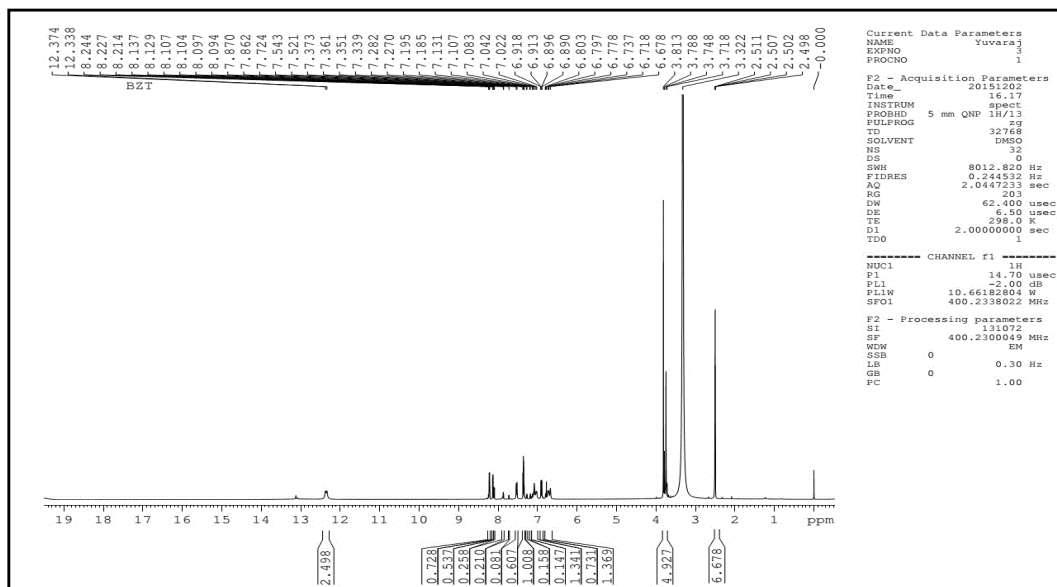
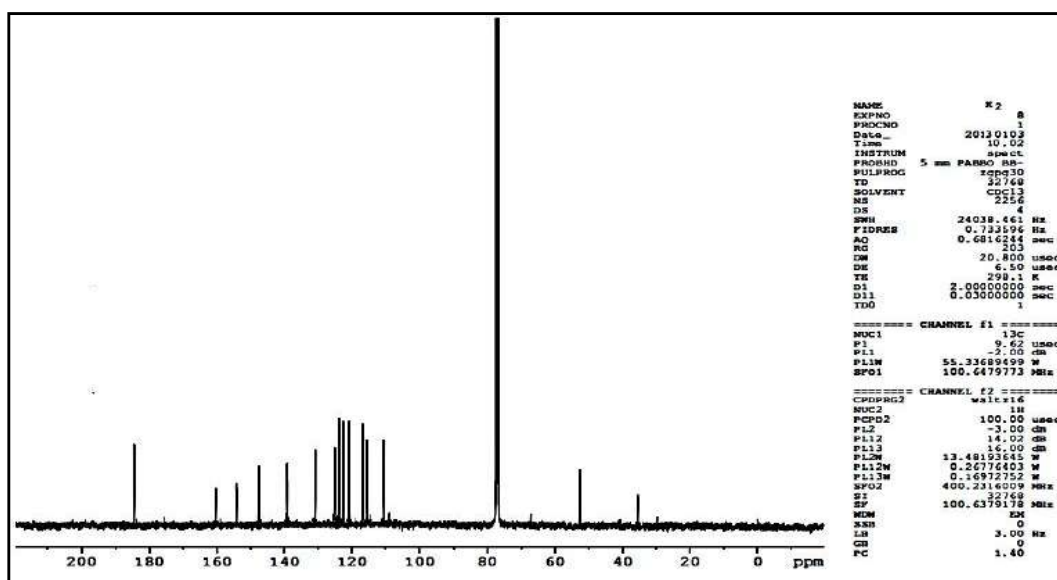


Figure 2.6 ^1H NMR spectrum of QB

Figure 2.7. ^1H NMR spectrum of $[\text{ZnCl}_2(\text{QB})_2]$ Figure 2.8 ^{13}C NMR spectrum of QB

2.3.4 Mass spectral studies

The recorded mass spectra of the QB and Zn complex have been illustrated in figure 2.9 and 2.10. The mass spectrum of the QB confirms the proposed formula and showed well defined molecular ion peak at m/z 366.01(365.25) due to $[\text{M}+1]$. The mass spectrum of the Zn(II) complex showed the molecular ion peak at m/z 863.20 (862.02) which is the evidence that the metal and the ligand are in 1:2 ratio as presented in figure 2.1.

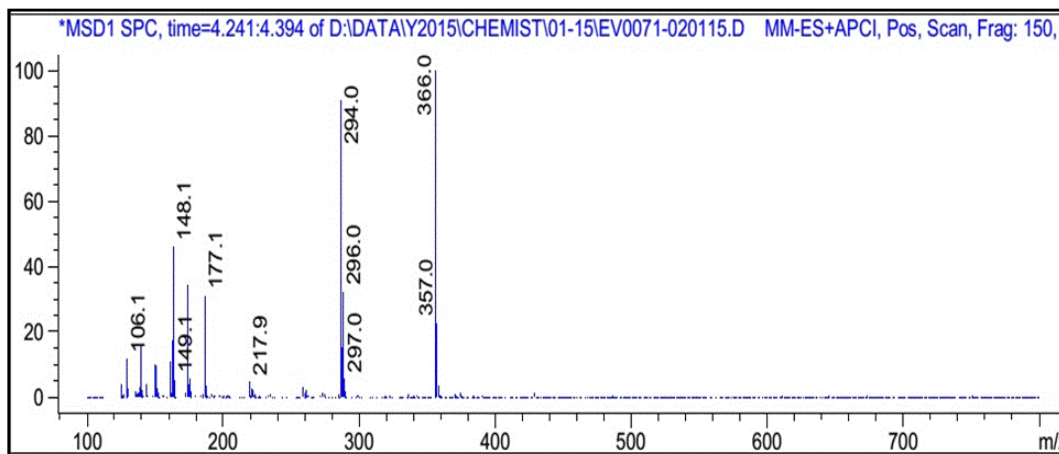
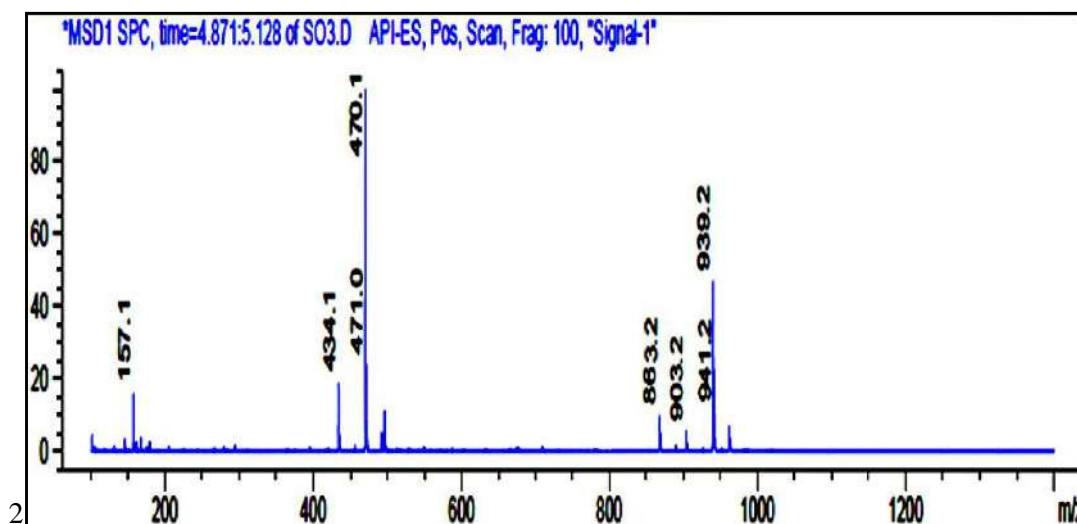


Figure 2.9 Mass spectrum of QB

Figure 2.10 Mass spectrum of $[\text{ZnCl}_2(\text{QB})_2]$

2.3.5 X-ray powder diffraction studies

The powder XRD diffraction is carried out for complexes, Co(II) and Cu(II) which showed prominent sharp peaks while no peaks for the remaining other complexes indicating that their amorphous nature, by evaluating the diffraction patterns of complexes Co(II) and Cu(II) given in figure 2.11 which reveals crystalline nature of the complexes [28, 29].

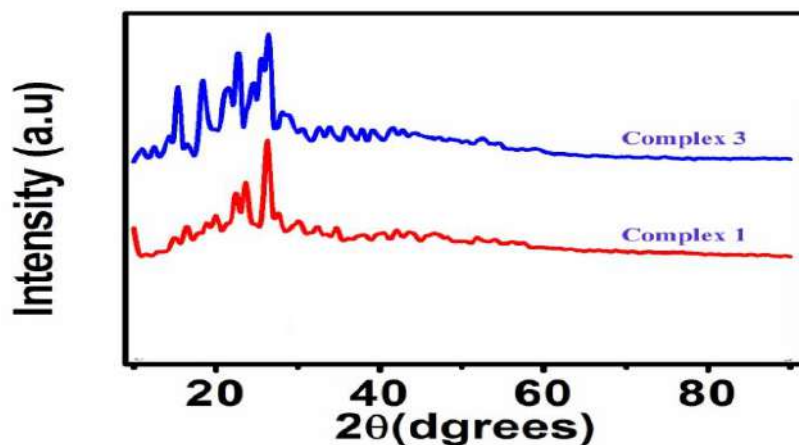


Figure 2.11 XRD Patterns of $[\text{CoCl}_2(\text{QB})_2] \cdot 2\text{H}_2\text{O}$ and $[\text{CuCl}_2(\text{QB})_2]$ Complex

The Miller indices (hkl) along with observed and calculated d angles, 2θ values, and relative intensities are given in tables 2.4 and 2.5. The average crystallite sizes of the complexes d_{XRD} were calculated using Debye Scherrer equation ($D = K\lambda/\beta \cos \theta$) Where D = Particle size, K = Dimensionless shape factor, λ = X-ray wavelength (0.15406 \AA) β = Line broadening at half the maximum intensity, θ = Diffraction angle. Complexes 1 and 3 have a crystallite size of 29.12 and 36.47 nm respectively suggesting that the complexes are in a monoclinic crystalline system.

Table 2.4 XRD data of $[\text{CoCl}_2(\text{QB})_2] \cdot 2\text{H}_2\text{O}$

Peak No	2θ	θ	$\text{Sin}\theta$	h k l	d		Intensity	a in \AA
					Cal	obs		
1	7.636	3.818	0.0665	1 1 0	11.57	11.568	20.9	5.65
2	8.45	4.225	0.0736	1 1 0	10.45	10.443	100	5.65
4	9.72	4.86	0.08472	4 2 0	9.088	9.089	51.9	5.65
5	13.58	6.79	0.1182	4 0 4	6.512	6.512	37.7	5.65
6	21.12	10.56	0.1832	6 6 1	4.203	4.202	16.8	5.65
7	21.90	10.95	0.1899	6 2 7	4.054	4.054	20.4	5.65

Table 2.5 XRD data of [CuCl₂(QB)₂]

Peak No	2θ	θ	Sinθ	h k l	d		Intensity	a in Å
					Cal	obs		
1	8.396	4.198	0.0732	110	10.51	10.52	100	3.62
2	10.528	5.264	0.0917	389	8.396	8.369	57.9	3.62
4	11.303	5.651	0.0984	414	7.825	7.822	71.0	3.62
5	12.833	6.416	0.1117	450	6.89	6.89	70.8	3.62
6	13.325	6.662	0.1160	420	6.63	6.639	56.6	3.62
7	14.707	7.353	0.1278	448	6.02	6.018	52.8	3.62
8	15.575	7.937	0.1380	431	5.57	5.578	57.4	3.62
9	16.845	8.422	0.1464	470	5.25	5.259	58.9	3.62

2.3.6 Electronic spectra and magnetic moment studies

To understand the nature of the M-L bond, the electronic spectra of all the compounds excepting Zn(II) complex were recorded in DMF solution in the range 200–800 nm and the data is presented in table 2.6 and figure 2.12. The Co(II) complex exhibited two absorption bands, in range of 23,094 cm⁻¹ and 20,000 cm⁻¹ are attributed to ⁴T_{1g}(F) → ⁴T_{2g}(F) (ν₁) and ⁴T_{1g}(F) → ⁴T_{1g}(P) (ν₂) transitions respectively. The Co(II) complex showed the magnetic moment of 4.4 B.M, corresponding to octahedral geometry [30]. Ni(II) complex exhibited three absorption bands in the region 14513 cm⁻¹, 21,321 cm⁻¹ and 25,839 cm⁻¹ attributed to the transitions ³A_{2g}(F) → ³T_{2g}(F) (ν₁), ³A_{2g}(F) → ³T_{1g}(F) (ν₂) and ³A_{2g}(F) → ³T_{1g}(P) (ν₃) transitions respectively and the observed magnetic moment was 3.6 B.M. These results suggest the presence of octahedral geometry around Ni(II) complex. In the case of Cu(II) complex, a broad band appeared at 20,883 cm⁻¹ and a weak shoulder at 27,855 cm⁻¹ were interpreted as ²E_g → ²A_{1g} and ²E_g → ²B_{1g} transitions respectively, the magnetic moment was found to be 1.81 B.M. Based on these results the structure of the complex is tentatively proposed to have square planar geometry [31, 32].

Table 2.6 UV-Vis data of QB and its metal complexes

Compound	Electronic transition $\nu(\text{cm}^{-1})$	μ_{eff} (BM)
QB	36764, 31645	-
1	23094, 20000	4.4
2	21321, 14513 and 25839	3.6
3	20883, 27855	1.81

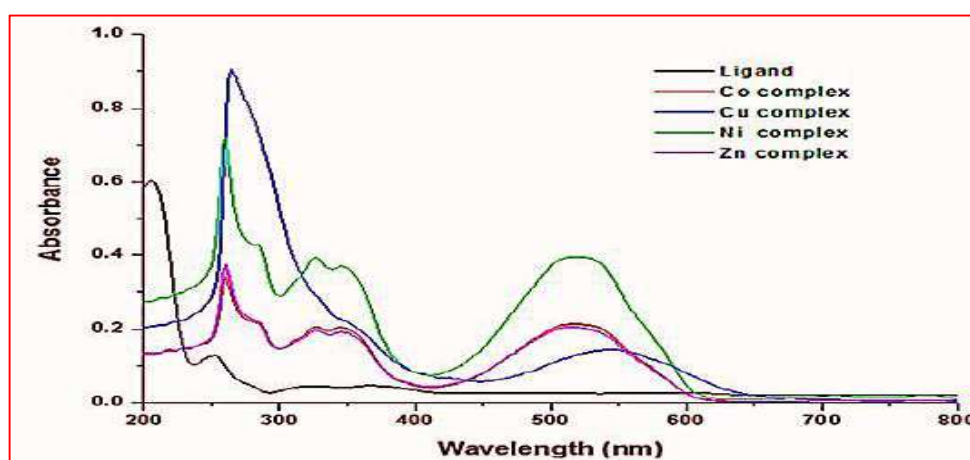


Figure 2.12 Electronic absorption spectra of QB and their metal complexes

2.3.7 Thermal studies

Thermal decomposition of all complexes showed in Figure 2.13. The Co(II) $[\text{Co}(\text{QB})_2\text{Cl}_2] \cdot 2\text{H}_2\text{O}$ decomposed in three stages. First stage resulted in a mass loss of 3.10% (Calc. 3.50%) corresponding to the loss of two lattice water molecules in the temperature range 40–85 °C. The mass loss of 61.05% (Calcd. 63.29%) was observed in second stage corresponding to the loss of coordinated quinoline moiety in the temperature range 213–303 °C. Third stage resulted in mass loss of 26% (Calcd. 27.46%) due to the dissociation of imidazole ring leaving CoO as residue from temperature range 303–652 °C. $[\text{Ni}(\text{QB})_2\text{Cl}_2] \cdot 2\text{H}_2\text{O}$ complex degraded in three steps. First stage involved a weight loss of 3.10% (Calc 3.50%) corresponding to the elimination of two lattice water molecules in the temperature range 90 to 110 °C. The second stage represented weight loss of 62.50 % (calculated 63.30%) which leads to the removal of coordinated sulphur associated imidazole sphere from the

temperature range 110 to 425 °C. Third stage resulted in weight loss (found 25.90% and calculated 27.47%) due to the loss of quinoline moiety from the temperature range 426 to 721°C, the residue was expected as NiO. The disintegration step of [Cu(QB)₂Cl₂] involves in two stages. The first stages occur in temperature range 95–456 °C due to the mass loss of 64.35% (Calcd. 65.29%) corresponding to elimination of imidazole moiety. The second step is in the temperature range 456–610°C resulted a mass loss of 27.65% (Calcd. 28.33%) corresponding to elimination of quinoline ring leaving CuO as the residue.

In the degradation method, kinetic and thermodynamic parameters of the Co(II), Ni(II) and Cu(II) metal complexes has been evaluated by Broido's graphical method for straight line decomposition portion of the thermodynamic analytical curve[33]. Energy of activation (E_a) is calculated by the slope of -ln(ln1/y) versus 1/T X10⁻³. The thermodynamic properties like change in enthalpy (ΔH), entropy(ΔS), free energy (ΔG) and frequency factor (lnA) are calculated using the standard equations by employing the Broido's relation: -ln[ln(1/y)] = E_a/RT_d-lnA-ln(8.314/T_d). Where y is the fraction of the complex undecomposed, T_d is the decomposition temperature, R is the gas constant and E_a is the activation energy in kJ.mol⁻¹.

Table 2.7 Thermal and Kinetic parameters of metal complexes

Compounds	Decomposition temperature [°C]	E _a [kJmol ⁻¹]	Frequency factor lnA [min ⁻¹]	ΔH [kJmol ⁻¹]	ΔS [J/K]	ΔG [kJmol ⁻¹]
[Co(QB) ₂ Cl ₂].2H ₂ O	302.84	20.085	10.869	3.564	-57.814	63.975
	328.98	--	6.7234	5.921	-132.848	43.711
[Ni(QB) ₂ Cl ₂].2H ₂ O	203.08	18.0691	15.271	2.378	-57.814	11.743
	318.32	--	6.7340	6.001	-132.848	43.710
[Cu(QB) ₂ Cl ₂]	278.91	17.092	5.614	2.914	-141.524	38.341
	381.25	--	6.562	13.556	-237.254	91.251

The TGA and kinetic parameters the Co(II), Ni(II) and Cu(II) metal complexes are tabulated in table. 2.7. The major weight loss for all the complexes was found in the temperature range 203.08 – 278.91°C. The Co(II) and Ni(II) complexes showed very high activation energies and rapid degradation of 20.084 and 18.069 kJmol⁻¹, While the Cu(II) complex exhibit higher thermal stability of 17.092 kJmol⁻¹. The negative values of ΔS indicated that the decomposition reactions are slower than the normal. The positive sign of ΔG values for the complexes assign that the free energy of the final residue is higher than that of the initial compound and all the decomposition steps are non-spontaneous processes and represented in figure 2.14.

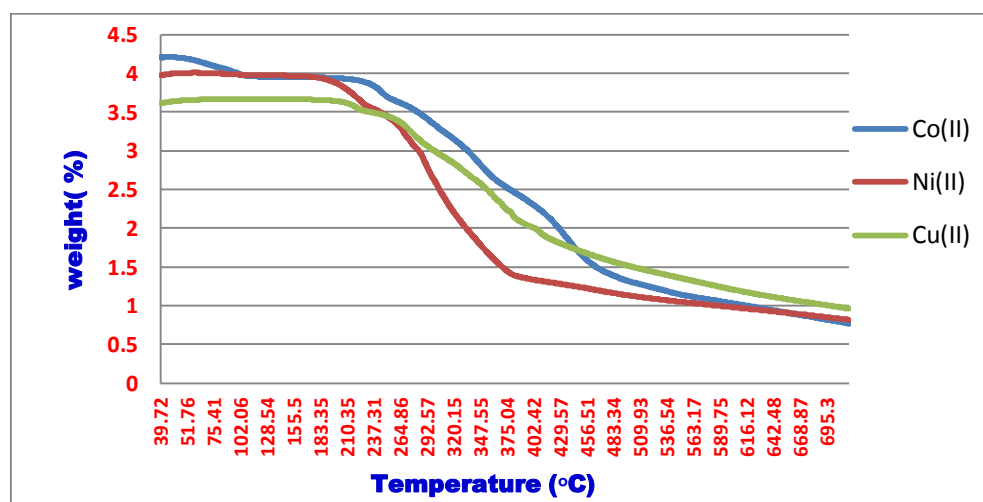
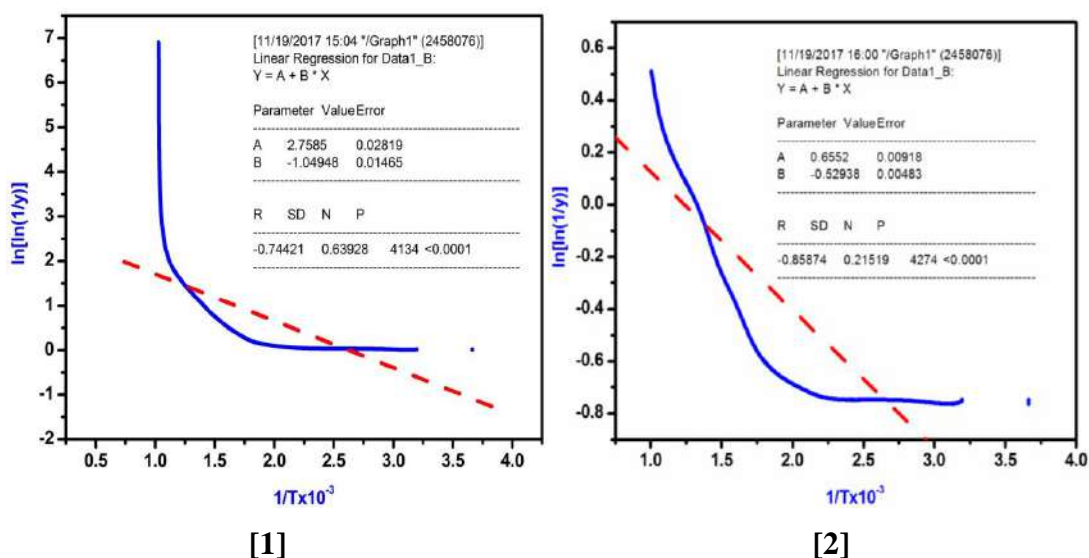
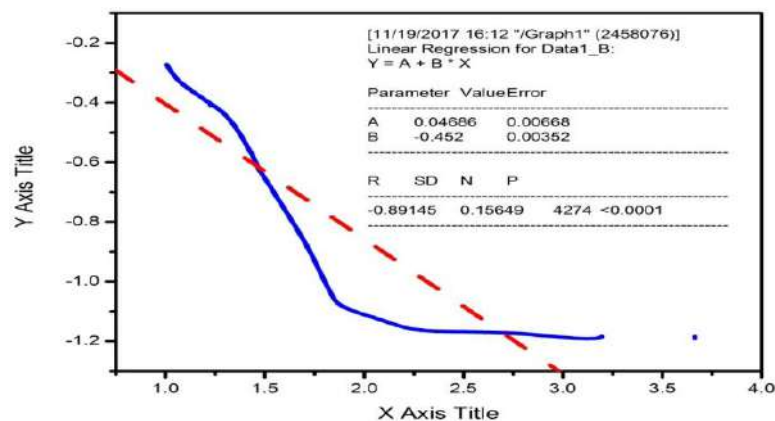


Figure 2.13 TGA and DTA curves of [Co(QB)₂Cl₂].2H₂O, [Ni(QB)₂Cl₂].2H₂O and [Cu(QB)₂Cl₂]





[3]

Figure 2.14 Linear fit graphs of [1] $[\text{Co}(\text{QB})_2\text{Cl}_2]\cdot 2\text{H}_2\text{O}$, [2] $[\text{Ni}(\text{QB})_2\text{Cl}_2]\cdot 2\text{H}_2\text{O}$ and [3] $[\text{Cu}(\text{QB})_2\text{Cl}_2]$

2.4 Procedures for biological evaluation

2.4.1 Cytotoxic activity

The cell lines MCF-7 (a-estrogen receptor-positive human breast cancer cells) and HeLa (b-human cervical cancer cell line) cell lines were obtained from National Centre for Cell Science, Pune. The cells were cultured in monolayers 25 cm 9.25 cm tissue culture flasks containing RPMI 1640 culture medium supplemented with 10 % fetal bovine serum (FBS) and 1 % penicillin. The cytotoxicity was determined using the 3-(4,5-dimethylthiazol-2-yl)-2,5-diphenyltetrazolium bromide (MTT) assay (Sigma) as described by Mosmann(20). Untreated cells were used as standards. Cytotoxicity was expressed as IC_{50} , *i.e.* the concentration of the drug that inhibits the growth of cancer cells by 50 % is compared to the control. Tamoxifen was used as the standard cytotoxic [34].

2.4.2 Molecular docking studies

In order to understand the binding interaction modes of the synthesized compounds in assessment to the competitive cytotoxicity effect, the molecular docking studies had been accomplished by way of the use of HEX 8.2 software [35]. The possible structures for the docking studies of the complexes have been drawn by Chem Sketch and Chem3D Ultra. The PDB format of protein epidermal growth factor receptor (EGFR) tyrosine kinase were retrieved from the RCSB Protein Data Bank (PDB ID: 1M17), The default parameters had been used for the

docking calculation with correlation kind form handiest, Fourier Transform, FFT steric experiment, FFT final search and MM refinement. A greater negative E-total value means that a strong binding interaction exists among drug and receptor which results in the inhibition of receptor activity.

2.4.3 Anti-lipase assay

Method:

Lipase inhibitory activity of different concentrations of methanol extract was tested by mixing 100 μ L of each concentration of methanol extract, 8mL of oil emulsion and 1mL of chicken pancreatic lipase followed by incubation of 60 minutes. The reaction was stopped by adding 1.5 mL of a mixture solution containing acetone and 95% ethanol (1:1). The liberated fatty acids were determined by titrating the solution against 0.02M NaOH (standardized by 0.01M oxalic acid) using phenolphthalein as an indicator.

The percentage inhibition of lipase activity was calculated using the formula: Lipase inhibition = $A - B/A \times 100$, where A is lipase activity, B is activity of lipase when incubated with the sample.

2.4.4 Antioxidant activity

The scavenging activity for the synthesized compounds by using DPPH method as per literature [36].The compounds of different concentrations (20–100 μ g/cm³)are dissolved in methanol and were introduced to each vials of 4 mL. To this test vials 3 mL of 0.004 % DPPH in methanol was added and the mixture have been incubated at ambient temperature for 30 min. Ascorbic acid is used as the standard. The absorbance reduced while the DPPH is scavenged by way of an antioxidant, through contribution of hydrogen to shape a strong DPPH molecule. DPPH scavenging activity calculated by the use of the following equation and the absorbance measured at 517 nm.

$$\text{Scavenging ratio (\%)} = [(A_i - A_o) / (A_c - A_o)] \times 100\%$$

Where A_i is the absorbance within the presence of the check compound; A_o is absorbance of the clean inside the absence of the check compound; A_c is the absorbance within the absence of the test compound.

2.4.5 In vitro antimicrobial activity

All the synthesized compounds were examined for their antimicrobial activity towards three bacterial and fungal strains using agar well diffusion method [37, 38]. All bacterial traces were maintained on nutrient agar medium at ± 37 °C and fungal strains were maintained on potato dextrose agar (PDA) at ± 25 °C. The test compounds had been dissolved in DMSO to get a concentration of 0.5 and 1 mg/mL. Sample-loaded plates were inoculated with the microorganism incubated at 37 °C for 24 h and culture was incubated at 25 °C for 60 h. Ciprofloxacin of 0.5 mg/mL and fluconazole of 0.5 mg/mL had been used as popular drugs for antibacterial and antifungal inhibition. The minimal concentration required for major boom of fungi was seemed as minimal inhibitory concentration (MIC). It was achieved by means of serial broth-dilution approach at distinctive concentrations like 1, 10, 25, 50 and 100 $\mu\text{g/mL}$. After the incubation time, the minimum inhibitory zone at which the microorganism increase became inhibited was measured in millimetres.

2.5 Results and discussion of biological evaluation

2.5.1 Cytotoxic activity

The complexes, Co(II), Ni(II) and Cu(II) are potent against both MCF-7 (estrogen receptor-positive human breast cancer) and HeLa (human cervical cancer cell line). IC_{50} values of the complex, Cu(II) against MCF-7 are slightly nearer to the standard Tamoxifen, while the complexes of Co(II) and Ni(II) showed appreciable cytotoxic effects towards HeLa. The QB and Zn(II) complex showed moderate activity towards the MCF-7 cells, while they were inactive towards HeLa. Complexation of QB to Co(II), Ni(II) and Cu(II) resulted in more cytotoxic effects, due to the presence imidazole nuclei in the ligand [39, 40], which is slightly more cytotoxic than the other complexes. Both QB and Zn(II) complex, were inactive against both breast cancer cell lines. The results of cytotoxic activity are given in table 2.8 and comparison of the activity is shown in figure 2.15.

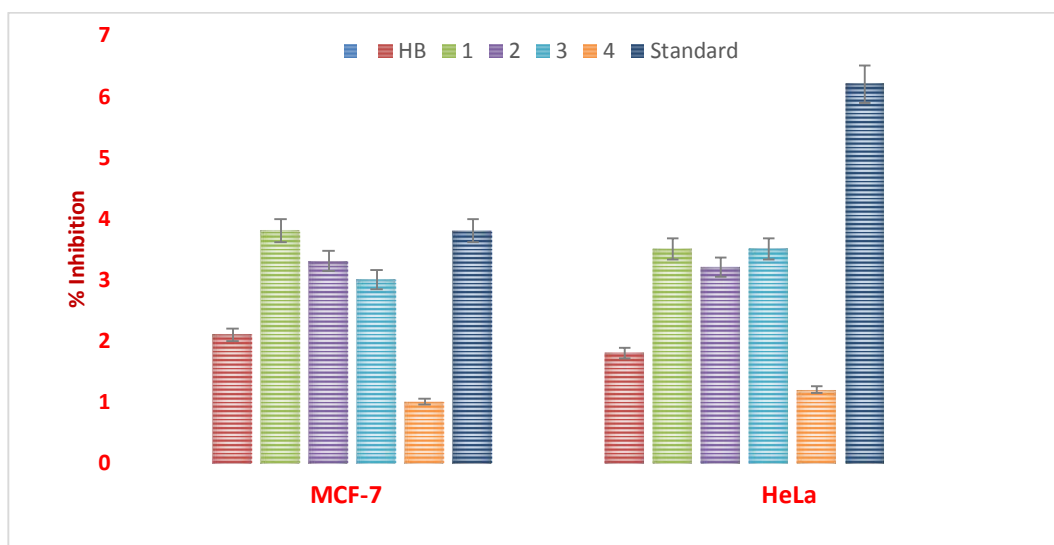


Figure 2.15 Comparison of cytotoxic (%) inhibition of QB and their metal complexes

Table 2.8 Cytotoxic potency (IC_{50} , μM) of the ligand and their metal complexes

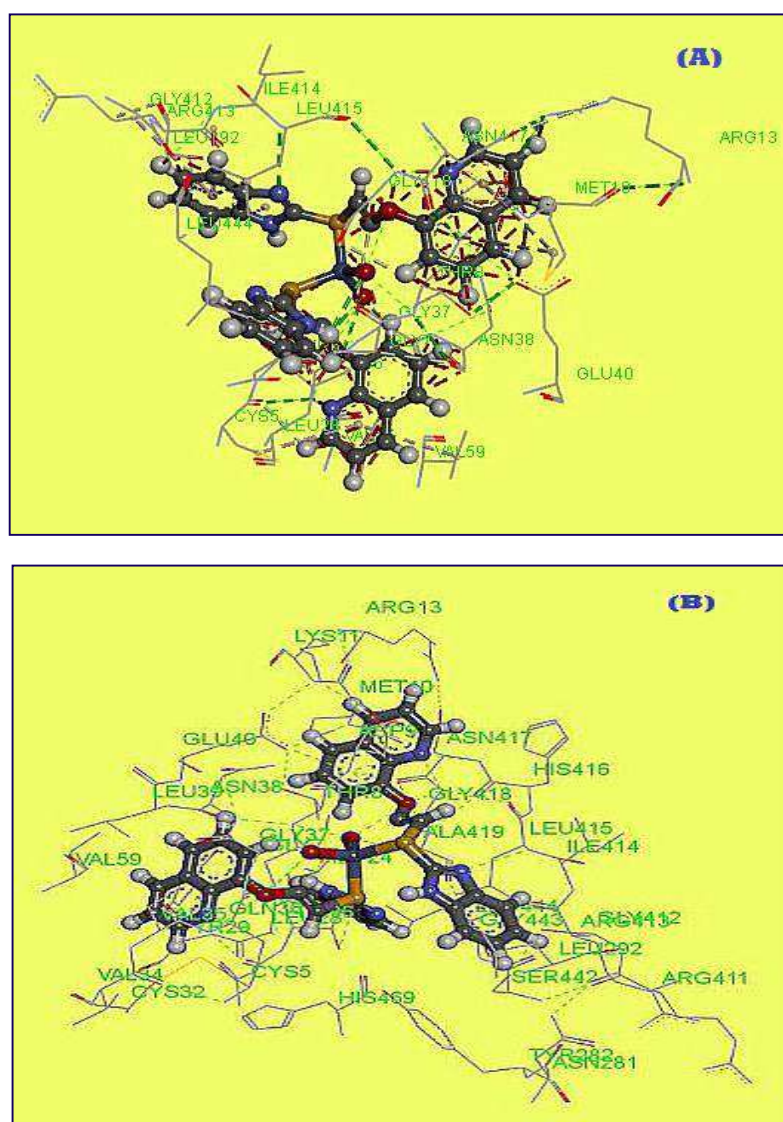
Compound names	MCF-7 ^a	HeL ^b
HB	1.20	>3.0
1	0.18	0.40
2	0.15	0.35
3	0.20	0.39
4	>4.0	>5.0
Standard	3.8	6.2

* IC_{50} is the inhibitory concentration at 50 %, i.e. the concentration of drug that inhibits the growth of cancer cells by 50 %. IC_{50} values $<0.5 \mu M$ indicate that the complex is potent, whereas IC_{50} scores of $0.5-5.0$ and $>5.0 \mu M$ indicate that the compound is moderately active and inactive respectively.

2.5.2 Molecular docking studies

Epidermal Growth Factor Receptor (EGFR) which is a tyrosine kinase receptor is an attractive tumour receptor for therapeutic interference due to its critical role of aberrant signalling in cancer cells [41]. The exceptional affinity modes of the docked compounds 2, 3, and 4 with EGFR tyrosine kinase is

represented in figure 2.16. The compounds Co(II), Ni(II) and Cu(II) showed docking score of -278.52, -265.33 and -244.96 kJmol⁻¹, respectively, exhibit good *in vitro* anticancer activity. All the docked compounds were analysed for various types of interactions like, hydrophobic bonding and Vander Waals interaction because, no compound was found to exhibit hydrogen bonding with the receptor [38, 39]. However, the QB and Zn(II) complex exhibited lower docking scores of -198.25 and 205.32 kJmol⁻¹ respectively. the hydrophobic pocket formed by amino acid residues Ala419, ThrR6, Tyr29 and Tyr420, Leu415, Cys32, Tyr29, Cys5, and Leu28, Val35, Glu40, Ala419, and Thr8. The obtained results showed a good correlation between the compounds and EGF receptor.



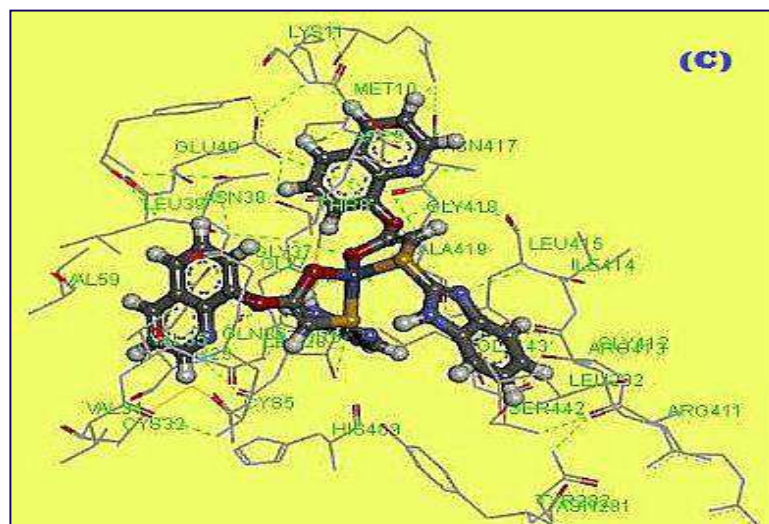


Figure 2.16 3D representation of (A) complex 1 (B) complex 2 and (C) complex 3 with epidermal growth factor receptor (EGFR) tyrosine kinase

2.5.3 Anti-lipase assay

All the compounds were evaluated with regard to pancreatic lipase activity and the data represented in table 2.9, among these, the ligand QB, Co(II) and Zn(II) complexes have no significant inhibitory effect, while the Ni(II) and Cu(II) complexes exhibits best anti-lipase activity [42-44]. It is noticed that, the order of inhibitory strength of the metal complexes towards the pancreatic lipase is Ni(II)>Cu(II)>QB>Co(II)>Zn(II) and they have the IC₅₀ values 0.26, 0.26, 1.24, 1.46, 1.81 μg/mL respectively, due to the conjugation of imidazole and quinoline ring at the ligand and their metal complexes showed higher activity when compared to the standard.

Table 2.9 Anti-lipase activity of ligand and their metal complexes

Compounds	% inhibition	IC ₅₀ (μg/mL)
QB	28.21	1.24
1	30.56	1.46
2	65.44	0.26
3	66.87	0.26
4C	30.77	1.81

2.5.4 Antioxidant activity

DPPH radical scavenging activity data represented in figure 2.17, it is showed that, due to the generation of DPPH free radical [45, 46]. It exhibits the absorption maximum at 517 nm. The results indicating that the complexes showed enhanced free radical scavenging effect, but lower when compared to ascorbic acid (vitamin C), a standard. The complex **3** exhibited highly potent scavenging activity almost close to the standard Vitamin C and complex **1** and **2** showed better inhibitions against free radical and the compounds QB and **4** showed moderate activity.

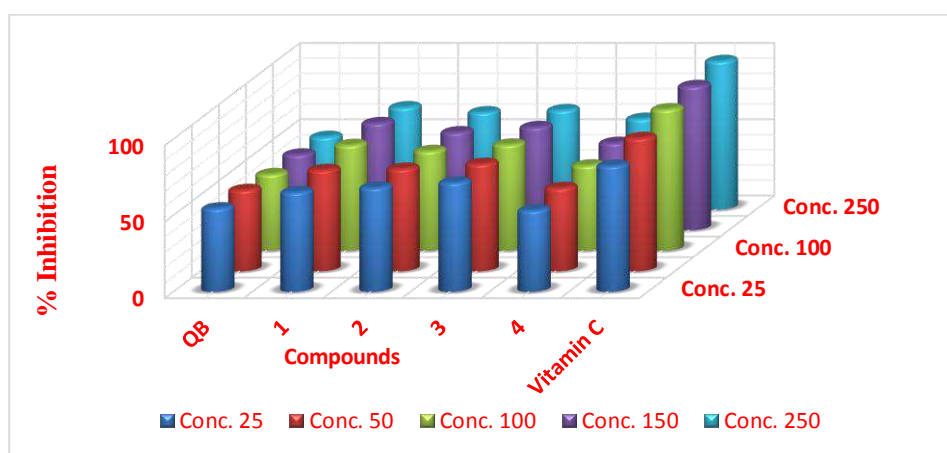


Figure 2.17 DPPH scavenging activity of QB and their metal complexes

2.5.5 In vitro antimicrobial activity

The antimicrobial activity results in two different concentrations of all synthesized QB and its metal complexes are collected in tables 2.10 and 2.11. The results revealed that the primary screening against the bacterial strains and fungal strains with different concentrations showed good zone of inhibition. The compounds **1**, **2** and **3** exhibited the highest antimicrobial activity against *Pseudomonas aeruginosa*, *Bacillus subtilis*, *Salmonella typhi* and *Aspergillus flavus*, and *Candida albicans*. The compound **QB** and the complex **4** showed the least activity against both bacterial and fungal strains. While the other complexes exhibit potent activity against tested fungal and bacterial strains at MIC values in different concentrations that are 1, 10, 25, 50, and 100 $\mu\text{g/mL}$. Against *Aspergillus flavus* and *Candida albicans*. The compounds **1**, **2** and **3** shows potential MIC values. The reason is that they have benzimidazole moiety in the **QB** [47, 48].

Table 2.10 Antimicrobial activity data of QB and their metal complexes

Compounds	Conc.m g/mL	Zone of inhibition in mm (mean \pm SD)				
		Antibacterial strains			Antifungal strains	
		P.aeruginosa \pm SD	B.subtilis \pm SD	S.typhi \pm SD	A.flavus \pm SD	C.albicans \pm SD
QB	1	10 \pm 0.2	10 \pm 0.1	11 \pm 0.3	08 \pm 0.3	08 \pm 0.3
	0.5	07 \pm 0.3	08 \pm 0.2	09 \pm 0.7	06 \pm 0.1	06 \pm 0.3
Co(II) -1	1	17\pm0.2	16\pm0.1	19\pm0.3	18\pm0.3	20\pm0.3
	0.5	07\pm0.3	08\pm0.2	09\pm0.1	10\pm0.2	08\pm0.3
Ni(II) -2	1	17\pm0.5	18\pm0.1	13\pm0.3	18\pm0.3	15\pm0.3
	0.5	11\pm0.8	07\pm0.6	07\pm0.3	11\pm0.5	12\pm0.4
Cu(II) -3	1	16\pm0.2	17\pm0.1	15\pm0.3	18\pm0.3	19\pm0.3
	0.5	10\pm0.5	08\pm0.2	07\pm0.4	14\pm0.1	12\pm0.3
Zn(II) -4	1	10 \pm 0.2	12 \pm 0.1	10 \pm 0.3	10 \pm 0.3	08 \pm 0.2
	0.5	08 \pm 0.3	08 \pm 0.3	09 \pm 0.1	06 \pm 0.2	06 \pm 0.3
Ciprofloxacin	1	18 \pm 0.40	20 \pm 0.3	22 \pm 0.4	-	-
	0.5	12 \pm 0.2	10 \pm 0.3	08 \pm 0.4	-	-
Fluconazole	1	-	-	-	20\pm0.1	22\pm0.3
	0.5	-	-	-	17\pm0.6	15\pm0.5

Table 2.11 MIC data of QB and metal their complexes

Compounds	Minimum inhibitory concentration (MIC μ g/mL)				
	P.aeruginosa	B.subtilis	S.typhi	A.flavus	C.albicans
QB	10.75	10.70	09.35	13.55	08.58
Co(II) -1	14.75	12.12	10.35	11.55	09.12
Ni(II) -2	15.24	13.11	10.10	13.55	09.25
Cu(II) -3	14.75	12.62	10.64	14.21	-
Zn(II) -4	11.75	08.11	08.24	10.55	07.55
Ciprofloxacin	15.75	13.70	12.35	-	-
Fluconazole	-	-	-	14.75	10.70

2.6 Conclusions

The complexes **1**, **2**, **3** and **4** has been derived from quinolin-8-yl [(5-methoxy-1H-benzimidazol-2-yl)sulfanyl]acetate the compounds were characterized by different spectral methods. The spectral data reveal that the metal ions coordinated through the thiol group and carbonyl oxygen atom which suggest that the bidentate nature. The XRD data of Co(II) and Cu(II) complexes reveals the nanocrystalline phase, The correlation of the experimental data allows assigning a octahedral geometry for Co(II) and Ni(II), complexes and square planar for Cu(II) complex, The theoretical study using DFT/B3LYP supports experimental evidences of the bonding sites of the ligand, geometry and the stability of the complexes. The cytotoxic activities were evaluated on two different cancerous cell lines in which the compounds **1**, **2** and **3** shows highly potent activity against MCF-7 (oestrogen receptor-positive human breast cancer) HeLa (human cervical cancer cell line) by MTT assay. Molecular docking studies reveal that the compounds **2**, **3** and **4** have comparatively least binding scores as compared to the EGFR tyrosine kinase receptor and may be considered as a potent cytotoxic agent. The complexes showed significant antioxidant activity compared to uncoordinated ligand, and among the studied complexes, the complex **3** exhibited promising antioxidant activity. In addition to this, the antimicrobial activity showed enhanced inhibition results for the compounds **1**, **2** and **4** against bacterial and fungal strains.

References

- [1] W.A Denny, G.W Rewcastle, B.C Baguley, Potential antitumor agents. 59. Structure-activity relationships for 2-phenylbenzimidazole-4-carboxamides, a new class of "minimal" DNA-intercalating agents which may not act via topoisomerase II, *J. Med Chem*, 33, 1990, 814–9.
- [2] S. Demirayak, U. Abu Mohsen, A. CagriKaraburun, Synthesis and anticancer and anti-HIV testing of some pyrazino[1,2-*a*]benzimidazole derivatives, *Eur J Med Chem*, 37, 2002, 255–60.
- [3] P. Sharma, R. Sharma, R. Tyagi, Inhibitors of cyclin dependent kinases: useful targets for cancer treatment, *Cur Cancer Drug Target*, 1, 2008, 53–75.
- [4] D. Carcanague, Y.K Shue, M.A Wuonola, M. Uria-Nickelsen, Novel structures derived from 2-[(2-pyridyl)methyl]thio]-1H-benzimidazole as anti-*Helicobacter pylori* agents, Part 2, C. Joubbran, J.K Abedi, *J Med Chem*, 45, 2002, 4300–9.
- [5] P. Lindberg, P. Nordberg, T. Alminger, The mechanism of action of the gastric acid secretion inhibitor omeprazole, A. Braendstroem, B. Wallmark, *J med chem*, 29, 1986, 1327–1329.
- [6] H. Kucukbay, B. Durmaz, Antifungal activity of organic and organometallic derivatives of benzimidazole and benzothiazole, *Arzneimittel forschung*, 47, 1997, 667–70.
- [7] D. Olender, J. Zwawiak, V. Lukianchuk, R. Lesyk, A, Kropacz, A. Fojutowski, Synthesis of some N-substituted nitroimidazole derivatives as potential antioxidant and antifungal agents, *Eur J Med Chem*, 44, 2009, 645–52.
- [8] G. Krishnamurthy, Synthesis and thermal degradation kinetics of some Cobalt (II) Complexes with 1,2-disubstituted benzimidazoles, *Journal. Teach. Research*, 17(1), 2010, 38-43.
- [9] G. Krishnamurthy, Shashikala N. Narashhimiah, Complexes of zinc(II) with 1,2-disubstituted Benzimidazoles, *Journal of chemical Research*, 2006, 766-768.

- [10] T. Fekner, J. Gallucci, M.K Chan, Ruffling-induced chirality: synthesis, metalation, and optical resolution of highly nonplanar, cyclic, benzimidazole-based ligands, *J American Chem Soc*, 126, 2004, 223–36.
- [11] H. Küçükbay, E. Cetinkaya, R. Durmaz, Synthesis and antimicrobial activity of substituted benzimidazole, benzothiazole and imidazole derivatives, *Arzneimittel forschung*, 45, 1995, 1331–4.
- [12] R. Durmaz, M. Köroğlu, H. Küçükbay, I. Temel, M.K Ozer, M. Refiq, Investigation of serum minimal inhibitory concentrations of some benzimidazole, imidazole and benzothiazole derivatives and their effects on liver and renal functions, *Arzneimittel forschung*, 48, 1998, 1179–84.
- [13] H. Zarrinmayeh, A.M Nunes, P.L Ornstein, D.M Zimmerman, M.B Arnold, D.A Schober, Synthesis and evaluation of a series of novel 2-[(4-chlorophenoxy)methyl]benzimidazoles as selective neuropeptide Y-Y1 receptor antagonists, *J Med Chem*, 41, 1998, 2709–19.
- [14] F. Hadizadeh, H. Hosseinzadeh, V. MotamedShariaty, M.S, Seifi, Kazemi, Synthesis and Antidepressant Activity of N-Substituted Imidazole-5-Carboxamides in Forced Swimming Test Model, *Ira J Pharm Res*, 7, 2010, 29–33.
- [15] G. Krishnamurthy, N. Shashikala, Synthesis of Ruthenium(II) Carbonyl Complexes with 2-Monosubstituted and 1,2-Diisubstituted Benzimidazoles, *Journal of Serb. Chem. Soc*, 74(10), 2009, 1085-1096.
- [16] P. Naik, P. Murumkar, R. Giridhar, M.R Yadav, Angiotensin II receptor type 1 (AT1) selective nonpeptidic antagonists--a perspective, *Bioorg & Med Chem*, 18, 2010, 8418–56.
- [17] K. Kubo, Y. Inada, Y. Kohara, Y. Sugiura, M. Ojima, K. Itoh, Nonpeptide angiotensin II receptor antagonists. Synthesis and biological activity of benzimidazoles, *J Med Chem*, 36, 1993, 1772–84.

- [18] N.H Hael, H. Nar, H. Priepke, U. Ries, J.M Stassen, W. Wiene, Structure-based design of novel potent nonpeptide thrombin inhibitors, *J Med Chem*, 45, 2002, 1757–66.
- [19] A.R Porcari, R.V Devivar, L.S Kucera, J.C Drach, L.B Townsend, Design, synthesis, and antiviral evaluations of 1-(substituted benzyl)-2-substituted-5,6-dichlorobenzimidazoles as nonnucleoside analogues of 2,5,6-trichloro-1-(beta-D-ribofuranosyl)benzimidazole, *J Med Chem*, 41, 1998, 1252–62.
- [20] S. Nithyanandan and P. Kannan, Photo Switchable pendant furyl and thienyl-fulgimides containing polypyrroles, *Polym Degrad Stab*, 98, 2013, 2224-2231.
- [21] Z. Zhou, R.G. Parr, Activation hardness: new index for describing the orientation of electrophilic aromatic substitution *J. Am. Chem. Soc.* 112, 1990, 5720-5724.
- [22] S. Praveen, M.A. Al-Alshaikh, C.Y. Panicker, A.A. El-Emam, V.V. Salian, B. Narayana, B.K. Sarojini, C.V. Alsenoy, Structural, thermal, linear and nonlinear optical studies of an organic optical limiter based on reverse saturable absorption, *J. Mol. Struct.* 1120, 2016, 317-326.
- [23] T. Roth, M.L Morningstar, P.L Boyer, S.H Hughes, R.W Buckheit, C.J Michejda, Synthesis and Biological Activity of Novel Non-nucleoside Inhibitors of HIV-1 Reverse Transcriptase. 2-Aryl-Substituted Benzimidazoles, *J Med Chem*, 40, 1997, 4199–207.
- [24] J. Pandey, V.K Tiwari, S.S Verma, V. Chaturvedi, S. Bhatnagar, S. Sinha, Synthesis and antitubercular screening of imidazole derivatives, *Eur J of Med Chem*, 44, 2009, 3350–5.
- [25] J. Singh, P. Grover, D.P Pathak, Synthesis, anticonvulsant activity and comparative QSAR study of some novel 1, 2, 5-trisubstituted benzimidazole derivatives, *Acta Pharm Scie*, 52, 2010, 511–522.

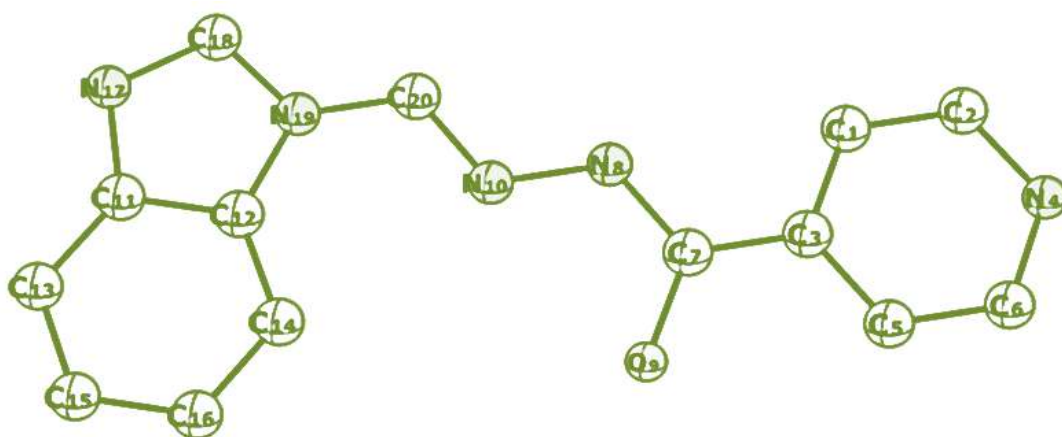
- [26] O.A El-Gammal, M.M Mostafa, Synthesis, characterization, molecular modeling and antioxidant activity of Girard's T thiosemicarbazide and its complexes with some transition metal ions, *Spectro chimica Acta Part A: Mol and Biomol Spect*, 127, 2014, 530–542.
- [27] S. Bhimagouda Patil, G. Krishnamurthy, H.S. Bhojya Naik, R. Prashant Latthe, Manjunath Ghate, Synthesis, characterization and antimicrobial studies of 2-(4-methoxy-phenyl)-5-methyl-4-(2-arylsulfanyl-ethyl)-2,4-dihydro-[1,2,4]triazolo-3-ones and their corresponding sulfones, *Eur J Med Chem*, 45, 2010, 3329-3334.
- [28] Subba Poojari, P. Parameswar Naik, G. Krishnamurthy, One-pot synthesis of thieno [2,3-d] pyrimidin-4-ol derivatives mediated by polyphosphonic anhydride, *Tetrahedron Letters*, 53, 2012, 4639-4643.
- [29] K. Nakamoto, *Infrared and Raman Spectra of Inorganic and Coordination Compounds: Part A: Theory and Applications in Inorganic Chemistry*, Sixth ed., John Wiley & Sons, Ltd, 2006.
- [30] D. N Sathyanarayana, *Vibrational Spectroscopy: Theory and Applications*, New Age International publications, 1996.
- [31] K.R. Sangeetha Gowda, H.S. Bhojya Naik, B. Vinay Kumar, C.N. Sudhamani, H.V. Sudeep T.R. Ravikumar Naik G. Krishnamurthy, Synthesis, antimicrobial, DNA-binding and photonuclease studies of Cobalt (III) and Nickel(II) Schiff base complexes, *Spectrochimica Acta Part A: Mol and Bio-mol Spect*, 105, 2013, 229–237.
- [32] Mustafa bal, Gokhanceyhan, Barısavar, Muhammetkose, Ahmet kayraldiz, Mukerrem kurtoglu, Synthesis and X-ray powder diffraction, electrochemical, and genotoxic properties of a new azo-Schiff base and its metal complexes, *Turk J Chem*, 38, 2014, 22 –241.

- [33] M.L. Sundararajan T. Jeyakumar J. Anandakumaran B. Karpanai Selvan, Synthesis of metal complexes involving Schiff base ligand with methylene dioxy moiety: Spectral, thermal, XRD and antimicrobial studies. *Spectrochimica Acta Part A: Molecular and Biomolecular Spectroscopy* 131, 2014, 82–93.
- [34] M.A Alaghaz, B.A. El-Sayed, A.A. El-Henawy, R.A.A Ammar, Synthesis, spectroscopic characterization, potentiometric studies, cytotoxic studies and molecular docking studies of DNA binding of transition metal complexes with 1,1-diaminopropane-Schiff base, *J. Mol Stru* 1035, 2013, 83-93.
- [35] B. Sreekanth, G. Krishnamurthy, H. S. Bhojya Naik, T. K. Vishnuvardhan, Cu(II) and Mn(II) Complexes Containing Macroacyclic Ligand: Synthesis, DNA Binding, and Cleavage Studies, *Nucleosides, Nucleotides and Nucleic Acids*, 31, 2012, 1-13.
- [36] J. Joseph, B. H. Mehta, Synthesis, characterization, and thermal analysis of transition metal complexes of polydentate ONO donor Schiff base ligand, *Russ J Coordination Chem*, 33, 2007, 124-129.
- [37] B.N. Bessy Raj, M.R. Prathapa chandra Kurup, E. Suresh, Synthesis, spectral characterization and crytal structure of N-2-hydroxy-4-nitrobenzoyl hydrazone and its square planar Cu(II) complex *Spectrochim. Acta A* 71, 2008, 1253.
- [38] H.B. El-Nassan, Synthesis antitumor activity and SAR study of novel [1 2 4] triazino [4,5-a] benzimidazole derivatives, *Eur. J. Med. Chem.* 53, 2012, 22-27.
- [39] D.W. Ritchie, Evaluation of protein docking predictions using Hex 3.1 in CAPRI Rounds 1 and 2, *Proteins*, 2003, 98-106.
- [40] B. Caliskan-Ergun, M. sukuroglu, T. Coban, E. Banoglu, S. Suzen, Screening and evaluation of antioxidant activity of some pyridazine derivatives, *J. Enzyme Inhib. Med. Chem.* 23, 2008, 225-229.
- [41] National Committee for Clinical Laboratory Standards (NCCLS). Performance standard for antimicrobial disc susceptibility test. Approved standard 7th ed. M2-A7 NCCLS document, Wayne Pa, 2000.

- [42] B. Garudachari, M.N. Satyanarayana, B. Thippeswamy, C.K. Shivakumar, K.N. Shivananda, G. Hegde, A.M. Isloor, Synthesis characterization and antimicrobial studies of some new quinoline incorporated benzimidazole derivatives, *Eur. J. Med. Chem.* 54, 2012, 900-906.
- [43] D. Seenaiiah, P. Ramachandra Reddy, G. Mallikarjuna Reddy, A. Padmaja, V. Padmavathi, N. Siva krishna, Synthesis, antimicrobial and cytotoxic activities of pyrimidinylbenzoxazole, benzothiazole and benzimidazole, *Eur. J. Med. Chem.* 77, 2014, 1-7.
- [44] M.A. Omar, Y.M. Shaker, S.A. Galal, M.M. Ali, S.M. Kerwin, J. Li, H.I. El Diwani, Synthesis and docking studies of novel antitumor, benzimidazoles, *Bioorg. Med. Chem.* 20, 2012, 6989-7001.
- [45] A .Hall, D. Parsonage, L .B Poole and P .A Karplus, Structural elucidation and physicochemical properties of an organic NLO crystal: 4-Nitrotoluene-2-sulphonic acid dihydrate, *J. Mol. Biol.* 10, 2010, 194.
- [46] W .A Bayoumi, M .A Elsayed, H .N Baraka and L. Abou-zeid, Synthesis and Biological Evaluation of a Series of Dithiocarbamates as New Cholinesterase Inhibitors, *Arch. Pharm. Chem. Life Sci.* 345, 2012, 902.
- [47] D.H.K Harinath Y Reddy, B .N Kumar, C.H Apparao and K. Sessaiah, Synthesis, spectral characterization and antioxidant activity studies of a bidentate Schiff base, 5-methyl thiophene-2-carboxaldehyde-carbohydrazone and its Cd(II), Cu(II), Ni(II) and Zn(II) complexes, *Spectrochim. Acta A*, 101, 2013, 264.
- [48] Patil, S.G, Patil, M.P, Maheshwari, V.L, Patil, R.H, In vitro lipase inhibitory effect and kinetic properties of di-terpenoid fraction from *Calatropisprocera* (Aiton). *Biocatal. Agric. Biotechnol.* 4, 2015, 57–585.

Chapter – 3

Co(II), Ni(II) and Cu(II) complexes of new mannich base of N'-(1H-benzimidazol-1-ylmethyl)pyridine-4-carbohydrazide: Spectral, XRD, DFT studies, molecular docking, antioxidant and antimicrobial studies.



3.1 INTRODUCTION

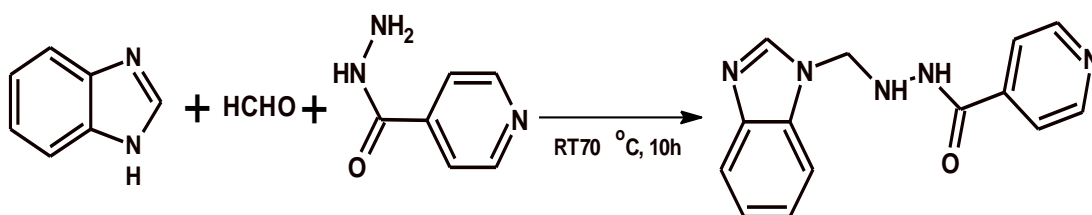
The metal complexes of benzimidazole and its derivatives have been evaluated for medicinal applications such as anticancer agents, antioxidant and enzyme inhibitors [1-8]. Isoniazid has been used as a front-line drug in the treatment of tuberculosis (TB), however; resistant to TB strains and have limited in its use. The major route of isoniazid resistance relies on KatG enzyme disruption, which does not promote an electron transfer reaction, reactivity of isoniazid metal complexes as prototypes for novel self-activating metallodrugs against TB. It is well known from the literature that benzimidazole compounds containing the amine moiety have a strong ability to form metal complexes. Therefore, it was thought worthwhile to synthesize some metal complexes of this type of Mannich base and investigate its bonding characteristics. Moreover, heterocyclic Mannich bases that are derived from the corresponding heterocyclic intermediates also possess various useful properties and the metal complexes of mannich bases have been studied extensively in recent years due to the selectivity and sensitivity of the ligands toward various metal ions [9, 10].

In the present study the author has reported the synthesis Co(II), Ni(II) and Cu(II) complexes derived from the new mannich base ligand, *N'*-(1*H*-benzimidazol-1-ylmethyl) pyridine-4-carbohydrazide (BI), and their characterization by elemental, spectral and XRD analysis. In addition, the antioxidant features of metal complexes *in-vivo* and *in-vitro* docking interactions have also been examined.

3.2 EXPERIMENTAL

3.2.1 Synthesis of ligand *N'*-(1*H*-benzimidazol-1-yl/methyl) pyridine-4-carbohydrazide [BI]

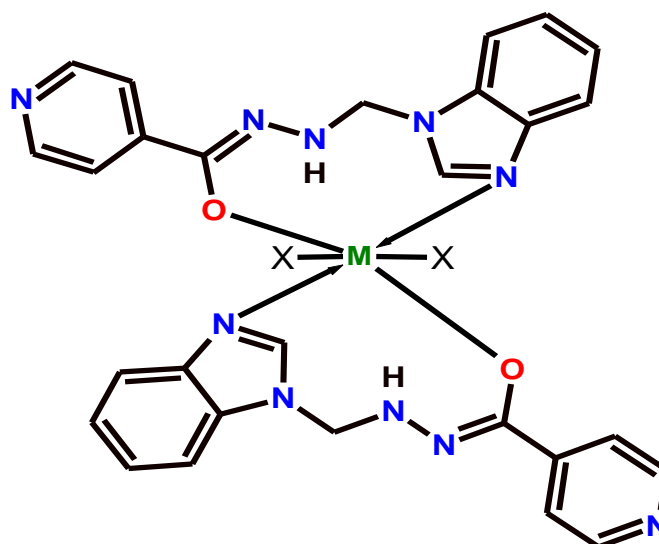
Isoniazid (0.01mol, 2.742g) was dissolved in 35 mL of anhydrous ethanol, to this benzimidazole (0.01mol, 2.362g) and formaldehyde solution (37%, 0.05mol) were added. The mixture was stirred at 70 °C for 10 h and the completion of the reaction was monitored by TLC, the reaction mixture was cooled and poured into crushed ice. The precipitate was collected by filtration and dried followed by recrystallization from the ethanol.



Scheme 3.1 Synthetic route of ligand (BI) via mannich base

3.2.2 General procedure for the synthesis of metal complexes $[M(\text{BI})_2\text{Cl}_2] \cdot n\text{H}_2\text{O}$.

The ethanolic solution of metal (II) chlorides (0.02mol) was added in drops to the ethanolic solution of ligand BI (0.04mol) and the mixture was refluxed on water bath at 70 °C for about 4-5h. The solid product obtained was filtered, washed with hot ethanol and dried under vacuum over anhydrous calcium chloride.

Figure 3.1 Proposed structure of metal complexes $[M=\text{Co}(\text{II}), \text{Ni}(\text{II}) \text{ and } \text{Cu}(\text{II})]$

3.3 Results and discussion

The analytical data of the metal complexes reveal that the reactions of metal (II) chlorides with the ligand occur in 1:2 (M:L) molar ratio. The observed molar conductance of the complexes in DMSO (ca. 10^{-2} M solution) are consistent with $\text{Co}(\text{II})$, $\text{Ni}(\text{II})$, $\text{Cu}(\text{II})$ complexes and are non-electrolytic in nature [11].

Table 3.1 Analytical data and molar conductance values of BI and their metal complexes

Compounds	Colour	Mol. Wt	Yield (%)	Calcd. (found) (%)			Molar conductance [$\Omega^{-1} \text{cm}^2 \text{mol}^{-1}$]
				C	H	N	
$\text{C}_{14}\text{H}_{13}\text{N}_5\text{O}$ (BI)	Creamy white	267.2	70	62.91 (61.91)	4.90 (3.96)	26.20 (25.31)	-
$[\text{CoCl}_2(\text{BI})_2] \cdot \text{H}_2\text{O}$ (1)	Dark green	661.08	65	56.86 (55.12)	4.09 (3.91)	23.68 (22.51)	14.20
$[\text{Ni}(\text{BI})_2] \cdot \text{Cl}_2$ (2)	Light blue	660.08	60	56.88 (55.81)	4.09 (3.97)	23.69 (22.51)	38.55
$[\text{CuCl}_2(\text{BI})_2] \cdot \text{H}_2\text{O}$ (3)	Light brown	663.08	63	56.42 (56.65)	4.06 (3.87)	10.66 (09.25)	17.81

3.2.1 Computations investigation and frontier molecular orbital analysis

The computational calculations of ligand QB performed by Becke's three parameter hybrid exchange functional (B3LYP) with support of chemcraft 1.7 software [12] has been used for visualization of optimized structures (figure 3.2 and 3.3), selected bond angles, bond length, dihedral angles (Table 3.2) and HOMO-LUMO of BI.

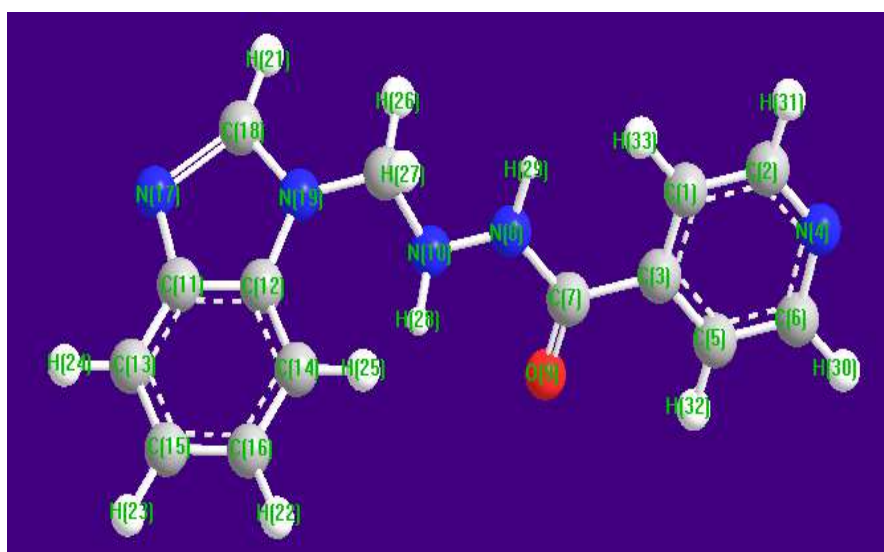


Figure 3.2 Optimized geometry of ligand BI

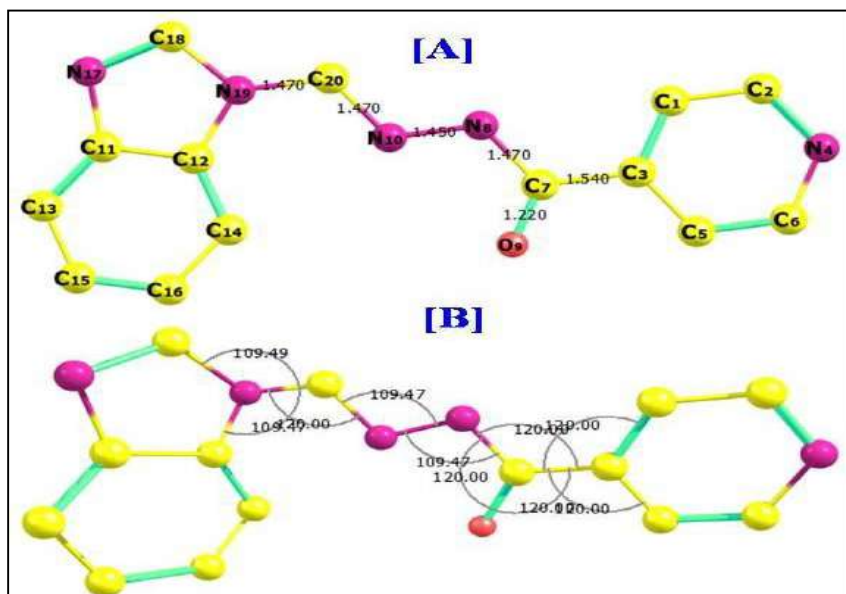


Figure 3.3 Standard bond lengths and bond angles of the ligand BI

Table 3.2 Selected structural parameters of ligand BI

Bond	Bond length (Å)	Angle	(°)	Dihedral angle	(°)
C(16)-H(22)	1.122	C(16)-H(22)	1.122	C(3)-C(7)-N(8)	120.000
N(17)-C(18)	1.659	N(17)-C(18)	1.659	C(3)-C(7)-O(9)	119.999
C(18)-N(19)	1.446	C(18)-N(19)	1.446	N(8)-C(7)-O(9)	119.999
C(18)-H(21)	1.122	C(18)-H(21)	1.122	C(7)-N(8)-N(10)	120.000
N(19)-C(20)	1.446	N(19)-C(20)	1.446	C(7)-N(8)-H(29)	119.999
C(20)-H(26)	1.122	C(20)-H(26)	1.122	N(10)-N(8)-H(29)	119.999
C(20)-H(27)	1.122	C(20)-H(27)	1.122	N(8)-N(10)-C(20)	109.500

The HOMO-LUMO gap of organic molecules is important because they transmit to particular movements of electrons and may be most generous for single electron transfer. This is useful for a number of reactions and has vast effects in organic semiconductors, the field where this gap is most vital. It has been found that molecules with large HOMO-LUMO gap are highly stable and unreactive; while those with small gaps are generally reactive [13]. By calculating the HOMO-LUMO

energy gap, one can easily determine the excitation energy of an organic derivative at its ground state [14].

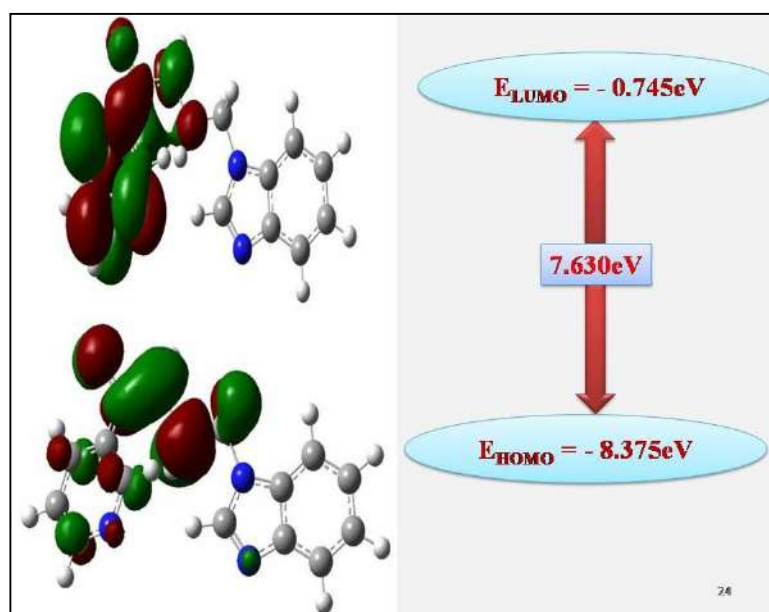


Figure 3.4 HOMO LUMO frontier orbitals of the ligand QB

HOMO-LUMO gap of ligand QB are shown in figure 3.4, since in the ligand electronic transition from HOMO orbitals to the LUMO orbitals is $\pi \rightarrow \pi^*$ transitions. Energy separation between the HOMO and LUMO ($\Delta\varepsilon = \varepsilon_{\text{LUMO}} - \varepsilon_{\text{HOMO}}$) of ligand BI is 7.630 eV

3.3.2 ^1H NMR and Mass spectra

The ^1H NMR spectrum of BI showed doublets in the region 10.12 to 9.83 ppm attributed to two $-\text{NH}$ protons and a singlet appears around 8.76 ppm for $-\text{CH}=\text{N}$ group proton. The multiplets appeared in the range 7.77 to 7.22 ppm attributed to aromatic protons of imidazole and isoniazid rings which evidence the structure of BI.

The ^1H NMR spectrum of the Zn(II) complex showed the presence of the amine group by a sharp signal at 10.25 ppm in uncoordinated ligand appeared at 10.12 ppm in the complex. The multiple signals observed in the range of 6.95 to 7.82 ppm attributed to aromatic protons of imidazole and Isoniazid rings, the results of NMR spectrum of complex confirm the bidentate nature of the ligand.

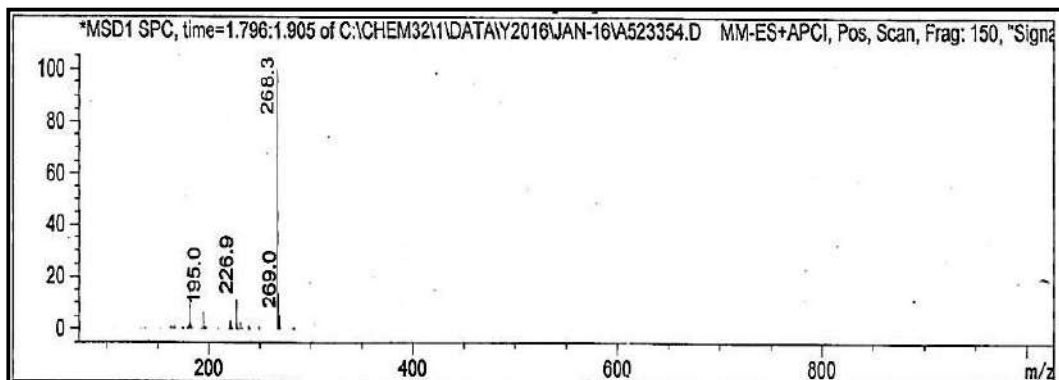


Figure 3.7 Mass spectrum of the BI

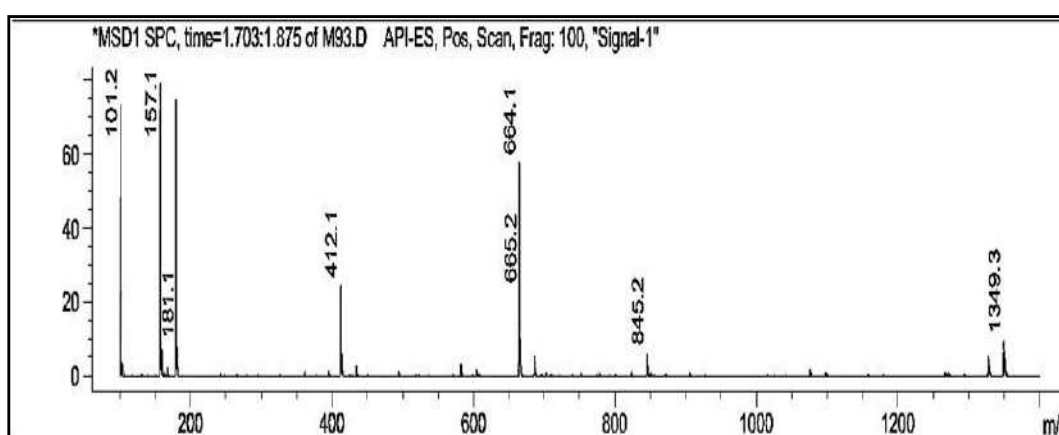


Figure 3.8 Mass spectrum of the Zn(II) complex

3.3.3 IR Spectra

The IR spectra recorded for uncoordinated ligand and their metal complexes as KBr pellets. A sharp band at 1704 cm^{-1} for $\nu(\text{C}=\text{O})$ and the position of $\nu(\text{C}=\text{O})$ band is shifted to the lower frequencies by $80\text{--}100\text{ cm}^{-1}$ in the spectra of the Co(II), Ni(II) and Cu(II) metal complexes, indicating that the coordination occurs through the oxygen atom [15]. The $\nu(\text{Ar-CH})$ stretching vibrations appeared at 2945 cm^{-1} and a medium intensity band appears at 1304 cm^{-1} for $\nu(\text{N-H})$. The band $\nu(\text{C}=\text{N})$ observed around 1535 cm^{-1} was shifted to lower frequencies in the spectra of all the complexes and appeared in the range $1500\text{--}1509\text{ cm}^{-1}$ indicating that coordination of $\nu(\text{C}=\text{N})$ occur *via* nitrogen atom of the ligand. In the coordination of the ligand to the metal ions new peak results in the range of $474, 475$ and 469 cm^{-1} which are due to $\nu(\text{M-N})$ bonding and are followed by 510 and 511 cm^{-1} due to $\nu(\text{M-O})$ mode of bonding [16,17].

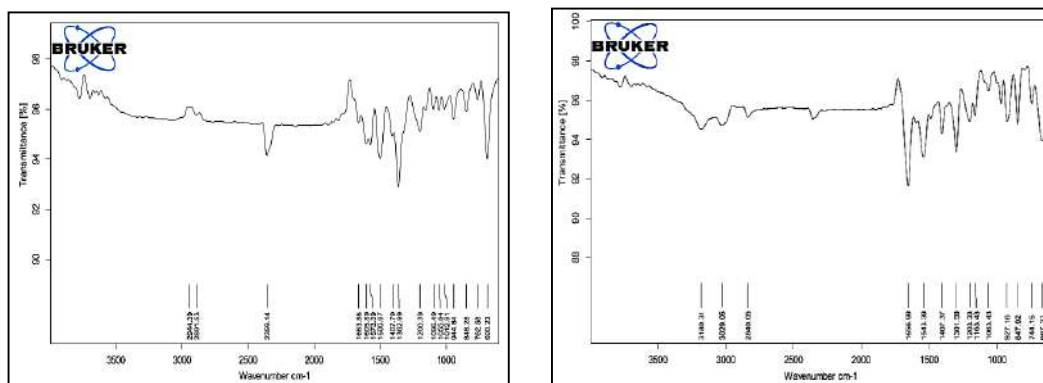


Figure 3.9 IR Spectra of BI and Co(II) Complex

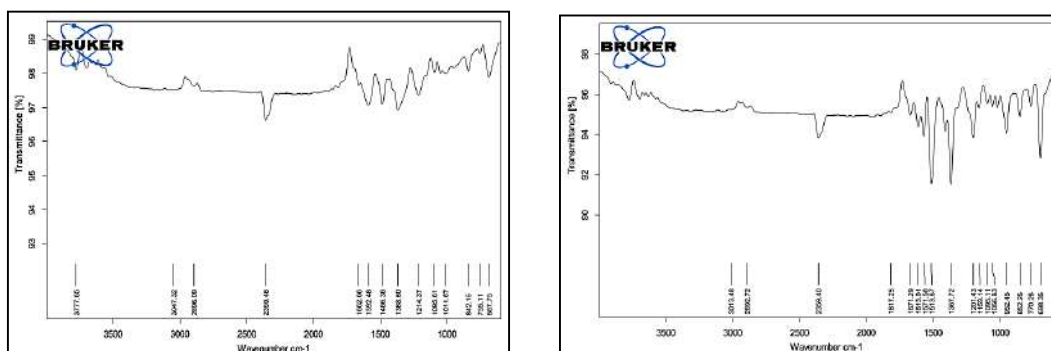


Figure 3.10 IR Spectra of Ni(II) and Cu(II) complexes

3.3.4 Electronic spectra and magnetic moments studies

The absorption band appeared at 32,051 and 33,898 cm^{-1} in the spectrum of BI are predominantly due to $n \rightarrow \pi^*$ and $\pi \rightarrow \pi^*$ transitions [18]. These transitions are shifted slightly in their metal complexes.

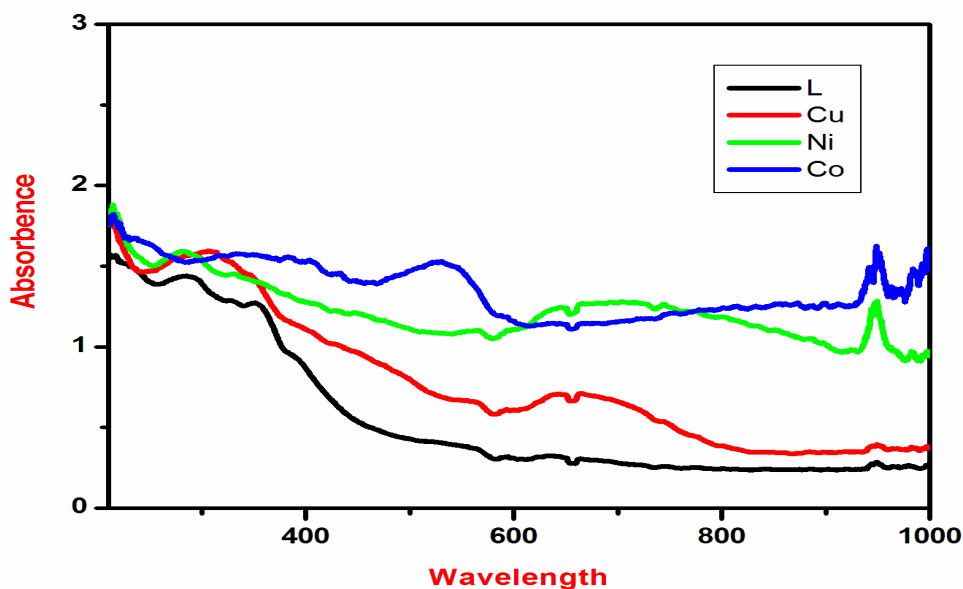


Figure 3.11 Uv-Visible spectra of the BI and their metal complexes

The d-d bands observed at 21,367 and 10,131 cm^{-1} for Co(II) complex are assigned as ${}^4\text{T}_{1g}(\text{F}) \rightarrow {}^4\text{T}_{2g}(\text{F})$ (ν_1) and $\rightarrow {}^4\text{A}_{2g}(\text{F})$ (ν_2) transitions and the magnetic moment is 1.94 B.M, represents octahedral geometry [19]. The electronic spectra of Ni(II) complex showed the bands at 20618 cm^{-1} corresponding to ${}^3\text{A}_{1g}(\text{F}) \rightarrow {}^3\text{T}_{1g}(\text{P})$ respectively and its magnetic moment is 5.18 B.M indicating a high spin octahedral geometry [20]. The copper complex show one board band at 15151 cm^{-1} and is assigned to the transitions ${}^2\text{B}_{1g} \rightarrow {}^2\text{A}_{1g}(\nu_1)$ also the determined magnetic moment is 1.83 B.M, indicating octahedral geometry[21].

Table 3.3 UV-Vis data of QB and its metal complexes

Compound	Electronic transition $\nu(\text{cm}^{-1})$	μ_{eff} (BM)
BI	32051, 31645	-
$[\text{CoCl}_2(\text{BI})_2] \text{H}_2\text{O}$ (1)	21367, 10131	1.94
$[\text{Ni}(\text{BI})_2] \text{Cl}_2 \cdot \text{H}_2\text{O}$ (2)	15873, 10266 cm^{-1}	3.63
$[\text{CuCl}_2(\text{BI})_2] \text{H}_2\text{O}$ (3)	15151	1.83

3.3.5 XRD analysis

The powder XRD diffraction pattern is carried out for all the complexes and the diffraction patterns of Co(II), Ni(II) and Cu(II) complexes showed that they are crystalline in nature as the spectra representing in figure 3.12, 3.13 and 3.14.

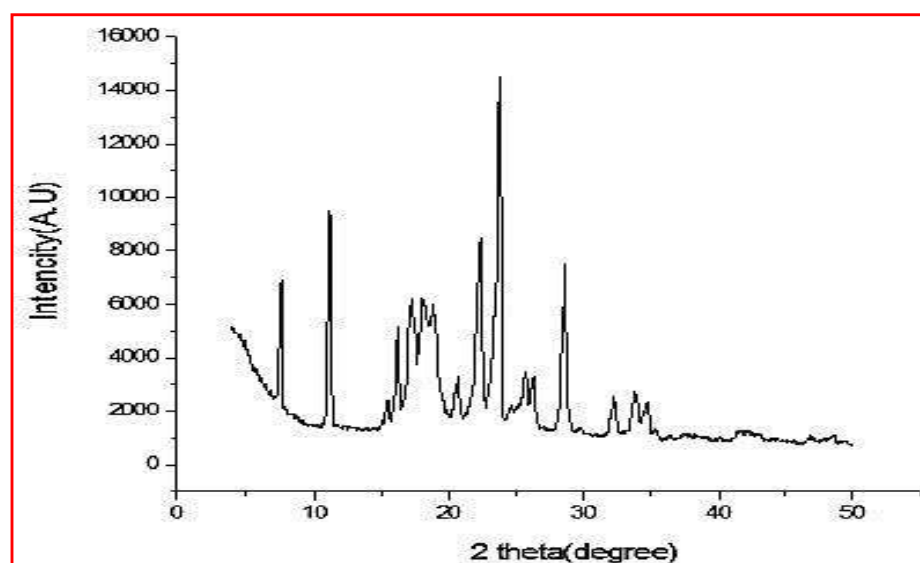


Figure 3.12 XRD patterns of $[\text{CoCl}_2(\text{BI})_2]$

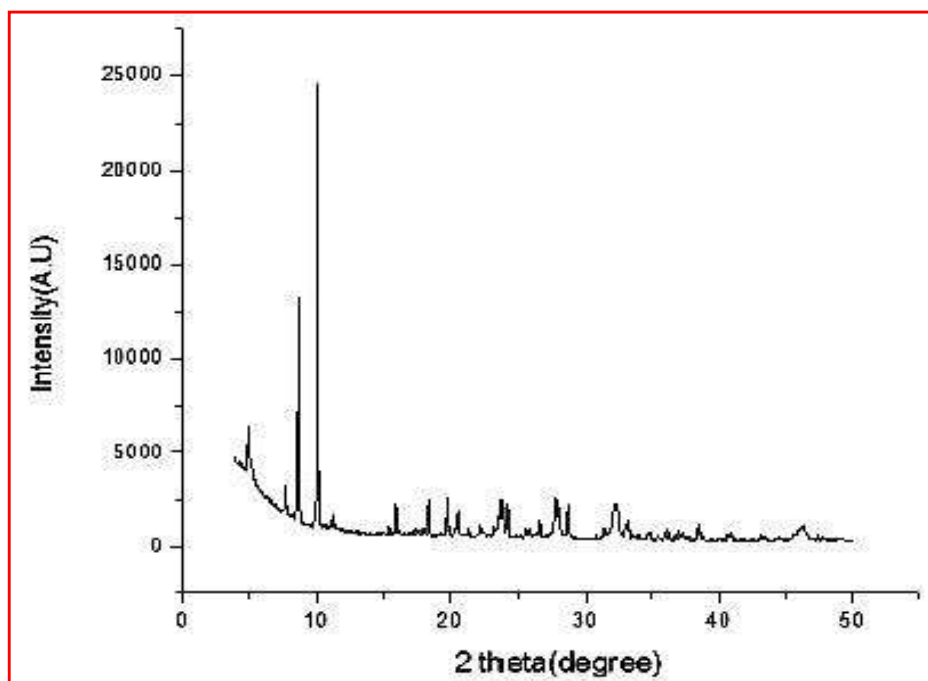


Figure 3.13 XRD patterns of [Ni (BI)₂]Cl₂ H₂O

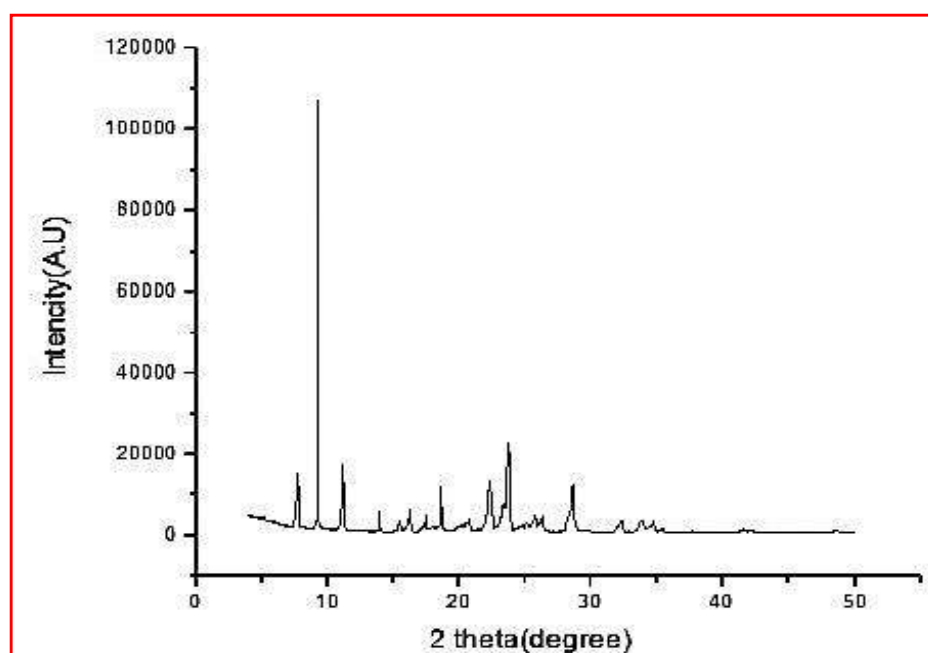


Figure 3.14 XRD pattern of [CuCl₂(BI)₂]

The Miller indices (hkl) along with observed and calculated d angles, 2θ , $\sin 2\theta$ values and the relative intensities, along with cell parameters are given in tables 3.3, 3.4 and 3.5. For [CoCl₂(BI)₂].H₂O, the lattice parameters and angle calculated are $a = 9.5496 \text{ \AA}$, $b = 15.4706 \text{ \AA}$, $c = 7.3935$, $\beta = 98.0241^\circ$, unit cell volume of the

complex 1.378×10^{-8} cm. $[\text{Ni}(\text{BI})_2]\text{Cl}_2 \cdot \text{H}_2\text{O}$ lattice parameters and angle calculated are $a = 11.9487 \text{ \AA}$, $b = 14.3386 \text{ \AA}$, $c = 13.4797$, $\beta = 94.8014^\circ$ unit cell volume of the complex 2.1261×10^{-8} cm and $[\text{CuCl}_2(\text{BI})_2]$ lattice parameters and angle calculated are $a = 13.4747 \text{ \AA}$, $b = 11.2711 \text{ \AA}$, $c = 8.6961$, $\beta = 90.245^\circ$, unit cell volume of the complex 1.378×10^{-8} cm. The average crystallite sizes of the complexes dxrd were calculated using Debye Scherrer equation ($D = K\lambda/\beta \cos \theta$) Where D = Particle size, K = Dimensionless shape factor, λ = Xray wavelength (0.15406 \AA) β = Line broadening at half the maximum intensity, θ = Diffraction angle. The $[\text{CoCl}_2(\text{BI})_2] \cdot \text{H}_2\text{O}$, $[\text{Ni}(\text{BI})_2]\text{Cl}_2 \cdot \text{H}_2\text{O}$ and $[\text{CuCl}_2(\text{BI})_2]$ having crystallite size of 93.28 nm (monoclinic), 33.54 nm (orthorhombic) and 63.31nm (monoclinic) respectively, suggesting that the complexes are in a nanocrystalline phase [21-23].

Table 3.4 XRD data of $[\text{CoCl}_2(\text{BI})_2] \cdot \text{H}_2\text{O}$

Peak No	2 θ	θ	Sin θ	d		Intensity
				Cal	Obs	
1	19.86	9.93	0.484001751	4.53	4.53	10.43
2	22.25	11.125	0.991636177	4.06	4.12	46.49
4	23.78	11.89	0.625966778	3.81	3.81	100
5	25.71	12.855	0.284638574	3.54	3.51	21.29
6	27.97	13.985	0.988444933	3.28	3.38	6.57
7	28.67	14.335	0.980494781	3.20	3.27	55.90
8	30.08	15.04	0.619388265	3.07	3.51	4.90
9	31.98	15.99	0.278312486	2.90	2.80	7.92
10	34.76	17.38	0.994879566	2.70	2.72	14.79
11	39.16	19.58	0.667200485	2.43	2.43	4.59

Table 3.5 XRD data of [Ni (BI)₂ Cl₂] H₂O

Peak No	2 θ	θ	Sin θ	d		Intensity
				Cal	Obs	
1	10.97	5.485	0.716090602	8.05	8.00	27.38
2	14.87	7.435	0.91350372	5.94	5.94	10.07
4	20.76	10.38	0.816441972	4.27	4.24	22.82
5	21.99	10.995	0.99999984	4.03	4.00	31.25
6	23.75	11.875	0.63759366	3.74	4.20	10.01
7	24.74	12.37	0.19511099	3.59	3.58	15.36
8	27.97	13.985	0.988444933	3.18	3.18	10.12
9	29.05	14.525	0.92573073	3.06	3.34	10.54
10	30.46	15.23	0.62289431	2.14	3.01	8.14
11	32.30	16.15	0.42778132	2.76	3.28	17.48

Table 3.6 XRD data of [CuCl₂(BI)₂]H₂O

Peak No	2 θ	θ	Sin θ	d		Intensity
				Cal	Obs	
1	19.79	9.895	0.453084237	4.48	4.46	98.96
2	20.58	10.29	0.761239268	4.31	4.14	73.17
4	22.37	11.185	0.982112532	3.96	4.00	43.61
5	24.19	12.095	0.45410786	3.67	3.25	84.83
6	25.53	12.765	0.197325851	3.48	3.48	37.33
7	26.59	13.295	0.665847662	3.34	3.04	50.69
8	27.79	13.895	0.970820607	3.20	3.32	100
9	29.17	14.585	0.90138753	3.05	3.311	19.97

3.4 Procedure of biological studies

3.4.1 DPPH radical scavenging assay

The free radical scavenging activity of the ligand, BI and complexes was measured *In vitro* by 2, 2- diphenyl-1-picrylhydrazyl (DPPH) assay. The stock solution was prepared by dissolving 24 mg DPPH with 100 mL methanol and stored at 20°C until required. The working solution was obtained by diluting DPPH solution with methanol to attain an absorbance of about 0.98 ± 0.02 at 517 nm using the spectrophotometer. All the tested samples in various concentrations (50, 75 and 100 $\mu\text{g/mL}$) were prepared in methanol and the homogeneous solutions were achieved by stirring. Aliquot of test sample (1 mL) was added to 4 mL of 0.004% (w/v) methanol solution of DPPH and then reaction mixture was vortexed for 1 min and kept at room temperature for 30 min in the dark to complete the reaction. The absorbance was read against blank at 517 nm. The synthetic antioxidant BHT was used as positive control [24, 25]. The ability of the tested samples at tested concentration to scavenge DPPH radicals was calculated using equation.

$$\text{Scavenging ratio (\%)} = [(A_i - A_o) / (A_c - A_o)] \times 100\%$$

Where A_i is the absorbance in the presence of the test compound; A_o is absorbance of the blank in the absence of the test compound; A_c is the absorbance in the absence of the test compound.

3.4.2 Ferric reducing antioxidant activity

The ferric reducing antioxidant activity was determined according to the method of Oyaizu. Various concentrations of the tested compounds, 25, 35 and 45 mM were mixed with 2.5 mL of phosphate buffer (0.2 M, pH 6.6) and 2.5 mL of 1% potassium ferric cyanide and incubated at 50°C for 20 min. 2.5 mL of 10% trichloro acetic acid was added to this mixture and centrifuged at 3000 rpm for 20 min. The upper layer (2.5 mL) was mixed with 2.5 mL of deionized water and 0.5 mL of 0.1% ferric chloride and the absorbance was measured at 650 nm using a spectrophotometer. Increase in the absorbance of the reaction mixture indicates higher reducing power. BHT was used as standard and compared with the reducing power of the synthesized BI and their metal complexes [26].

3.4.3 Molecular docking

Molecular modeling studies were performed by using *Hex* 8.0.0 protein-ligand docking in PDB formats. The parameters used for docking include: correlation type-shape only, FFT mode -3D, grid dimension -0.6, receptor range -180, ligand range -180, twist range -360, distance range -40. The starting coordinates of the human antioxidant enzyme in complexes with the competitive inhibitor *DTT* (PDB: 3MNG) were taken from the Protein Data Bank (<http://www.rcsb.org/pdb>) [27, 28]. The selected ligands were docked against the lead competitive inhibitor ligand DTT at the crystal enzyme structure of the target protein and the best energy conformations of receptor ligand were studied and the energy of binding was calculated as the difference between the energy of the complex and the individual energies of enzyme and ligand.

3.5 Results and discussion biological studies

3.5.1 DPPH radical scavenging activity

DPPH radical scavenging activity data of the synthesized ligand and their metal complexes exhibited that all the compounds having highly potency activity represented in figure 3.15. The metal complexes exhibited more radical scavenging activity than that of the uncoordinated BI. The $[\text{CuCl}_2(\text{BI})_2]$ complex exhibited effective antioxidant activity almost close to the standard BHT, and the BI. The other complexes, $[\text{CoCl}_2(\text{BI})_2]\cdot\text{H}_2\text{O}$ and $[\text{Ni}(\text{BI})_2]\text{Cl}_2\cdot\text{H}_2\text{O}$ showed moderate antioxidant activity when compared to BHT. The activity is due the presence imidazole and isoniazid nucleus in the ligand which is coordinated to the metal ion [29].

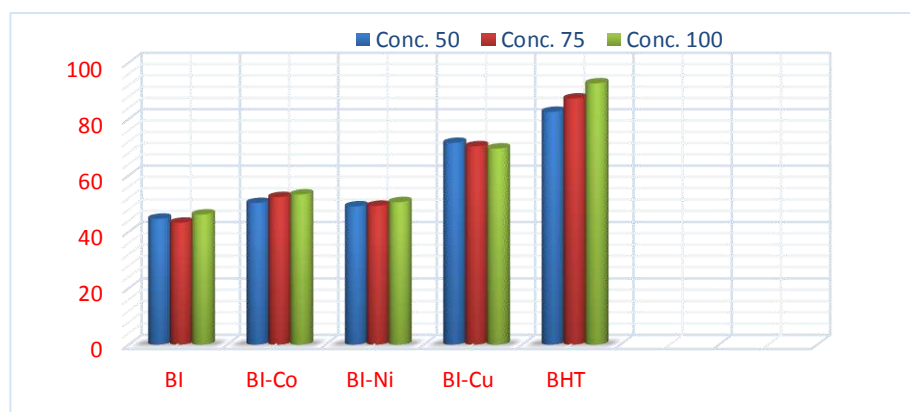


Figure 3.15 DPPH scavenging data of BI and their metal complexes

3.5.2 Ferric reducing antioxidant activity

In this activity, the reducing power of each compound depends on the colour change of the solution from yellow to green and blue. The existence of reducers (i.e., antioxidants) causes the reaction of Fe^{3+} / ferricyanide complex to the ferrous form, after addition of trichloro acetic acid and ferric chloride, the Perl's Prussion blue that can be monitored at 700 nm [30]. The reducing power of the standard (BHT) at various concentrations showed higher absorbance value. The ligand, BI showed least activity, while the Ni(II) complex exhibits highest reducing activity and the Co(II) as well as Cu(II) complexes showed moderate activity. The order of reducing power of the ligand and their metal complexes is given by $\text{BHT} > \text{Ni} > \text{Co} > \text{Cu} > \text{ligand BI}$ and the results shown in the figure 3.16.

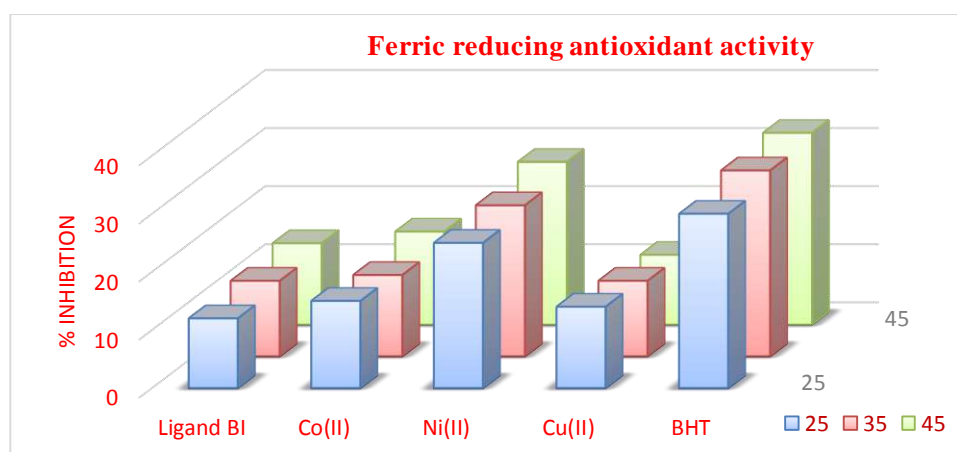
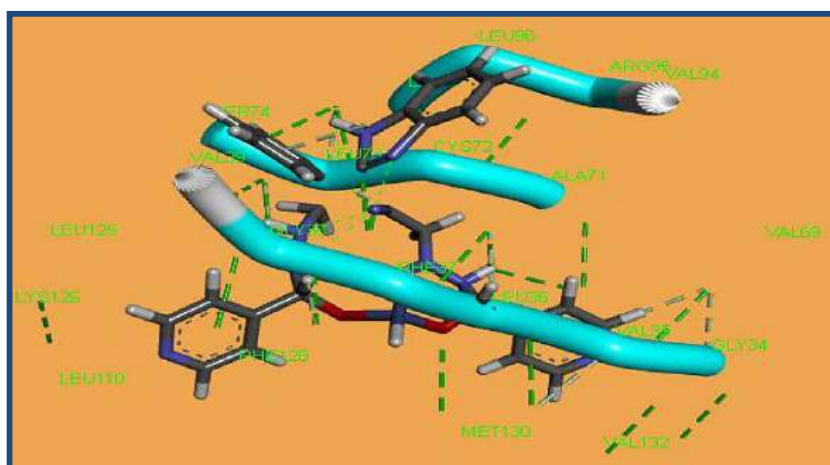


Figure 3.16 Ferric reducing scavenging data of BI and their metal complexes

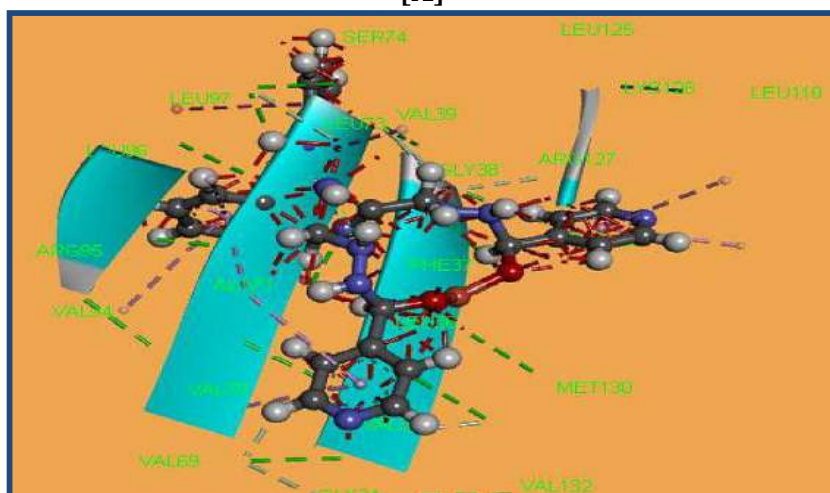
3.5.3 Molecular docking studies

In order to interrupt the binding interactions modes *In-vitro* activity of BI and their metal complexes with human antioxidant enzyme of competitive inhibitor DTT (PDB: 3MNG) [31]. The binding energy all the complexes showed prominent binding interactions, $[\text{CoCl}_2(\text{BI})_2]$ exhibits the -297.24 Kcal/mol , while $[\text{Ni}(\text{BI})_2]\text{Cl}_2 \cdot \text{H}_2\text{O}$ showed -295.57 Kcal/mol and $[\text{CuCl}_2(\text{BI})_2]$ gives highest binding energy of -334.14 Kcal/mol with human antioxidant 3MNG protein receptor by the key of amino acids LEU-97, VAL-69, ALA-71, CYS-72, PHE-37. Hydrophobic and hydrophilic spheres are used to recognize the interactive positions which will be the potential ligand binding sites in each possible position. Finally, the molecular docking studies for the selected compounds revealed that the synthesized

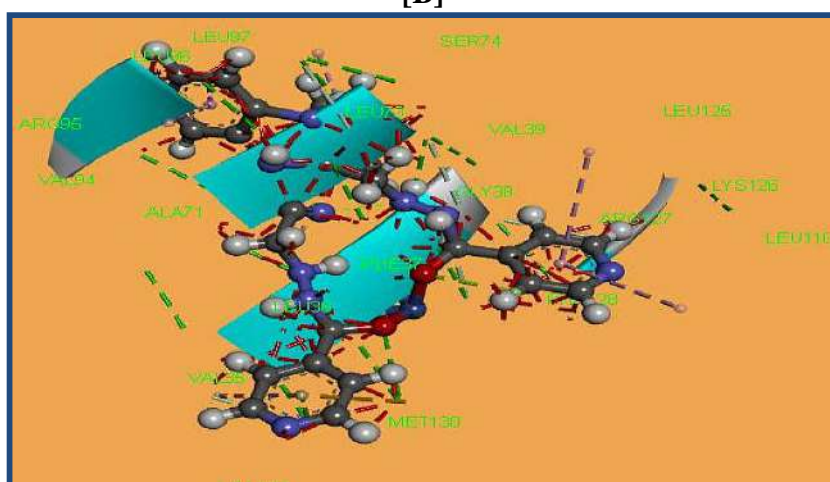
compounds are antioxidant competitive inhibitors in comparison to antioxidant inhibitor DTT at 3MNG binding receptor as shown in figure 3.17.



[A]



[B]



[C]

Figure 3.17 Binding interaction of [A] Co(II), [B] Ni(II) and [C] Cu(II) complexes with 3MNG receptor

3.5.4 Antimicrobial activity

All the synthesized complexes and BI have been examined towards three bacterial and fungal strains using of agar well diffusion method [32-34] as data represent in table 3.6 and figure 3.18. All the bacterial traces were maintained on nutrient agar medium at ± 37 °C and fungal strains were maintained on potato dextrose agar (PDA) at ± 25 °C. The test compounds had been dissolved in DMSO. Sample-loaded plates were inoculated with the microorganism incubated at 37 °C for 24 h and culture was incubated at 25 °C for 60 h. DMSO as control and chloramphenicol and fluconazole is used as standards for bactericide and fungicide. All the synthesized complexes and BI showed inhibition property, among them Ni(II) and Cu(II) complexes showed excellent when compared to the standard. The compounds were also tested for minimal inhibitory concentration (MIC) values [35-38]. The MIC values of less than 25 μ g/mL are given in table 3.7, it observed that ligand (BI) and Co(II) complex have least activity, while Ni(II) and Cu(II) complexes showed the promising activity.

Table 3.7 Antimicrobial data – Zone inhibition

Compounds	Antibacterial zone inhibition in mm (mean \pm SD)			Antifungal zone inhibition in mm (mean \pm SD)		
	S. aureus	B. subtilis	E. coli	S. coccus	C. albicans	A. niger
BI	03 \pm 0.3	05 \pm 0.2	05 \pm 0.7	04 \pm 0.4	03 \pm 0.1	-
Co(II)	06 \pm 0.3	-	07 \pm 0.3	08 \pm 0.2	-	06 \pm 0.3
Ni(II)	14 \pm 0.2	12 \pm 0.4	10 \pm 0.2	10 \pm 0.6	09 \pm 0.2	11 \pm 0.3
Cu(II)	13 \pm 0.1	15 \pm 0.1	12 \pm 0.3	08 \pm 0.4	10 \pm 0.1	10 \pm 0.3
Chloramphenicol	15 \pm 0.2	16 \pm 0.3	13 \pm 0.3	12 \pm 0.2	11 \pm 0.4	13 \pm 0.3
Fluconazole	-	-	-	12 \pm 0.2	10 \pm 0.1	12 \pm 0.3
DMSO	0	0	0	0	0	0

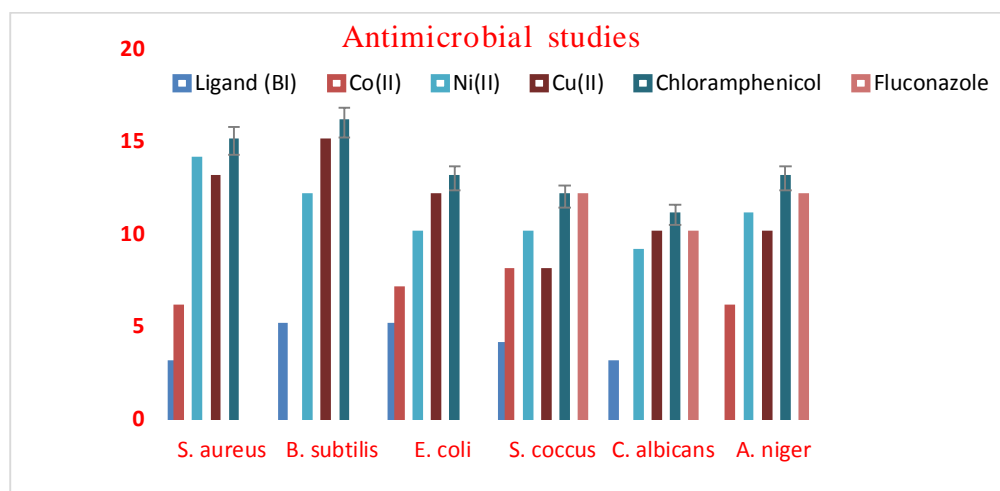


Figure 3.18 Graphical representations of antimicrobial studies

Table 3.8 Antimicrobial data – minimal inhibitory concentration

Compounds	MIC of the compounds in 25 μ mL					
	S. aureus	B. subtilis	E. coli	S. coccus	C. albicans	A. niger
BI	10	-	12	09	08	-
Co(II)	11	10	-	08	10	11
Ni(II)	18	21	17	19	21	15
Cu(II)	19	20	22	17	13	22

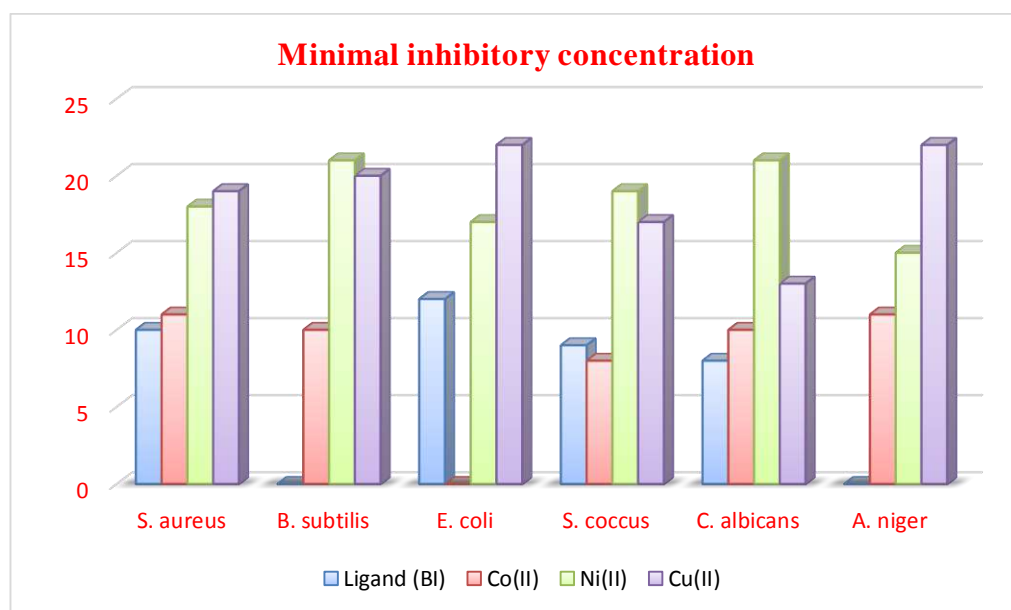


Figure 3.19 Graphical representation of Minimal inhibitory concentration [MIC]

3.6 Conclusion

The new mannich base ligand synthesized *N'*-(1*H*-benzimidazol-1-ylmethyl)pyridine-4-carbohydrazide (BI) and characterized. The spectral data showed that the ligand coordinated through carbonyl oxygen and the imidazole nitrogen which imply that bidentate in nature. The electronic spectra and magnetic moment data suggest that octahedral geometry for Co(II), Ni(II) and Cu(II) complexes, From the XRD data it was found that Co(II), Cu(II), possessing monoclinic and Ni(II) complex showed orthorhombic crystallite phase, DFT calculations at B3LYP level using chemcraft 1.3 of synthesized ligand BI has been carried out and derived some fruitful structural information. Antioxidant activity enhances on complexation with metal ions, resulting promising scavenging activity for all complexes. The Cu(II) complex give highest and prominent activity almost equal to that of standard BHT. The molecular docking studies of synthesized compounds are carried out, which reveal the excellent binding energy interactions of the metal complexes with protein enzyme *DTT* (*PDB: 3MNG*).

References

- [1] P. Singla, V. K. Luxami, Paul. Benzimidazole-biologically attractive scaffold for protein kinase inhibitors. RSC Advance. (4), 2014, 12422-12440.
- [2] A. Kamal, V.S Reddy, K. Santosh, G.B Kumar, A.B Shaik, R. Mahesh, S.S Chourasiya, I. Bin Sayeed, S. Kotamraju. Synthesis of imidazo[2,1-*b*][1,3,4]thiadiazole chalcones as apoptosis inducing anticancer agents. Medicinal chemistry Communication. (11), 2014, 51718-1723.
- [3] A. Kamal, M.P.N Rao, P. Swapna, V. Srinivasulu, C. Bagul, A.B. Shaik, K. Mullagiri, J. Kovvuri, V.S Reddy, K. Vidyasagar, N. Nagesh. Synthesis of β -carboline–benzimidazole conjugates using lanthanum nitrate as a catalyst and their biological evaluation. Organic & biomolecular chemistry, (12), 2014, 2370-2387.
- [4] A. Kamal, A.V.S Rao, V.L Nayak, N.V.S Reddy, K. Swapna, G. Ramakrishna, M. Alvala. Synthesis and biological evaluation of imidazo[1,5-*a*]pyridine-benzimidazole hybrids as inhibitors of both tubulin polymerization and PI3K/Akt pathway. Organic & biomolecular chemistry, (12), 2014, 9864-9880.
- [5] A. Kamal, S. Ponnampalli, M.P.N. Rao, K. Mullagiri, V.L. Nayak, B. Chandrakant. Synthesis of imidazo-thiadiazole–benzimidazole conjugates as mitochondrial apoptosis inducers. Medicinal chemistry communication. (5), 2014, 1644-1650.
- [6] M Hanif. M.A.H Nawaz, M.V Babak, J. Iqbal, A. Roller, B.K. Keppler, C.G. Hartinger, Ruthenium^{II}(η^6 -arene) Complexes of Thiourea Derivatives: synthesis, characterization and urease inhibition. Molecules, (19), 2014, 8080-8092.
- [7] M Hanif. M.A.H Nawaz, C.G. Hartinger. Synthesis of [Ru^{II}(η^6 -*p*-cymene)(PPh₃)₂(L)Cl]PF₆ complexes with carbohydrate-derived phosphites, imidazole or indazole co-ligands. Inorganica chimica acta. 380, 2012, 211-215.

- [8] H. Khalid, M. Hanif, M.A. Hashmi, T. Mahmood, K. Ayub, M. Monim-ul-Mehboob. Copper complexes of bioactive ligands with superoxide dismutase activity. *Mini-review medicinal chemistry*, (13), 2013, 1944-1956.
- [9] G. Krishnamurthy Synthesis of Ruthenium(II) Carbonyl Complexes with 2-Monosubstituted and 1,2-Diisubstituted Benzimidazoles & Shashikala N, *Journal of Serb. Chem. Soc.*, 74(10), 2009, 1085-1096.
- [10] B. Roopashree, V. Gayathri, A. Gopi, K.S. Devaraju. Synthesis, characterizations, and antimicrobial activities of binuclear ruthenium(III) complexes containing 2-substituted benzimidazole derivatives. *Journal of coordination chemistry*, (65), 2012, 4023-4040.
- [11] L. Muruganandam, K. Krishna kumar, Synthesis, characterization and antimicrobial studies of a new mannich base *n*-[morpholino (phenyl)methyl]acetamide and its cobalt(II), nickel(II) and copper(II) metal complexes. *E-journal of chemistry*. 9(2), 2012, 875-882.
- [12] M.A. Abdel Nasser, A. Alaghaz, Badr, El-Sayed. A. Ahmed, El-Henawy, A.A. Reda, Ammar. Synthesis, spectroscopic characterization, potentiometric studies, cytotoxic studies and molecular docking studies of DNA binding of transition metal complexes with 1, 1-diaminopropane–Schiff base. *Journal of molecular structure*, 1035, 2013, 83–93.
- [13] S. Nithyanandan and P. Kannan, Photo Switchable pendant furyl and thienyl fulgimides containing polypyrroles, *Polym Degrad Stab*, 98, 2013, 2224-2231.
- [14] Z. Zhou, R.G. Parr, Activation hardness: new index for describing the orientation of electrophilic aromatic substitution *J. Am. Chem. Soc.* 112, 1990, 5720-5724.
- [15] S. Praveen, M.A. Al-Alshaikh, C.Y. Panicker, A.A. El-Emam, V.V. Salian, B. Narayana, B.K. Sarojini, C.V. Alsenoy, Structural, thermal, linear and nonlinear optical studies of an organic optical limiter based on reverse saturable absorption, *J. Mol. Struct.* 1120, 2016, 317-326.

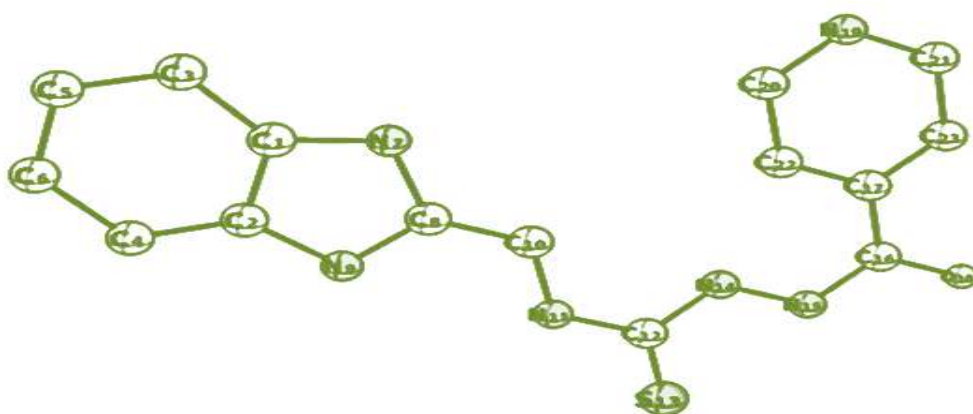
- [16] A. Ashraf, W.A Siddiqui, J Akbar, G. Mustafa, H. Krautscheid, N Ullah. Metal complexes of benzimidazole derived sulfonamide: Synthesis, molecular structures and antimicrobial activity. *Inorganic chimca acta*. 443, 2016, 179–85.
- [17] K.R Sangeetha Gowda, H.S Bhojya Naik, B Vinay Kumar, C.N Sudhamani, H.V Sudeep, T.R Ravi kumar Naik, G. Krishnamurthy. Synthesis, antimicrobial, DNA-binding and photonuclease studies of Cobalt (III) and Nickel (II) Schiff base complexes. *Spectro chimica acta part A: Mol and Bio-mol spect* 105, 2013, 229–237.
- [18] K. Nakamoto, *Infrared and Raman Spectra of Inorganic and Coordination compounds*, 1986. 4th ed. John Wiley and Sons, New York, 257.
- [19] D. N Sathyanarayana, *Vibrational Spectroscopy: Theory and Applications*, New Age International publications, 1996.
- [20] B. Sreekanth, G. Krishnamurthy, H. S. Bhojya Naik & T. K. Vishnuvardhan, Cu(II) and Mn(II) Complexes Containing Macroacyclic Ligand: Synthesis, DNA Binding, and Cleavage Studies, *Nucleosides, Nucleotides and Nucleic Acids*, 31(1), 2012, 1-13.
- [21] Subba Poojari, Parameshwar Naik P, Krishnamurthy G, Jithendra Kumara K.S, Sunil Kumar N, Sathish Naik, Anti-inflammatory, antibacterial and molecular docking studies of novel spiro-piperidine quinazolinone derivatives. *Journal of Taibah Univ. Sci*, 23, 2016, 10-25.
- [22] B. Sreekanth, G Krishnamurthy, H. S. Bhojya Naik, T. K. Vishnuvardhan. Cu(II) and Mn(II) complexes containing macroacyclic ligand: Synthesis, DNA binding, and cleavage studies. *Nucleosides, Nucleotides and Nucleic Acids*, 2012, 311–313.
- [23] S. Tabassum, W.M. Al-Asbahy, M. Afzal, F. Arjmand, V. Bagchi, *Dalton Trans.* 41 2012, 4955–4964.
- [24] R.M. Silverstein, G.C. Bassler, *Spectrometric Identification of Organic compounds*, Wiley, New York, 1964.

- [25] A.B.P Lever. Inorganic electronic spectroscopy. 2nd ed. Amsterdam; New York: Elsevier; 1984 863.
- [26] H.K. Fun, P.S. Patil, S.M. Dharmaprakash, S. Chantrapromma, I.A. Razak, *Acta cryst.* 64E, 2008, 1814-1815.
- [27] B. Mustafa, C. Gokhan, A. Baris, K. Muhammet, K. Ahmet, K. Mukerrem. Synthesis and X-ray powder diffraction, electrochemical, and genotoxic properties of a new azo-Schiff base and its metal complexes. *Turkish journal of chemistry.* (38), 2014, 22-241.
- [28] J. Joseph, B. H. Mehta, Synthesis, characterization, and thermal analysis of transition metal complexes of polydentate ONO donor Schiff base ligand. *Russian journal of coordination chemistry,* (33), 2007, 124-129.
- [29] Y. Harinath, D. Subbarao, C. Suresh, K. Sessaiah. Synthesis, characterization and studies on antioxidant and molecular docking of metal complexes of 1-(benzo[d]thiazol-2-yl)thiourea. *Journal of chemical sciences.* 128, 2016, 43-51.
- [30] N.D. Shashikumar, G. Krishnamurthy, H.S. Bhojya Naik, M.R. Lokesh and K. S. Jithendra kumara, Synthesis of new biphenyl-substituted quinoline derivatives, preliminary screening and docking studies. *J. chem. sci.* 126, 1, 2014, 205–212.
- [31] Bhimagouda S. Patil, Krishnamurthy G, Lokesh M. R. , Shashikumar N. D., Bhojya Naik H. S. Prashant R. Latthe, Manjunath Ghate, Synthesis of some novel 1,2,4-triazole and 1,3,4-oxadiazole derivatives of biological interest, *Med Chem Res* 22, 2013, 3341–3349.
- [32] D.W. Ritchie, Evaluation of protein docking predictions using Hex 3.1 in CAPRI rounds 1 and 2, *Proteins,* 2003, 98-106.
- [33] K. Thanigaimani, S. Arshad, N.C. Khalib, I.A. Razak, C. Arunagiri, A. Subashini, S.F. Sulaiman, N.S. Hashim, K.L. Ooi, *Spectrochim. acta,* 149A, 2015, 90-102.

- [34] B.V.S. Kumar, S.D. Vaidya, R.V. Kumar, S.B. Bhirud, R.B. Mane, Synthesis and anti-bacterial activity of some novel 2-(6-fluorochroman-2-yl)-1-alkyl/acyl/ aroyl-1H-benzimidazoles, *Eur. J. Med. Chem.* 41, 2006, 599-604.
- [35] S. Bhimagouda Patil, G. Krishnamurthy, H.S. Bhojya Naik, R.Prashant, Lathe, Manjunath Ghate, Synthesis, characterization and antimicrobial studies of 2-(4-methoxy-phenyl)-5-methyl-4-(2-arylsulfanyl-ethyl)-2,4-dihydro-[1,2,4] triazolo-3-ones and their corresponding sulfones, *European Journal of Medicinal Chemistry*, 45, 2010, 3329-3334.
- [36] D. Sharma, B. Narasimhan, P. Kumar, V. Judge, R. Narang, E.D. Clercq, J.J. Balzarini, Synthesis antimicrobial and antiviral activity of substituted benzimidazoles, *Enzy. Inhibi. Med. Chem.* 24, 2009, 1161.
- [37] Shashikumar N.D, Krishnamurthy G, Bhojya Naik H.S, A facile synthesis of novel cyclic esters of γ -keto acid derivatives by Heck coupling reaction" *Journal of Heterocyclic Chem*, 51, 2014, E354.
- [38] G.A. Kilgil, N. Altanlar, Synthesis and antimicrobial activities of some new benzimidazole derivatives, *IL Farm.* 58, 2003, 1345-1350.

Chapter – 4

Synthesis, characterization, spectral, thermal, DFT, molecular docking and biological studies of benzimidazol-2-ylmethyl)-2-(pyridin-4-yl carbonyl) hydrazine carbothio amide and their Co(II), Ni(II) and Cu(II) complexes



4.1 INTRODUCTION

The benzimidazole moiety is part of the chemical structure of vitamin B₁₂ which is one of the biologically significant naturally occurring compounds [1]. Benzimidazole and its derivatives have involved continuing interest over the years because of their varied biological activities *viz.* anticancer [2], antihypertensive [3], antiviral [4], anti-inflammatory [5] vasodilator [6] and antimicrobial [7-9]. Moreover, as a typical heterocyclic ligand, the large benzimidazole rings not only can afford potential supramolecular recognition sites for π - π stacking interactions, but also act as hydrogen bond acceptors and donors to accumulate multiple coordination geometry [10]. Transition metal complexes containing benzimidazole-based ligand are a subject of intensive research which not only owing to their rich coordination chemistry but also due to a number of established and prospective application areas [11-14] and is responsible for the possibility of further research, such as design of structural probes and the development of novel therapeutics.

The aim of the present work is to deal specifically the coordination properties of N-(*1H*-benzimidazol-2-ylmethyl)-2-(pyridin-4-ylcarbonyl) hydrazine carbothioamide (L) concerning its interactions with Co(II), Ni(II), and Cu(II) complexes, spectral characterization and thermal decomposition studies serve as important tools for the interpretation of structures of molecules and also biological and analytical importance. The molecular docking study have been performed to investigate the interaction and binding energies of the complexes with tyrosinase enzyme by using *HEX 8.0* for antioxidant activity, The compounds were also performed to investigate against the growth of *in vitro* bacteria and pathogenic fungi.

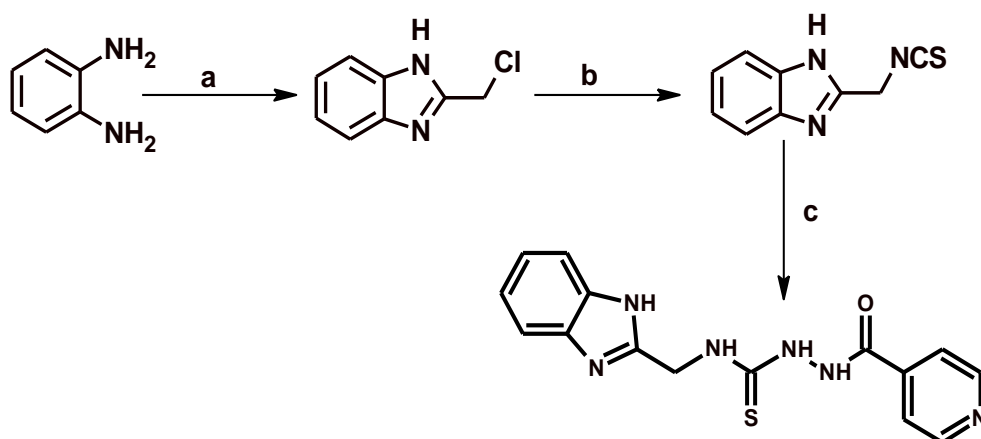
4.2 Experimental

4.2.1 Preparation of N-(*1H*-benzimidazol-2-ylmethyl)-2-(pyridin-4-ylcarbonyl) hydrazine carbothioamide (BPH)

The key intermediate 2-(chloromethyl)-*1H*-benzimidazole was synthesized by following literature method from commercially available benzene-1,2-diamine as reported previously [15-16].

A mixture of 2-(chloromethyl)-1*H*-benzimidazole (0.5 mmol) in 30 mL of dry ethanol was added to a solution of potassium thiocyanate (0.6 mmol) in 10 mL dry ethanol and the reaction mixture was refluxed for 6h, forming isocyanate derivative as an intermediate. After cooling, the white precipitate of potassium chloride was filtered off. To the filtrate solution the isonicotinic hydrazide (0.5 mmol) was added and allowed to reflux with continuous stirring for about 8h. The reaction was monitored by TLC (chloroform: methanol, 0.9:0.2). After completion of the reaction, the solution was poured into crushed ice; the solid so obtained was collected by filtration to afford ligand BPH.

Yellow solid: Yield 72%; mp 181 °C; Anal. Calcd for $C_5H_{14}N_6OS$ (%): C, 56.83; H, 5.30; N, 29.46. Found: C, 55.75; H, 5.19; N, 28.65. IR (KBr): m (cm^{-1}): (-NH) 3380, (-C=N) 1668, (-C=S) 1557, (-C=O) 1520, (-C=C) 1441. 1H NMR (DMSO- d_6) δ (ppm): 7.96-7.25, (m, Ar1H), 8.82 - 8.53 (s -NH 1H), 4.17 - 4.07 (dd- CH_2^1H). MS: m/z 328.96.



Scheme 1. (a) Chloroacetyl Chloride, 5 N HCl, reflux, 4 h; (b) KSCN, EtOH reflux, 6 h; (c) isonicotinic hydrazide reflux, 8h.

4.2.2 Preparation of the Metal Complexes

Hot solution of hydrated metal chlorides [0.1 mmol, Co(II), Ni(II) and Cu(II)] in absolute ethanol was added to the hot solution of the ligand (BPH) (0.2 mmol) in ethanol (25 mL). The resulting solution was stirred under reflux for 5-6 h. The coloured complex precipitated was then collected by filtration and washed with distilled water and hot ethanol. The physical properties and analytical data of the metal complexes are given in table 4.1.

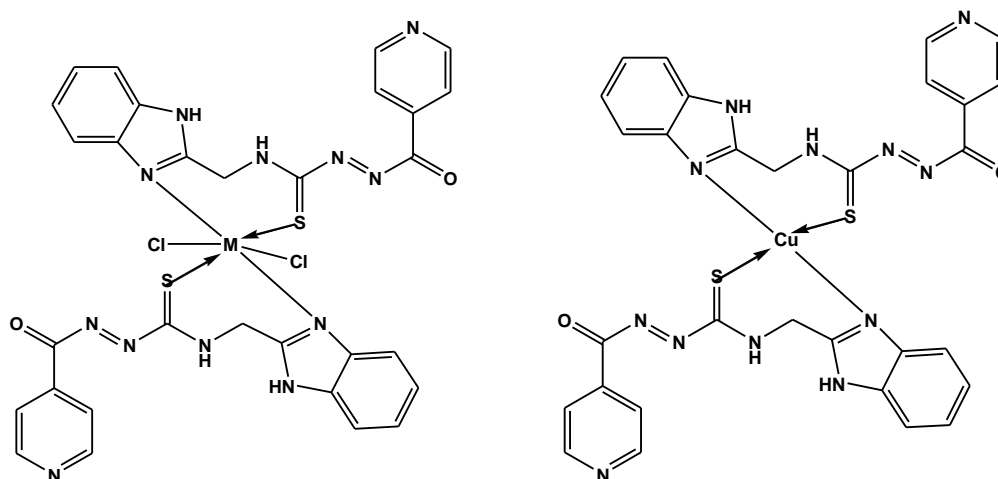


Figure 4.1 Proposed structure of metal complexes [M=Co(II), Ni(II) and Cu(II)]

4.3 Results and discussion

The synthetic route for the new ligand (BPH) is shown in Scheme 1. The complexes were prepared by reaction of BPH with metal halides in the ratio of 1:2 using absolute ethanol. The molar conductance values of the complexes in DMF at a concentration of 10^{-3} M at room temperature are in the range of $31-70 \text{ ohm}^{-1} \text{ cm}^2 \text{ mol}^{-1}$ [17]. For Ni(II) and Cu(II) complexes the molar conductance value is slightly more than expected when compared to non-electrolytic complexes in DMF indicates that, there may be partial dissociation of complexes in DMF solution. In the case of Co(II) complex, high molar conductance value imply uni-uni valent that the complex is electrolytic in nature and the values are presented in Table 4.1.

Table 4.1 Physical properties and analytical data of the metal complexes

Compound	Colour	Mol.Wt	Yield (%)	Calcd. (found) (%)			Molar conductance ($\text{ohm}^{-1} \text{ cm}^2 \text{ mol}^{-1}$)	M.p [$^{\circ} \text{C}$]
				C	H	N		
[CoCl(BPH) ₂].Cl. H ₂ O	Dark green	777.03	65	46.28 (46.13)	3.11 (3.46)	21.59 (21.23)	62.4	298-300
[NiCl ₂ (BPH) ₂].2 H ₂ O	Light blue	776.06	60	46.29 (46.54)	3.11 (3.01)	21.60 (21.10)	21.6	302-305
[CuCl ₂ (BPH) ₂]. H ₂ O	Light brown	711.09	63	50.36 (50.21)	3.40 (3.75)	23.60 (23.80)	14.4	315-31

Table 4.2 Selected structural parameters of BPH

Bond	Bond length (Å)	Angle	(°)	Dihedral angle	(°)
C(6)-H(31)	1.122	C(1)-N(7)-C(8)	107.555	C(1)-N(7)-C(8)	107.555
N(7)-C(8)	1.252	N(7)-C(8)-N(9)	112.905	N(7)-C(8)-N(9)	112.905
C(8)-N(9)	1.451	N(7)-C(8)-C(10)	123.433	N(7)-C(8)-C(10)	123.433
C(8)-C(10)	1.540	N(9)-C(8)-C(10)	123.656	N(9)-C(8)-C(10)	123.656
N(9)-H(35)	1.028	C(2)-N(9)-C(8)	103.752	C(2)-N(9)-C(8)	103.752
C(10)-N(11)	1.446	C(2)-N(9)-H(35)	120.381	C(2)-N(9)-H(35)	120.381
C(10)-H(33)	1.122	C(8)-N(9)-H(35)	120.506	C(8)-N(9)-H(35)	120.506

Frontier molecular orbital analysis

The HOMO-LUMO gap of organic molecules is important because they transmit to particular movements of electrons and may be most generous for single electron transfer. As seen, the HOMO orbital of the ligands is localized on the benzimidazole rings. But the LUMO orbital is mainly localized on the isonicotinic hydrazide ring and its substitutions. It has been found that molecules with large HOMO-LUMO gap are highly stable and unreactive; while those with small gaps are generally reactive [19]. By calculating the HOMO-LUMO energy gap, one can easily determine the excitation energy of an organic derivative at its ground state [20].

HOMO-LUMO gap of ligand BPH are shown in figure 4.4, since in the ligand electronic transition from HOMO orbitals to the LUMO orbitals is $\pi \rightarrow \pi^*$ transitions. Energy separation between the HOMO and LUMO ($\Delta\varepsilon = \varepsilon_{\text{LUMO}} - \varepsilon_{\text{HOMO}}$) of QB is 7.995 eV respectively.

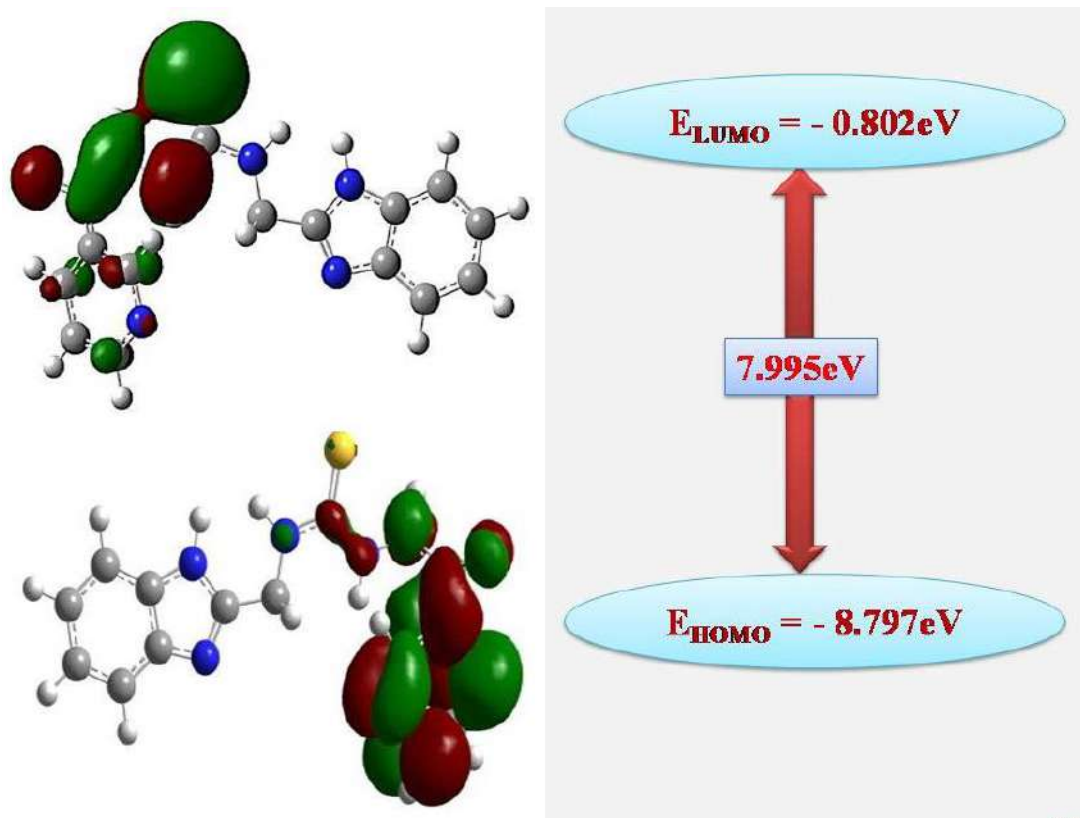


Figure 4.4 HOMO LUMO frontier orbitals of the BPH

4.3.2 ^1H NMR and Mass Spectral studies

^1H NMR spectrum of the BPH recorded in DMSO-d_6 is showed in figure 4.5, confirm its structure by displaying a singlet in the range in between 8.82 and 8.53 ppm for secondary amine hydrogen of imidazole ring. The multiplets observed in the range of 7.96–7.25 ppm are assigned to aromatic protons of both imidazole and isonicotinic hydrazide rings and two doublets in the region 4.17–4.07 ppm for $-\text{CH}_2$ protons. The ^1H NMR spectrum of the Ni(II) complex gave the resonance in the range 12.35 to 13.11 ppm, which indicates shifting of $-\text{NH}$ protons and also appearance of multiplets due to aromatic protons in the range 7.14 to 8.21 ppm as it shown in the figure 4.6. The mass spectrum of the BPH and its Cu(II) complex is depicted in figure 4.7 and 4.8 respectively. The spectrum showed a molecular ion peak at m/z 328.96, which is almost equivalent to the expected.

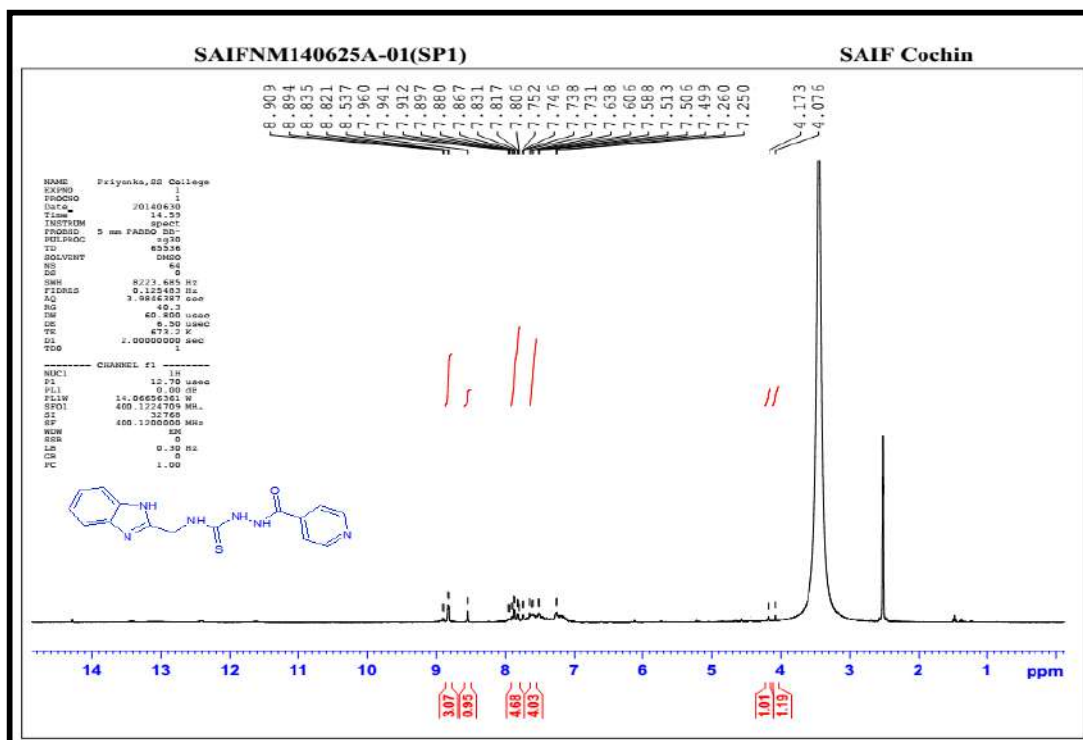
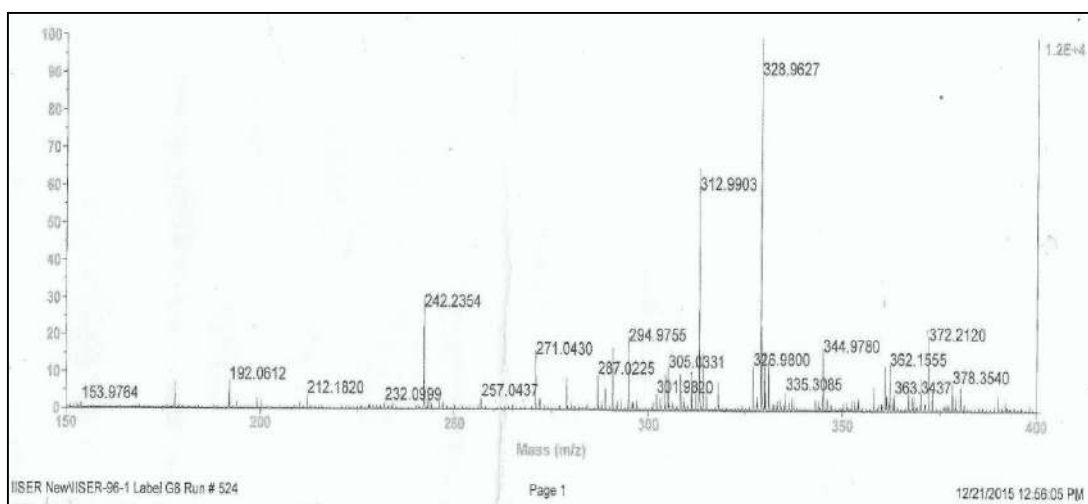
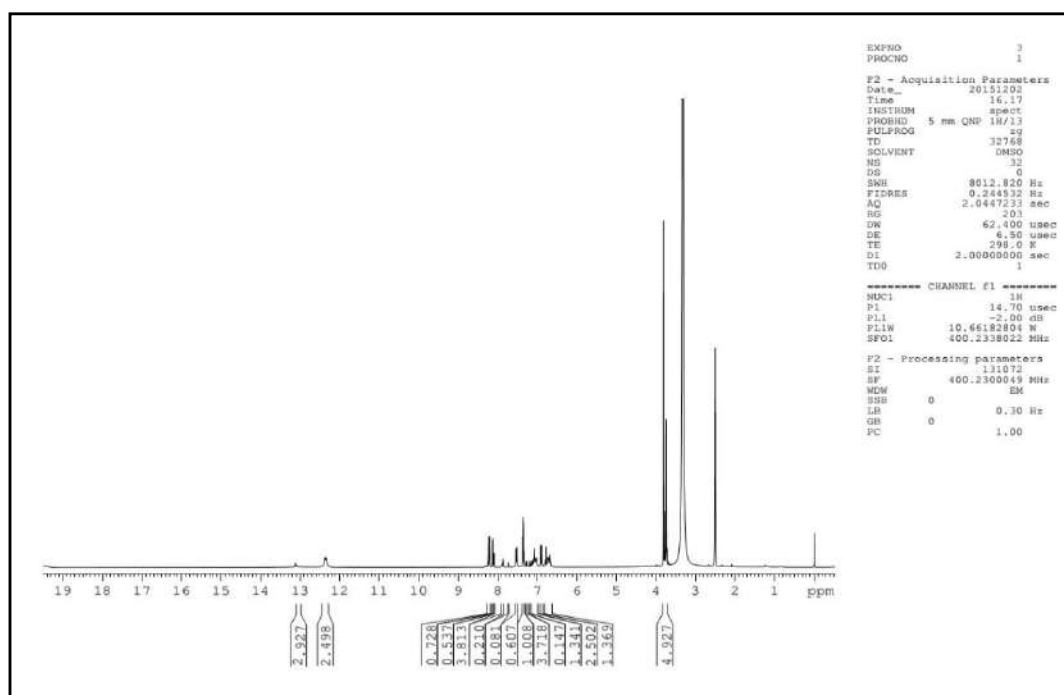
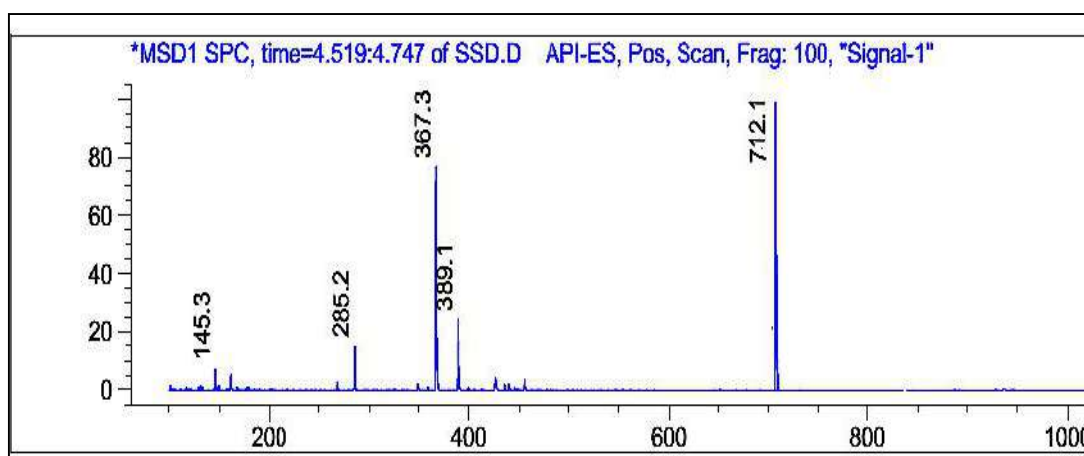
Figure 4.5 ^1H NMR spectrum of the BPH

Figure 4.6 Mass spectrum of the BPH

Figure 4.7 ^1H NMR spectrum of $[\text{NiCl}_2(\text{BPH})_2] \cdot 2\text{H}_2\text{O}$ Figure 4.8 Mass spectrum of $[\text{CuCl}_2(\text{BPH})_2] \cdot \text{H}_2\text{O}$

4.3.3 IR spectral studies

The prominent IR frequencies of the BPH and metal complexes are presented in table 4.3 and figure 4.9. The characteristic bands of the ligand are appeared 3380 cm^{-1} $\nu(-\text{NH})$ of benzimidazole ring, 1668 cm^{-1} $\nu(-\text{C}=\text{N})$, 1557 cm^{-1} $\nu(-\text{C}=\text{O})$, of isonicotinic hydrazide, 1520 cm^{-1} $\nu(-\text{C}=\text{S})$ and 1441 cm^{-1} $\nu(\text{C}=\text{C})$ of ligand indicates that the isocyanate intermediate compound was formed by condensation from isoniazid. The IR spectrum of the metal complexes showed that

the band at 1668 cm^{-1} assigned to the $\nu(\text{-C=N})$ vibration of the ligand and it is shifted to lower frequency 1611 , 1617 , and 1604 cm^{-1} after complexation with the Co(II) , Ni(II) and Cu(II) metal ions respectively. This shift indicates the coordination of the ligand to the metal ions through nitrogen of isonicotinic hydrazide. As similar to this, $\nu(\text{-C=S})$ band observed at 1520 cm^{-1} is shifted to lower frequency, suggesting a weak (-C=S) stretching vibration, this confirms that the coordination of the metal complexes has taken place through M-N and M-S atoms of the ligand [21-25].

Table 4.3 Characteristic IR bands of the ligand and its complexes

Compound	$\nu(\text{NH})$	$\nu(\text{C=N})$	$\nu(\text{C=O})$	$\nu(\text{C=S})$	$\nu(\text{C=C})$	$\nu(\text{M-N})$	$\nu(\text{M-S})$
BPH	3380	1668	1557	1520	1441	740	687
[CoCl(L)₂]Cl. H₂O	3267	1611	1555	1450	1381	742	691
[NiCl₂(L)₂].2H₂O	3393	1617	1618	1468	1353	743	698
[CuCl₂(L)₂].H₂O	3265	1604	1608	1372	1320	742	697

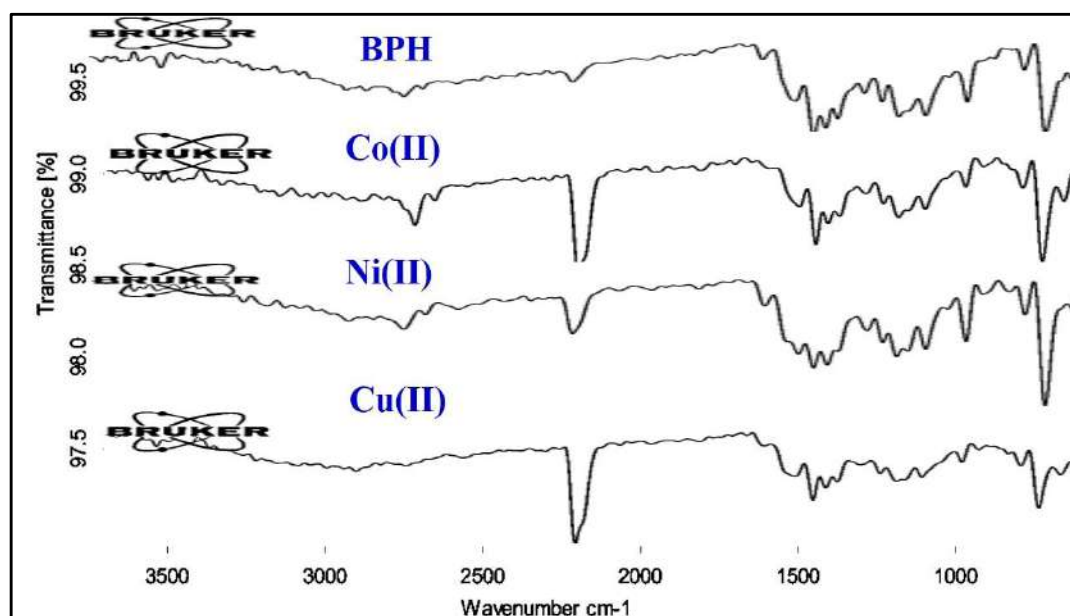


Figure 4.9 IR spectra of BPH and their metal complexes

4.3.4 Electronic Spectral Studies

The UV-visible spectral data of the ligand and their Co(II) , Ni(II) and Cu(II) complexes are given in the figure 4.10. The electronic spectra of the free ligand

showed two adsorption bands in the region of 280 to 310 nm due to $\pi \rightarrow \pi^*$ transition. The visible spectra of all the complexes in DMF displayed clear bands in the range of 535 to 785 nm and the broad low laying shoulder at 380 to 420 nm due to the red shift showed $\pi \rightarrow d_{x^2-y^2}$ LMCT transition in all complexes [26]

UV-visible spectrum of the Co(II) complex exhibited an electronic transition at $24,390 \text{ cm}^{-1}$ (410 nm) and another at $18,518 \text{ cm}^{-1}$ (540 nm) may be assigned to ${}^4A_2, {}^4E \rightarrow {}^4A_2(P)$ and ${}^4A_2, {}^4E \rightarrow {}^4E(P)$ respectively [27]. The molar conductance also shows that uni-univalent electrolytic behavior in DMF hence the complex is expected to have square pyramidal geometry. The Ni(II) complex showed the bands at $16,393 \text{ cm}^{-1}$ (610 nm) and $25,000 \text{ cm}^{-1}$ (400 nm) due to ${}^3A_{2g}(F) \rightarrow {}^3T_{1g}(F)$ (ν_2) and ${}^3A_{2g}(F) \rightarrow {}^3T_{1g}(P)$ (ν_3) respectively. The conductance measurement values indicate that the complex is non-electrolytic behavior therefore the structure of the complex is tentatively proposed to have octahedral geometry [28]. The electronic spectra of Cu(II) complex showed a low intensity broad band around $24,390 \text{ cm}^{-1}$ (410nm) and $13,517 \text{ cm}^{-1}$ (760nm) nm assignable to ${}^2E_g \rightarrow {}^2T_{2g}$ transition (d^9), [29] which are due to tetragonal geometry.

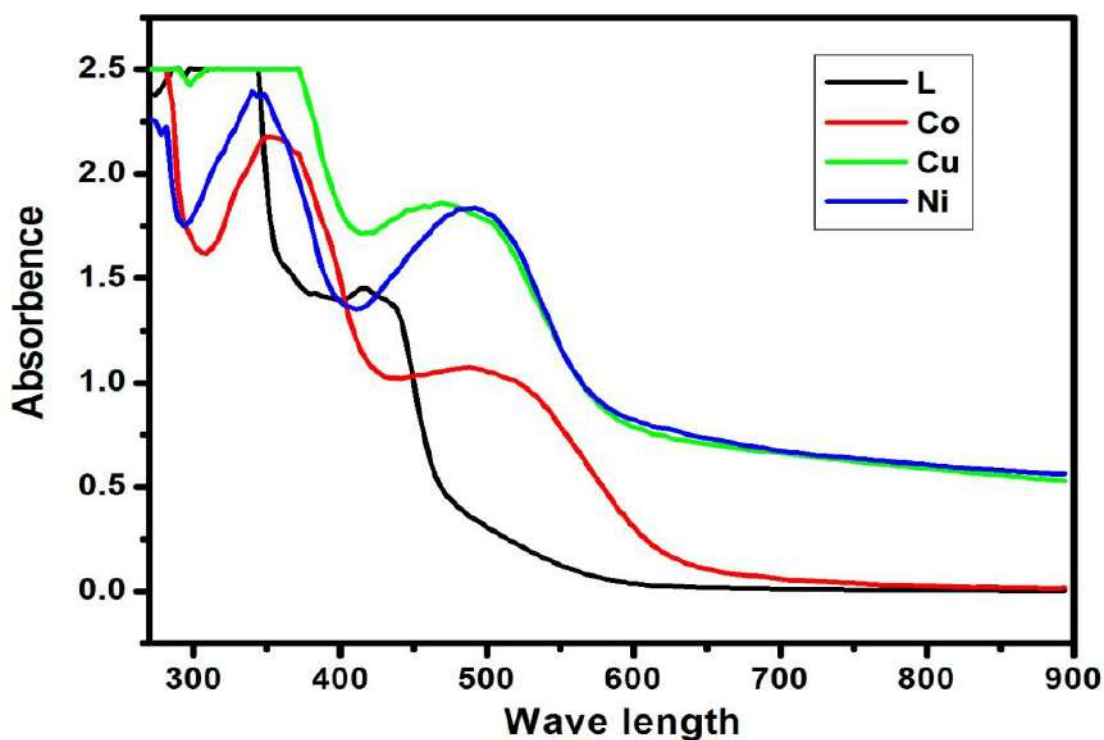


Figure 4.10 Electronic absorption spectrum of BPH and their metal complexes

4.3.5 Thermal studies of the metal complexes

The thermal behavior of Co (II), Ni (II) and Cu (II) complexes has been studied in the temperature range 50-800 °C as represented in figure 4.11 and the data tabulated table 4.4.

The Co(II) complex exhibits decomposition in three steps. The first step of decomposition occurs in the temperature range of 30-90 °C by mass loss of 4.81 % (Calcd. mass loss 4.01 %) for a molecule water of hydration. The second and third steps found within the range 250-310 °C and 420-850 °C with an estimated mass loss 81.92 % (Calcd. Mass loss 81.00 %) which are responsible for decomposition of the remaining organic part (C₅H₁₄N₆OS) and finally leaving CoO as a residue. Ni(II) complex exhibits thermal decomposition in two steps. The first step estimated mass loss of 8.63 % (Calcd. mass loss 8.90 %) in the temperature range of 30-110 °C corresponds to the loss of two lattice water molecules. The second step found within the range 290-900 °C with an estimated overall mass loss 73.99 % (Calcd. Mass loss 72.27 %) which is responsible for decomposition of the remaining part of the ligand (C₅H₁₄N₆OS) leaving behind NiO as the residue. The TGA for Cu(II) chelate represent three steps. The first step of decomposition within the temperature range 30–140 °C corresponds to the loss of two lattice water molecules with a mass loss of 14.91% (calcd. mass loss 14.30%).

The another step of decomposition takes place at 270-850 °C corresponds to the removal of the ligand (C₅H₁₄N₆OS) and finally leaving behind CuO as residue.

Table 4.4 Thermogravimetric data of Co(II), Ni(II) and Cu(II) complexes.

Complexes	TG range [°C]	Estimated (calcd.) %	Total mass loss	Metallic Residue (n*)
[CoCl(BPH) ₂]Cl. H ₂ O	30-90 280-850	4.81 (4.05) 81.92 (81.00)	86.73 (85.11)	CoO (3)
[NiCl ₂ (BPH) ₂].2H ₂ O	30-110 290-900	8.63 (8.09) 73.99 (72.27)	82.62 (80.36)	NiO (2)
[CuCl ₂ (BPH) ₂].H ₂ O	30-140 270-850	14.91 (14.30) 70.31 (68.11)	85.22 (83.21)	CuO (3)

n* = number of decomposition steps

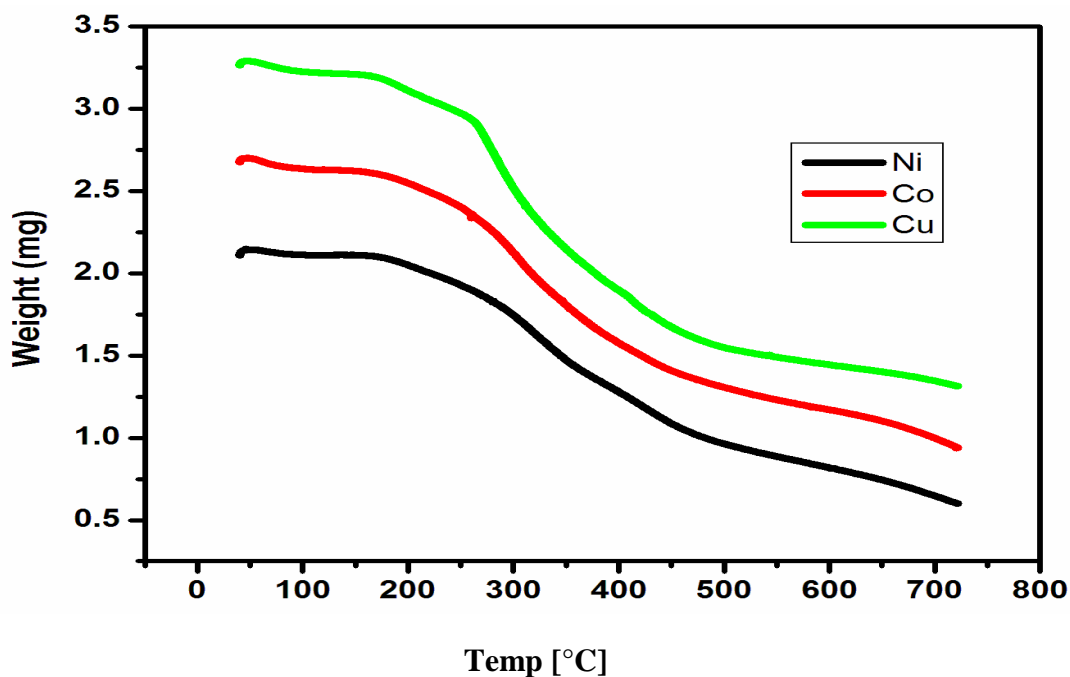
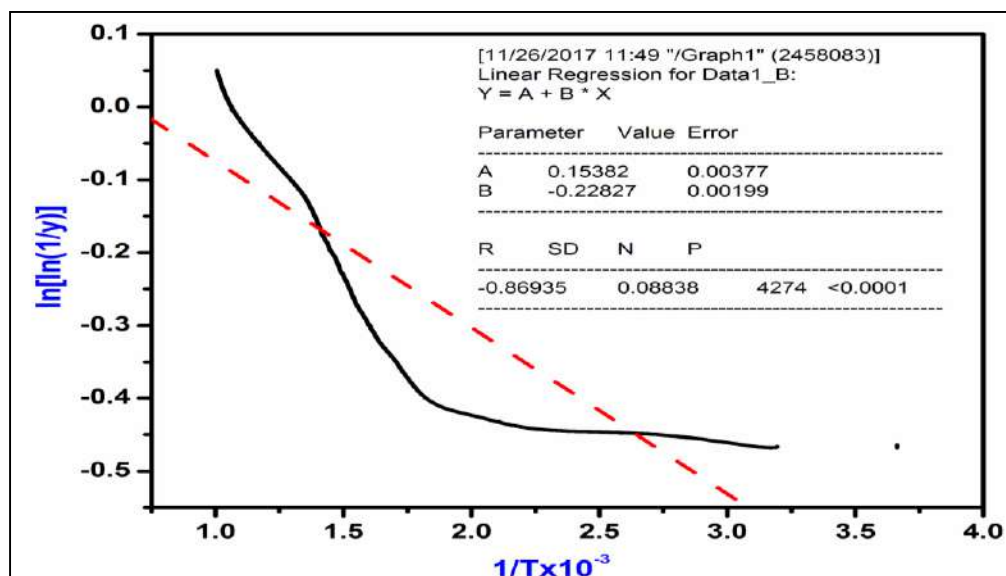
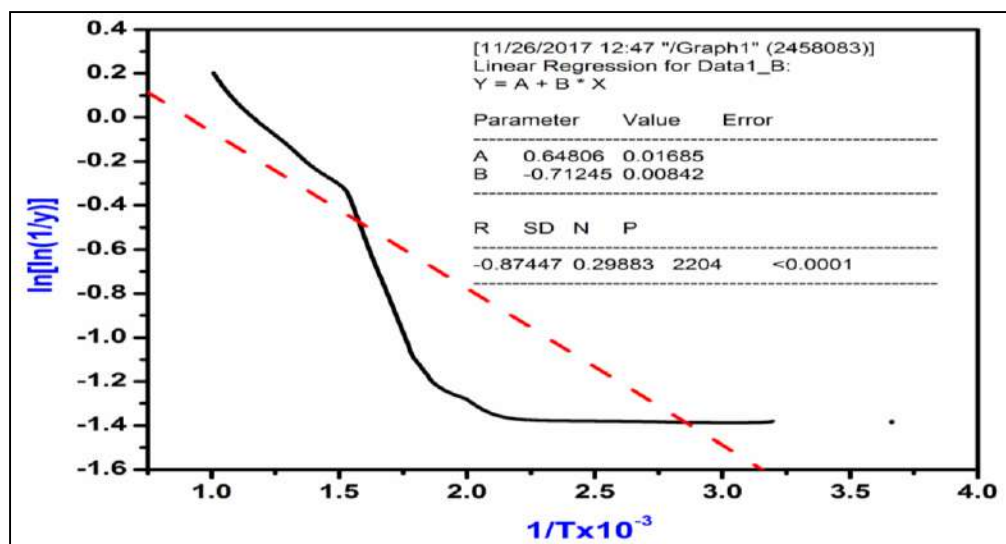


Figure 4.11 Thermogravimetric (TGA/DTG) curves of metal complexes

The degradation method, kinetic and thermodynamic parameters of the Ni(II) and Cu(II) metal complexes has been evaluated by Broido's graphical method for straight line decomposition portion of the thermodynamic analytical curve [30]. Energy of activation (E_a) were calculated by the slope of $-\ln(\ln(1/y))$ versus $1/T \times 10^{-3}$. The thermodynamic properties like change in enthalpy (ΔH), entropy (ΔS), free energy (ΔG) and frequency factor ($\ln A$) are calculated using the standard equations by employing the Broido's relation: $-\ln[\ln(1/y)] = E_a/RT_d - \ln A - \ln(8.314/T_d)$. Where y is the fraction of the complex un-decomposed, T_d is the decomposition temperature, R is the gas constant and E_a is the activation energy in kJ mol^{-1} .

Table 4.5 Thermal and Kinetic parameters of Ni(II) and Cu(II) metal complexes

Compounds	Decomposition temperature [°C]	E_a [kJ mol^{-1}]	Frequency factor $\ln A$ [min^{-1}]	ΔH [kJ mol^{-1}]	ΔS [J/K]	ΔG [kJ mol^{-1}]
[NiCl ₂ (BPH) ₂].2H ₂ O	347.86	18.215	15.271	2.378	-57.8	11.7
	378.77	19.662	8.691	6.190	-19.4	39.2
[CuCl ₂ (BPH) ₂].H ₂ O	212.72	6.7752	6.2542	4.9053	-144.3	32.05
	303.76	5.7143	5.7411	6.0241	-156.3	41.03

Figure 4.12 Linear fit graphs of $[\text{NiCl}_2(\text{BPH})_2] \cdot 2\text{H}_2\text{O}$ Figure 4.13 Linear fit graphs of $[\text{CuCl}_2(\text{BPH})_2] \cdot \text{H}_2\text{O}$

The TGA and kinetic parameters the Ni(II) and Cu(II) metal complexes are tabulated table 4.5 and represented in figure 4.12 and 4.13. The major weight loss for all the complexes was found in the temperature range 212 – 378. °C. The Ni(II) complex showed very high activation energies and rapid degradation of 19.662 and 18.215 kJmol^{-1} , the Cu (II) complex showed least activation energies. The negative values of ΔS indicated that the decomposition reactions are slower than normal. The positive sign of ΔG values for the complexes indicate that the free energy of the final residue is higher than that of the initial compound and all the decomposition steps are non-spontaneous processes.

4.4 Procedures of biological studies

4.4.1 Molecular Docking Studies

The docking is a method which involves the prediction of ligand conformation and orientation in the binding receptacle of the receptor. All the synthesized compounds were screened for docking analysis carried out with antioxidant strain tyrosinase enzyme (PDB ID: 3NM8) from *Bacillus megaterium* by HEX 8.0 and compared with uncoordinated ligand. The receptor was downloaded from RCSB protein data bank. Docking was performed with HEX 8.0 [31-33], by SP Fourier Transform, FFT steric scan, FFT final search and MM refinement. A more negative E-total energy value implies that a strong binding interaction exists between drug and receptor which leads to the inhibition of receptor activity.

The enzyme structure containing hetero molecules were removed before docking was carried out. The corresponding CIF files of derivatives were converted into PDB file using Argus lab [34, 35]. The ligands were converted to 2D and 3D energy-minimized conformations using Hex 3D Ultra 8.0 and the conformation was visualized using Acceryl Discovery Studio 3.1 Client.

4.4.2 Antioxidant Activity studies

The free radical scavenging activity of the fractions was measured *in vitro* by 2, 2- diphenyl-1-picrylhydrazyl (DPPH) assay according to the method described in the reports [36, 37]. The stock solution was prepared by dissolving 24 mg DPPH with 100 mL methanol and stored at 20 °C until required. The working solution was obtained by diluting DPPH solution with methanol to attain an absorbance of about 0.98 ± 0.02 at 517 nm using the spectrophotometer. A 3 mL aliquot of this solution was mixed with 100 μ L of the sample at various concentrations (10 - 500 μ g/ml). The reaction mixture was shaken well and incubated in the dark for 15 min. at room temperature. Then the absorbance was measured at 517 nm. The control was prepared as above without the sample.

$$\text{Scavenging ratio (\%)} = [(A_i - A_o) / (A_c - A_o)] \times 100\%$$

Where A_i is the absorbance in the presence of the test compound; A_o is absorbance of the blank in the absence of the test compound; A_c is the absorbance in the absence of the test compound.

4.4.3 Antimicrobial Activity

***In vitro* antibacterial and antifungal studies**

The *in-vitro* antibacterial and antifungal activity of the ligand and their metal complexes was determined by well plate method [38-41]. The following Gram positive and negative bacteria were used as test organism *Escherichia coli*, *Bacillus subtilis* and *Salmonella typhi* and fungal strains are *Candida albicans*, *Aspergillus flavus* and *cladosporium* to investigate the activity. The test compounds were dissolved in dimethyl sulfoxide (DMSO) at a concentration of 25, 50 and 100µ/mL and incubated at 37 °C for 24 h for bacteria and 38 h for fungi, the diameter of the zone of inhibition around each well plate was measured after the incubation period.

4.3.4 Anti-lipase assay

Method:

Lipase inhibitory activity of different concentrations of methanol extract was tested by mixing 100µL of each concentration of methanol extract, 8mL of oil emulsion and 1mL of chicken pancreatic lipase followed by incubation of 60 minutes. The reaction was stopped by adding 1.5 mL of a mixture solution containing acetone and 95% ethanol (1:1). The liberated fatty acids were determined by titrating the solution against 0.02M NaOH (standardized by 0.01M oxalic acid) using phenolphthalein as an indicator.

Percentage inhibition of lipase activity was calculated using the formula: Lipase inhibition = $A - B/A \times 100$, where A is lipase activity, B is activity of lipase when incubated with the sample.

[4.5] Results and discussion of biological studies

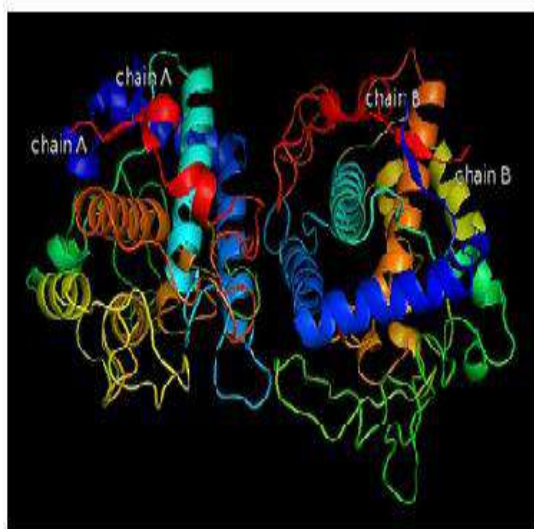
4.5.1 Molecular Docking Studies

Molecular docking analysis of all the compounds have been carried out against protein receptor tyrosinase enzyme (PDB ID: 3NM8) from *Bacillus megaterium*, in order to rationalize the obtained biological data and to explain the possible interactions that might takes place with the amino acid residue.

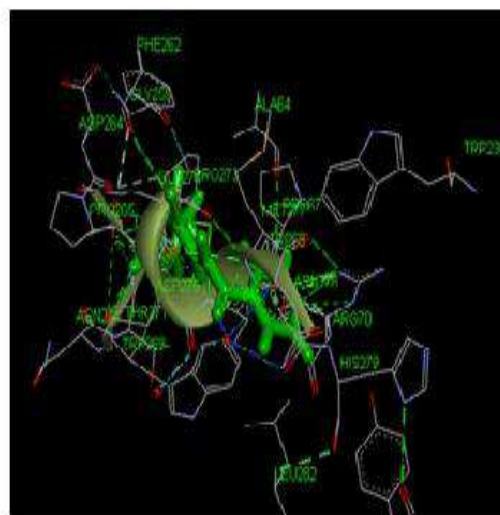
Table 4.6 Docking study results of the BPH and their metal complexes

Compounds	Total energy value (E-total)
BPH	-221.80
[CoCl(BPH) ₂]Cl. H ₂ O	-287.27
[NiCl ₂ (BPH) ₂].2H ₂ O	-281.88
[CuCl ₂ (BPH) ₂].H ₂ O	-286.24

It can be concluded that the receptor with metal complexes fits best with the highest binding energy for the compounds [CoCl(BPH)₂]Cl. H₂O (energy value -287.27 KJ/mol⁻¹), followed by [NiCl₂(BPH)₂].2H₂O (energy value -281.88 KJ/mol⁻¹), and [CuCl₂(BPH)₂].H₂O (energy value -286.24 KJ/mol⁻¹). The uncoordinated ligand showed least binding energy with energy value of -221.80 KJ/mol⁻¹. The docking studies showed that Tyr267A, Pro268A, Ala44A, Leu282, Tyr267B His60, and Pro268B amino acids in the tyrosinase enzyme (PDB ID: 3NM8) may play major role in substrate binding or catalysis and given Figure 4.14 and table 4.6.



(A)



(B)

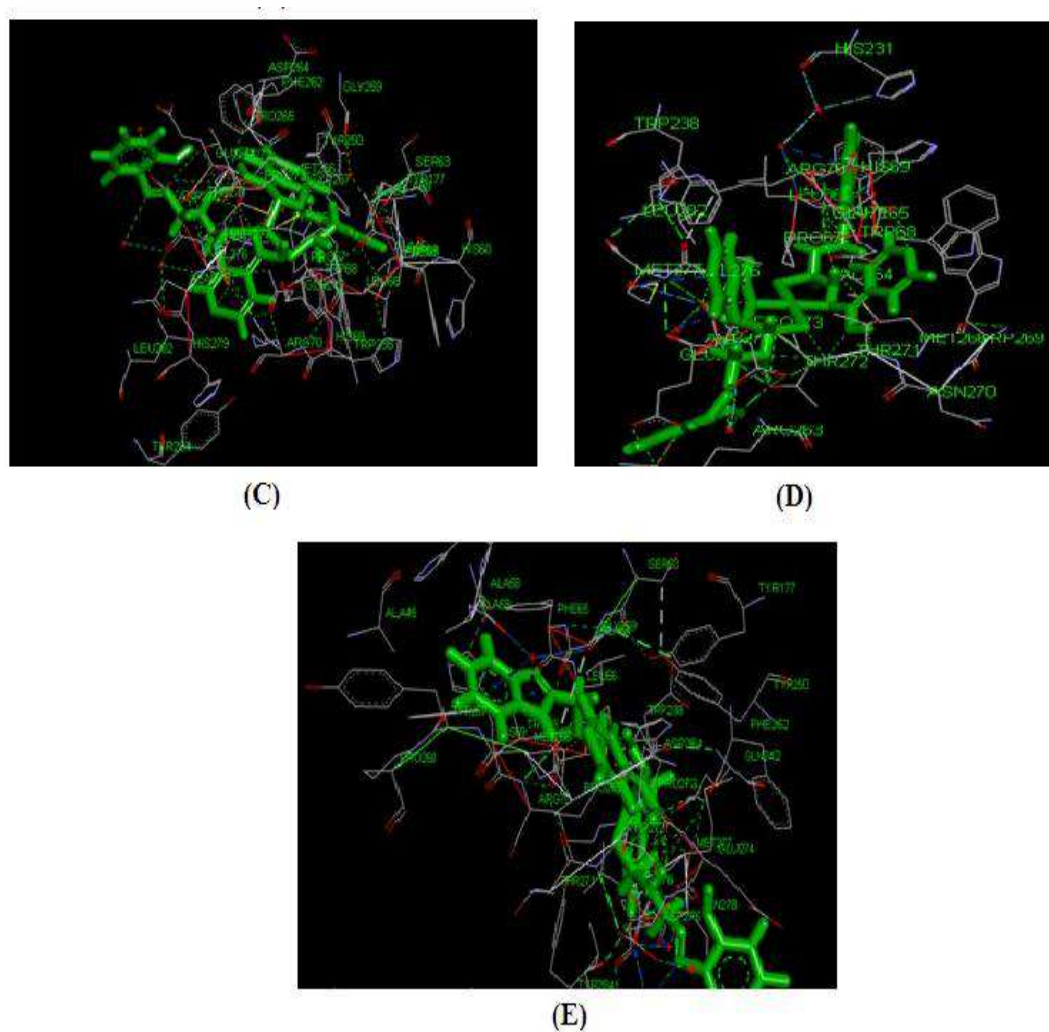


Figure 4.14 3-Dimensional (3D) interactions of BPH and their complexes (A) Tyrosinase enzyme (PDB ID: 3NM8) from *Bacillus megaterium*. (B) $[\text{CoCl}(\text{BPH})_2]\text{Cl} \cdot \text{H}_2\text{O}$ (C) $[\text{NiCl}_2(\text{BPH})_2] \cdot 2\text{H}_2\text{O}$ and (D) $[\text{CuCl}_2(\text{BPH})_2] \cdot \text{H}_2\text{O}$.

4.5.2 Antioxidant Activity

According to relevant literature reports [42, 43] some transition metal complexes exhibit potential antioxidant activity therefore, the free radical scavenging activity of all compounds was measured using the DPPH method. The ascorbic acid was used as the standard. The tested compounds showed significant DPPH scavenging activity (>60%) at 100 mg concentration (figure 4.15). All complexes exhibited potent scavenging activity, among them Cu(II) and Ni(II) complexes showed highest scavenging activity compared with the standard excepting the ligand which showed slightly lower activity than those of the complexes.

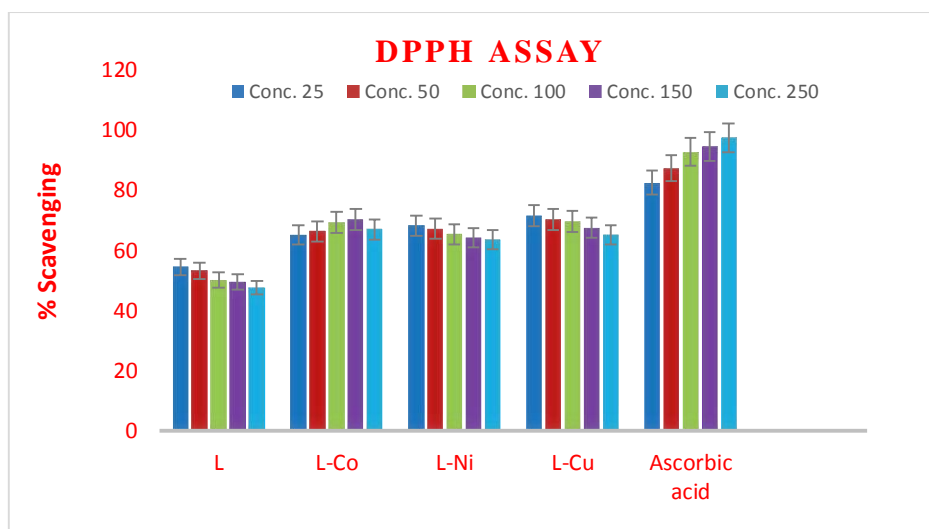


Figure 4.15 Radical scavenging activities of the BPH and their complexes

4.5.3 Antimicrobial Activity

In vitro antibacterial and antifungal assay

The results of the tested compounds shown in tables 4.7 and 4.8 indicate that all the complexes exhibit higher inhibition efficiency than the free ligand against various tested microbial strains. The chelation reduces the polarity of the ligand due to the overlap of the ligand orbitals and partial sharing of the positive charge of the metal ions with donor groups. Further, it increases the delocalization of π -electrons over the whole chelate ring and enhances the lyophilic nature of the complexes [44, 45].

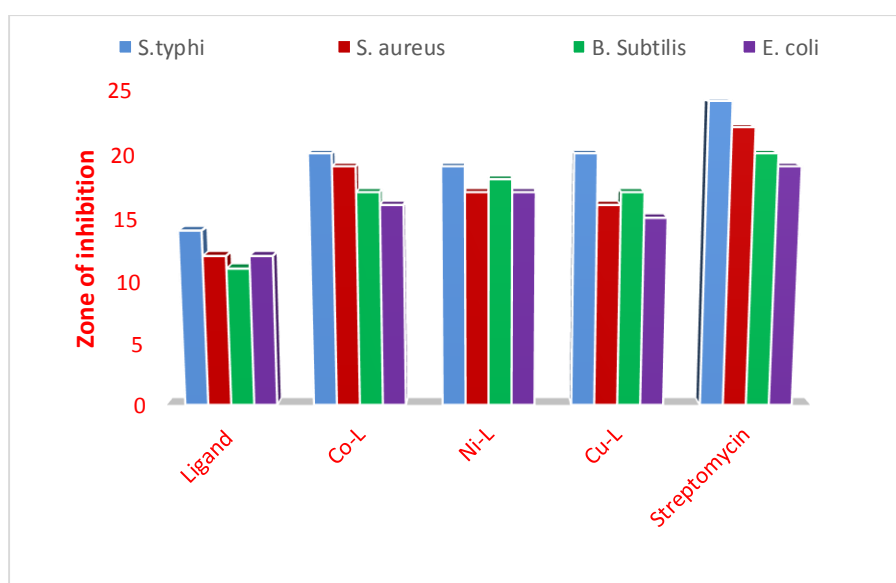


Figure 4.16 Antibacterial activities of BPH and their metal complexes

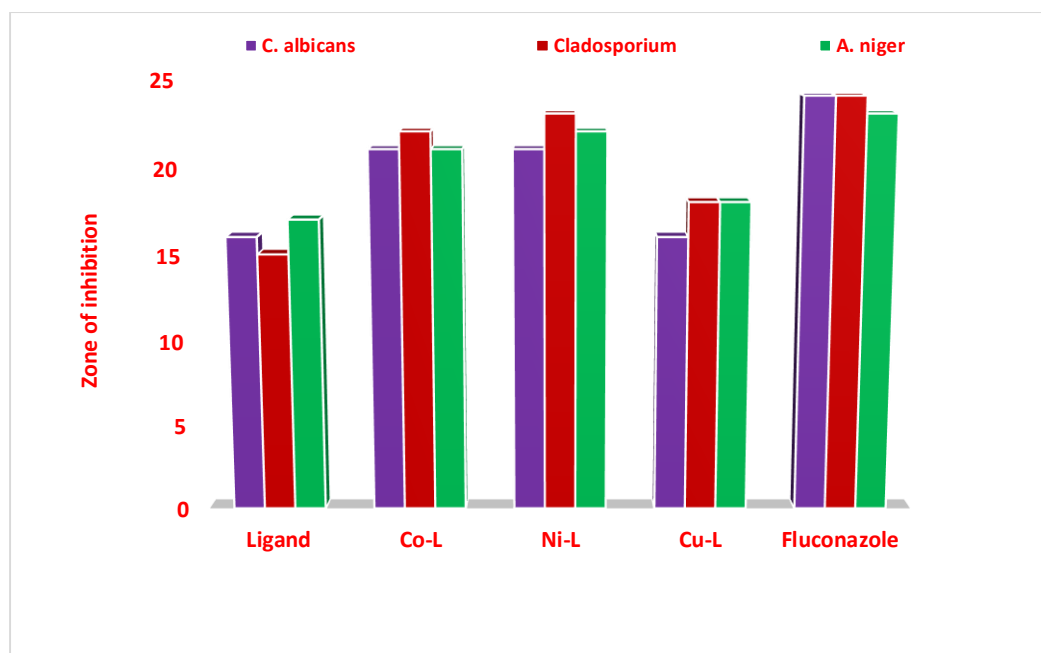


Figure 4.17 Antifungal activities of BPH and their metal complexes

The chelating tends to make the benzimidazole derivatives to act as more powerful and potent bacteriostatic agents, thus inhibiting the growth of bacteria and fungi. The Co(II), Ni(II) and Cu(II) complexes exhibit eminent efficiency than the free ligand compared to standard drug Streptomycin for bacterial activity. For fungal activity the Co(II) and Ni(II) complexes shows good efficiency than that of Cu(II) complex and free ligand when compared to the standard drug Fluconazole as represented in figure 4.16 and 4.17.

Table 4.7 Antimicrobial results of BPH and their metal complexes

Compounds	Conc(μgml^{-1})	% inhibition against bacteria			
		<i>S.typhi</i>	<i>S. aureus</i>	<i>B. Subtilis</i>	<i>E. coli</i>
BPH	25	08 \pm 0.3	05 \pm 0.5	04 \pm 0.3	06 \pm 0.3
	50	06 \pm 0.5	03 \pm 0.2	02 \pm 0.1	04 \pm 0.5
	100	04 \pm 0.5	04 \pm 0.5	04 \pm 0.5	04 \pm 0.5
[CoCl(BPH)₂]Cl. H₂O	25	11 \pm 0.1	09 \pm 0.2	13 \pm 0.1	12 \pm 0.2
	50	13 \pm 0.4	12 \pm 0.6	12 \pm 0.3	13 \pm 0.4
	100	20 \pm 0.3	16 \pm 0.4	17 \pm 0.4	16 \pm 0.4
[NiCl₂(BPH)₂].2H₂O	25	12 \pm 0.5	11 \pm 0.5	13 \pm 0.1	12 \pm 0.5
	50	14 \pm 0.4	13 \pm 0.4	14 \pm 0.3	10 \pm 0.4
	100	19 \pm 0.4	17 \pm 0.3	16 \pm 0.2	10 \pm 0.4
[CuCl₂(BPH)₂].H₂O	25	12 \pm 0.5	11 \pm 0.2	13 \pm 0.3	12 \pm 0.3
	50	13 \pm 0.3	12 \pm 0.1	14 \pm 0.2	13 \pm 0.4
	100	20 \pm 0.4	16 \pm 0.3	17 \pm 0.4	15 \pm 0.2
Streptomycin	25	12 \pm 0.1	11 \pm 0.2	13 \pm 0.3	12 \pm 0.5
	50	15 \pm 0.4	14 \pm 0.2	15 \pm 0.3	14 \pm 0.4
	100	24 \pm 0.5	18 \pm 0.5	18 \pm 0.4	17 \pm 0.2

Table 4.8 Antimicrobial results of BPH and their metal complexes

Compounds	Conc(μgml^{-1})	% inhibition against fungi		
		<i>C. albicans</i>	<i>Cladosporium</i>	<i>A. niger</i>
[CoCl(BPH)₂]Cl. H₂O	25	13 \pm 0.3	12 \pm 0.3	11 \pm 0.3
	50	15 \pm 0.4	13 \pm 0.1	14 \pm 0.4
	100	22 \pm 0.5	23 \pm 0.2	20 \pm 0.2
[NiCl₂(BPH)₂].2H₂O	25	12 \pm 0.3	11 \pm 0.5	10 \pm 0.3
	50	14 \pm 0.2	14 \pm 0.1	13 \pm 0.4
	100	21 \pm 0.5	22 \pm 0.6	21 \pm 0.1
[CuCl₂(BPH)₂].H₂O	25	10 \pm 0.3	10 \pm 0.5	10 \pm 0.3
	50	12 \pm 0.2	12 \pm 0.2	11 \pm 0.1
	100	18 \pm 0.4	19 \pm 0.2	19 \pm 0.2
Fluconazole	25	13 \pm 0.3	12 \pm 0.5	12 \pm 0.3
	50	16 \pm 0.5	15 \pm 0.2	15 \pm 0.1
	100	23 \pm 0.5	24 \pm 0.5	23 \pm 0.5

4.5.4 Anti-lipase assay

Lipase inhibitory activity of different concentrations (1mg, 2mg) for the ligand and their metal complexes was carried out. The ligand showed lesser activity compared to Co(II), Ni(II) and Cu(II) metal complexes. The result indicates that the Co(II) and Ni(II) ion coordinated to the ligand play an important role in the physiological activity, most likely as a result of good conjugation of imidazole and isonicotinic hydrazide ring. The complex is conducive to form interaction between chicken pancreatic lipase enzymes. The interactions found, are π - π stacking interaction and σ - π interaction. Therefore, Co(II) and Ni(II) complexes have the strongest inhibitory activity compared with the Cu(II) complex and the free ligand.

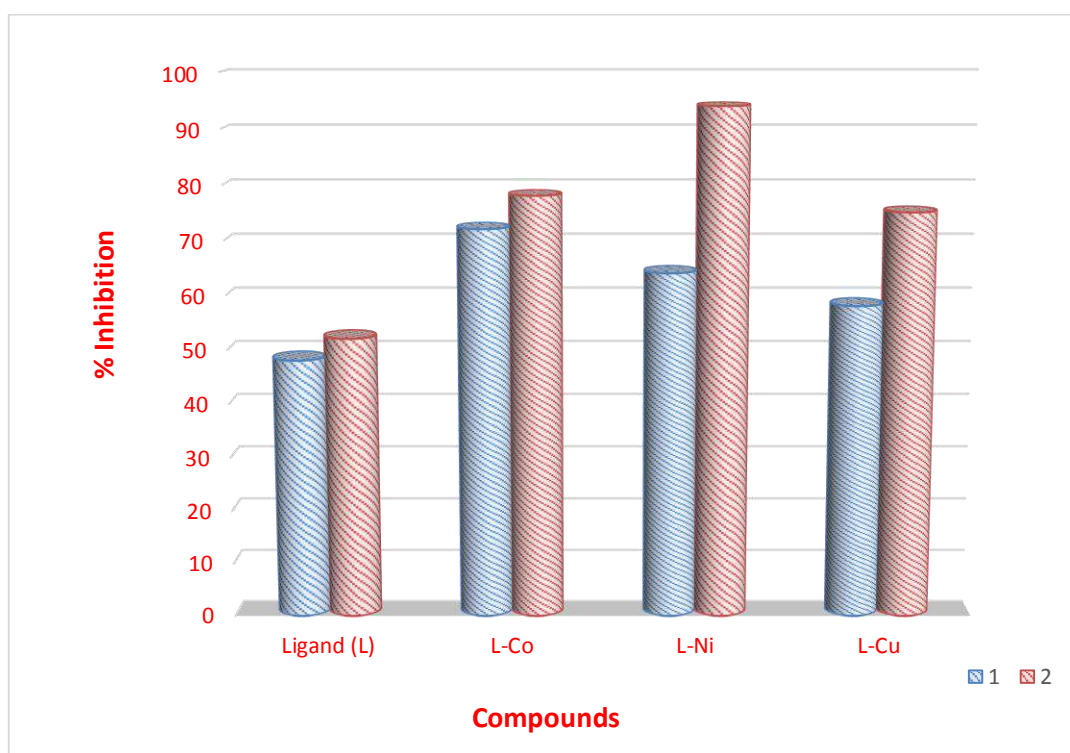


Figure 4.18 Graphical representation of anti-lipase assay

4.6 Conclusion

A series of Co(II), Ni(II) and Cu(II) metal complexes with new N-(*1H*-benzimidazol-2-ylmethyl)-2-(pyridin-4-ylcarbonyl)hydrazinecarbothioamide (BPH) have been successfully prepared and characterized by using various spectral and analytical techniques. The structure of the ligand was established by ¹H NMR, LCMS followed by IR, UV-visible spectroscopy and thermal studies indicate that the ligand is coordinated through N and S atoms, The theoretical study using DFT/B3LYP supports experimental evidences of the bonding sites of the BPH, geometry and the stability of the complexes. All the complexes and BPH were screened for DPPH free radical scavenger activity. The results revealed that, among the complexes [CuCl₂(BPH)₂].2H₂O and [NiCl₂(BPH)₂].2H₂O exhibited good scavenging property than the [CoCl(BPH)₂].Cl. H₂O and free ligand. The antibacterial and antifungal studies reveal that, the ligand and metal complexes were found to be highly active due to existence of imidazole moiety along with the metal ions. The comparative docking studies was also carried out on synthesized ligand and its metal complexes indicate higher binding energy for [CoCl(BPH)₂].Cl. H₂O and less binding energy for [NiCl₂(BPH)₂].2H₂O and [CuCl₂(BPH)₂].2H₂O complexes with the tyrosinase enzyme (PDB ID: 3NM8).

References

- [1] R.M. Acheson, *An Introduction to the Chemistry of Heterocyclic Compounds*, third ed., Wiley India Pvt Ltd New Delhi, 2008, 1-3.
- [2] H.M. Refaat, Synthesis and anticancer activity of some novel 2-substituted benzimidazole derivatives, *Eur. J. Med. Chem.* 45, 2010, 2949-2956.
- [3] G.A. Kilgil, N. Altanlar, Synthesis and antimicrobial activities of some new benzimidazole derivatives, *IL Farm.* 58, 2003, 1345-1350.
- [4] C. Kus, A.G. Kilgil, B.C. Eke, M. Iscan, Synthesis and antioxidant properties of some novel benzimidazole derivatives on lipid peroxidation in the rat liver, *Arch. Pharm. Res.* 27, 2004, 156-163.
- [5] K. Bahrami, M.M. Khodaei, F. Naali, Mild and highly efficient method for the synthesis of 2-arylbenzimidazoles and 2-arylbenzothiazoles, *J. Org. Chem.* 73, 2008, 6835-6837.
- [6] H.B. El-Nassan, Synthesis, antitumor activity and SAR study of novel [1,2,4] triazino [4,5-a] benzimidazole derivatives, *Eur. J. Med. Chem.* 53, 2012, 22-27.
- [7] R. Sawant, D. Kawade, Synthesis and biological evaluation of some novel 2-phenyl benzimidazole-1-acetamide derivatives as potential anthelmintic agents, *Acta Pharm.* 61, 2011, 353-361.
- [8] B. Zhou, B. Li, W. Yi, X. Bu, L. Ma, Synthesis, antioxidant and antimicrobial evaluation of some 2-arylbenzimidazole derivatives, *Bioorg. Med. Chem. Lett.* 23, 2013, 3759-3763.
- [9] K. Achar, K.M. Hosamani, H.R. Seetharamareddy, In-vivo analgesic and anti-inflammatory activities of newly synthesized benzimidazole derivatives, *Eur. J. Med. Chem.* 45, 2010, 2048-2054.
- [10] M. Alamgir, D.St.C. Black, N. Kumar, Synthesis, reactivity and biological activity of benzimidazoles, *Top. Heterocycl. Chem.* 9, 2007, 87-118.

- [11] B.C. Eke, M.O. Puskullu, E. Buyukbingol, M. Smis, A study on the antioxidant capacities of some benzimidazoles in rat tissues, *Chem. Biol. Interact.* 113, 1998, 65-67.
- [12] C. Beaulieu, Z. Wang, D. Denis, G. Greig, S. Lamontagne, G. O'Neill, D. Slipetz, J. Wang, Benzimidazoles as new potent and selective DP antagonists for the treatment of allergic rhinitis, *Bioorg. Med. Chem. Lett.* 14, 2004, 3195-3199.
- [13] F. Arjmand, B. Mohani, S. Ahmad, Synthesis, antibacterial, antifungal activity and interaction of CT-DNA with a new benzimidazole derived Cu(II) complex, *Eur. J. Med. Chem.* 40, 2005, 1103-1110.
- [14] S.Satyanarayana, J.C.Cabrowiak, J.B.Chaires, Tris(phenanthroline) ruthenium (II) enantiomer interactions with DNA: mode and specificity of binding, *Biochemistry* 32, 1993, 2573-2584.
- [15] U.S. Patent 4714764, 1987, *Chem. Abstr.* 1983, 98, 46775h.
- [16] V.P. Devmurari, P. Shivanand, M.B. Goyani, N.P. Jivani, *International Journal of ChemTech Research* 2, 2010, 681-689.
- [17] J.A. Dean, *Lange's Hand Book of Chemistry*, 14 ed., 1992, McGraw-Hill, New York.
- [18] B.K. Singh, U.K. Jetley, R.K. Sharma, B.S. Garg, *Spectrochim. Acta A* 68, 2007, 63-73.
- [19] S. Nithyanandan and P. Kannan, Photo Switchable pendant furyl and thienylfulgimides containing polypyrroles, *Polym Degrad Stab.* 98, 2013, 2224-2231.
- [20] Z. Zhou, R.G. Parr, Activation hardness: new index for describing the orientation of electrophilic aromatic substitution *J. Am. Chem. Soc.* 112, 1990, 5720-5724.

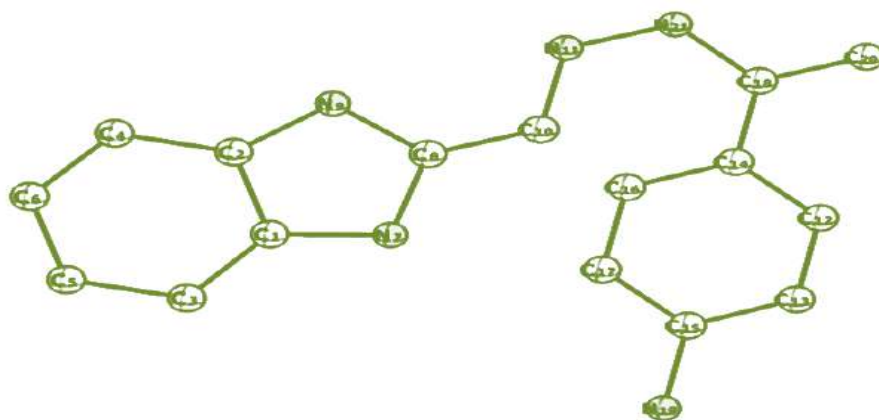
- [21] S. Praveen, M.A. Al-Alshaikh, C.Y. Panicker, A.A. El-Emam, V.V. Salian, B. Narayana, B.K. Sarojini, C.V. Alsenoy, Structural, thermal, linear and nonlinear optical studies of an organic optical limiter based on reverse saturable absorption, *J. Mol. Struct.* 1120, 2016, 317-326.
- [22] K. Nakamoto, *Infrared and Raman Spectra of Inorganic and Coordination compounds*, 1986. 4th ed. John Wiley and Sons, New York, 257.
- [23] D. N Sathyanarayana, *Vibrational Spectroscopy: Theory and Applications*, New Age International publications, 1996.
- [24] C. Preti, G. Tosi, Synthesis antitumor activity and SAR study of novel [1,2,4] triazino [4,5-a] benzimidazole derivatives, *Aust. J. Chem.* 20, 1976, 543-549.
- [25] R. Pilbrow, *Transition Ion Electron Paramagnetic Resonance*, Oxford Science Publications, Oxford, 1990.
- [26] A.B.P Lever. *Inorganic electronic spectroscopy*. 2nd ed. Amsterdam; New York: Elsevier; 1984 863.
- [27] J. Joseph, B. H. Mehta, Synthesis, characterization, and thermal analysis of transition metal complexes of polydentate ONO donor Schiff base ligand, *Russ J Coordination Chem*, 33, 2007, 124-129.
- [28] B.N. Bessy Raj, M.R. PrathapachandraKurup, E. Suresh, Synthesis, spectral characterization and crystal structure of N-2-hydroxy-4-nitrobenzoyl hydrazone and its square planar Cu(II) complex *Spectrochim. Acta A* 71, 2008, 1253.
- [29] K. Thanigaimani, S. Arshad, N.C. Khalib, I.A. Razak, C. Arunagiri, A. Subashini, S.F. Sulaiman, N.S. Hashim, K.L. Ooi, *Spectrochim. acta*, 2015, 149A 90-102.
- [30] S. Ganguly, G. Yadav, Molecular docking studies of novel benzimidazole analogs as HIV-1-RT inhibitors with broad spectrum chemotherapeutic properties, *Int. J. Drug Des. Dis*, 2013, 4.

- [31] J. Zhu, C.F. Wu, X. Li, G.S. Wu, S. Xie, Q.N. Hu, Z. Deng, M.X. Zhu, H. Luo, X. Hong, Synthesis biological evaluation and molecular modeling of substituted 2-aminobenzimidazoles as novel inhibitors of acetylcholinesterase and butyryl-cholinesterase, *Bioorg. Med. Chem. Lett.* 21, 2013, 4218-4224.
- [32] H.T.M. Van, W.-J. Cho, Structural modification of 3-arylisquinolines to isoindolo[2,1-b]isoquinolinones for the development of novel topoisomerase I inhibitors with molecular docking study, *Bioorg. Med. Chem. Lett.* 19, 2009, 2551-2554
- [33] C. Kus, G.A. Kilcigil, S. Ozbey, F.B. Kaynak, M. Kaya, T. Coban, B.C. Eke, Synthesis and antioxidant properties of novel N-methyl-134-thiadiazol-2-amine and 4-methyl-2H-124-triazole-3 (4H)-thione derivatives of benzimidazole class, *Bioorg. Med. Chem.* 16, 2008, 4294-4303.
- [34] Y. Harinath, D. Subbarao, C. Suresh, K. Seshaiiah. Synthesis, characterization and studies on antioxidant and molecular docking of metal complexes of 1-(benzo[d]thiazol-2-yl)thiourea. *Journal of chemical sciences.* (128), 2016, 43-51.
- [35] U. Chaveerach, A. Meenongwa, Y. Trongpanich, C. Soikum, P. Chaveerach, DNA binding and cleavage behaviors of copper(II) complexes with amidino-O-methylurea and N-methylphenyl-amidino-O-methylurea, and their antibacterial activities, *Polyhedron* 29, 2010, 731-738.
- [36] B.V.S. Kumar, S.D. Vaidya, R.V. Kumar, S.B. Bhirud, R.B. Mane, Synthesis and anti-bacterial activity of some novel 2-(6-fluorochroman-2-yl)-1-alkyl/acyl/ aryl-1H-benzimidazoles, *Eur. J. Med. Chem.* 41, 2006, 599-604.
- [37] D. Sharma, B. Narasimhan, P. Kumar, V. Judge, R. Narang, E.D. Clercq, J.J. Balzarini, Synthesis antimicrobial and antiviral activity of substituted benzimidazoles, *Enzy. Inhibi. Med. Chem* 24, 2009, 1161.

- [38] G.A. Kilcgil, N. Altanlar, Synthesis and antimicrobial activities of some new benzimidazole derivatives, *IL Farm.* 58, 2003, 1345-1350.
- [39] N.D. Shashikumar, G. Krishnamurthy, H.S. Bhojya Naik, M.R. Lokesh and K. S. Jithendra kumara, Synthesis of new biphenyl-substituted quinoline derivatives, preliminary screening and docking studies. *J. chem. sci.* 126, 1, 2014, 205–212.
- [40] V. Padmavathi, B.C. Venkatesh, A. Muralikrishna, A. Padmaja, The reactivity of Gem cyanoester ketene dithiolates towards the development of potent antioxidant heterocycles, *Chem. Pharm. Bull.* 60, 2012, 449-458.
- [41] S. Bhimagouda Patil, G. Krishnamurthy, H.S. Bhojya Naik, R.Prashant, Latthe, Manjunath Ghate, Synthesis, characterization and antimicrobial studies of 2-(4-methoxy-phenyl)-5-methyl-4-(2-arylsulfanyl-ethyl)-2,4-dihydro-[1,2,4] triazolo-3-ones and their corresponding sulfones, *European Journal of Medicinal Chemistry*, 45, 2010, 3329-3334.
- [42] F. Rahaman, B.H.M Mruthyunjayaswamy, Synthesis, Spectral Characterization, Grain Size Effect, Antimicrobial, DNA Cleavage and Anticancer Activities of Cobalt(II), Nickel(II), Copper(II) and Zinc(II) Complexes of Schiff Base, *Complex Metals*, 31, 2014, 88–95.
- [43] D.H.K Harinath Y Reddy, B .N Kumar, C.H Apparao and K. Sessaiah, Synthesis, spectral characterization and antioxidant activity studies of a bidentate Schiff base, 5-methyl thiophene-2-carboxaldehyde-carbohydrazone and its Cd(II), Cu(II), Ni(II) and Zn(II) complexes, *Spectrochim. Acta A*, 101, 2013, 264.
- [44] Patil, S.G., Patil, M.P., Maheshwari, V.L., Patil, R.H, *In vitro* lipase inhibitory effect and kinetic properties of di-terpenoid fraction from *Calatropisprocera* (Aiton). *Biocatal. Agric. Biotechnol.* 4, 2015, 57–585.
- [45] G.A. Kilcgil, N. Altanlar, Synthesis and antimicrobial activities of some new benzimidazole derivatives, *IL Farm.* 58, 2003, 1345-1350.

Chapter – 5

Studies on the synthesis, spectral, biological evaluation of 4-{(1Z)-1-[2-(1H-benzimidazol-2-ylmethyl)hydrazinylidene] ethyl} phenol and 4-{(1Z)-1-[2-(1H-benzimidazol-2-ylmethyl)hydrazinylidene]ethyl}aniline and their transition metal complexes



5.1. INTRODUCTION

The metal complexes with benzimidazole motifs are useful compounds of bioinorganic interest [1, 2]. since the imidazole ring is a structural fragment of histidine that provides an essential metal binding site in metalloproteins (one or more benzimidazole units are bound to metal ions in almost all copper and zinc metalloproteins or, e.g., in nickel-containing urease) and thus has intense effects on their biological actions [3, 4]. It is also well known that amino group acts as the primary anchor site for metal ions and, as such, is able to promote stepwise deprotonation and subsequent coordination of other successive binding sites, leading to the formation of hydrolytically stable, fused, five-membered chelate rings with M–N bonds. Thus, complexes formed between metal ions and different types of bio-ligands, namely hetero-aromatic nitrogen bases, may be considered as models for substrate–metal ion–enzyme interactions and other metal ion-mediated biochemical interactions [5-10]. Newly, benzimidazole-derived drugs have received much consideration owing to the fact that benzimidazole residue is a constituent of vitamin B₁₂, which supports their potential use as therapeutics [11-19].

In view of the above applications of benzimidazole derivatives the author in this chapter describes the synthesis and characterization of 4-{(1Z)-1-[2-(1H-benzimidazol-2-ylmethyl)hydrazinylidene]ethyl}phenol (LB) and 4-{(1Z)-1-[2-(1H-benzimidazol-2-ylmethyl)hydrazinylidene]ethyl}aniline (BN), their metal complexes and their characterization by various spectral methods. The powder XRD analysis and thermal degradation studies also been done. The cytotoxic studies and molecular docking interactions for the ligand metal complexes have been carried out with protein enzyme receptor.

5.2 Experimental

5.2.1 Materials and physical measurements

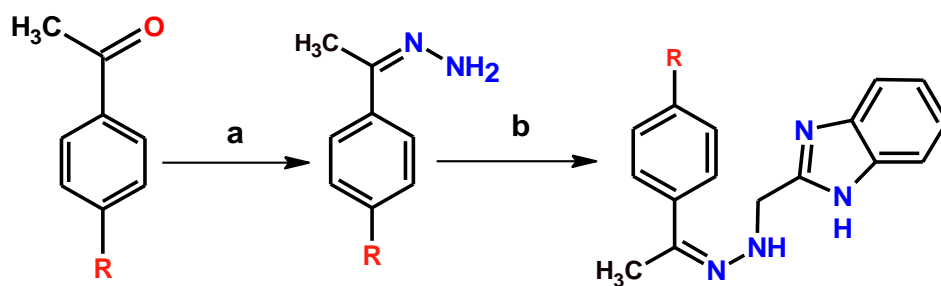
The materials used for the synthesis and physical techniques used for the analysis have been discussed in the previous chapters

5.2.2 Synthesis of the ligands 4-[(*IZ*)-1-[2-(*IH*-benzimidazol-2-ylmethyl)hydrazinylidene]ethyl]phenol (LB) and 4-[(*IZ*)-1-[2-(*IH*-benzimidazol-2-ylmethyl)hydrazinylidene]ethyl]aniline (BN)

The ligand, LB was synthesized by reacting a mixture of each 2-(Chloromethyl) benzimidazole (0.01mol, 1.8g), in dry DMF 30 mL and potassium carbonate (0.01mol, 1.62g). To this solution 4-[(*IZ*)-1-hydrazinylideneethyl]phenol (0.01mol, 1.32g.), was added and refluxed by stirring for 12 h. The reaction mixture was cooled and poured into crushed ice. The precipitate was collected by filtration, dried and then recrystallized from the ethanol the reaction pathway is represented in scheme 5.1. Similarly, the another ligand, BN was synthesized by heating the mixture of 2-(Chloromethyl)benzimidazole (0.01mol, 1.8g) in dry DMF 30 mL and potassium carbonate (0.01mol, 1.62g) and 4-[(*IZ*)-1-hydrazinylideneethyl]aniline (0.01mol, 1.32g.) was added to the above solution by stirring for 12 h. The workup procedure is same as described for the LB.

$C_{16}H_{16}N_4O$ (**LB**): Creamy white solid, yield (75%), M.p 183-185 °C. Anal, Cald (%):C(68.55%) H(5.75%) N(19.99%). Found C(65.9%) H(5.2%) N(18.5%). IR $\nu(\text{cm}^{-1})$ 3673 (OH), 3320(NH), 2987 (Ar CH), 1597(C=N) , 1394(CH₃). ¹H-NMR (DMSO-d₆; δ ppm): 12.96(1H, NH) imidazole ring, 10.18(1H, OH), 7.86 to 7.13(8H, aromatic protons), 4.7 to 4.4(2H, CH₂), 3.37 to 3.35(3H, CH₃). LC-MS (Found): m/z 280.32 (281.35).

$C_{16}H_{17}N_5$ (**BN**): light yellow solid, yield (72%), M.p -189-192 °C. Anal, Cald (%):C(68.79%) H(6.13%) N(25.07%). Found C(67.19%) H(5.32%) N(24.25%). IR $\nu(\text{cm}^{-1})$ 3673 (OH), 3320(NH), 2987 (Ar CH), 1597(C=N) , 1394(CH₃). ¹H-NMR (DMSO-d₆; δ ppm): 12.96(1H, NH) imidazole ring, 10.18(1H, OH), 7.86-7.13(8H, aromatic protons), 4.7- 4.4(2H, CH₂), 3.37-3.35(3H, CH₃). LC-MS (Found): m/z 279.33(280.21).



R = OH [LB] and R = NH₂ [BN]

Scheme 5.1 Scheme for the synthesis LB and BN [a] N₂H₄, dry C₂H₅OH [b] 2-(chloromethyl)benzimidazole DMF, K₂Cr₂O₇.

5.2.4 Synthesis of the metal complexes

The ethanolic solution of metal (II) chlorides (0.02mol) was added in drops to the ethanolic solution of the ligand LB (0.04mol) and the resulting mixture was refluxed on a water bath at 70 °C for about 4-5h. The solid product so obtained was filtered, washed with hot ethanol and dried in vacuum over anhydrous calcium chloride.

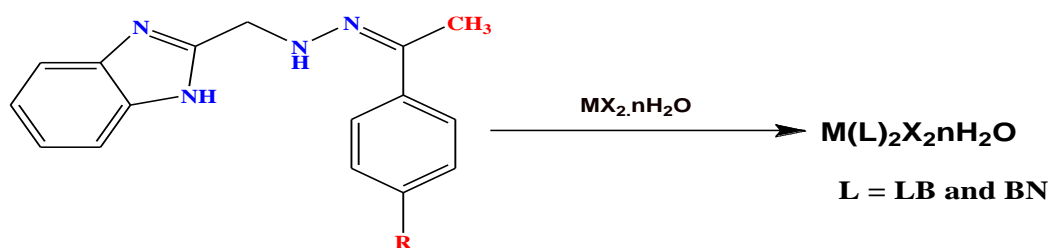


Figure 5.1 Proposed structure of metal complexes [M=Co(II), Ni(II) and Cu(II)]

Similarly to the solution of ligand BN (0.04mol), the solution of metal (II) chlorides were added drop wise and were refluxed for about 4-5 h, yield the solid product. The synthesized complexes were collected by following the procedure as described for the complexes of LB.

5.3 Results and Discussion

The analytical data of the metal complexes reveal that the reactions of metal (II) chlorides and ligands occurred in 1:2 (M:L) molar ratio, The observed molar conductance of the complexes in DMSO (10⁻³ M solution) are in consistent with Co(II), Ni(II) and Cu(II) complexes and are non-electrolytic in nature [20]. The

slightly higher conductance value obtained may be due to partial dissociation of the complexes upon dissolving in DMSO.

Table 5.1 Physical properties and analytical data of LB, BN and their metal complexes

Compounds	Colour	Mol. Wt	Yield (%)	Calcd. (found) (%)				Molar conductance (ohm ⁻¹ cm ² mol ⁻¹)
				C	H	N	M	
Co(LB) ₂ Cl ₂ ·2H ₂ O	pale green	690.48 (691.3)	62	55.66 (55.92)	4.67 (4.81)	16.23 (15.91)	8.54 (8.23)	25
Co(BN) ₂ Cl ₂ ·2H ₂ O	Dark brown	686.17 (687.5)	60	55.81 (55.92)	4.45 (4.11)	18.25 (17.96)	8.41 (8.73)	29
[Ni(LB) ₂ Cl ₂].2H ₂ O	Light blue	690.48 (691.8)	63	55.68 (55.34)	4.67 (4.92)	16.23 (15.96)	8.50 (8.15)	21
Ni(BN) ₂ Cl ₂ ·2H ₂ O	pale green	687.48 (688.5)	65	55.61 (55.45)	4.45 (4.63)	18.12 (17.89)	8.22 (7.97)	27
[Cu(LB) ₂ Cl ₂]. H ₂ O	Light red	695.10 (696.8)	70	55.29 (55.91)	4.64 (4.54)	16.12 (15.90)	9.14 (8.97)	30
[Cu(BN) ₂ Cl ₂]. H ₂ O	maroon	691.16 (692.3)	68	55.81 (55.92)	4.45 (4.11)	18.23 (17.92)	9.71 (9.34)	32

5.3.1 ¹H NMR studies

The ¹H NMR spectra of ligand LB and BN are represented in figure 5.2 and 5.3 respectively, both the ligands having almost similar structural features, the LB showed a singlet at 12.96 ppm due to -NH and 10.18 ppm for -OH protons and the aromatic protons for both imidazole and acetophenone motifs resonated in the range 7.86 to 7.13 ppm. While in ligand BN, a signal at 5.37 to 5.16 ppm and 10.11 ppm for NH₂ and NH protons respectively and the signals in the range 7.92 to 7.01 ppm for aromatic protons. The singlet for -CH₂ protons appeared at 4.7 ppm for LB and at 4.4 ppm for BN, followed by this the -CH₃ protons signal appeared at 3.37 and 3.35 ppm for LB and BN respectively.

The ^1H NMR spectrum of $[\text{Ni}(\text{LB})_2\text{Cl}_2]\cdot 2\text{H}_2\text{O}$ complex showed that the position of $-\text{NH}$, $-\text{OH}$, Ar-H and CH_2 protons signals remains unchanged. Based on this, it can be concluded that these signals are in the expected region and shift only slightly due to the coordination of the ligand to the metal ion and the spectrum represented in the figure 5.4.

The signal due NH moiety is disappeared at 10.11 ppm in the spectra of $[\text{Ni}(\text{BN})_2\text{Cl}_2]\cdot 2\text{H}_2\text{O}$ indicate that coordination of the ligand has occurred through N-atom of imidazole NH group of the ligand BN, and the spectrum is represented in the figure 5.5.

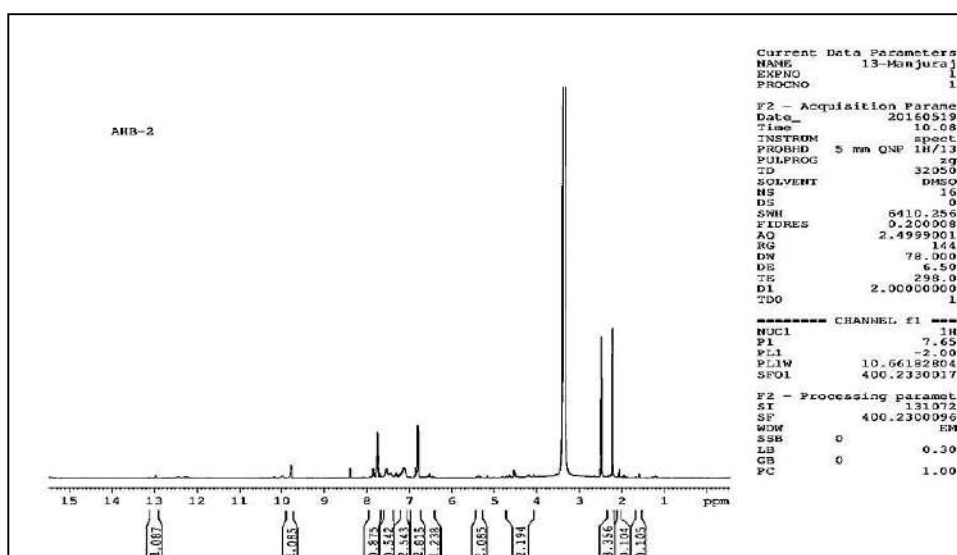


Figure 5.2 ^1H NMR spectrum of LB

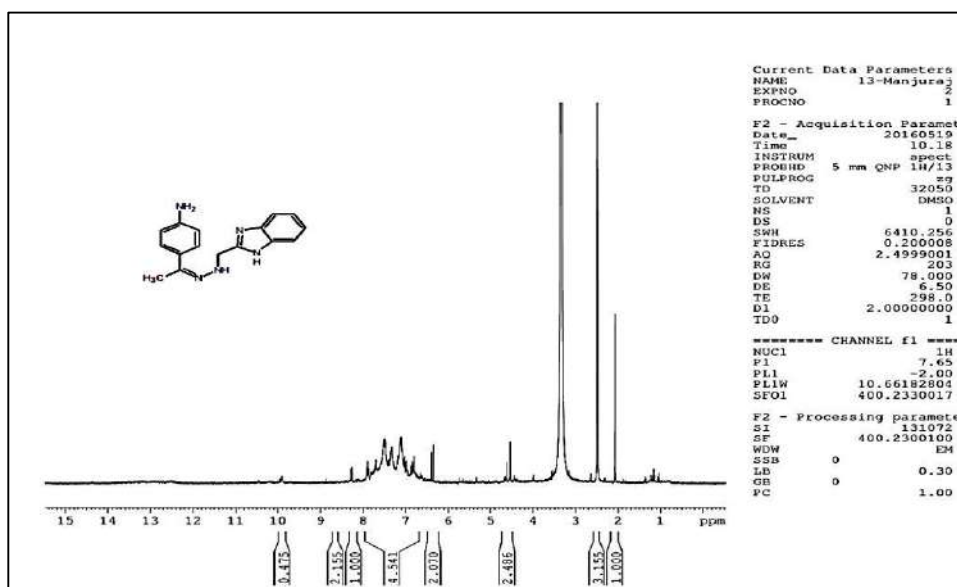


Figure 5.3 ^1H NMR spectrum of the BN

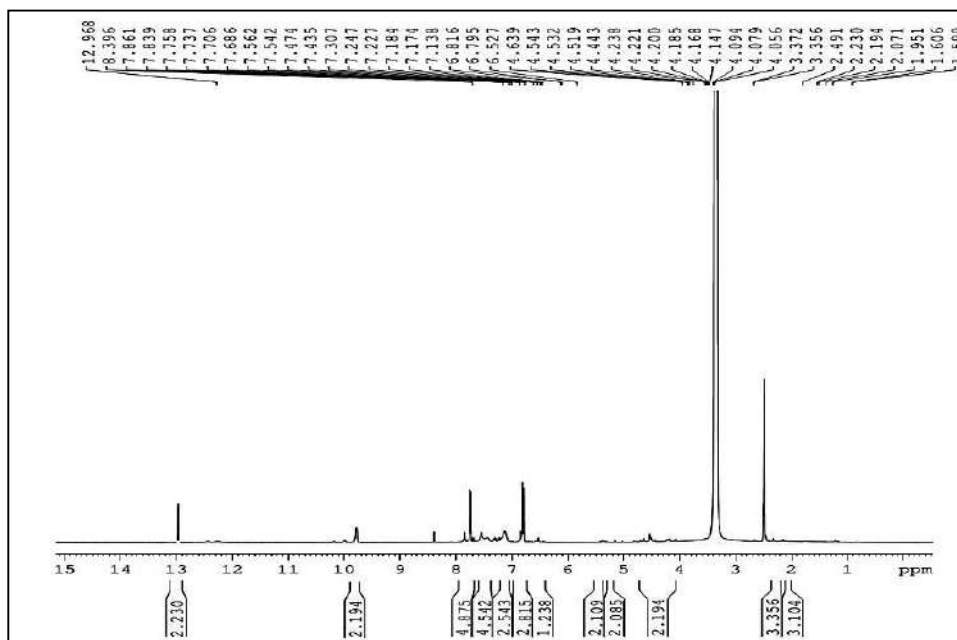


Figure 5.4 ^1H NMR spectrum of $[\text{Ni Cl}_2 (\text{LB})_2] \cdot 2\text{H}_2\text{O}$

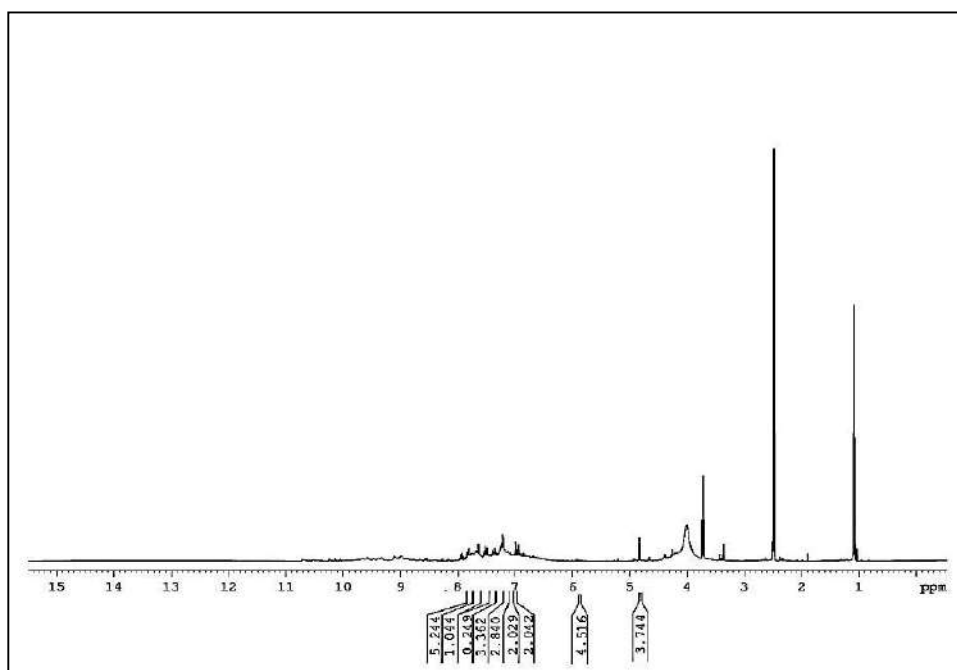


Figure 5.5 ^1H NMR spectrum of $[\text{Ni Cl}_2 (\text{BN})_2] \cdot 2\text{H}_2\text{O}$

5.3.2 Mass spectral studies

In the mass spectrum, the molecular ion peak M and $[M+1]$ appeared at m/z 280 (281), that is equivalent to the molecular weight of LB, and for BN m/z 279 (280) which corresponds to molecular ion peak M and $[M+1]$ respectively and the spectrum are showed in figure 5.6 and 5.7 respectively.

The molecular ion peak of $[\text{CoCl}_2(\text{LB})_2]\cdot 2\text{H}_2\text{O}$ and $[\text{NiCl}_2(\text{LB})_2]\cdot 2\text{H}_2\text{O}$ obtained at $[\text{M}+2]$ at m/z 690.48 (691.28) and 690.24 (691.31) respectively and are represented in figure 5.8. The molecular ion peak of $[\text{CoCl}_2(\text{BN})_2]\cdot 2\text{H}_2\text{O}$ and $[\text{NiCl}_2(\text{BN})_2]\cdot 2\text{H}_2\text{O}$ complexes showed prominent peaks at m/z 687.17(688.52) and 686.17(687.22) and presented in figure 5.9.

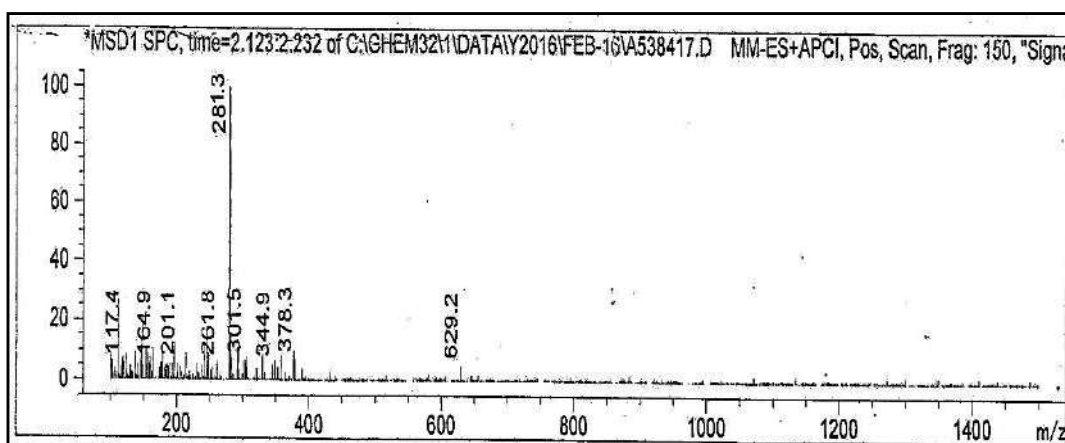


Figure 5.6 Mass spectrum of the LB

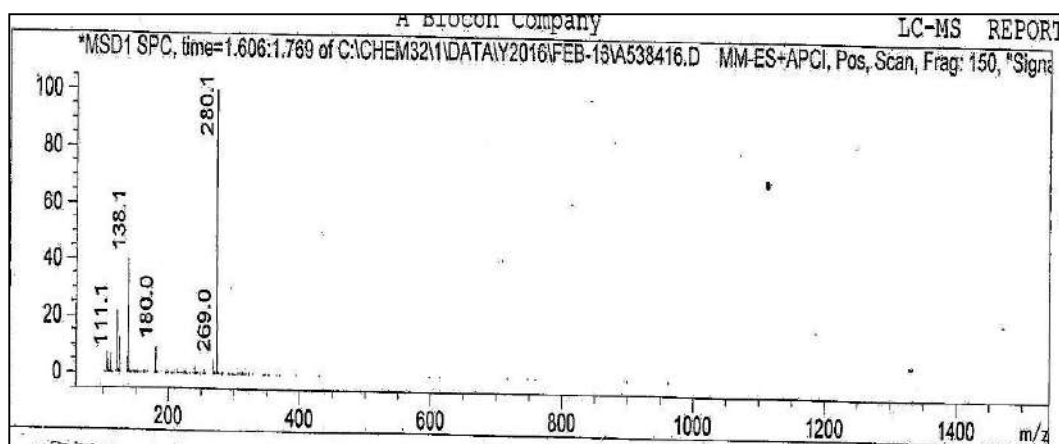
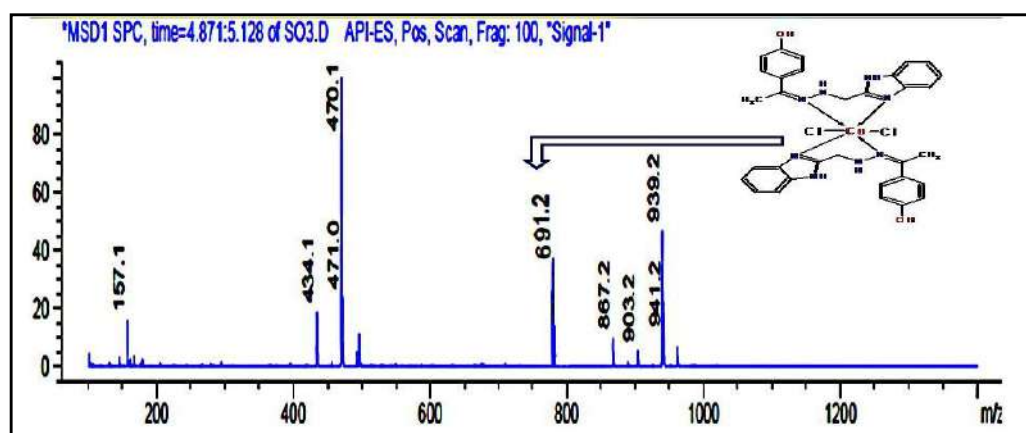


Figure 5.7 Mass spectrum of the BN

Figure 5.8 Mass spectrum of the $[\text{CoCl}_2(\text{LB})_2]\cdot 2\text{H}_2\text{O}$

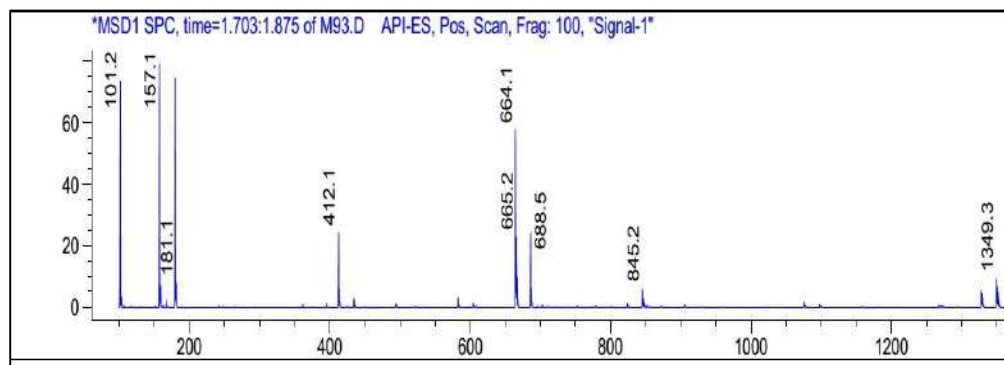


Figure 5.9 Mass spectrum of the $[\text{CoCl}_2(\text{BN})_2] \cdot 2\text{H}_2\text{O}$

5.3.3 Electronic spectra and magnetic moment studies

The electronic spectrum of the ligands LB, BN as well as their metal complexes were recorded as DMF solvent (10^{-3} M) and are represented in figure 5.10. The intense absorption band observed at $32,258\text{ cm}^{-1}$, $30,303\text{ cm}^{-1}$ in the spectrum of LB and two bands at $37,037\text{ cm}^{-1}$, $29,850\text{ cm}^{-1}$ in the spectrum of BN is predominantly due to $\pi-\pi^*$, $n\rightarrow\pi^*$ transitions in the complexes are shifted to a longer wavelength as a consequence of coordination to the metal. [21].

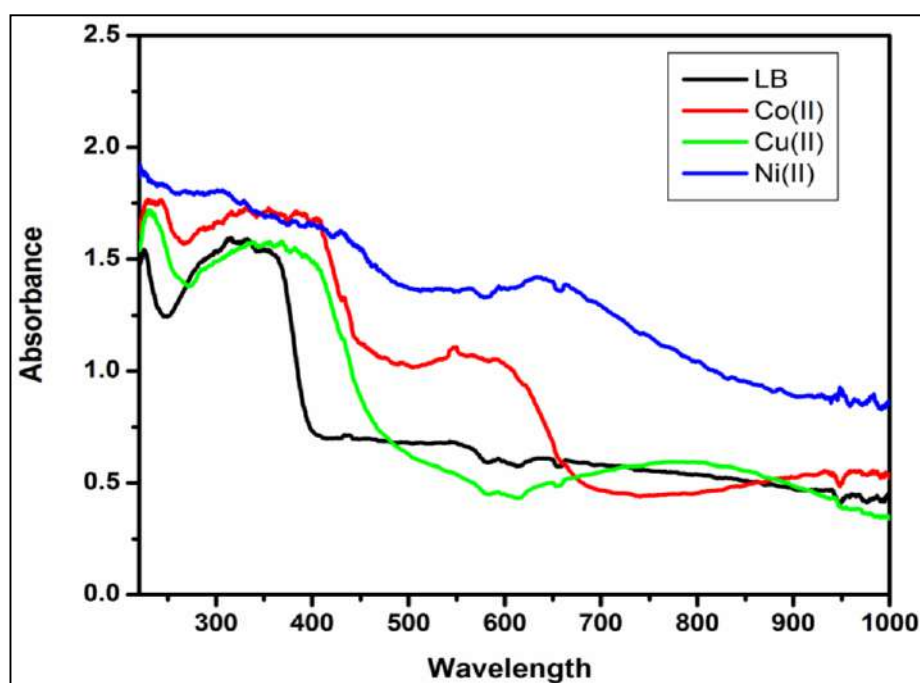


Figure 5.10 Electronic spectra of metal complexes

The d-d bands observed at $23,640\text{ cm}^{-1}$ and $20,833\text{ cm}^{-1}$ for $[\text{Co}(\text{LB})_2\text{Cl}_2] \cdot 2\text{H}_2\text{O}$ complex are assigned as ${}^4\text{T}_{1g}(\text{F}) \rightarrow {}^4\text{T}_{2g}(\text{F}) (\nu_1)$ and $\rightarrow {}^4\text{A}_{2g}(\text{F})$

(ν_2) transitions, and the magnetic moment obtained was 4.51 B.M, consistent to the high spin octahedral geometry [22], Similarly for the $\text{Co}(\text{BN})_2\text{Cl}_2 \cdot 2\text{H}_2\text{O}$ showed two bands at 15,971 and 15,886 cm^{-1} corresponds to the transition ${}^4\text{T}_1(\text{F}) \rightarrow {}^4\text{A}_2(\text{F})$ and ${}^4\text{T}_1(\text{F}) \rightarrow {}^4\text{T}_1(\text{P})$, that suggest the octahedral geometry for the complex. The electronic spectra of $[\text{Ni}(\text{LB})_2\text{Cl}_2] \cdot 2\text{H}_2\text{O}$ complex showed the bands at 22,228 cm^{-1} and 19,607 cm^{-1} corresponding to ${}^3\text{A}_{2g} \rightarrow {}^3\text{T}_{2g}$ (F) (ν_1) and ${}^3\text{A}_{2g} \rightarrow {}^3\text{T}_{2g}$ (F) (ν_2) respectively and the magnetic moment is 2.87 B.M leads to octahedral geometry [23]. While the electronic spectra of $\text{Ni}(\text{BN})_2\text{Cl}_2 \cdot 2\text{H}_2\text{O}$ complex also showed two bands, one at 18681 cm^{-1} and another at 15886 cm^{-1} which assigned to ${}^3\text{A}_{2g}(\text{F}) \rightarrow {}^3\text{T}_{1g}$ (ν_1) and ${}^3\text{A}_{2g}(\text{F}) \rightarrow {}^3\text{T}_{1g}$ (ν_2) ascribed to the transitions, these bands suggest that octahedral geometry for the complex. The $[\text{Cu}(\text{LB})_2\text{Cl}_2] \cdot \text{H}_2\text{O}$ showed a board band at 14705 cm^{-1} which corresponds to the ${}^2\text{T}_{2g} \rightarrow {}^2\text{E}_g$ transition and the magnetic moment is 2.31 B.M, indicating distorted octahedral geometry [24]. Whereas the $[\text{Cu}(\text{BN})_2\text{Cl}_2] \cdot \text{H}_2\text{O}$ complex displayed one broad band in the range 12984 to 13651 cm^{-1} due to ${}^2\text{E}_g(\text{F}) \rightarrow {}^2\text{T}_{2g}$ transition which implies that the distorted octahedral geometry [25].

5.3.4 IR Spectra

The IR spectra of the ligands and their complexes were taken as KBr pellets. The spectrum of LB gave a board bands for $\nu(\text{OH})$ and $\nu(\text{NH})$ at 3673 cm^{-1} and 3324 cm^{-1} respectively and these bands appear nearly at the same or slightly shifted position in the spectra of their metal complexes, indicating that no participation of $\nu(\text{OH})$ and $\nu(\text{NH})$ group upon complexation. In the spectrum of the BN, the band due to $\nu(\text{NH})$ appeared at 3309 cm^{-1} , while it on complexation their band position shifted to lower frequency and appear in the range 3220 – 3203 cm^{-1} .

In the IR spectrum of LB $\nu(\text{C}=\text{N})$ band observed around 1597 cm^{-1} and 1590 cm^{-1} for BN and these are shifted to lower frequencies in the corresponding metal complexes [26]. The $\nu(\text{Ar}-\text{CH})$ stretching vibrations appeared at 2987 cm^{-1} and a medium intensity band appeared at 1394 cm^{-1} while for $\nu(\text{CH}_3)$ of methyl ketone group. The $\nu(\text{C}=\text{N})$ band observed around 1597 cm^{-1} and was shifted to lower frequencies in the spectra of all the complexes 1489 – 1585 cm^{-1} indicating that azomethine nitrogen atom coordinated to the metal ion [27]. The sharp band

appeared at 935 cm^{-1} due to $\nu(\text{N-N})$ of the ligands, which shifted to the lower frequency in their complexes indicating that the coordination of nitrogen atom. The appearance of new peaks at 474, 469 and 475 cm^{-1} are due to $\nu(\text{M-N})$ bonding [28, 29].

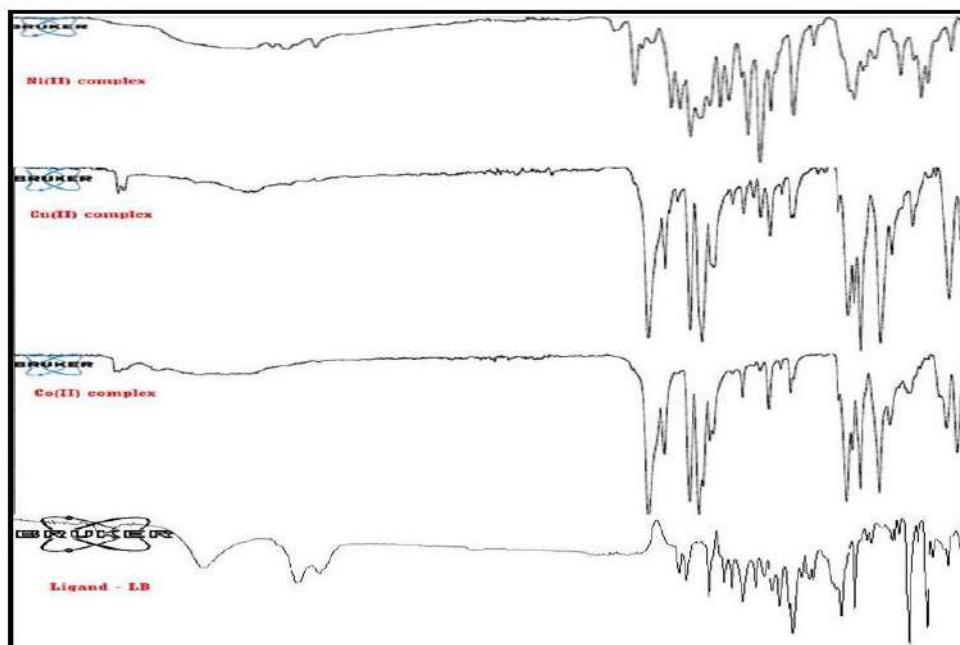


Figure 5.11 IR Spectra of LB and their metal complexes

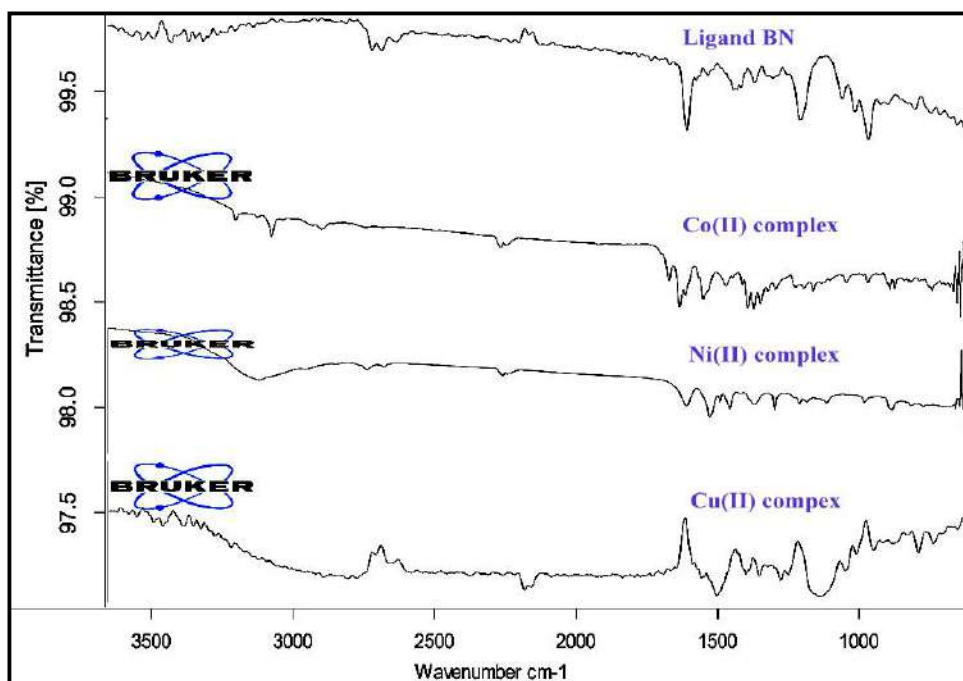


Figure 5.12 IR spectra of BN and their metal complexes

5.3.5 Thermal gravimetric studies

Thermal decomposition patterns of all the complexes with LB are showed in figures 5.13, 5.14, 5.15. The $[\text{Co}(\text{LB})_2\text{Cl}_2] \cdot 2\text{H}_2\text{O}$ decomposed in three stages. First stage resulted in a mass loss of 7.10% (Calcd. 8.50%) corresponding to the loss of two lattice water molecules in the temperature range 70-95 °C. In the second stage, the mass loss of 61.05% (Calcd. 63.29%) was observed and is corresponding to the loss of $\text{C}_8\text{H}_{10}\text{N}_2\text{O}$, 2HCl in the temperature range 160–303 °C. Third stage of dissociation occurred above 300 °C with the mass loss of 26% (Calcd. 27.46%) is due to the decomposition of $\text{C}_7\text{H}_6\text{N}_2$ ring and leaving behind CoO as residue. The $[\text{Ni}(\text{LB})_2\text{Cl}_2] \cdot 2\text{H}_2\text{O}$ degraded in three steps. The first stage involved a weight loss of 6.10% (Calcd 8.23%) corresponding to the elimination of two lattice water molecules in the temperature range 90-110 °C. The second stage represents weight loss of 62.50 % (calculated 63.30%) which leads to the removal of coordinated $\text{C}_7\text{H}_6\text{N}_2\text{HCl}$ in the temperature range 110 to 425 °C. The third stage resulted with the weight loss of 25.90% (calculated 27.47%) due to the dissociation of $\text{C}_8\text{H}_{10}\text{N}_2\text{O}$ from the temperature 426 °C and above. The residue was expected as NiO . The disintegration steps of $[\text{Cu}(\text{LB})_2\text{Cl}_2]$ occurred in three stages. The first stage occurred in temperature range 95–120 °C due to the loss of two lattice water molecules with the mass loss 8.23% (Calcd. 9.45%). In the second stage, the weight loss found to be 38.50 % (calcd 40.30%) which leads to the removal of coordinated $\text{C}_8\text{H}_{10}\text{N}_2\text{OHCl}$ in the temperature range 180 – 340 °C. The third stage resulted with the weight loss (found 25.90% and calcd 27.47%) indicating dissociation of $\text{C}_7\text{H}_6\text{N}_2$ moiety and leaving behind CuO above 300 °C.

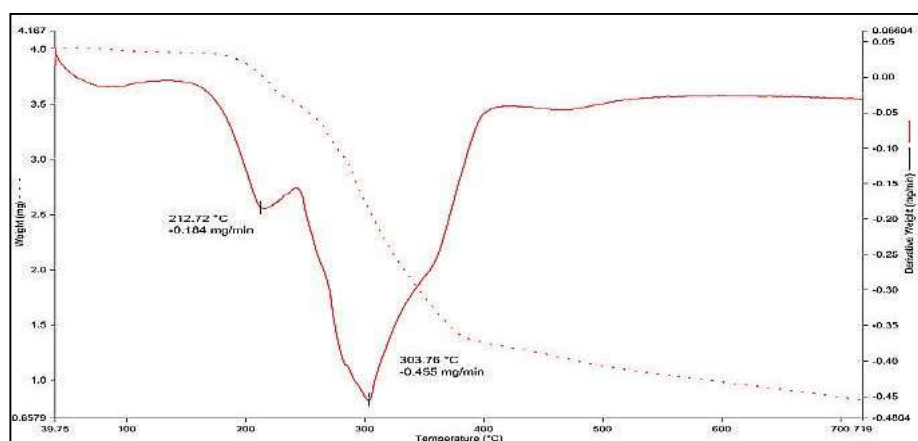
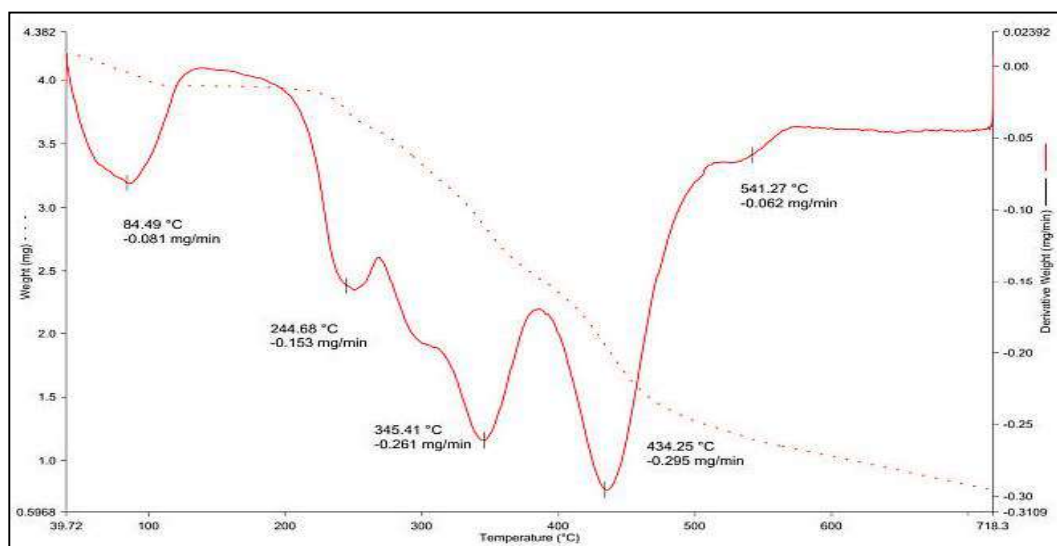
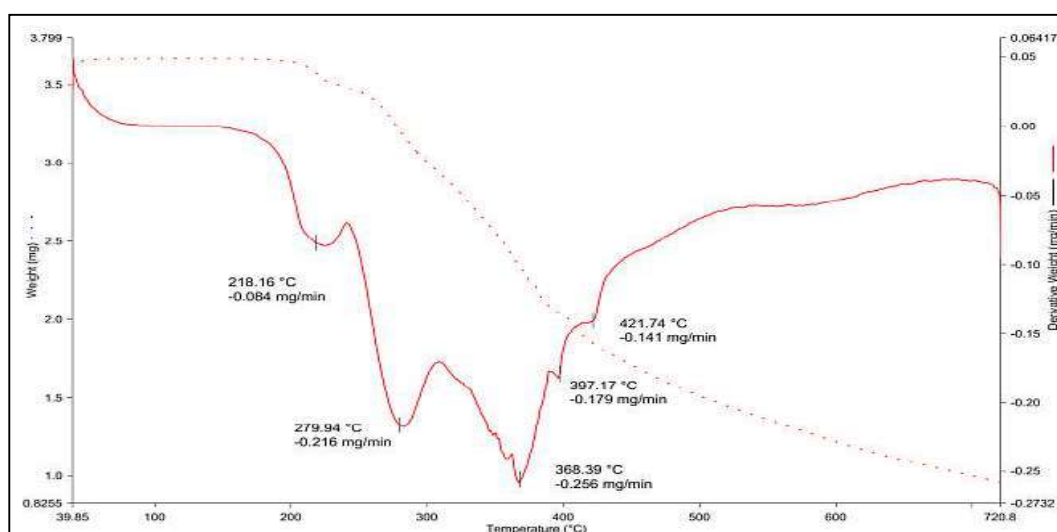
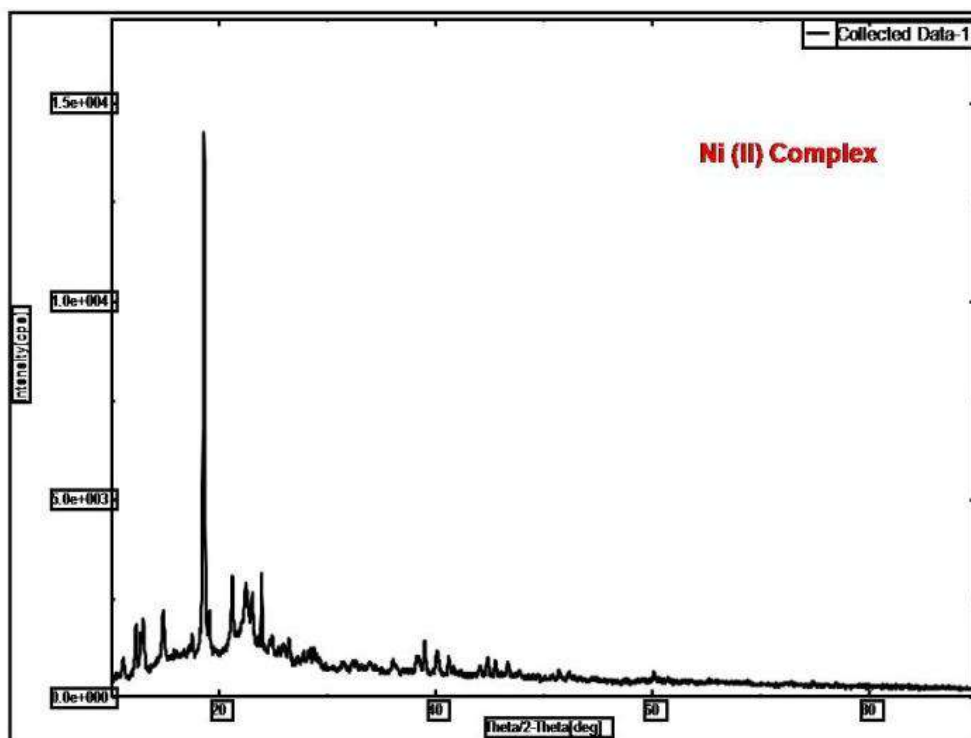
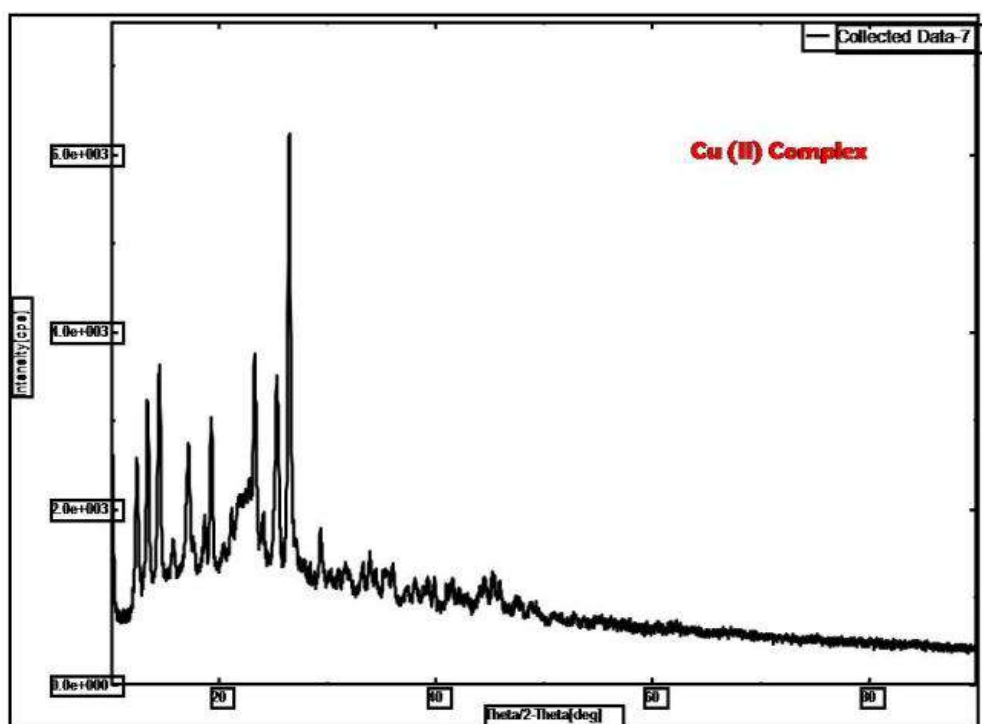


Figure 5.13 TGA pattern of $[\text{Co}(\text{LB})_2\text{Cl}_2] \cdot 2\text{H}_2\text{O}$

Figure 5.14 TGA pattern of [Ni(LB)₂Cl₂] 2H₂OFigure 5.15 TGA pattern of [Cu(LB)₂Cl₂]

5.3.6 XRD studies

The powder X-ray diffraction studies were carried out for all the complexes of LB. The XRD pattern indicate that Co(II) complex is amorphous in nature, while the diffraction patterns showed crystalline nature for Ni(II) and Cu(II) complexes. The X-ray diffraction pattern of the complexes are represented in figure 5.16 and 5.17.

Figure 5.16 X-ray diffraction pattern of $[\text{Ni}(\text{LB})_2\text{Cl}_2] \cdot 2\text{H}_2\text{O}$ Figure 5.17 X-ray diffraction pattern of $[\text{Cu}(\text{L})_2\text{Cl}_2]$

The Miller indices (*hkl*) along with observed and calculated *d* angles, 2θ values and relative intensities are given in Tables 5.2 and 5.3. The average crystalline size of the complexes (dxrd) were calculated using Debye Scherrer equation ($D = K\lambda/\beta\cos\theta$) Where *D* = Particle size, *K* = Dimensionless shape factor, λ = X-ray wavelength (0.15406Å) β = Line broadening at half the maximum intensity, θ = Diffraction angle. The complexes of Ni(II) and Cu(II) have a crystalline size of 29.12 and 36.47 nm respectively suggesting that the complexes are in a nanocrystalline phase[30, 31].

Table 5.2 The XRD data of the [Ni(LB)₂Cl₂] 2H₂O

Peak No	2θ	θ	Sin θ	h k l	d		Intensity	a in Å
					Cal	obs		
1	7.636	3.818	0.0665	1 1 0	11.57	11.568	20.9	5.65
2	8.45	4.225	0.0736	1 1 0	10.45	10.443	100	5.65
4	9.72	4.86	0.08472	4 2 0	9.088	9.089	51.9	5.65
5	13.58	6.79	0.1182	4 0 4	6.512	6.512	37.7	5.65
6	21.12	10.56	0.1832	6 6 1	4.203	4.202	16.8	5.65
7	21.90	10.95	0.1899	6 2 7	4.054	4.054	20.4	5.65

Table 5.3 The XRD data of the [Cu(LB)₂Cl₂]

Peak No	2θ	θ	Sin θ	h k l	d		Intensity	a in Å
					Cal	obs		
1	8.396	4.198	0.0732	110	10.51	10.52	100	3.62
2	10.528	5.264	0.0917	389	8.396	8.369	57.9	3.62
4	11.303	5.651	0.0984	414	7.825	7.822	71.0	3.62
5	12.833	6.416	0.1117	450	6.89	6.89	70.8	3.62
6	13.325	6.662	0.1160	420	6.63	6.639	56.6	3.62
7	14.707	7.353	0.1278	448	6.02	6.018	52.8	3.62
8	15.575	7.937	0.1380	431	5.57	5.578	57.4	3.62
9	16.845	8.422	0.1464	470	5.25	5.259	58.9	3.62

5.4 Procedures of biological studies

5.4.1 Antioxidant activity

The free radical scavenging activity of the LB, BN and their metal complexes were measured *in vitro* by 2, 2'-diphenyl-1-picrylhydrazyl (DPPH) assay [32]. The procedure is given in the earlier chapters

5.4.2 Anti-lipase assay

Lipase inhibitory activity method of the LB, BN and their metal complexes, and their related procedure were discussed in the previous chapters [33].

5.4.3 Molecular docking analysis

The molecular docking of the uncoordinated ligand and their metal complexes was carried out with epidermal growth factor receptor EGFR; PDB: 2A91 as cancer receptor, which have been discussed in the previous chapters.

5.4.4 Cytotoxic activity

In the study of *in-vitro* anticancer activity, MCF-7 (estrogen receptor-positive human breast cancer cell line) and HeLa (human cervical cancer cell line) cell lines were obtained from the National Centre for Cell Science, Pune. The cells were cultured in 25 cm and 9.25 cm tissue culture flasks containing RPMI 1640 culture medium supplemented with 10 % foetal bovine serum (FBS) and 1 % penicillin. The cytotoxicity was determined using the 3-(4,5-dimethylthiazol-2-yl)-2,5-diphenyltetrazolium bromide (MTT) assay (Sigma) as described by Mosmann. Controls that contained untreated cells were included for each sample. Cytotoxicity was expressed as IC₅₀ (µg), (the value which corresponds to the concentration required for 50 % inhibition cell viability). Tamoxifen was used as the standard cytotoxin [34].

5.5 Results and discussion of biological studies

5.5.1 Antioxidant activity

DPPH radical scavenging activity data of the synthesized ligands and their metal complexes exhibited that all the compounds having highly potential activity as it is compared in figures 5.18 and 5.19. The metal complexes exhibited more radical

scavenging activity than either of the ligands. The $[\text{Cu}(\text{LB})_2\text{Cl}_2]\cdot\text{H}_2\text{O}$ exhibited effective antioxidant activity which is almost close to the standard BHT. While $[\text{Co}(\text{LB})_2\text{Cl}_2]\cdot 2\text{H}_2\text{O}$ and $[\text{Ni}(\text{LB})_2\text{Cl}_2]\cdot 2\text{H}_2\text{O}$ exhibited moderate activity. Similarly $[\text{Ni}(\text{BN})_2\text{Cl}_2]\cdot 2\text{H}_2\text{O}$ and $[\text{Co}(\text{BN})_2\text{Cl}_2]\cdot 2\text{H}_2\text{O}$ complexes showed highest scavenging activity towards DPPH radical, while the $[\text{Cu}(\text{BN})_2\text{Cl}_2]\cdot\text{H}_2\text{O}$ exhibited least activity. The antioxidant activity of the complexes and ligands is appreciable due to presence imidazole nucleus of the ligand and its coordination with metal ion in their complexes [35, 36].

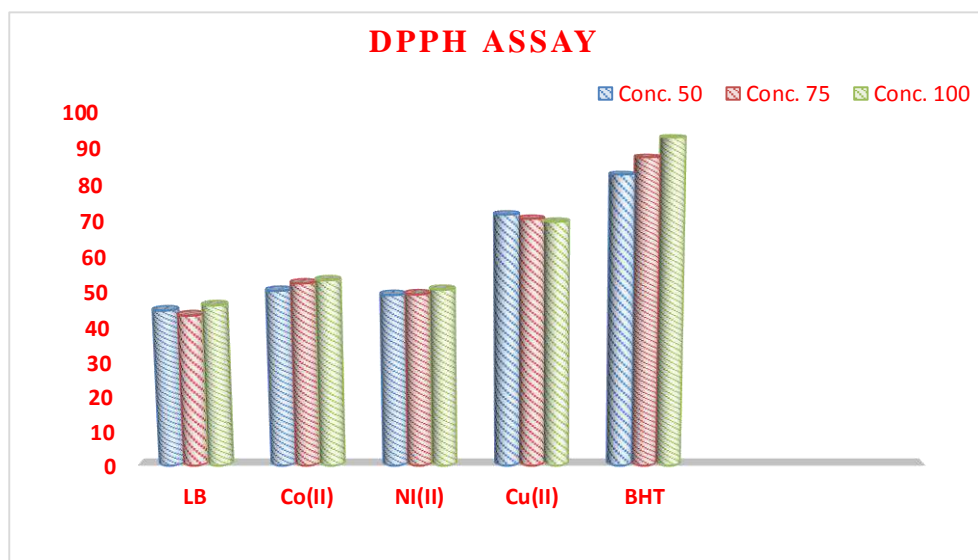


Figure 5.18 DPPH radical scavenging activity of LB and their metal complexes

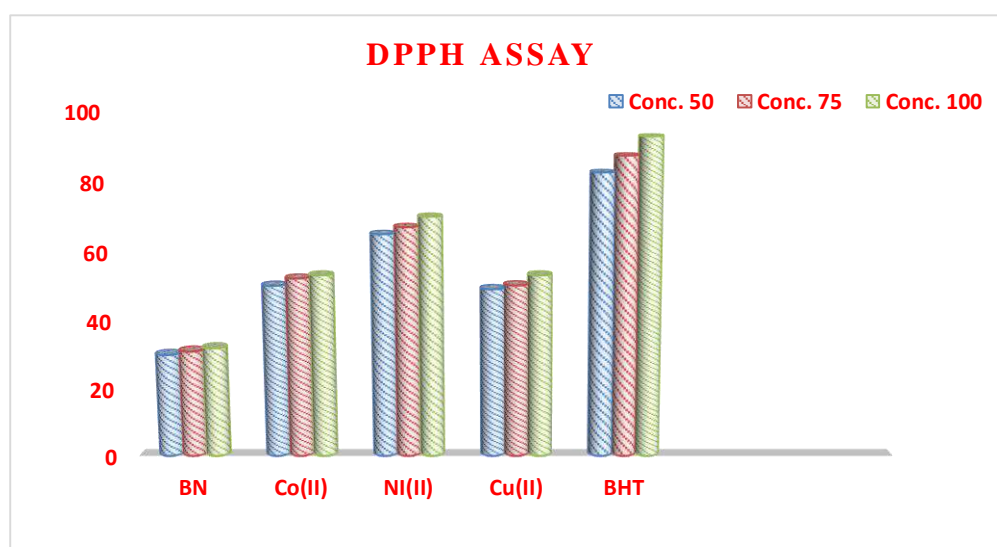


Figure 5.19 DPPH radical scavenging activity of BN and their metal complexes

5.5.2 Anti-lipase assay

Lipase inhibitory activity of different concentrations (1mg, 2mg) was carried for the ligands LB and BN and their metal complexes. The ligands showed lesser activity compared to their metal complexes. The graphical representation of the activity of metal complexes of LB and BN are shown in figure 5.19 and 5.20 respectively. The result indicates that in the Co(II), Ni(II) and Cu(II) complexes of the ligands play an important role for their physiological activity, because of good conjugation of imidazole and isonicotinic hydrazide rings. The metal complexes of the LB showed more potent inhibition compared to the complexes of BN. The metal complex is conducive to form interaction between chicken pancreatic lipase enzyme. The π - π stacking interaction and are found to have σ - π interaction [37].

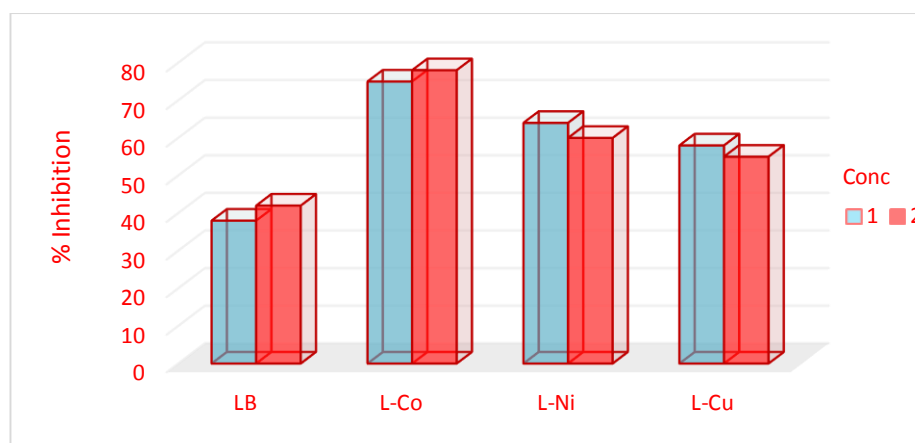


Figure 5.20 Anti-lipase assay of LB and their metal complexes

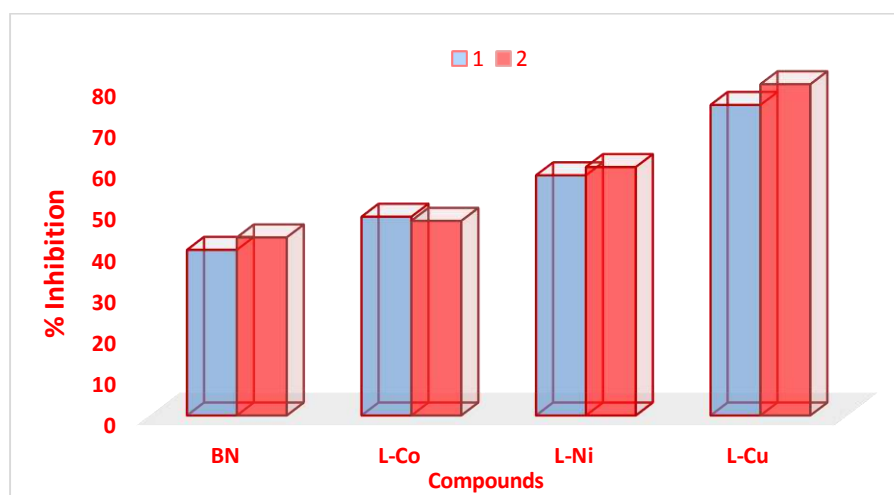


Figure 5.21 Anti-lipase assay of BN and their metal complexes

5.5.3 Docking studies

The docking scores of the LB and their metal complexes are presented in table 5.4. In accordance with cytotoxic activity, the receptor EGFR tyrosine kinase showed the least binding energy $-205.24 \text{ kcal mol}^{-1}$ with LB [39, 40], whereas their complexes, $[\text{Co}(\text{LB})_2\text{Cl}_2]\cdot 2\text{H}_2\text{O}$ and $[\text{Cu}(\text{LB})_2\text{Cl}_2]\cdot \text{H}_2\text{O}$ exhibits highest binding interaction of -321.42 and $-321.07 \text{ kcal mol}^{-1}$ respectively on the active sites of the target receptor with different types of amino acids. In addition, the $[\text{Ni}(\text{LB})_2\text{Cl}_2]\cdot 2\text{H}_2\text{O}$ also having good dockings score of $-291.64 \text{ kcal mol}^{-1}$. All the complexes exhibited hydrogen bonding with active amino acid sites with highest binding affinity and these are represented in the figure 5.22 and 5.23. The binding interactions are compared to the standard Actinoin [38, 39].

Table 5.4 Binding energy values of LB and their metal complexes

Compounds	ΔG (Kcal/mol)	Interacting of amino acids
LB	-204.25	GLN36, ASP9, THR6, TYR29, ALA419, CYS5, MET24, CYS32, ALA419, GLY37 LEU415, CYS32, TYR29, CYS5, LEU28, VAL35, GLU40, ALA419, THR8 GLN36, ASN417, ASN417, GLN85, LEU28, CYS5, LEU415, VAL35
$[\text{Co}(\text{LB})_2\text{Cl}_2]\cdot 2\text{H}_2\text{O}$	-321.42	
$[\text{Ni}(\text{LB})_2\text{Cl}_2]\cdot 2\text{H}_2\text{O}$	-291.64	
$[\text{Cu}(\text{LB})_2\text{Cl}_2]\cdot \text{H}_2\text{O}$	-321.07	
Actinoin(Std)	-235.99	

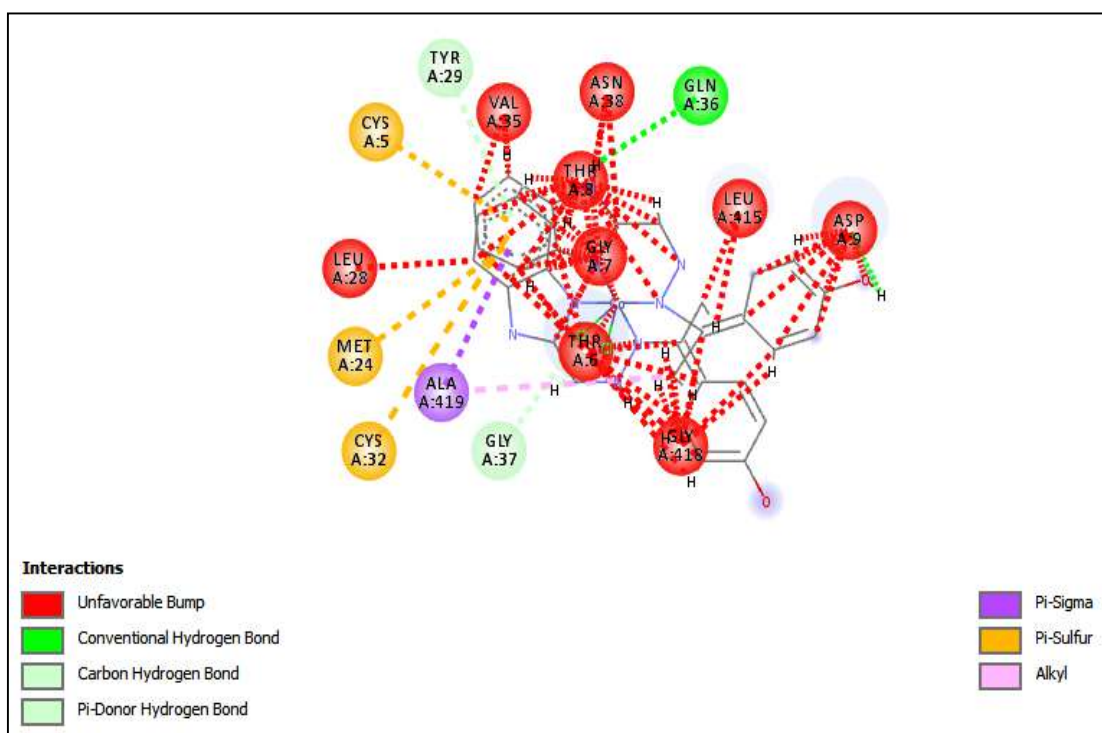
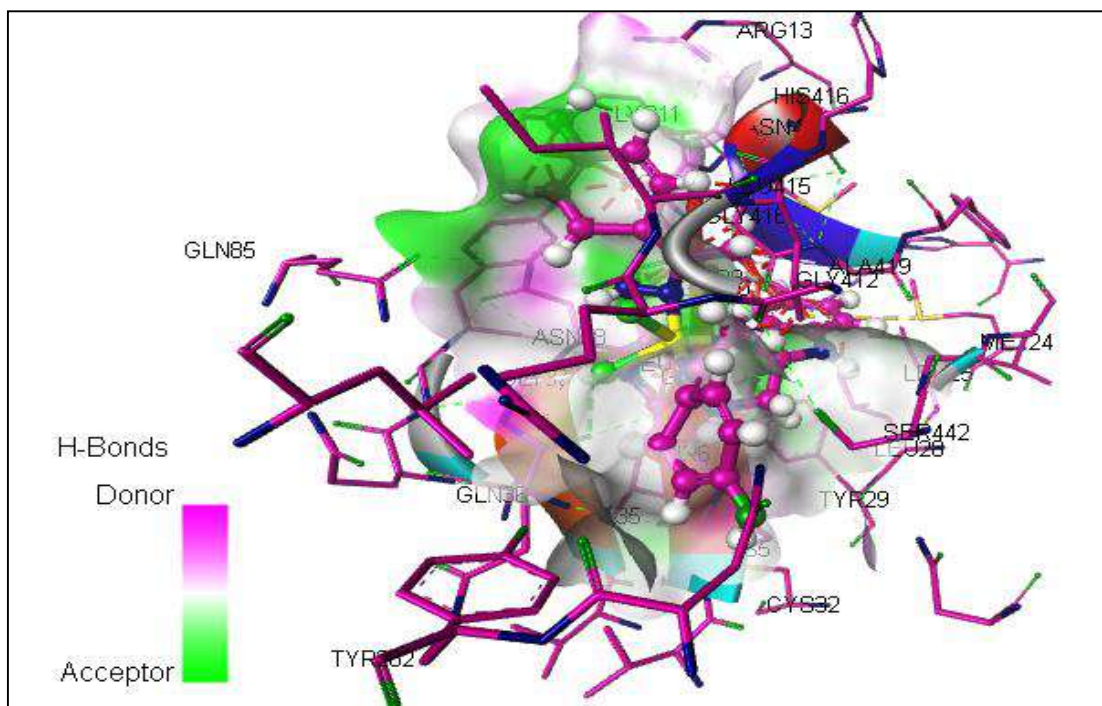


Figure 5.22 3D Interaction and hydrogen bonding of $[\text{Co}(\text{LB})_2\text{Cl}_2]\cdot 2\text{H}_2\text{O}$ with amino acids of receptor 2A91 and 2D interaction

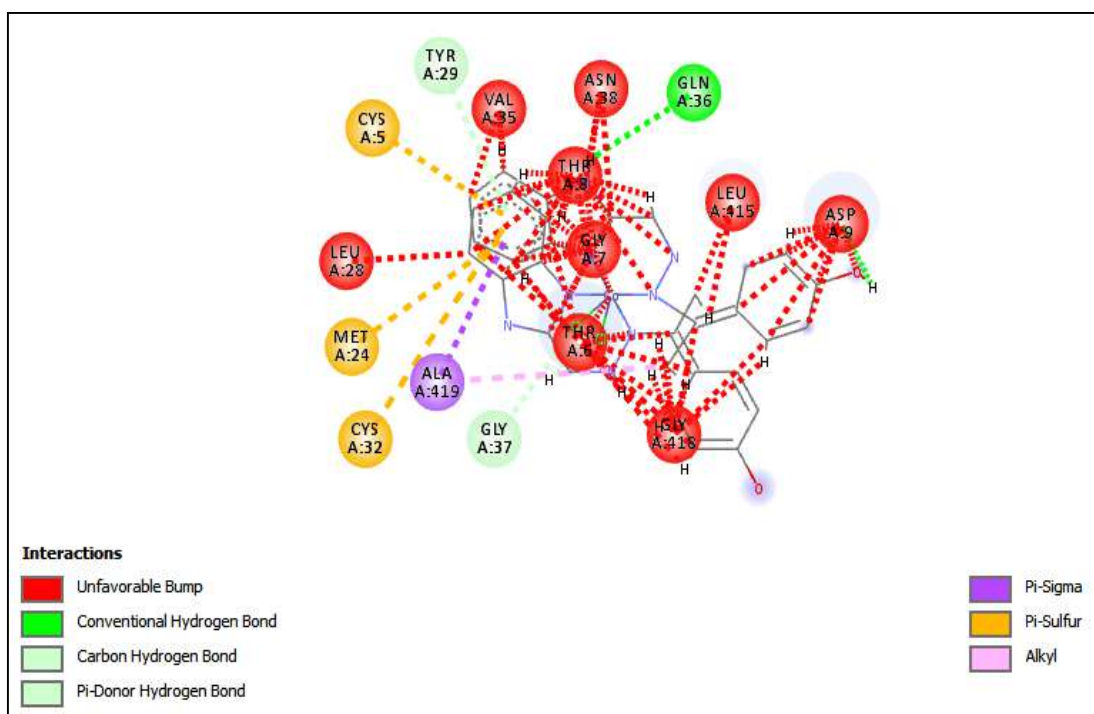
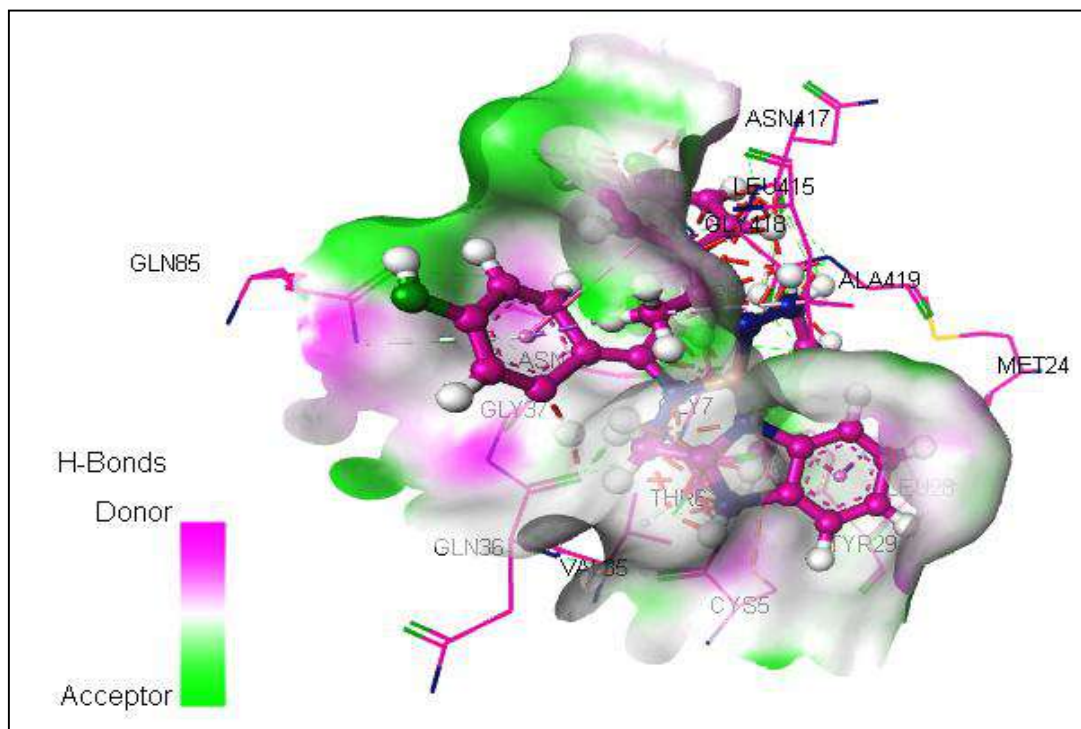


Figure 5.23 3D Interaction and hydrogen bonding of $[\text{Cu}(\text{LB})_2\text{Cl}_2] \cdot \text{H}_2\text{O}$ with amino acids of receptor 2A91 and 2D interaction

5.5.3 Cytotoxic activity

The cytotoxicity assay of the compounds against two tumor cell lines MCF-7 (oestrogen receptor-positive human breast cancer) HeLa (human cervical cancer cell line), and the IC₅₀ values compared with the standard tamoxifen and are collected in table 5.5. The obtained results indicated that, all the complexes showed potent cytotoxicity effect, the IC₅₀ value from 6.8 to 10.24 of [Cu(LB)₂Cl₂] \cdot H₂O showed relatively high inhibition towards HeLa cell line and slightly lesser activity towards MCF-7 cell lines [40-44]. The remaining metal complexes showed promising activity against HeLa cell lines. This variation could be due to the selective inhibition of the complexes towards cancer cell lines. The IC₅₀ value of LB, [Co(LB)₂Cl₂] \cdot 2H₂O and [Ni(LB)₂Cl₂] \cdot 2H₂O is 1.20 to 5.2 showed considerably less inhibitory activity towards both cells lines when compared to the standard tamoxifen and the results are represented in figure 5.24 and 5.25.

Table 5.5 IC₅₀ values of LB and its complexes on MCF-7^a and HeL^b cancer cells.

Compounds	MCF-7 ^a	Inhibition %	HeL ^b	Inhibition %
LB	1.2	15.21	>15.0	24.18
[Co(LB)₂Cl₂]\cdot2H₂O	3.8	37.58	5.2	51.21
[Ni(LB)₂Cl₂]\cdot2H₂O	5.0	50.11	>20.0	30.24
[Cu(LB)₂Cl₂]\cdot H₂O	6.8	70.58	10.24	83.12
Tamoxifen	7.5	-	12.5	-

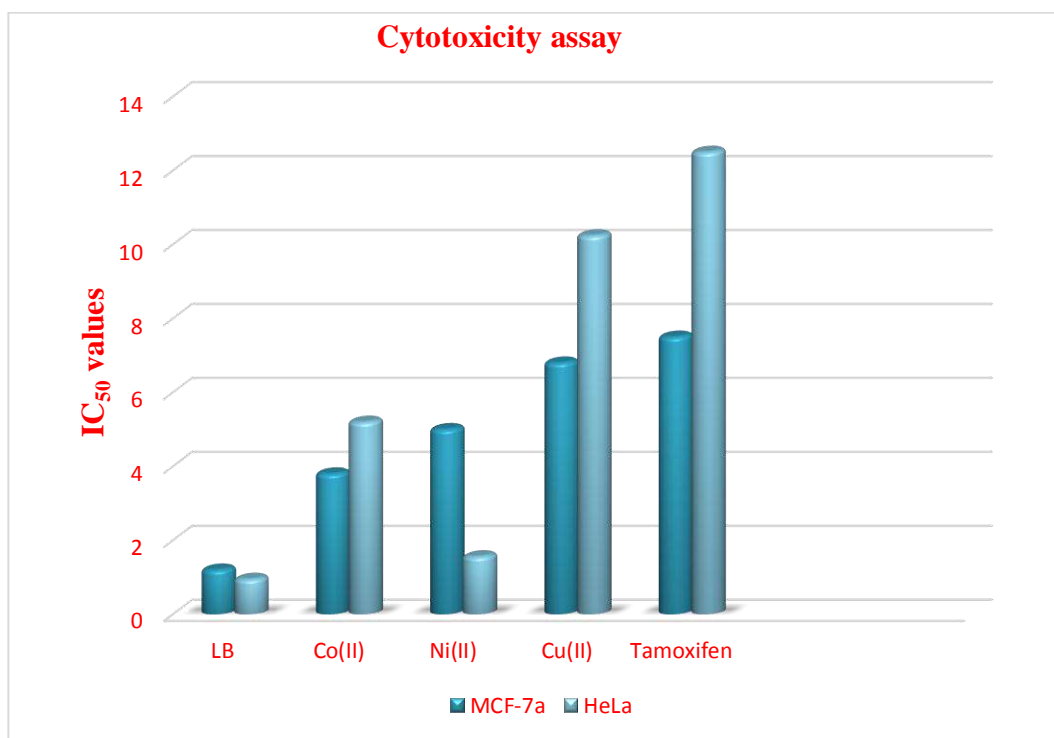


Figure 5.24 Cytotoxicity activity (IC₅₀ values) of LB and their metal complexes

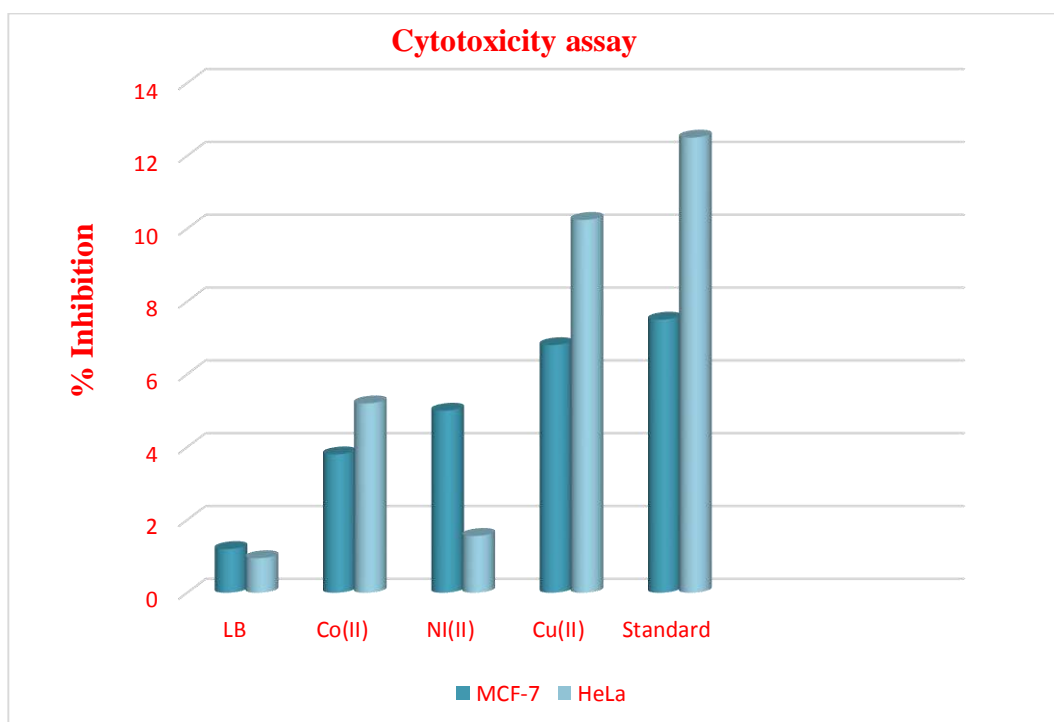


Figure 5.25 Cytotoxicity activity (Inhibition %) of B and their metal complexes

5.6 Conclusions

The Co(II), Ni(II), and Cu(II) complexes with 4-((1Z)-1-[2-(1H-benzimidazol-2-ylmethyl)hydrazinylidene]ethyl)phenol (LB) and 4-((1Z)-1-[2-(1H-benzimidazol-2-ylmethyl)hydrazinylidene]ethyl)aniline (BN) were synthesized and characterized by elemental analysis, mass, IR, ¹H NMR electronic spectra, magnetic studies, molar conductance. For LB and their metal complexes, the TGA and XRD analysis was carried out. The spectral studies suggest that the ligand is bidentate in nature, For the LB and their metal complexes, the cytotoxic activities were evaluated on two different MCF-7 and HeLa cancerous cell lines in which [Cu(LB)₂Cl₂] \cdot H₂O showed promising cytotoxic inhibition while the LB, [Co(LB)₂Cl₂] \cdot 2H₂O and [Ni(LB)₂Cl₂] \cdot 2H₂O complexes exhibited a moderate activity. The molecular docking studies reveal that the complexes have comparatively good binding scores as compared to the *EGFR tyrosine kinase* receptor may be considered as a potent cytotoxic agent. All the complexes showed significant DPPH antioxidant activity compared to both the uncoordinated ligands also, among the studied complexes, [Co(LB)₂Cl₂] \cdot 2H₂O, [Cu(LB)₂Cl₂] \cdot H₂O, Ni(BN)₂Cl₂] \cdot 2H₂O and Co(BN)₂Cl₂] \cdot 2H₂O complexes exhibited promising antioxidant activity. The anti-lipase activity for both the ligands and their respective metal complexes showed best inhibitory activity.

References

- [1] Y. Bansal, O. Silakari, The therapeutic journey of benzimidazoles: a review, *Bioorgan Med. Chem.* 20, 2012, 6208-6236.
- [2] Y.L. Yao, Y.X. Che, J.M. Zheng, The coordination chemistry of benzimidazole- 5,6-dicarboxylic acid with Mn(II), Ni(II), and Ln(III) complexes (Ln $\frac{1}{4}$ Tb, Ho, Er, Lu), *Cryst. Growth Des.* 8, 2008, 2299-2306.
- [3] C.H. Chen, W.S. Huang, M.Y. Lai, W.C. Tsao, J.T. Lin, Y.H. Wu, T.H. Ke, L.Y. Chen, C.C. Wu, Versatile, benzimidazole/amine-based am-bipolar compounds for electroluminescent applications: single-layer, blue, fluorescent OLEDs, hosts for single-layer, phosphorescent OLEDs, *Adv. Funct. Mater.* 19, 2009, 2661-2670.
- [4] G.G. Mohamed, Z.H. Abd El-Wahab, Salicylidene-2-aminobenzimidazole Schiff base complexes of Fe(III), Co(II), Ni(II), Cu(II), Zn(II) and Cd(II), *J. Therm. Anal. Calorim.* 73, 2003, 347-359.
- [5] M.R. Maurya, A. Kumar, M. Ebel, D. Rehder, Synthesis, characterization, reactivity, and catalytic potential of model vanadium(IV, V) complexes with benzimidazole-derived ONN donor ligands, *Inorg. Chem.* 45, 2006, 5924-5937.
- [6] M.R. Maurya, M. Bisht, A. Kumar, M.L. Kuznetsov, F. Avecilla, J.C. Pessoa, Synthesis, characterization, reactivity and catalytic activity of oxidovanadium(IV), oxidovanadium(V) and dioxidovanadium(V) complexes of benzimidazole modified ligands, *Dalton T* 40, 2011, 6968-6983.
- [7] O. Dayan, S. Demirmen, N. Ozdemir, Heteroleptic ruthenium(II) complexes of 2-(2-pyridyl) benzimidazoles: a study of catalytic efficiency towards transfer hydrogenation of acetophenone, *Polyhedron* 85, 2015, 926-932.
- [8] G. Krishnamurthy, Synthesis and thermal degradation kinetics of some Cobalt(II) Complexes with 1,2-disubstituted benzimidazoles, *Journal. Teach. Resear.* 17(1), 2010, 38-43.

- [9] O. Dayan, N. Ozdemir, Z. Serbetci, M. Dincer, B. Cetinkaya, O. Buyukgungor, Synthesis and catalytic activity of ruthenium(II) complexes containing pyridine-based tridentate triamines ('NNN') and pyridine carboxylate ligands (NO), *Inorg. Chim. Acta* 392, 2012, 246-253.
- [10] O. Dayan, S. Dayan, I. Kani, B. Cetinkaya, Ruthenium(II) complexes bearing pyridine-based tridentate and bidentate ligands: catalytic activity for transfer hydrogenation of aryl ketones, *Appl. Organomet. Chem.* 26, 2012, 663-670.
- [11] N.M. Shavaleev, S.V. Eliseeva, R. Scopelliti, J.C.G. Bunzli, Designing simple tridentate ligands for highly luminescent europium complexes, *Chem-Eur J.* 15, 2009, 10790-10802.
- [12] G. Krishnamurthy, N. Shashikala, Synthesis of Ruthenium(II) Carbonyl Complexes with 2-Monosubstituted and 1,2-Diisubstituted Benzimidazoles, *Journal of Serb. Chem. Soc.* 74(10), 2009, 1085-1096.
- [13] H. Kucukbay, B. Cetinkaya, S. Guesmi, P.H. Dixneuf, New (carbene)ruthenium-arene complexes: preparation and uses in catalytic synthesis of furans, *Organometallics* 15, 1996, 2434-2439.
- [14] S. Samai, K. Biradha, Chemical and mechano responsive metal-organic gels of bis(benzimidazole)-based ligands with Cd(II) and Cu(II) halide salts: self sustainability and gas and dye sorptions, *Chem. Mater* 24, 2012, 1165-1173.
- [15] V.C.O. Njar, A.M.H. Brodie, Discovery and development of galeterone (TOK-001 or VN/124-1) for the treatment of all stages of prostate cancer, *J. Med. Chem.* 58, 2015, 2077-2087.
- [16] Y.L. Yao, Y.X. Che, J.M. Zheng, The coordination chemistry of benzimidazole-5,6-dicarboxylic acid with Mn(II), Ni(II), and Ln(III) complexes (Ln $\frac{1}{4}$ Tb, Ho, Er, Lu), *Cryst. Growth Des.* 8, 2008, 2299-2306.

- [17] J. Dhanaraj Chellaian, J. Johnson, Spectral characterization, electrochemical and anticancer studies on some metal(II) complexes containing tridentate quinoxaline Schiff base, *Spectrochimica Acta Part A: Molecular and Biomolecular Spectroscopy* 127, 2014, 396-404.
- [18] S. Singh, J. Gupta, S.S. Kanwar, Antilipase, antiproliferatic and antiradical activities of methanolic extracts of *Vinca major*. *J. Pharmacognosy Phytochem.* 3, 2014, 53-64.
- [19] N.D. Shashikumar, G. Krishnamurthy, H.S. Bhojya Naik, M.R. Lokesh and K. S. Jithendra kumara, Synthesis of new biphenyl-substituted quinoline derivatives, preliminary screening and docking studies. *J. chem. sci.* 126, 1, 2014, 205–212.
- [20] V. Padmavathi, B.C. Venkatesh, A. Muralikrishna, A. Padmaja, The reactivity of Gem cyanoester ketene dithiolates towards the development of potent antioxidant heterocycles, *Chem. Pharm. Bull.* 60, 2012, 449-458.
- [21] G. Krishnamurthy Synthesis, molecular modeling and biological activity of zinc(II) salts with 1,4-bis(benzimidazol-2-yl)benzene, *Journal of Chemistry*, 41, 2013, 54-96.
- [22] Q.Y. Yu, B.X. Lei, J.M. Liu, Y. Shen, L.M. Xiao, R.L. Qiu, D.B. Kuang, C.Y. Su, Ruthenium dyes with heteroleptic tridentate 2,6-bis(benzimidazol-2-yl)-pyridine for dye-sensitized solar cells: enhancement in performance through structural modifications, *Inorg. Chim. Acta* 392, 2012, 388-395.
- [23] A.K. Vannucci, J.F. Hull, Z. Chen, R.A. Binstead, J.J. Concepcion, T.J. Meyer, Water oxidation intermediates applied to catalysis: benzyl alcohol oxidation, *J. Am. Chem. Soc.* 134, 2012, 3972-3975.
- [24] J. Diez, J. Gimeno, A. Lledos, F.J. Suarez, C. Vicent, Imidazole based ruthenium(IV) complexes as highly efficient bifunctional catalysts for the redox isomerization of allylic alcohols in aqueous medium: water as cooperating ligand, *Acs Catal.* 2, 2012, 2087-2099.

- [25] W.J. Ye, M. Zhao, W.M. Du, Q.B. Jiang, K.K. Wu, P. Wu, Z.K. Yu, Highly active ruthenium(II) complex catalysts bearing an unsymmetrical NNN ligand in the (asymmetric) transfer hydrogenation of ketones, *Chem-Eur J.* 17, 2011, 4737-4741.
- [26] G. Krishnamurthy, Shashikala N. Narashimiah, Complexes of zinc(II) with 1,2-disubstituted Benzimidazoles, *Journal of chemical Research*, 12, 2006, 766-768.
- [27] G. Krishnamurthy, Synthesis, Characterization of Ruthenium(III) chloride Complexes with Some 1,2-Disubstituted Benzimidazoles and their Catalytic Activity, *Synthesis and Reactivity in Inorganic, Metal-Organic, and Nano-Metal Chemistry*, 41(6), 2011, 590-597.
- [28] F. Arjmand, M. Muddassir, Chiral preference of L-tryptophan derived metal based antitumor agent of late 3d-metal ions (Co(II), Cu(II) and Zn(II)) in comparison to d- and dl-tryptophan analogues: their in vitro reactivity towards CT DNA, 50-GMP and 50-TMP, *Eur. J. Med. Chem.* 45, 2010, 3549–3557.
- [29] J.R. Lakowicz, G. Webber, Quenching of fluorescence by oxygen. Probe for structural fluctuations in macromolecules, *Biochemistry* 12, 1973, 4161-4170.
- [30] A. Wolfe, G.H. Shimer, T. Meehan, Polycyclic aromatic hydrocarbons physically intercalate into duplex regions of denatured DNA, *Biochemistry* 26, 1987, 6392-6396.
- [31] H.T.A. Mohsen, F.A.F. Ragab, M.M. Ramla, H.I.E. Diwani, Novel benzimidazolepyrimidine conjugates as potent anti-tumor agents, *Eur. J. Med. Chem.* 45, 2010, 2336-2344.
- [32] S. Demirayak, I. Kayagil, L. Yurttas, Microwave supported synthesis of some novel 13-diarylpyrazino[12-a]benzimidazole derivatives and investigation of their anticancer activities, *Eur. J. Med. Chem.* 46, 2011, 411-416.

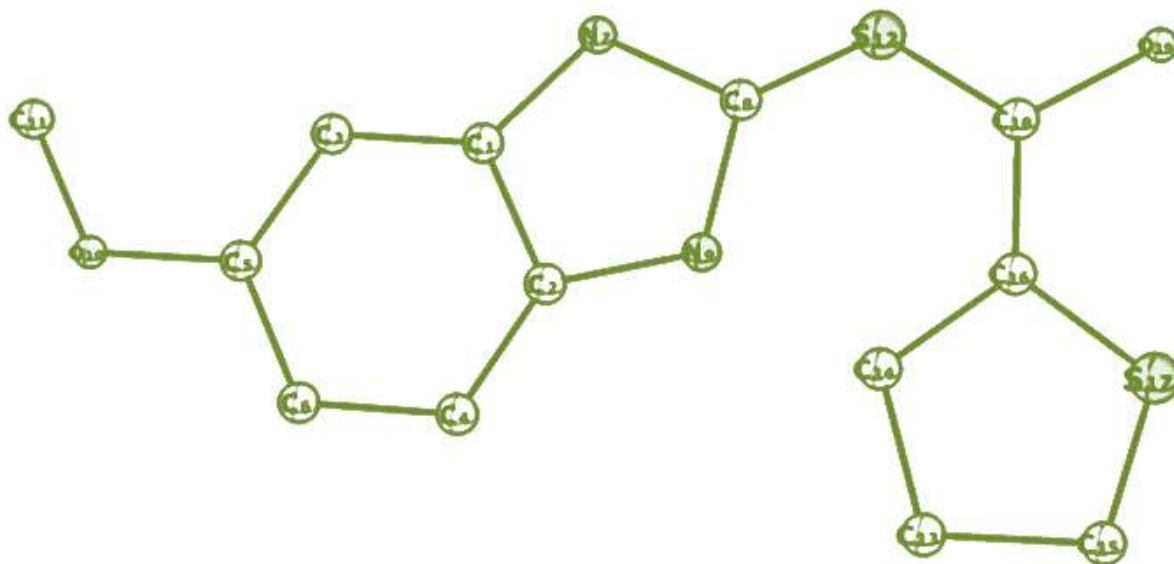
- [33] S. Demirayak, A. Usama, A.C. Mohsen, K. Agri, Synthesis and anticancer and anti-HIV testing of some pyrazino[12-a]benzimidazole derivatives, *Eur. J. Med. Chem.* 37, 2002, 255-260.
- [34] A. Kamal, P. Praveen Kumar, K. Sreekanth, B.N. Seshadri, P. Ramulu, Synthesis of new benzimidazole linked pyrrolo [21-c][1,4] benzodiazepine conjugates with efficient DNA-binding affinity and potent cytotoxicity, *Bioorg. Med. Chem. Lett.* 18, 2008, 2594-2598.
- [35] E. Moriarty, M. Carr, S. Bonham, M.P. Carty, F. Aldabbagh, Synthesis and toxicity towards normal and cancer cell lines of benzimidazole quinines containing fused aromatic rings and 2-aromatic ring substituents, *Eur. J. Med. Chem.* 45, 2010, 3762-3769.
- [36] E.J. Hanan, B.K. Chan, A.A. Estrada, D.G. Shore, J.P. Lyssikatos, Mild and general one-pot reduction and cyclization of aromatic and heteroaromatic 2-nitroamines to bicyclic 2H-imidazoles, *Syn-lett* 18, 2010, 2759-2764.
- [37] D. Yang, D. Fokas, J. Li, L. Yu, C.M. Baldino, A versatile method for the synthesis of benzimidazoles from o-nitroanilines and aldehydes in one step via a reductive cyclization, *Synthesis* 1, 2005, 47-56.
- [38] D. Seenaiiah, P. Ramachandra Reddy, G. Mallikarjuna Reddy, A. Padmaja, V. Padmavathi, N. Siva krishna, Synthesis, antimicrobial and cytotoxic activities of pyrimidinyl benzoxazole, benzothiazole and benzimidazole, *Eur. J. Med. Chem.* 77, 2014, 1-7.
- [39] Subba Poojari, P. Parameswar Naik, G. Krishnamurthy, One-pot synthesis of thieno [2,3-d] pyrimidin-4-ol derivatives mediated by polyphosphonic anhydride, *Tetrahedron Letters*, 53, 2012, 4639-4643.
- [40] R.V. Shingalapur, K.M. Hosamani, R.S. Keri, M.H. Hugar, Derivatives of benzimidazole pharmacophore: synthesis anticonvulsant antidiabetic and DNA cleavage studies, *Eur. J. Med. Chem.* 45, 2010, 1753-1759.

- [41] K. Achar, K.M. Hosamani, H.R. Seetharamareddy, In-vivo analgesic and antiinflammatory activities of newly synthesized benzimidazole derivatives, *Eur. J. Med. Chem.* 45, 2010, 2048-2054.
- [42] Subba Poojari, P. Parameswar Naik, G. Krishnamurthy, Synthesis of macrocycles containing 1,3,4-oxadiazole and pyridine moieties, *Tetrahedron Letters* 55, 2014, 305–309.
- [43] A.O. El-Nezhawy, A.R. Biuomy, F.S. Hassan, A.K. Ismaiel, H.A. Omar, Design synthesis and pharmacological evaluation of omeprazole-like agents with anti-inflammatory activity, *Bioorg. Med. Chem.* 21, 2013, 1661-1670.
- [44] M. Ishikawa, K. Nonoshita, Y. Ogino, Y. Nagae, D. Tsukahara, H. Hosaka, H. Hosaka, H. Maruki, S. Ohyama, R. Yoshimoto, K. Sasaki, Y. Nagata, T. Nishimura, Discovery of novel 2-(pyridine-2-yl)-1H-benzimidazole derivatives as potent glucokinase activators, *Bioorg. Med. Chem. Lett.* 19, 2009, 4450-4454.

Chapter – 6

Part A

Metal complexes of S-1H-benzimidazol-2-yl thiophene-2-carbothioate: Synthesis, spectral characterization, XRD, DFT, molecular docking and biological studies



INTRODUCTION

Benzimidazole derivatives are structural isosters of naturally occurring nucleotides, which allow them to interact easily with the biopolymers of the living system which is responsible for their numerous biological activities and functions [1-5]. The benzimidazole containing thiophene and sulfanyl derivatives possess many important pharmacological activities such as potent bacterial, fungal, anticonvulsant, antioxidant and cytotoxic agents [6-8]. In addition to this, the transition metal complexes with benzimidazole derivatives are used as catalysts, optical materials, chemical sensors, and biological probes [9, 10]. In view of the above versatile applications of benzimidazole derivatives and their transition metal complexes, the author in this chapter made an attempt to synthesis a series of benzimidazole derivatives containing 2-mercapto benzimidazole and benzimidazole-2-ylmethanethiol moieties as well as their some 3d metal ion complexes and characterized them by various spectral techniques and the pharmacological evaluation and molecular docking have also been studied

For the convenience of discussion the present chapter is divided into two parts

Part-A

6.1 Synthesis, characterization and biological evaluation of S-(1H-benzimidazole-2-yl)thiophene-2-carbothioae [BTC] and their metal complexes

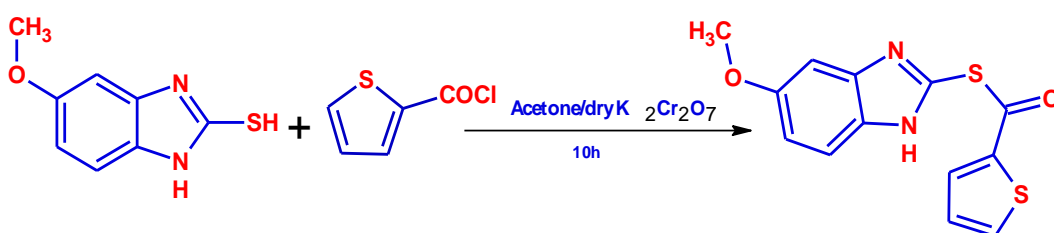
Part-B

6.2 Synthesis, characterization and biological evaluation of of 2-[(thiophen-2-yl)sulfanyl)methyl]-1H-benzimidazole [BT] and their metal complexes

6.1 EXPERIMENTAL

6.1.1 Synthesis of S-(1H-benzimidazole-2-yl) thiophene-2-carbothioate [BTC]

A solution of 5-methoxy-2-mercaptobenzimidazole (1.83g, 0.01mol) in 30mL of acetone with 2-thiophencarboxylchloride (1.46g, 0.01mol), was refluxed for 16h, on oil bath with stirrer. The resulting solution was poured into ice cold water. The white precipitate formed was collected through filtration, washed with hot water and dried under vacuum and then recrystallized from the methanol. The reaction path is showed in scheme 6.1



Scheme 6.1 Preparation of the BTC

6.1.2 Synthesis of the metal complexes

Methanolic solution of metal (II) chlorides [1mol, Co(II), Ni(II), Cu(II) and Zn(II)] was added in drops separately to a methanolic solution of the ligand (2 mol) and the reaction mixture was refluxed on a water bath for 3-4h. The solid separated was obtained by filtration, washed with hot methanol and dried under vacuum over anhydrous calcium chloride. The physical properties and the analytical data are collected in table 6.1.

6.1.3 Results and discussion

The BTC was prepared by condensation of 5-methoxy-2-mercaptobenzimidazole and 2-thiophencarboxylchloride (scheme 6.1), which on further reaction with the metal chlorides yield the resultant complexes with metal: ligand in the ratio 1:2, and represented in figure 6.1.1

Table 6.1.1 Physical properties and analytical data of the metal complexes

Compounds	Colour	Mol.Wt	Yield (%)	Calcd. (found) (%)				Molar conductance ($\text{ohm}^{-1} \text{cm}^2 \text{mol}^{-1}$)	M.P °C
				C	H	N	M		
[CoCl ₂ (BTC) ₂]	Dark green	706.23	65	44.07 (43.98)	2.56 (2.91)	7.91 (6.14)	8.32 (6.81)	22	>300
[NiCl ₂ (BTC) ₂]	Light blue	705.16	62	44.09 (42.78)	2.56 (1.71)	7.91 (6.52)	8.29 (6.12)	35	>300
[Cu(BTC) ₂ Cl ₂]	Dark brown	713.89	60	43.79 (40.25)	2.54 (1.62)	7.86 (6.87)	8.91 (7.25)	32	>300
[Zn(BTC) ₂ Cl ₂]	Light cream	711.89	65	43.68 (41.15)	2.54 (2.08)	7.84 (6.70)	9.15 (8.56)	24	>300

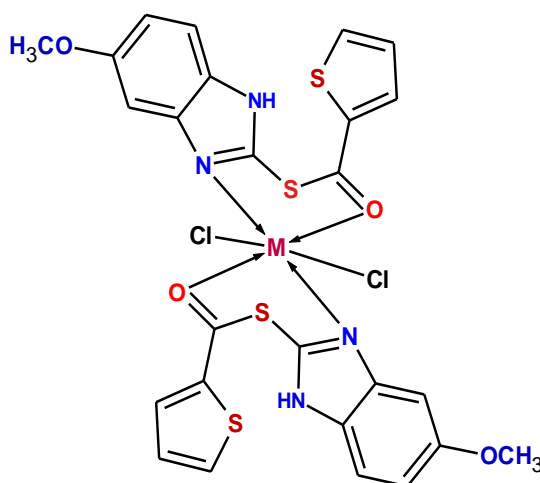


Figure 6.1.1 Proposed structure of metal complexes [M=Co(II), Ni(II), Cu(II) and Zn(II)]

6.1.4 IR spectral studies

The IR spectrum of the ligand and their metal complexes recorded in KBr pellets. The spectrum showed characteristic bands at 3304 cm^{-1} , 1676 cm^{-1} and 1498 cm^{-1} are assigned to (NH), (C=O) and (C=N) stretching frequencies respectively and for (C-S-C) stretching, a band appeared at 791 cm^{-1} [12], In the Cu(II) complex, the absence of (-NH) suggest the coordination through (-NH) group upon deprotonation.

While, in Co(II), Ni(II) and Zn(II) complexes, the band of (C=O) shifted from 1581, 1585, 1589 cm^{-1} and for (C=N) 1423, 1421, 1432 cm^{-1} respectively [13, 14]. The new bands appeared in the spectra of the complexes are at 587, 588, and 574 cm^{-1} are due to M-O vibrations and the bands for M-N appeared at 437, 447, 441 and 474 cm^{-1} . The appearance of these new bands supports the involvement of oxygen and nitrogen atoms. The IR spectra of the ligand and their complexes are represented in figures 6.1.2 to 6.1.5 and their data are given in table 6.1.2.

Table 6.1.2 IR spectral data of the ligand and their metal complexes

Compounds	-NH	C=O	Ar-CH	C-S-C	C=N	M-O	M-N
Ligand BTC	3304	1676	3063	791	1498	-	-
Co(II)	3448	1581	3028	774	1423	578	437
Ni(II)	3478	1585	2945	774	1421	589	447
Cu(II)	-	1621	2988	785	1489	-	441
Zn(II)	3235	1589	2984	761	1432	574	474

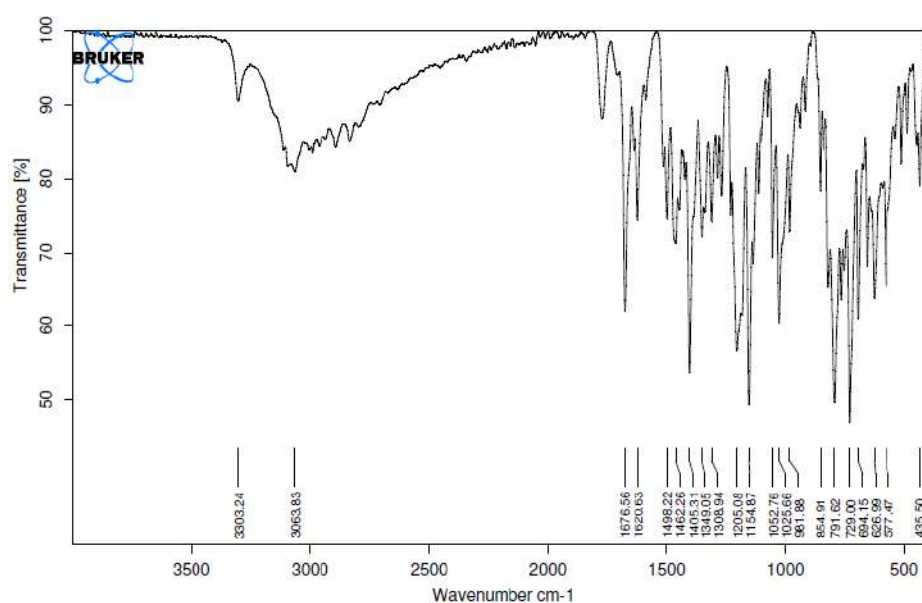
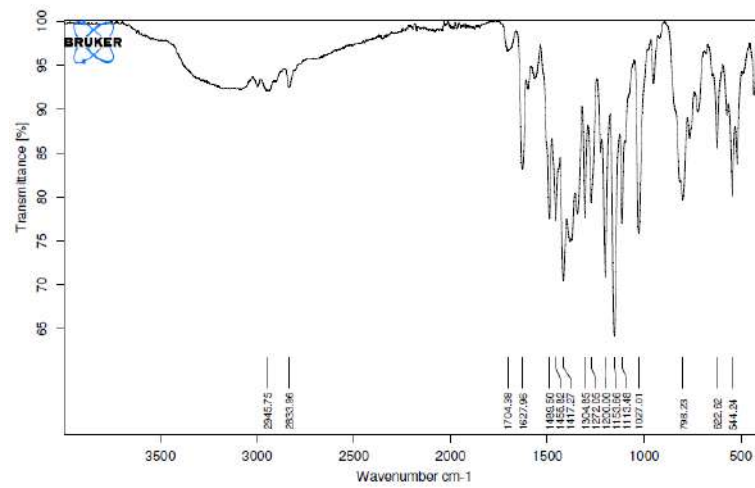
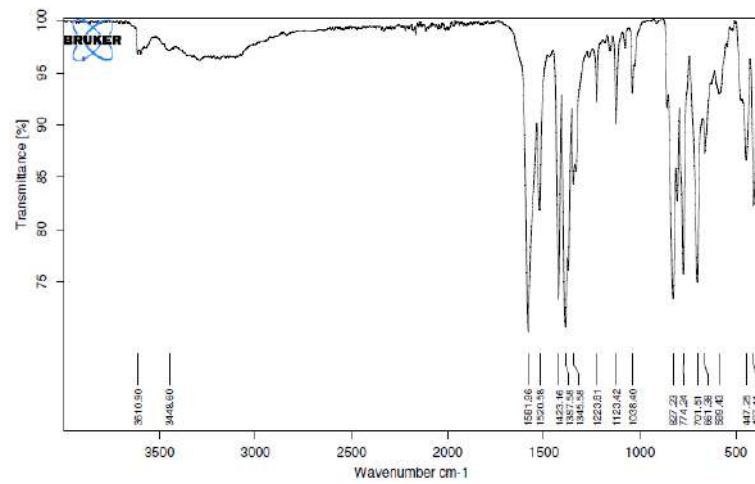
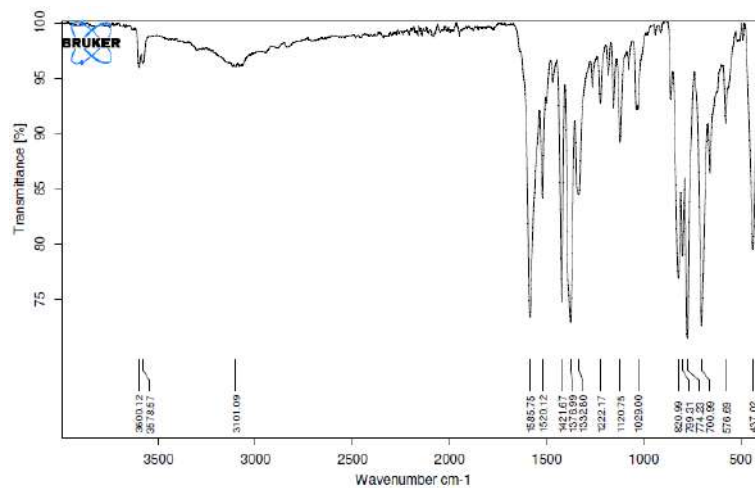


Figure 6.1.2 IR spectrum of BTC

Figure 6.1.3 IR spectrum of $[\text{Cu}(\text{BTC})_2\text{Cl}_2]$ Figure 6.1.4 IR spectrum of $[\text{Ni}(\text{BTC})_2\text{Cl}_2]$ Figure 6.1.5 IR spectra of $[\text{CoCl}_2(\text{BTC})_2]$

6.1.5 Uv-visible studies

The Uv-visible spectrum of the ligand BTC recorded in DMF solution at ca. 10^{-3} m exhibits two bands at 33,353 and 28,571 cm^{-1} suggesting the presence of $\pi-\pi^*$, $n\rightarrow\pi^*$ transitions respectively [15]. Analogous bands are also appeared in the spectra of the complexes. The Ni(II) complex showed a band at 20,381 cm^{-1} and the another at 21,739 cm^{-1} which corresponds to the transitions ${}^3A_{2g} \rightarrow {}^3T_{2g}$ (F) (ν_1) and ${}^3A_{2g} \rightarrow {}^3T_{1g}$ (F) (ν_2) transitions suggest an octahedral geometry [16], while the Co(II) complex exhibits two bands at 22,238 and 20,233 cm^{-1} corresponds ${}^4T_1(\text{F}) \rightarrow {}^4A_2(\text{F})$ and ${}^4T_1(\text{F}) \rightarrow {}^4T_1(\text{P})$ transitions respectively, for an octahedral geometry [17]. The electronic spectrum Cu(II) complex showed a board band at 25,841 cm^{-1} which is assignable to the transition of ${}^2E_g \rightarrow {}^2T_{2g}$, which arise due to the distorted octahedral geometry [18].

Table 6.1.3 Uv-Visible data of the ligand and their metal complexes

Compounds	λ_{max} (cm^{-1})	Band assignments	Geometry
BTC	33353, 28571	$\pi-\pi^*$, $n\rightarrow\pi^*(\text{LMCT})$	-
$[\text{CoCl}_2(\text{BTC})_2]$	20381, 21739	${}^4T_1(\text{F}) \rightarrow {}^4A_2(\text{F})$ ${}^4T_1(\text{F}) \rightarrow {}^4T_1(\text{P})$	Octahedral geometry
$[\text{NiCl}_2(\text{BTC})_2]$	20381, 21739	${}^3A_{2g} \rightarrow {}^3T_{2g}$ (F) (ν_1) ${}^3A_{2g} \rightarrow {}^3T_{1g}$ (F) (ν_2)	Octahedral geometry
$[\text{CuCl}_2(\text{BTC})_2]$	25841	${}^2E_g \rightarrow {}^2T_{2g}$	Distorted octahedral geometry

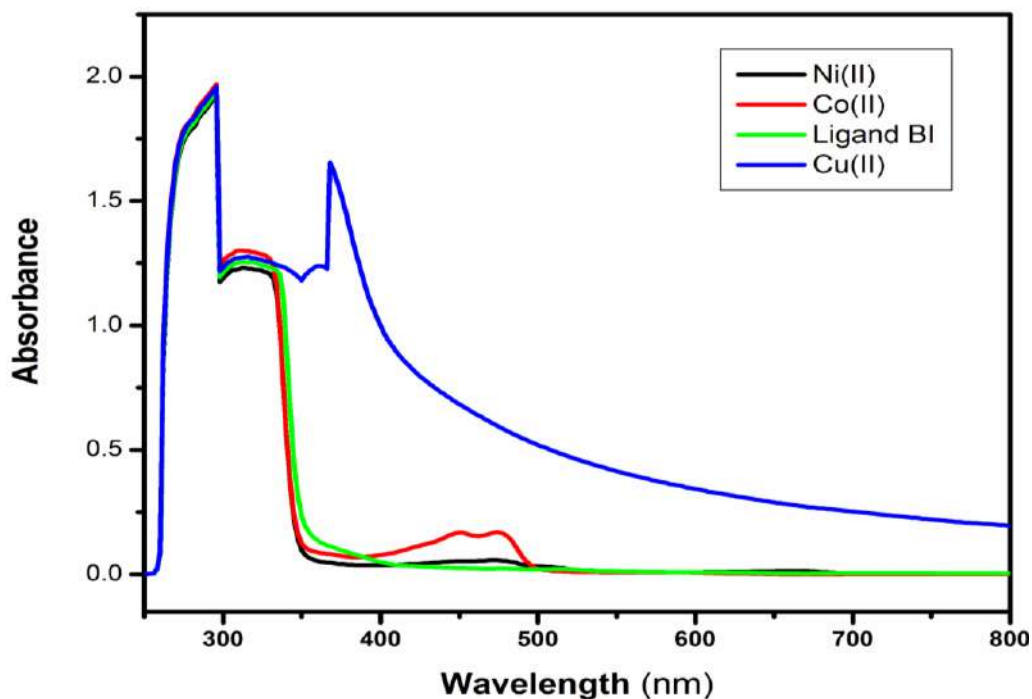


Figure 6.1.6 Uv-Visible spectrum of the BTC and their metal complexes

6.1.6 ^1H NMR and mass studies

The proton NMR spectra of the BTC and Zn(II) complex were recorded in DMSO- d_6 solution using tetramethylsilane (TMS) as an internal standard. The spectrum of the ligand exhibits (-NH) signal at 11.41 ppm. The singlet due to three protons (-OCH₃) appears at 2.40 and 2.44 ppm. The (-CH=N) proton signal obtained at 8.22 ppm and the six aromatic protons at 7.27 to 7.57 ppm. In the Zn(II) complex, the signal due to the proton (-CH=N) of the ligand is shifted towards downfield and appeared at 8.55 ppm suggesting azomethine nitrogen involved in the coordination. Further, the signals shifted slightly in the Zn(II) complex also confirms the involvement of (C=N) of the ligand in the coordination. The structure of the complexes represented in the figure 6.1.8. The mass spectrum of the ligand showed a peak at 290.9(289.2) corresponding to the molecular ion M and M+1 respectively. The Co(II) and Ni(II) complexes exhibit the molecular ion peaks at m/z 706.23 (707.9) and 705.16 (706.2) respectively. For the complexes, the obtained molecular ion peaks confirms the proposed structure and is represented in figures 6.1.9 and 6.1.10.

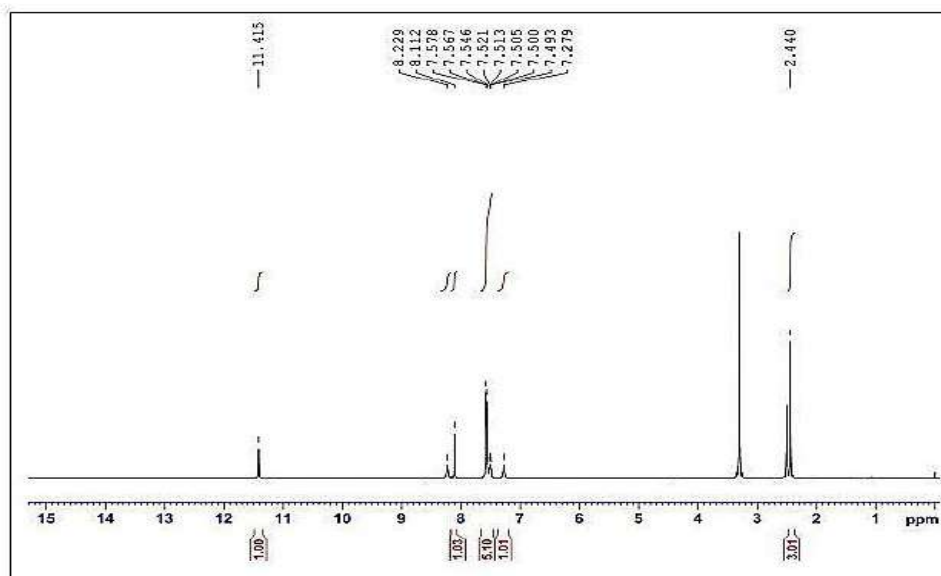
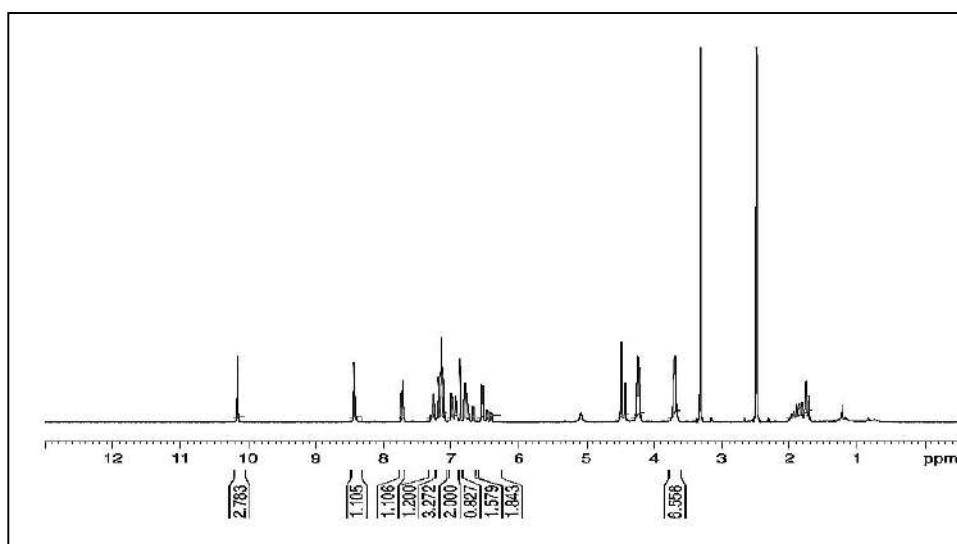
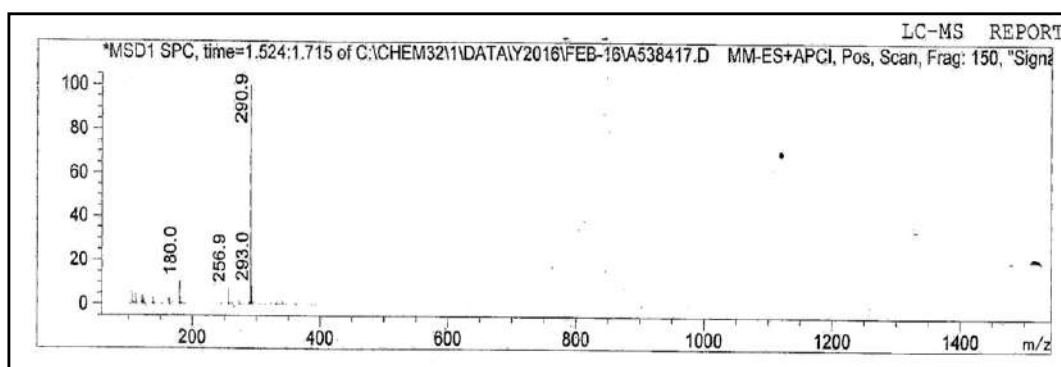
Figure 6.1.7 ¹H NMR spectrum of BTCFigure 6.1.8 ¹H NMR spectrum of [Zn(BTC)₂Cl₂]

Figure 6.1.9 Mass spectrum of BTC

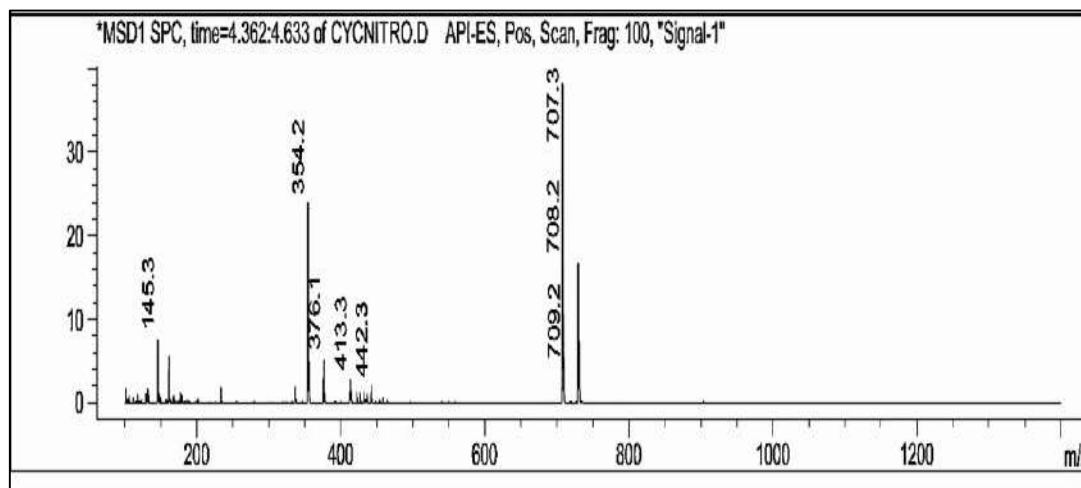


Figure 6.1.10 Mass spectrum of $[\text{CoCl}_2(\text{BTC})_2]$

6.1.7 X-ray powder diffraction studies

The crystal lattice parameters of Co(II), Ni(II) and Cu(II) complexes with BTC were recorded in the range of 5° to 80° using X-ray diffractometer and are represented in figures 6.1.11 to 6.1.13. All the three complexes exhibited sharp peaks due to crystalline nature excepting the ligand and Zn(II) complex which showed the properties similar to the amorphous nature.

The diffractograms and associated data depict the 2θ value for each peak, the relative intensity and inter-planar spacing (d -values). This indexing method also yield the Miller indices (hkl), and half width full maximum values of all the metal complexes. The average crystalline sizes of the complexes dxrd were calculated using Debye Scherrer equation ($D = K\lambda/\beta\cos \theta$) Where D = Particle size, K = Dimensionless shape factor, λ = X-ray wavelength (0.15406\AA) β = Line broadening at half the maximum intensity, θ = Diffraction angle. The complexes of Co(II), Ni(II) and Cu(II) have a crystalline size of 27.58, 26.13 and 35.14 nm respectively suggesting that the complexes are in a nanocrystalline phase [19, 21].

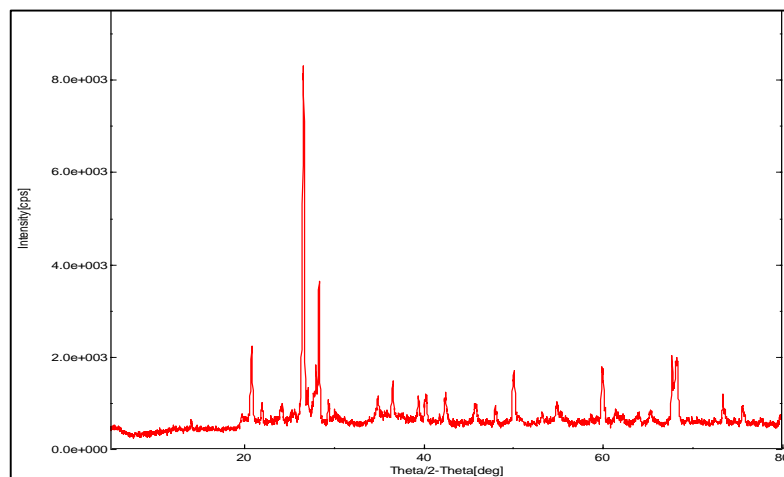


Figure 6.1.11 XRD pattern of [CoCl₂(BTC)₂]

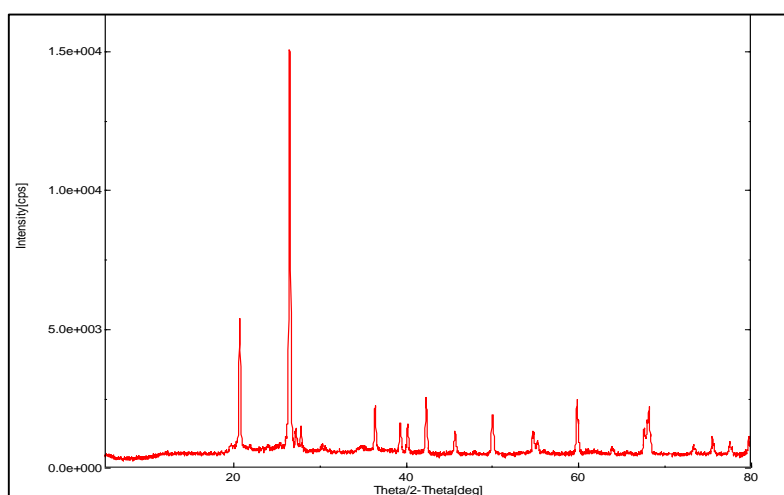


Figure 6.1.12 XRD pattern of [NiCl₂(BTC)₂]

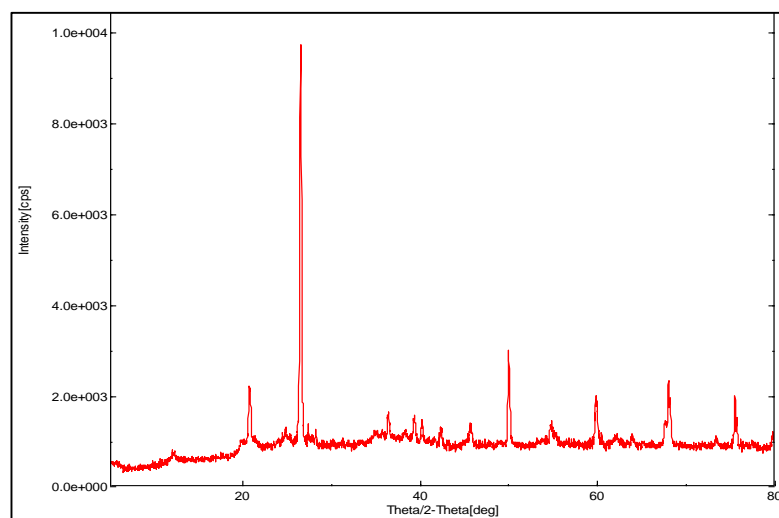


Figure 6.1.13 XRD pattern of [CuCl₂(BTC)₂]

6.1.8 Frontier molecular orbital analysis

The computational calculations of ligand QB performed by Becke's three parameter hybrid exchange functional (B3LYP) with support of chemcraft 1.7 software [22]. The E_{HOMO} and E_{LUMO} energy of the BTC and Co(II) complex are calculated to evaluate the energy gap and represented in figure 6.1.14 and 6.1.15. The global reactivity descriptors as chemical hardness, electrochemical potential, electrophilicity and chemical hardness. Calculation of molecular orbital coefficients indicates that the possible coordination sites of the ligand are -N=N- (azo) and C-O (phenolic) group that binds the metal ion [40].

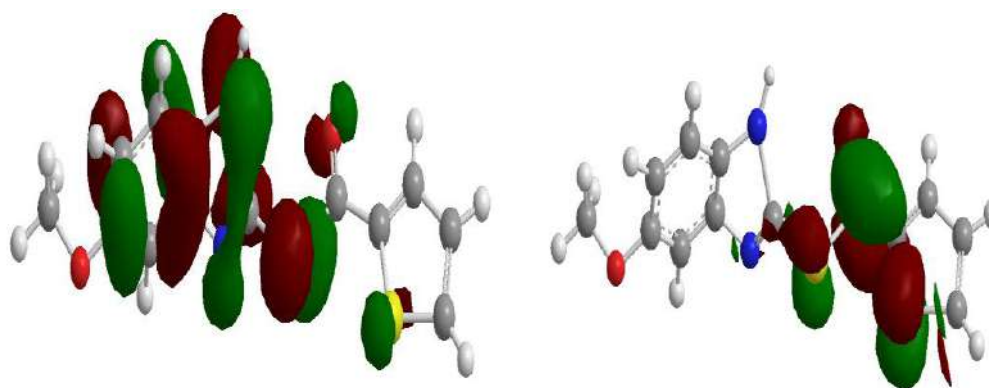


Figure 6.1.14 HOMO-LUMO frontier orbitals of BTC

The E_{HOMO} and E_{LUMO} values are found negative which indicate the stability of the ligand and its complexes [41, 42]. The decrease of E_{HOMO} values of the complexes when compared to the value of the ligand confirms the weakening of metal-ligand sites.

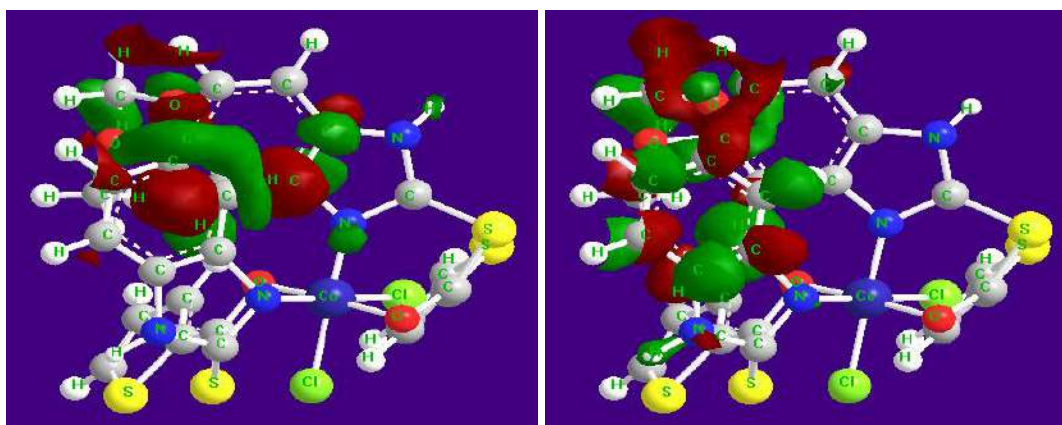


Figure 6.1.15 HOMO-LUMO frontier orbitals of Co(II) complex

The frontier molecular orbitals and the energy band gap elucidate the charge transfer interaction within the molecule, i.e., chemical reactivity values as electronegativity ($\chi = (E_{\text{LUMO}} + E_{\text{HOMO}})/2$), chemical potential ($\mu = -\chi = (E_{\text{LUMO}} + E_{\text{HOMO}})/2$), global hardness ($\eta = (E_{\text{LUMO}} - E_{\text{HOMO}})/2$), global softness ($S = 1/2\eta$) and global electrophilicity index ($\omega = \mu^2/2\eta$) are given in the table 6.1.4.

Table 6.1.4 Calculated quantum chemical parameters for BTC and Co(II) complex

Compound	HOMO in (eV)	LUMO in (eV)	ΔE in (eV)	χ pauling	η in (eV)	σ	μ in (eV)	S	ω in (eV)
BTC	-9.822	-2.720	7.102	-3.551	1.77	0.564	3.551	0.886	11.178
Co(II)	-12.548	-13.312	0.768	-12.93	0.382	2.617	12.93	1.30	7.037

6.1.9 Procedures of biological studies

6.1.10 *In vitro* α -Amylase Inhibitory Assay

The assay was carried out by following the standard method with slight modifications [22]. Starch azure (2mg) was suspended in 0.2 mL of 0.5M *Tris*-HCl buffer (pH 6.9) containing 0.01 M CaCl_2 (substrate solution). The tubes containing substrate solution were boiled for 5 min and then pre-incubated at 37 °C for 5 min. The ligand and their complexes were dissolved in DMSO in order to attain the concentrations of 15, 30 and 45 $\mu\text{g/mL}$. Then, 0.2 mL of particular concentration was added to the tube containing the substrate solution. In addition, 0.1 mL of porcine pancreatic amylase in *Tris*-HCl buffer (2units/mL) was added to the tube containing the ligand and complex solutions and substrate solution. The reaction was carried out at 37 °C for 10 min. The reaction was stopped by adding 0.5 mL of 50% acetic acid in each tube. The absorbance of resulting supernatant was measured at 595 nm using spectrophotometer (Perkin Elmer Lambda 25 UV-VIS spectrophotometer). Acarbose a known α -amylase inhibitor was used as a standard drug. The experiments were repeated thrice.

The α -amylase inhibitory activity was calculated by using following formula: The α -amylase inhibitory activity = $(A_c - A_s) / A_b \times 100$, where A_c , A_s , and A_b are defined as the absorbance of 100% enzyme activity (only solvent with enzyme), 0%

enzyme activity (only solvent without enzyme) a test sample (with enzyme) and a blank (a test sample without enzyme) respectively.

6.1.11 *In Vitro* DPPH free Radical Scavenging Activity

The scavenging activity for the synthesized compounds by using DPPH method as per literature [23, 24]. The compounds of concentrations (20 µg/mL) are dissolved in menthaol and were introduced to each vials of 4 mL. To this test vials 3 cm³ of 0.004 % DPPH in methanol was added and the mixtures was incubated at the ambient temperature for 30 min. Ascorbic acid is used as the standard. The absorbance reduced as the DPPH is scavenged by way of an antioxidant, through contribution of hydrogen to shape a strong DPPH molecule. DPPH scavenging activity calculated by using the following equation and absorbance measured at 517 nm.

$$\text{Scavenging ratio (\%)} = [(A_i - A_o) / (A_c - A_o)] \times 100\%$$

Where A_i is the absorbance within the presence of the check compound; A_o is absorbance of the clean inside the absence of the check compound; A_c is the absorbance within the absence of the test compound.

6.1.12 *In Vitro* antifungal activity

The synthesized ligand, BTC and their metal complexes were tested for antifungal activity with different fungal strains *Candida albicans*, *Aspergillus flavus* and *Microspora griseus* by using agar well diffusion method [25, 26]. Dimethyl sulphoxide (DMSO) was used as solvent control. The fungal culture was inoculated on potato dextrose agar media (20 mL). The test compounds were dissolved in DMSO to get a concentration of 1 mg/mL, and 100 µL of this sample was loaded into the wells of agar plates directly. Plates inoculated with the fungal culture were incubated at 25 °C for 72 h. All the evolution was done in triplicates. Fluconazole was used as the standard. The lowest concentration required for arresting the growth of fungi was regarded as minimum inhibitory concentration (MIC). It was performed by serial broth-dilution method standards, at different concentrations like 10, 25 and 50 µg/mL. After the incubation period, the minimum inhibitory zone at which the microorganism growth was inhibited was measured in millimeters.

6.1.13 Molecular docking studies

The docking is a method which involves the prediction of ligand conformation and orientation in the binding receptacle of the receptor. All the synthesized compounds were screened for docking analysis carried out with the starting coordinates of the human antioxidant enzyme in complex with the competitive inhibitor DTT (PDB ID: 3NMG) by HEX 8.0 and compared with uncoordinated ligand. The receptor was downloaded from RCSB protein data bank. A rigid body docking was performed with HEX 8.0 [27-28], by SP Fourier Transform, FFT steric scan, FFT final search and MM refinement. A more negative E-total energy value implies that a strong binding interaction exists between drug and receptor which leads to the inhibition of receptor activity. The corresponding CIF files of derivatives were converted into PDB file using Argus lab. The ligands were converted to 2D and 3D energy-minimized conformations using Hex 3D Ultra 8.0 and the conformation was visualized using Acceryl Discovery Studio 3.1 Client.

6.1.14 Results and discussion of biological results

6.1.15 *In vitro* α -Amylase Inhibitory Assay

The α -amylase inhibitor assay was carried out for the BTC and their metal complexes, with different concentrations of 15, 30 and 45 $\mu\text{g/mL}$ by using porcine pancreatic amylase enzyme is shown in figure 6.1.14.

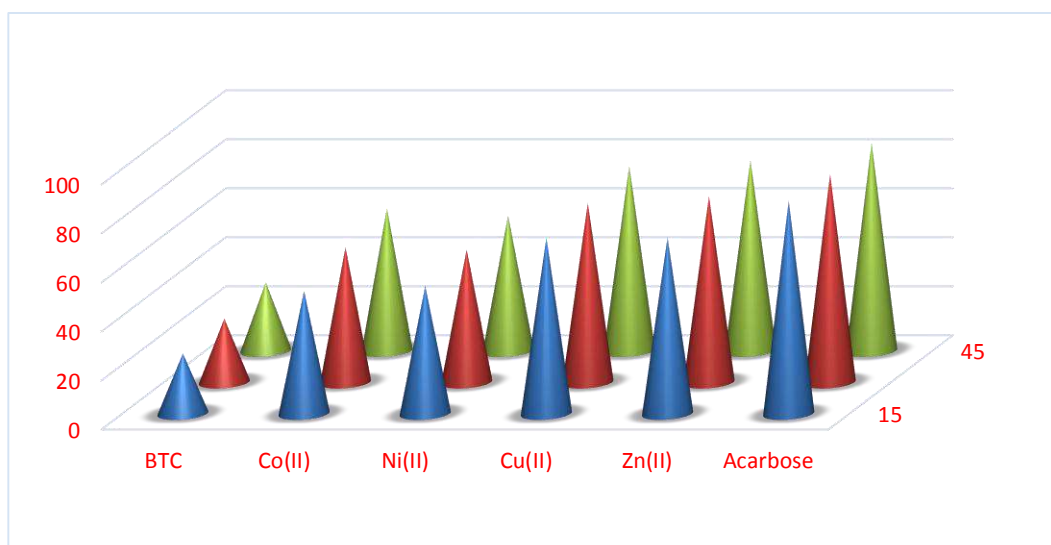


Figure 6.1.16 Graphical representation of α -Amylase Inhibitory

The coordination of the metal ion with heterocyclic imidazole and thiophene moieties with the ligand showed promising amylase inhibition activity is represented in the figure 6.1.16 and table 6.1.5. In which the uncoordinated BTC showed lowest activity, while we compared IC₅₀ values and the standard Acarbose values, the Ni(II) complex showed little lesser activity when compared to Cu(II) while Zn(II) metal complex exhibited highest inhibition activity.

Table 6.1.5 α -Amylase inhibitory assay data of ligand and their metal complexes

Compounds	Conc. $\mu\text{g/mL}$	% Inhibition	IC ₅₀ $\mu\text{g/mL}$
BTC	15	38.21	21.45
	30	41.47	
	45	41.8	
[Co(BTC) ₂]Cl ₂	15	42.14	22.14
	30	42.84	
	45	43.55	
[Ni(BTC) ₂]Cl ₂	15	36.14	20.45
	30	37.41	
	45	39.21	
[Cu(BTC) ₂]Cl ₂	15	68.47	41.63
	30	71.54	
	45	73.11	
[Zn(BTC) ₂]Cl ₂	15	75.77	42.21
	30	76.1	
	45	76.74	

6.1.16 *In Vitro* DPPH free Radical Scavenging Activity Assay

The DPPH scavenging activity performed for the synthesized BTC and Co(II), Ni(II), Cu(II) and Zn(II) complexes. The picrylhydrazyl (purple) radical has been reduced to picrylhydrazine (pale yellow) by antioxidant compounds and the values are given in table 6.1.6. The decreasing in the absorbance of the solution

indicates that the free radical scavenging capacity of the tested compounds and the absorbance of solution decreases proportionally as the increases of non-radical forms of DPPH [29].

Table 6.1.6 DPPH Scavenging IC₅₀ (µg/cm³) data

Compounds	DPPH Scavenging IC ₅₀ (µg/cm ³)
BTC	13±0.1
[Co(BTC) ₂]Cl ₂	22±0.2
[Ni(BTC) ₂]Cl ₂	19±0.4
[Cu(BTC) ₂]Cl ₂	21±0.2
[Zn(BTC) ₂]Cl ₂	14±0.3
BHT	24±0.5

The Co(II) and Cu(II) complexes showed promising scavenging activity with IC₅₀ (µg/cm³) value of (22±0.2 and 21±0.20) while the Ni(II) and Zn(II) complexes showed moderate activity when compared with the standard BHT, The uncoordinated ligand has minimum inhibition activity represented in figure 6.1.17.

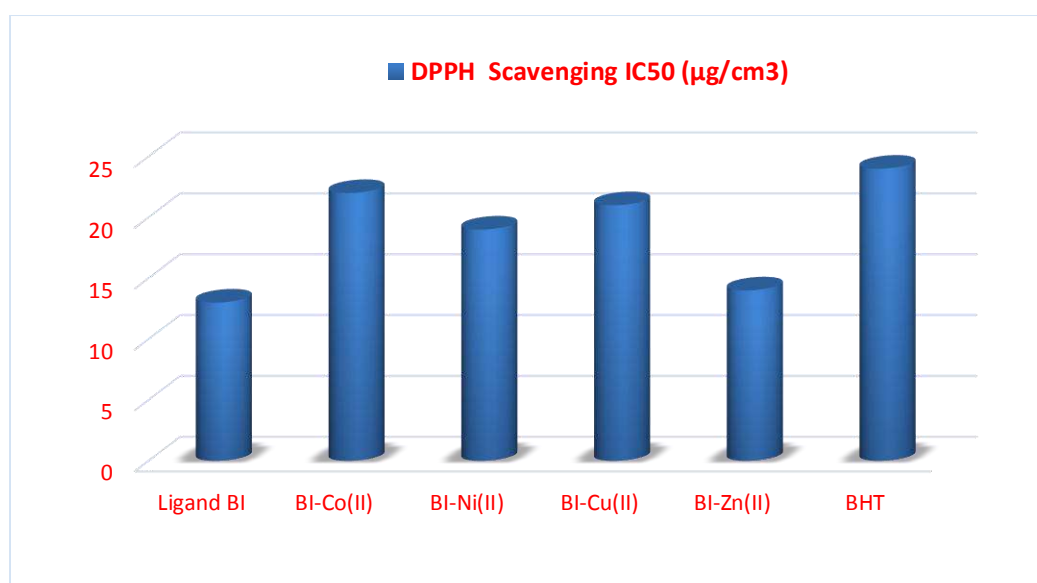


Figure 6.1.17 Graphical representation of DPPH scavenging activity

6.1.17 *In Vitro* antifungal activity

The investigation of antifungal activity reveal that the BTC and their metal complexes showed varying results of antifungal activity with the fungal strains [30, 31], The Cu(II) complex showed highest zone inhibition against *Candida albicans*, *Aspergillus flavus* and *Microspora griseus*, whereas the Ni(II) and Co(II) complexes showed good zone of inhibition, due to the presence of metal ions with two heterocyclic moieties such as benzimidazole and thiophene, which enhances the potential activity, while the uncoordinated ligand and its Zn(II) complex exhibited a moderate activity when compared to the standard Fluconazole.

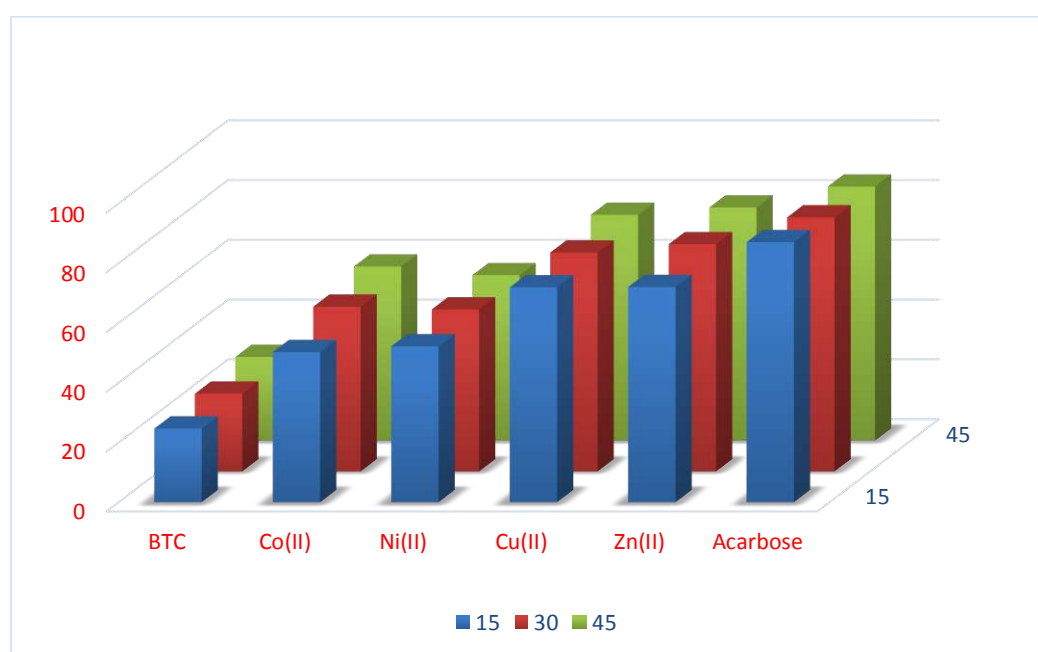


Figure 6.1.18 Graphical representation of antifungal activity of the BTC and their metal complexes

The MIC values suggests that the selective and effective zone inhibition of synthesized metal complexes. The Cu(II) complex with *Candida albicans* (15.23 µg/mL) and *Aspergillus flavus* (14.54 µg/mL) strains and Ni(II) and Co(II) complexes with *Microspora griseus* (08.35, 09.11 µg/mL) strain showed fairly good activity, comparable to standard Fluconazole. The values are tabulated in table 6.1.7.

Table 6.1.7 Minimum inhibitory concentration data of the BTC and their metal complexes

Compounds	Minimum inhibition concentration (MIC $\mu\text{g/mL}$)		
	<i>Aspergillus flavus</i>	<i>Candida albicans</i>	<i>Microspora griseus</i>
BTC	08.21	07.84	6.19
$[\text{Co}(\text{BTC})_2\text{Cl}_2]$	11.21	10.25	09.11
$[\text{Ni}(\text{BTC})_2\text{Cl}_2]$	10.32	12.91	08.35
$[\text{Cu}(\text{BTC})_2\text{Cl}_2]$	14.54	15.23	09.63
$[\text{Zn}(\text{BTC})_2\text{Cl}_2]$	08.66	07.87	6.44
Fluconazole	15.24	15.45	10.41

6.1.18 Molecular docking studies

In correlation with antioxidant activity, it is significant to carry out *in silico* docking studies. The human antioxidant enzyme receptor in complex with the competitive inhibitor DTT (PDB ID: 3NMG) revealed that the good docking interactions with different amino acids and the E-total score [32]. The Ni(II) complex showed maximum binding affinity towards enzyme receptor 3NMG of -366.21kcal/mol, while Co(II), Cu(II) and Zn(II) complexes exhibiting good binding interactions docking scores of -298.14, -281.74 and 280.45 kcal/mol. But the ligand BTC showed least binding interactions of -186.71 kcal/mol. The ligand and receptor interactions involve binding different amino acids like His6, Phe20, Thr136, Ser165, Phe167, Glu198, Phe200, Val236, Thr237, Leu250 and Leu253.

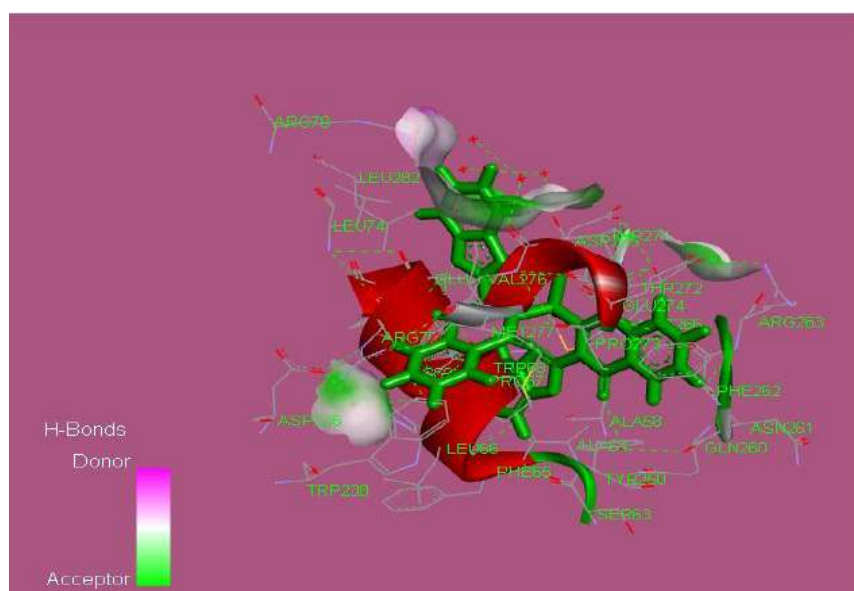


Figure 6.1.19 3D interactions of $[\text{Cu}(\text{BTC})_2\text{Cl}_2]$

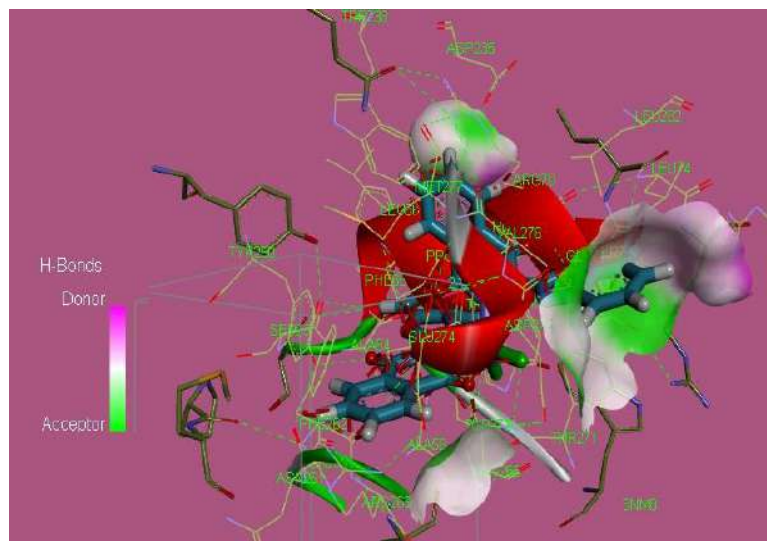


Figure 6.1.20 3D interactions of [Co(BTC)₂]Cl₂

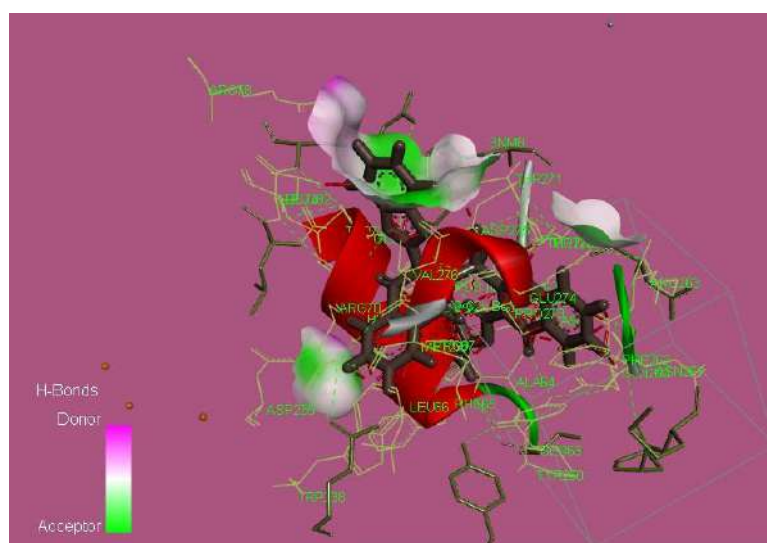


Figure 6.1.21 3D interactions of [Ni(BTC)₂]Cl₂

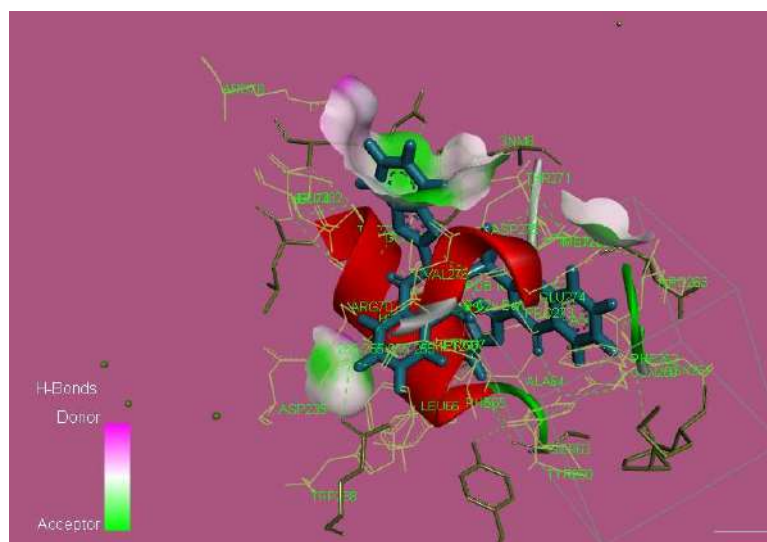


Figure 6.1.22 3D interactions of [Zn(BTC)₂]Cl₂

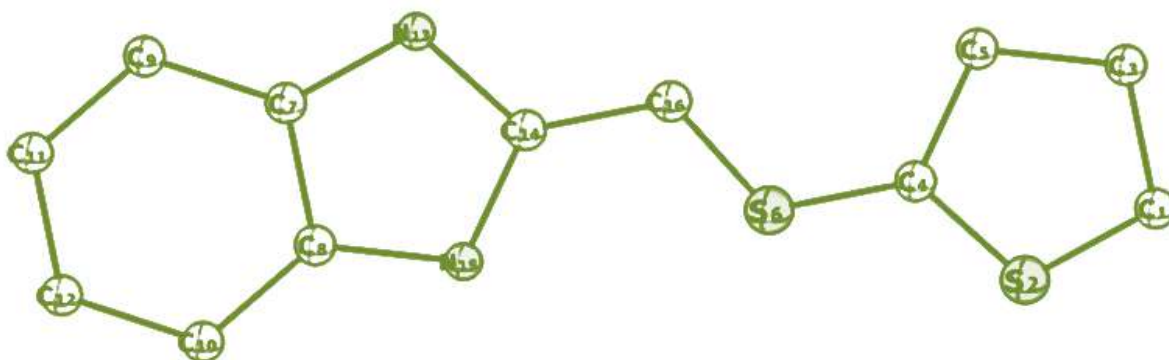
6.1.19 Conclusion

To summarize this work, the ligand BTC and their complexes have been synthesized, characterized by various physical and analytical techniques ^1H NMR, LC-mass, FT-IR, Uv-Visible spectroscopy. The spectral evidence suggest that the coordination of metal ions with carbonyl oxygen and azomethine nitrogen atom which is having bidentate nature. The XRD studies suggest that the crystalline nature of Co(II), Ni(II) and Cu(II) complexes, The DFT study of the BTC and the Co(II) complex is used to calculate the bond length, bond angle, HOMO, LUMO and dipole moment values. The calculated HOMO-LUMO energy gap shows that a charge transfer occurs within the molecule. The ligand and their metal complexes investigated for *In vitro* α -Amylase activity with porcine pancreatic amylase enzyme, showed promising activity with metal complexes. Further the DPPH free radical scavenging activity was carried out, which exhibits potential scavenging activity with metal complexes and least activity towards the ligand. In correlation the docking studies have been done by using human antioxidant enzyme receptor DTT (PDB ID: 3NMG), which supports the wet study data of antioxidant studies. The antifungal activity was performed with *Candida albicans*, *Aspergillus flavus* and *Microspora griseus* by agar well diffusion method.

Chapter – 6

Part B

The transition metal complexes of 2-[(thiophen-2-ylsulfanyl)methyl]-1H-benzimidazole : Synthesis, characterization, molecular docking and biological studies

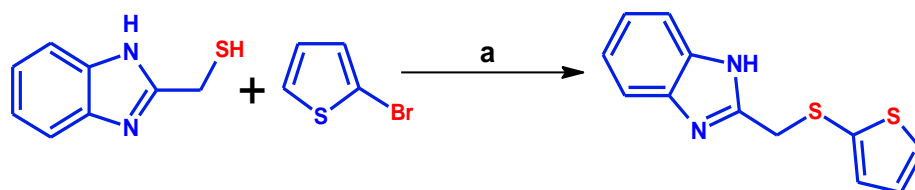


6.2 EXPERIMENTAL

6.2.1 Synthesis of 2-[(thiophen-2-yl/sulfanyl)methyl]-1H-benzimidazole [BT]

1H-benzimidazol-2-ylmethanethiol (0.1 mmol) was dissolved in DMF, to this solution (0.1 mmol) 2-bromothiophene was added drop wise and a catalytic amount of KI was added. The reaction mixture refluxed with stirring under a N₂ atmosphere at 80 °C for 5h. Then the solvent was removed under vacuum, cooled at room temperature, poured into ice, filtered, washed with warm water. The light brown product of BT was obtained after recrystallization from DMF/H₂O.

Ligand BT: Yield: 72%, Mp: 210 °C, Anal, Cald, for C(58.51%) H(4.09%) N(11.37%), Found: C(56.23%) H(3.11%) N(9.15%).MS(LC): 247.12 (248.34)



Scheme 1. a) DMF, KI, 80°C, N₂ reflux 12-14h

6.2.2 Synthesis of the metal complexes

The ethanolic (25mL) solution of ligand BT (0.1mol) was mixed with Co(II), Ni(II) and Cu(II) metal chlorides (0.2mol) in ethanol (25mL) solution with metal–ligand ratio 1:2. The mixture was refluxed for 4 h. The solid product was precipitated on cooling and collected by filtration and washed with hot ethanol until the washing becomes colorless. The product was dried in vacuum over CaCl₂.

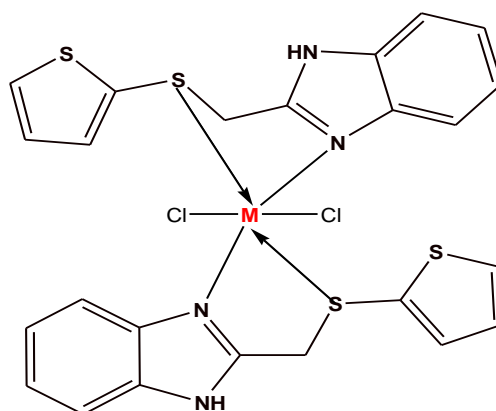


Figure 6.2.1 Proposed structure of metal complexes [M=Co(II), Ni(II), Cu(II) and Zn(II)]

6.2.3 RESULTS AND DISCUSSION

The results indicate that all metal complexes are colored, stable and having high melting points above 300 °C. The molar conductance values of Co(II), Ni(II), Cu(II) and Zn(II) metal complexes are in the range of 30 to 35 $\Omega^{-1}\text{cm}^3$ in DMF solution at concentration 10^{-3} M and are non-electrolytes [33] and having the molar ratio of metal:ligand as 1:2, as represented in table 6.2.1.

Table 6.2.1 Physical properties and analytical data of the metal complexes

Compounds	Colour	Mol. Wt	Yield (%)	Calcd. (found) (%)				Molar conductance ($\text{ohm}^{-1} \text{cm}^2 \text{mol}^{-1}$)
				C	H	N	M	
$[\text{CoCl}_2(\text{BT})_2] \cdot \text{H}_2\text{O}$	Dark brown	620.93	54	46.30 (46.17)	3.24 (2.99)	9.00 (8.94)	9.47 (8.53)	30
$[\text{NiCl}_2(\text{BT})_2] \cdot \text{H}_2\text{O}$	Light maroon	619.93	50	46.32 (46.78)	3.24 (3.05)	9.02 (8.82)	9.43 (9.12)	33
$[\text{CuCl}_2(\text{BT})_2]$	Dark green	624.92	52	41.73 (41.52)	2.92 (2.71)	8.11 (8.01)	9.20 (8.93)	35
$[\text{ZnCl}_2(\text{BT})_2]$	Light cream	625.11	53	45.83 (45.94)	3.20 (3.08)	8.91 (9.03)	10.40 (10.56)	31

6.2.4 IR spectral studies

IR spectrum of the ligand and their complexes were recorded as KBr pellets, it provides the information regarding the coordination of the metal ions with BT. The IR spectrum of BT showed a band at 3185 cm^{-1} is due to (-NH) stretching, and band at 1606 cm^{-1} is due to (C=N) at 1606 cm^{-1} stretching and the 986 cm^{-1} is presence of (C-S-C) stretching at 986 cm^{-1} which supports the formation of coordination band. In their complexes, the band due to C=N group is appeared at $1596\text{-}1599 \text{ cm}^{-1}$ signifying the coordination of azomethine nitrogen with metal ions. Moreover, it is further supported by M-N characteristic bands at $445\text{-}456 \text{ cm}^{-1}$. In addition to this, the band of (C-S-C) also shifted to 965 cm^{-1} indicating that the coordination of metal ions and the appearance of new bands in the range $590\text{-}596 \text{ cm}^{-1}$ also supports this [13, 34].

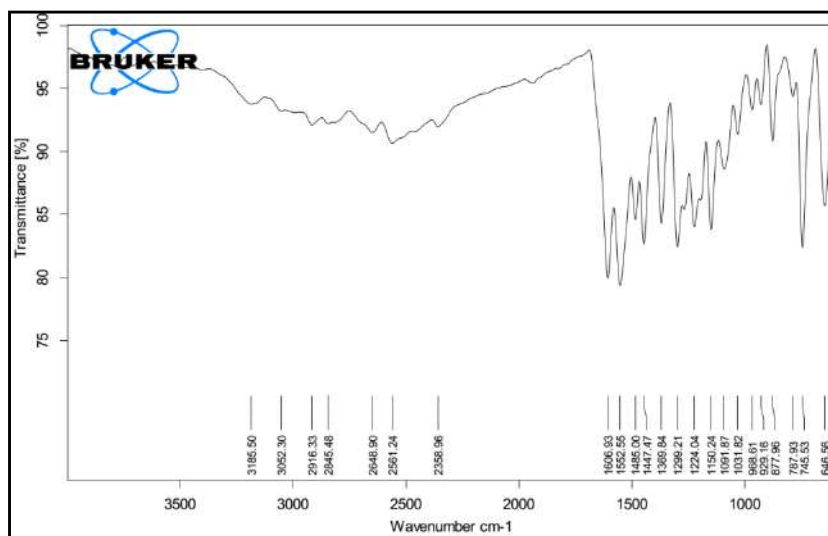
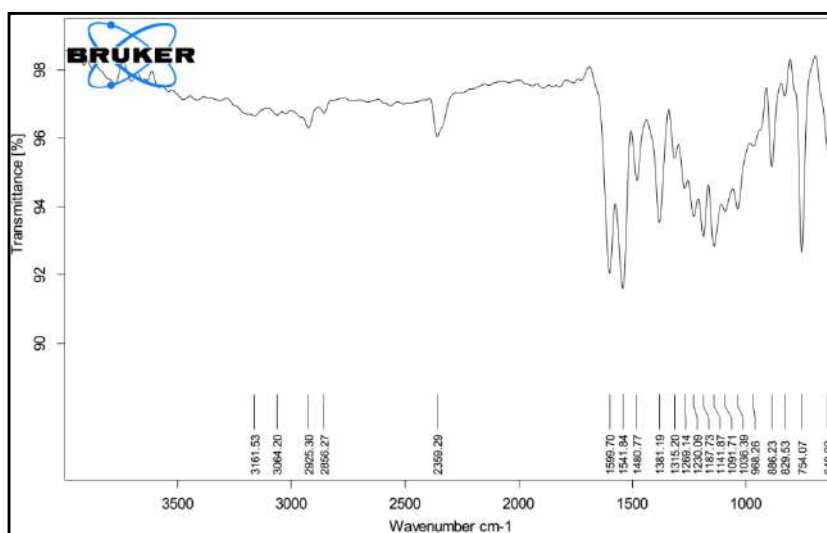
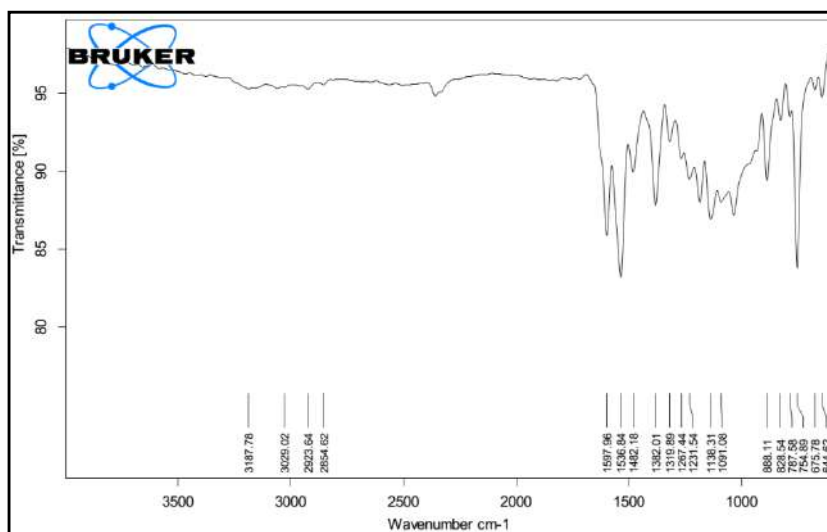


Figure 6.2.2 IR spectrum of BT

Figure 6.2.3 IR spectrum of [CoCl₂(BT)₂].H₂OFigure 6.2.4 IR spectrum of [NiCl₂(BT)₂].H₂O

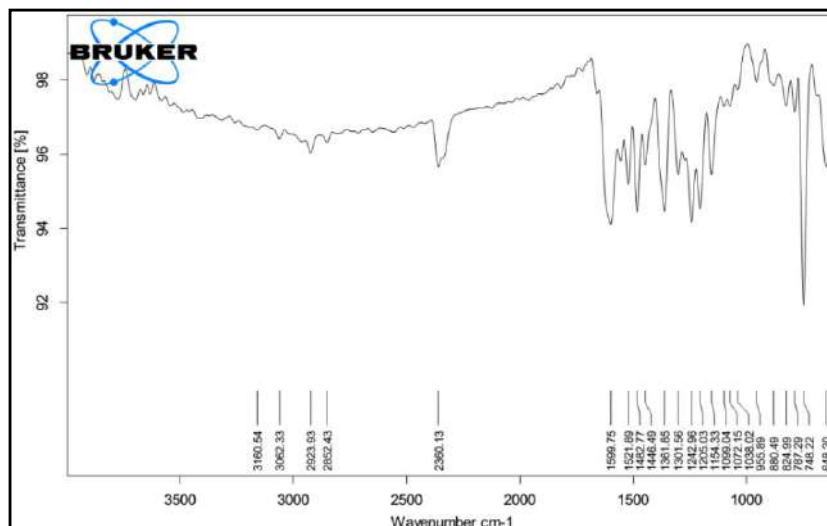


Figure 6.2.5 IR spectrum of $[\text{CuCl}_2(\text{BT})_2]$

6.2.5 Uv-Visible spectroscopy and magnetic moment studies

The BT exhibits the absorption band around 262 nm and 324 nm which are assigned to $\pi \rightarrow \pi^*$, $n \rightarrow \pi^*$ and on complexation the $n \rightarrow \pi^*$ transitions and are shifted to lower frequencies suggest the coordination of imine nitrogen atom with the metal ions [35]. The Co(II) complex exhibits bands at 21,302 and 20,408 cm^{-1} assigned to as ${}^4\text{T}_1(\text{F}) \rightarrow {}^4\text{A}_2(\text{F})$ and ${}^4\text{T}_1(\text{F}) \rightarrow {}^4\text{T}_1(\text{P})$ transitions respectively and the magnetic moment at 4.0 BM that supports the octahedral geometry. The electronic spectra of Ni(II) complex showed two bands 24,154 and 19,379 cm^{-1} corresponds to ${}^3\text{A}_{2g} \rightarrow {}^3\text{T}_{2g}(\text{F})$ (ν_1) and ${}^3\text{A}_{2g} \rightarrow {}^3\text{T}_{1g}(\text{F})$ (ν_2) transitions, and the magnetic moment of 2.7 BM suggest an octahedral geometry. The Cu(II) complex showed a board band at 18,832 cm^{-1} assigned to the transition ${}^2\text{B}_{1g}(\text{F}) \rightarrow {}^2\text{A}_{1g}$ and the obtained magnetic moment of 1.8 BM confirms the octahedral geometry [36].

6.2.6 ${}^1\text{H}$ NMR and Mass studies

The ${}^1\text{H}$ NMR spectrum of BT in DMSO showed a singlet at 12.40 ppm assigned for (-NH) proton and the peaks in the region 7.33 to 7.54 ppm were assigned for chemical shift for hydrogen of symmetrical aromatic rings and the two moieties which bridges by $-\text{CH}_2$ protons at 4.43 ppm appear as a singlet. The Zn(II) complex also showed a signal due to proton of (-NH) group but shifted to down field and appeared at 11.42 ppm compared to the position of the ligand. The multiplet protons of imidazole and thiophene moiety also shifted to 7.11 to 7.89 ppm

respectively and also the signal due to $-\text{CH}_2$ group proton shifted to down field and appeared at 3.91 ppm which indicates the formation complex and the spectra are represented in figure 6.2.6 and 6.2.7.

The mass spectrum of the ligand observed that $m/z = 247.3$ (248.3) corresponds to the molecular ion peak due to (M+1). The Zn(II) complex exhibits the molecular ion peak at $m/z = 625.11$ (626.21) which is represented in figure 6.2.8 and 6.2.9.

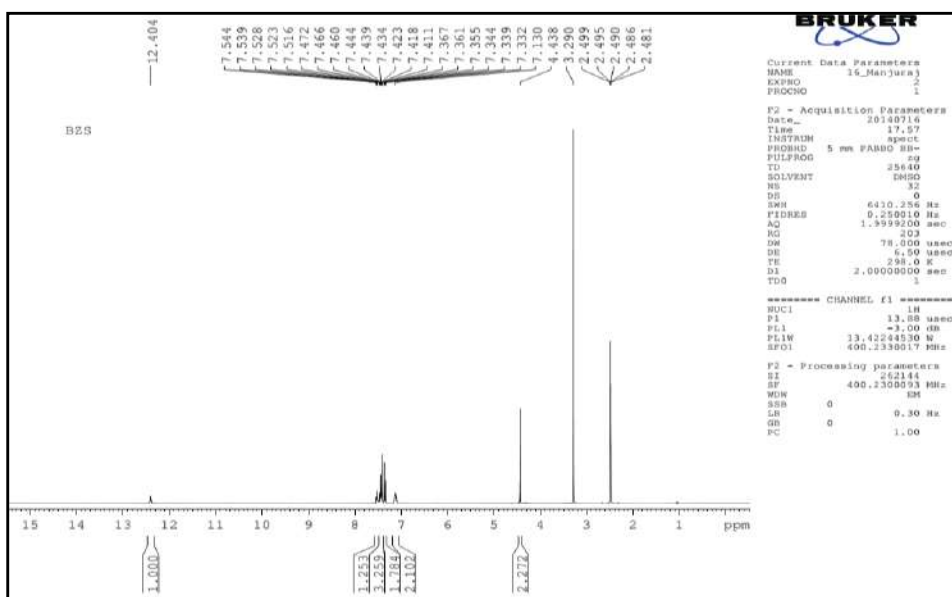


Figure 6.2.6 ^1H NMR spectrum of BT

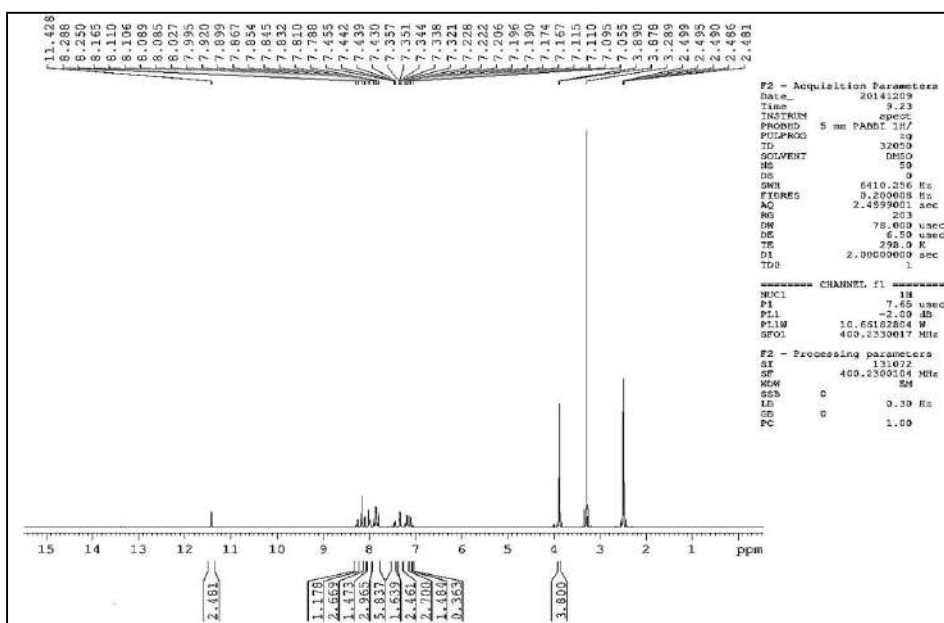


Figure 6.2.7 ^1H NMR spectrum of $[\text{ZnCl}_2(\text{BT})_2]$

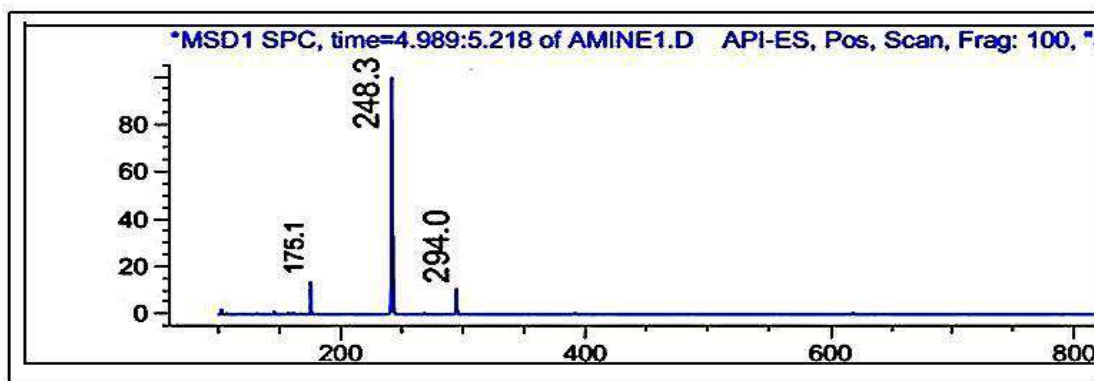
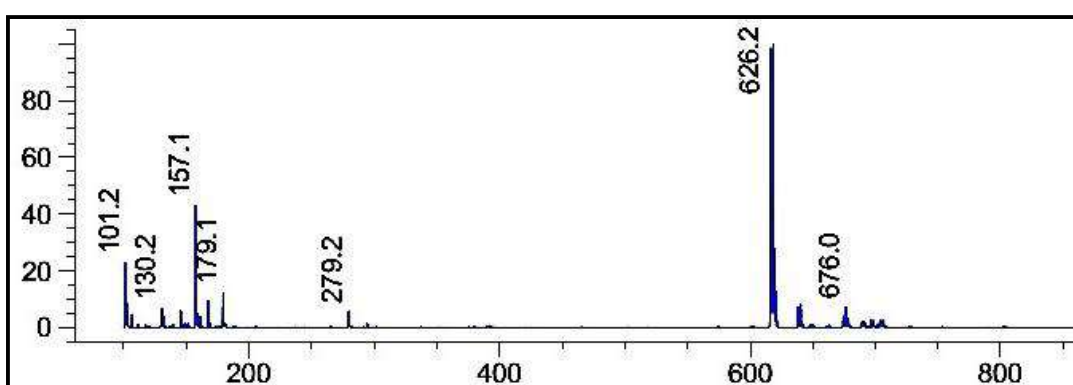


Figure 6.2.8 Mass spectrum of BT

Figure 6.2.9 Mass spectrum of $[\text{ZnCl}_2(\text{BT})_2]$

6.2.7 Results and discussion of biological activities

6.2.8 *In vitro* antimicrobial activity

Antimicrobial activity in two different concentrations of all synthesized BT and its metal complexes were evaluated and the results are tabulated in tables 6.2.2 and 6.2.2. The results of primary screening against the bacterial strains and fungal strains with different concentrations showed good zone of inhibition. The compounds Co(II), Ni(II) and Cu(II) exhibited the highest antimicrobial activity against *Pseudomonas aeruginosa*, *Bacillus subtilis*, *Salmonella typhi* and *Aspergillus flavus*, and *Candida albicans*. The compounds BT and the Zn(II) complex showed least activity against both bacterial and fungal strains. While it exhibited similar activity against tested fungal organisms with MIC values which gives significant activity at different concentrations *i.e.*, 1, 10, 25, 50, and 100 $\mu\text{g}/\text{mL}$. Against *Aspergillus flavus* and *Candida albicans*, the compounds Co(II), Ni(II) and Cu(II) complexes shows potential MIC values, which may be due to the presence of benzimidazole moiety in the BT [37, 38].

Table 6.2.2 Antimicrobial activity data of BT and its metal complexes

Compounds	Conc.mg/mL	Zone of inhibition in mm (mean \pm SD)				
		Antibacterial strains			Antifungal strains	
		P.aeruginosa \pm SD	B.subtilis \pm SD	S.typhi \pm SD	A.flavus \pm SD	C.albicans \pm SD
BT	1	09 \pm 0.2	10 \pm 0.1	11 \pm 0.3	08 \pm 0.3	08 \pm 0.3
	0.5	07 \pm 0.3	08 \pm 0.2	-	06 \pm 0.1	06 \pm 0.3
[CoCl ₂ (BT) ₂].H ₂ O	1	17\pm0.2	16\pm0.1	19\pm0.3	18\pm0.3	20\pm0.3
	0.5	07\pm0.3	08\pm0.2	09\pm0.1	10\pm0.2	08\pm0.3
[NiCl ₂ (BT) ₂].H ₂ O	1	17\pm0.5	18\pm0.1	13\pm0.3	18\pm0.3	15\pm0.3
	0.5	11\pm0.8	07\pm0.6	07\pm0.3	11\pm0.5	12\pm0.4
[CuCl ₂ (BT) ₂]	1	16\pm0.2	17\pm0.1	15\pm0.3	18\pm0.3	19\pm0.3
	0.5	10\pm0.5	08\pm0.2	07\pm0.4	-	12\pm0.3
[ZnCl ₂ (BT) ₂]	1	10 \pm 0.2	12 \pm 0.1	10 \pm 0.3	10 \pm 0.3	08 \pm 0.2
	0.5	08 \pm 0.3	-	09 \pm 0.1	06 \pm 0.2	06 \pm 0.3
Ciprofloxacin	1	21 \pm 0.40	22 \pm 0.3	24 \pm 0.4	-	-
	0.5	19 \pm 0.2	13 \pm 0.3	13 \pm 0.4	-	-
Fluconazole	1	-	-	-	23\pm0.1	20\pm0.3
	0.5	-	-	-	18\pm0.6	13\pm0.5

Table 6.2.3 Minimum inhibitory concentration data of BT and its metal complexes

Compounds	Minimum inhibitory concentration (MIC μ g/mL)				
	P.aeruginosa	B.subtilis	S.typhi	A.flavus	C.albicans
BT	10.75	10.70	09.35	13.55	08.58
[CoCl ₂ (BT) ₂].H ₂ O	14.75	12.12	10.35	11.55	09.12
[NiCl ₂ (BT) ₂].H ₂ O	15.24	13.11	10.10	13.55	09.25
[CuCl ₂ (BT) ₂]	14.75	12.62	10.64	14.21	-
[ZnCl ₂ (BT) ₂]	11.75	08.11	08.24	10.55	07.55
Ciprofloxacin	15.75	13.70	12.35	-	-
Fluconazole	-	-	-	14.75	10.70

6.2.9 Antioxidant activity

DPPH radical scavenging activity data represented in figure 6.2.10. Due to the generation of DPPH free radical it showed the absorption maximum at 517 nm [39]. The metal complexes showed significantly higher activity than uncoordinated BT. Also the complexes exhibited enhanced free radical scavenging effect but lower when compared to the ascorbic acid (vitamin C) a standard. The Cu(II) complex exhibited highly potent scavenging activity which is almost close to the standard vitamin C and the complexes of Ni(II) and Co(II) ions have a better inhibitions against the free radicals whereas the other compounds BT and Zn(II) complex showed a moderate activity.

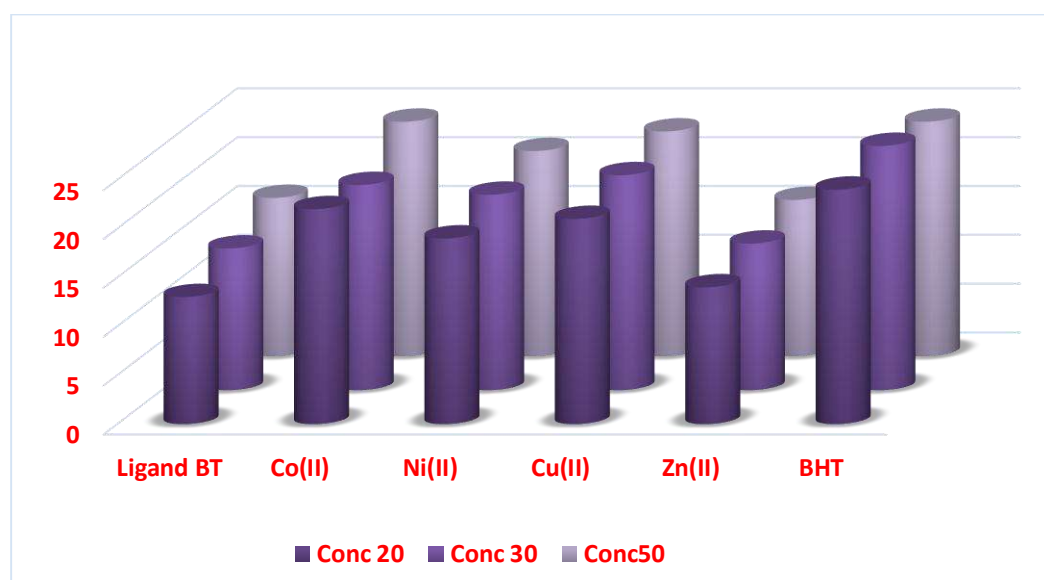


Figure 6.2.10 Antioxidant activity of BT and its metal complexes

6.2.10 Molecular docking

In accordance with antioxidant activity, it is significant to carry out *in silico* docking studies. The human antioxidant enzyme receptor in complex with the competitive inhibitor DTT (PDB ID: 3NMG) revealed that the good docking interactions with different amino acids and E-total score [40]. The Ni(II) complex showed excellent binding affinity towards enzyme receptor 3NMG of -287.16 kcal/mol, while Co(II) and Cu(II) complexes also exhibit good binding interactions docking score of -257.11 and -222.99 kcal/mol. But the ligand, BT showed a least binding interactions of -197.73 kcal/mol. The ligand and the receptor interactions

involves binding with different amino acids like His6, Phe20, Thr136, Ser165, Phe167, Glu198, Phe200, Val236, Thr237, Leu250 and Leu253.

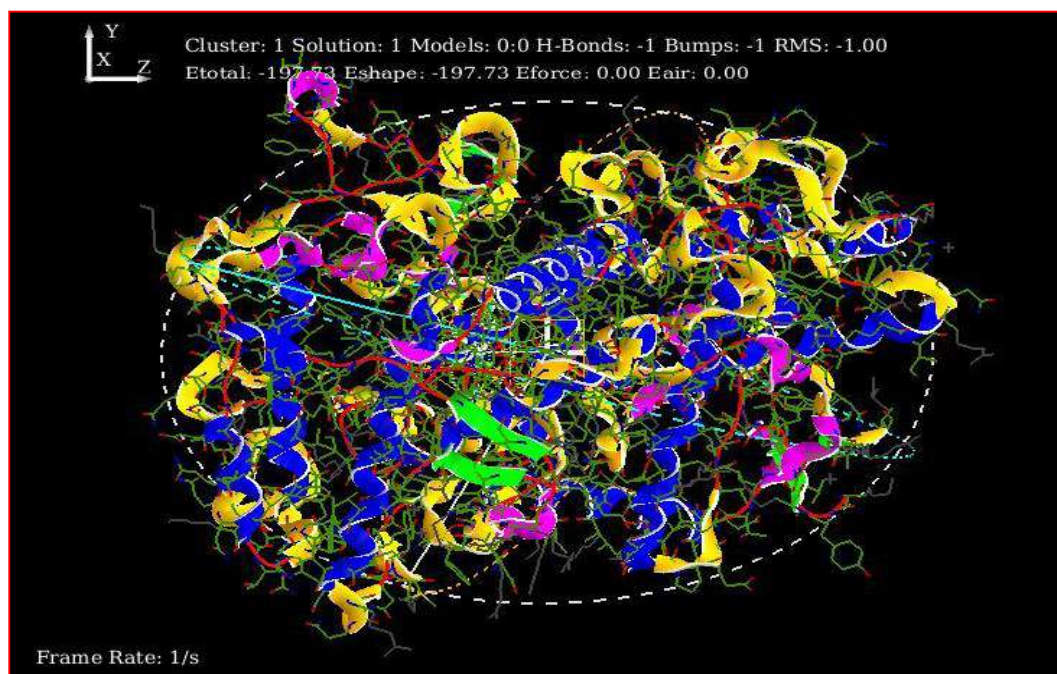


Figure 6.2.11 3D interactions of BT

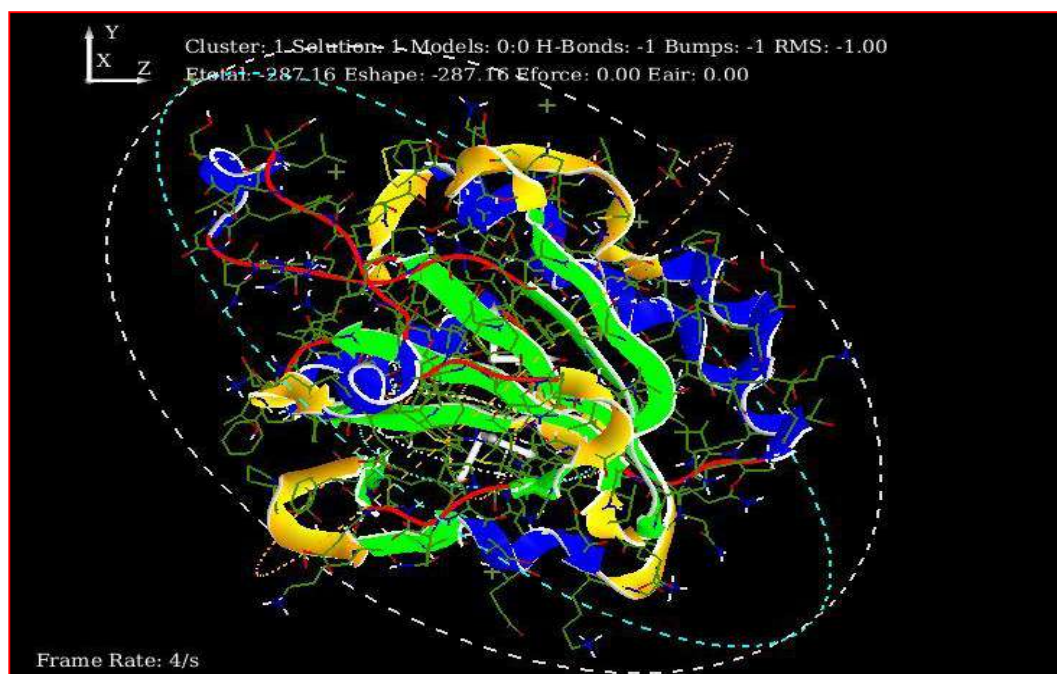
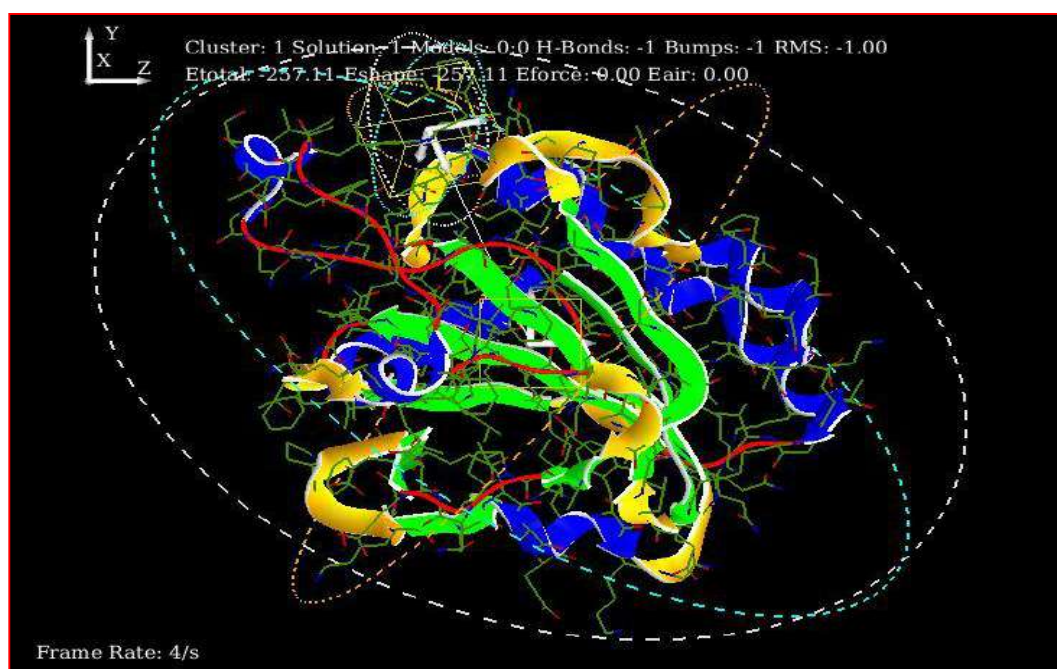
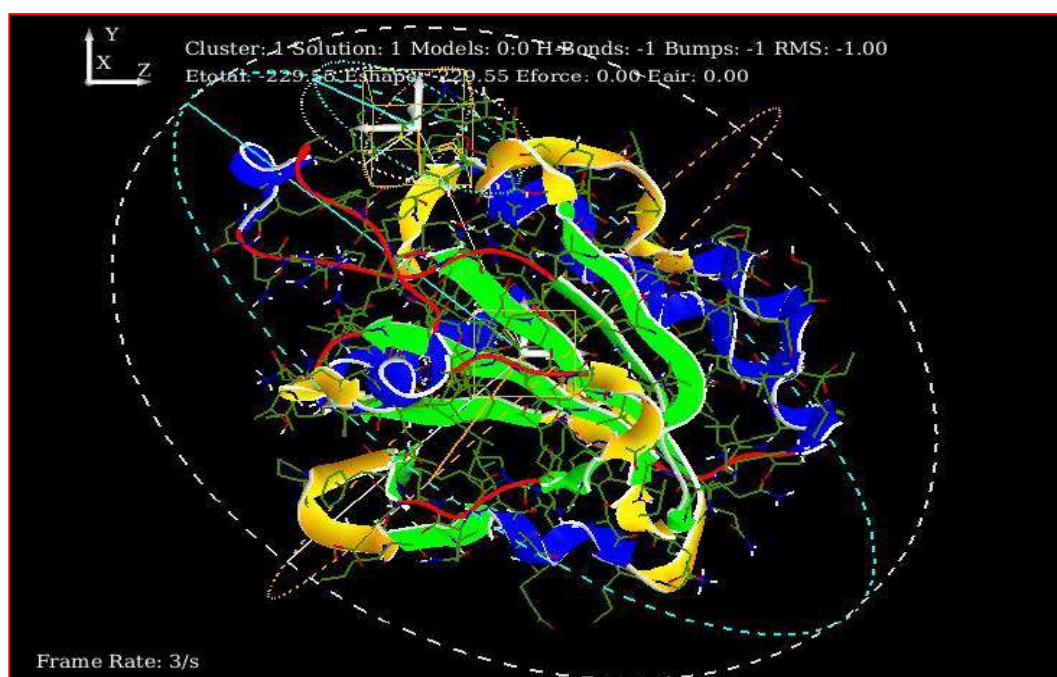


Figure 6.2.12 3D interactions of [CoCl₂(BT)₂].H₂O

Figure 6.2.13 3D interactions of [NiCl₂(BT)₂].H₂OFigure 6.2.14 3D interactions of [CuCl₂(BT)₂]

6.2.10 Conclusion

In outline, the ligand 2-[(thiophen-2-ylsulfanyl)methyl]-1H-benzimidazole [BT] and their metal complexes were synthesized and structurally characterized by elemental analysis, molar conductance, Uv-Visible spectra, ¹H NMR, and IR spectral techniques, which suggest the bidentate nature of the ligand, which coordinate through tertiary nitrogen of imidazole and sulphur atoms to the metal ion. The ligand and metal complexes were tested for the antimicrobial activity, which showed a potential inhibition against different pathogens reveal that the metal complexes are biologically active. The antioxidant activity of metal complexes also showed prominent inhibition against DPPH radical than that of the ligand and it is compared with *In silico* docking with human antioxidant enzyme receptor DTT (PDB ID: 3NMG).

References

- [1] B.V.S Kumar, S.D Vidya, R.V Kumar, S.B Bhirud, R.B Mane Synthesis and anti-bacterial activity of some novel 2-(6-fluorochroman-2-yl)-1-alkyl/ acyl/ aroyl-1H-benzimidazoles. *Eur J Med Chem* 41, 2006, 599–604.
- [2] D. Kumar, M.R Jacob, M.B Reynolds, S.M Kerwin, Synthesis and evaluation of anticancer benzoxazoles and benzimidazoles related to UK-1. *Bioorg Med Chem* 10, 2002, 3997–4004.
- [3] M. Andrzejewska, L. Yopez-Mulia, A. Tapia, R. Cedillo-Rivera, A.E Laudy, B.J Starosciak, Z. Kazimierczuk, Synthesis, and antiprotozoal and antibacterial activities of S-substituted 4,6- dibromo- and 4,6-dichloro-2-mercapto benzimidazoles, *Eur J Pharm Sci* 21, 2004, 323–329.
- [4] M.A Ismail, R. Brun, T. Wenzler, F.A Tanious, W.D Wilson, D.W Boykin, Dicationic biphenyl benzimidazole derivatives as antiprotozoal agents. *Bioorg Med Chem* 12, 2004, 5405–5413.
- [5] H. Nokano, T. Inoque, N. Kawasaki, H. Miyataka, H. Matsumoto, T. Taguchi, N.Inagaki, H. Nagai, T. Satoh, Synthesis and biological activities of novel antiallergic agents with 5-lipoxygenase inhibiting action. *Bioorg Med Chem* 8, 2000, 373–380.
- [6] K. Starcevic, M. Kralj, K. Ester, I. Sabol, M. Grce, K. Pavelic, G. Karminski-Zamola () Synthesis, antiviral and antitumor activity of 2-substituted-5-amidino-benzimidazoles. *Bioorg Med Chem* 15, 2007, 4419–4426.
- [7] R. Abonia, E. Cortes, B. Insuasty, J. Quiroga, M. Noguerras, J. Cobo, Synthesis of novel 125-trisubstituted benzimidazoles as potential antitumor agents, *Eur. J. Med. Chem.* 46,2011, 4062-4070.
- [8] H.T.A. Mohsen, F.A.F. Ragab, M.M. Ramla, H.I.E. Diwani, Novel benzimidazole pyrimidine conjugates as potent anti-tumor agents, *Eur. J. Med. Chem.* 45 2010, 2336-2344.

- [9] N.S. Pawar, D.S. Dalal, S.R. Shimpi and P.P. Mahulikar, Studies of microbial activity of N-alkyl and N acyl-2-(4-thiazolyl)-1H-benzimidazoles, *Eur. J.Pharm. Sci.*21, 2004,115.
- [10] B. Shao, J. Huang, Q. Sun, K.J. Valenzano, L. Schmid, S. Nolan 4-(2-Pyridyl) piperazine-1-benzimidazoles as potent TRPV1 antagonists. *Bioorg Med Chem Lett* 15, 2005, 719-723
- [11] A.T Mavrova, K.K Anichina, D.I Vuchev, J.A Issenov, P.S Denkova, M.S Kondeva, M.K Micheva, Antihelminthic activity of some newly synthesized 5(6)-(un) substituted-1H-benzimidazol- 2-ylthioacetylpiperazine derivatives. *Eur J Med Chem* 41, 2006, 1412-1420.
- [12] G. Krishnamurthy, N. Shashikala, Synthesis of Ruthenium(II) Carbonyl Complexes with 2-Monosubstituted and 1,2-Diisubstituted Benzimidazoles, *Journal of Serb. Chem. Soc.* 74(10), 2009, 1085-1096.
- [13] G. Krishnamurthy Synthesis, molecular modeling and biological activity of zinc(II) salts with 1,4-bis(benzimidazol-2-yl)benzene, *Journal of Chemistry*, 41, 2013, 54-96.
- [14] K. Nakamoto, *Infrared and Raman Spectra of Inorganic and Coordination Compounds*, fourth ed., Wiley Interscience, New York, 1986.
- [15] D. N Sathyanarayana, *Vibrational Spectroscopy: Theory and Applications*, New Age International publications, 1996.
- [16] R. Mithun, P. Biswarup, K.P. Ashis, D.J. Eluvathingal, N. Munirathinam, R.C. Akhil, *Inorg. Chem.* 46, 2007, 11122-11129.
- [17] B. Mustafa, C. Gokhan, A. Baris, K. Muhammet, K. Ahmet, K. Mukerrem. Synthesis and X-ray powder diffraction, electrochemical, and genotoxic properties of a new azo-Schiff base and its metal complexes. *Turkish journal of chemistry.* (38), 2014, 22-241.

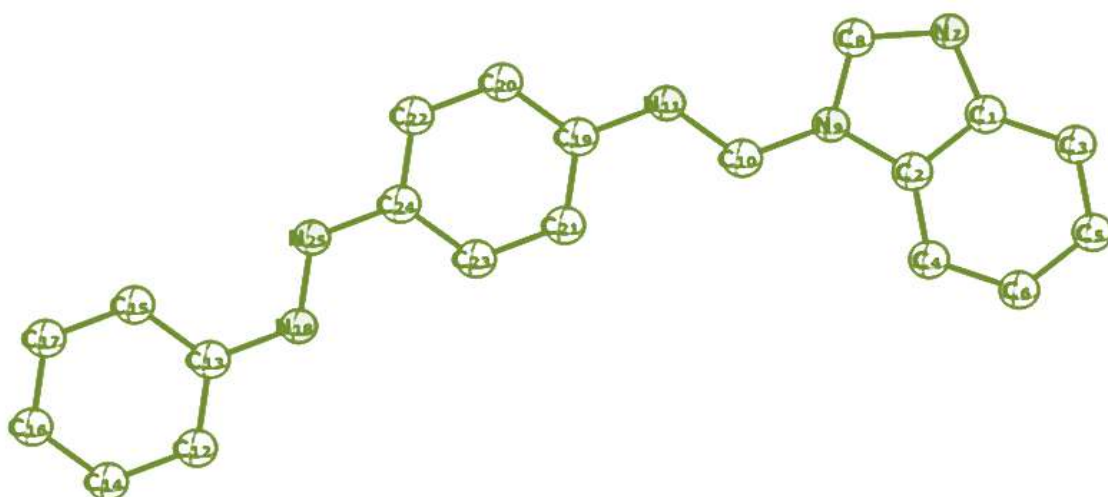
- [18] B. Sreekanth, G. Krishnamurthy, H. S. Bhojya Naik & T. K. Vishnuvardhan, Cu(II) and Mn(II) Complexes Containing Macroacyclic Ligand: Synthesis, DNA Binding, and Cleavage Studies, *Nucleosides, Nucleotides and Nucleic Acids*, 31(1), 2012, 1-13.
- [19] Subba Poojari, Parameshwar Naik P, Krishnamurthy G, Jithendra Kumara K.S, Sunil Kumar N, Sathish Naik, Anti-inflammatory, antibacterial and molecular docking studies of novel spiro-piperidine quinazolinone derivatives. *Journal of Taibah Univ. Sci*, 23, 2016, 10-25.
- [20] J. Joseph, B. H. Mehta, Synthesis, characterization, and thermal analysis of transition metal complexes of polydentate ONO donor Schiff base ligand. *Russian Journal of coordination chemistry*. (33), 2007, 124-129.
- [21] A. Sharma, R.T Singh, S.S Handa. Estimation of Phyllanthin and Hypophyllanthin by High performance liquid chromatography in *Phyllanthus amarus*. *Phytochem Anal*, 4, 1993, 226–9.
- [22] I. Kerimov, A.G. Kilcgil, B.C. Eke, N. Altanlar, M.J. Iscan, Synthesis antifungal and antioxidant screening of some novel benzimidazole derivatives, *Enzy. Inhibi. Med. Chem*. 22, 2007, 696-701
- [23] C. Kus, A.G. Kilcgil, B.C. Eke, M. Iscan, Synthesis and antioxidant properties of some novel benzimidazole derivatives on lipid peroxidation in the rat liver, *Arch. Pharm. Res*. 27, 2004, 156-163.
- [24] Y. Harinath, D. Subbarao, C. Suresh, K. Seshaiiah. Synthesis, characterization and studies on antioxidant and molecular docking of metal complexes of 1-(benzo[d]thiazol-2-yl)thiourea . *Journal of chemical sciences*. (128), 2016, 43-51.
- [25] N.D. Shashikumar, G. Krishnamurthy, H.S. Bhojya Naik, M.R. Lokesh and K. S. Jithendra kumara, Synthesis of new biphenyl-substituted quinoline derivatives, preliminary screening and docking studies. *J. chem. sci*. 126, 1, 2014, 205–212.

- [26] B. Zhou, B. Li, W. Yi, X. Bu, L. Ma, Synthesis antioxidant and antimicrobial evaluation of some 2-arylbenzimidazole derivatives, *Bioorg. Med. Chem. Lett.* 23, 2013, 3759-3763.
- [27] D. Joshi, K. Parikh, Synthesis and evaluation of novel benzimidazole derivatives as antimicrobial agents, *Med. Chem. Res.* 23, 2014, 1290-1299.
- [28] H.H. Jardosh, C.B. Sangani, M.P. Patel, R.G. Patel, One step synthesis of pyrido [12-a] benzimidazole derivatives of aryloxypyrazole and their antimicrobial evaluation, *Chin. Chem. Lett.* 24, 2013, 123-126.
- [29] M.A Abdel Nasser, A. Alaghaz, Badr, El-Sayed. A. Ahmed, El-Henawy, A.A Reda, Ammar. Synthesis, spectroscopic characterization, potentiometric studies, cytotoxic studies and molecular docking studies of DNA binding of transition metal complexes with 1,1-diaminopropane–Schiff base. *Journal of molecular structure.* 1035, 2013, 83–93.
- [30] M.M. Omar, G.G. Mohamed, *Spectrochim. Acta Part A Mol. Biomol. Spectrosc.* 61, 2005, 929-936.
- [31] C. Koradin, W. Dohle, A.L. Rodriguez, B. Schmid, P. Khochel, *Tetrahedron* 59, 2003, 1571-1587.
- [32] A.G. Shadia, H.H. Khaled, M.H. Ahmed, S.Y. Nabil, Synthesis and antitumor activity of novel benzimidazole-5-carboxylic acid derivatives and their transition metal complexes as topoisomerase II inhibitors, *Eur. J. Med. Chem.* 45, 2010, 5685-5691.
- [33] D. Sharma, B. Narasimhan, P. Kumar, V. Judge, R. Narang, E.D. Clercq, J.J. Balzarini, Synthesis antimicrobial and antiviral activity of substituted benzimidazoles, *Enzy. Inhibi. Med. Chem.* 24, 2009, 1161.
- [34] G.A. Kilcgil, N. Altanlar, Synthesis and antimicrobial activities of some new benzimidazole derivatives, *IL Farm.* 58, 2003, 1345-1350.

- [35] B. Sreekanth, G Krishnamurthy, H. S. Bhojya Naik, T. K. Vishnuvardhan. Cu(II) and Mn(II) complexes containing macrocyclic ligand: Synthesis, DNA binding, and cleavage studies. *Nucleosides, Nucleotides and Nucleic Acids*, 2012, 311–313.
- [36] S. Sujarani, A. Ramu, Docking of imines, cytotoxicity and DNA interaction studies of metal(II) complexes, *Journal of Molecular Structure* 1059, 2014, 299-308.
- [37] K. Thanigaimani, S. Arshad, N.C. Khalib, I.A. Razak, C. Arunagiri, A. Subashini, S.F. Sulaiman, N.S. Hashim, K.L. Ooi, *Spectrochim. acta*, 149A, 2015, 90-102.
- [38] B.V.S. Kumar, S.D. Vaidya, R.V. Kumar, S.B. Bhirud, R.B. Mane, Synthesis and anti-bacterial activity of some novel 2-(6-fluorochroman-2-yl)-1-alkyl/acyl/ aroyl-1H-benzimidazoles, *Eur. J. Med. Chem.* 41, 2006, 599-604.
- [39] H.B. Mallesh, G.Krishnamurthy, N. Shashikala, Reactions of 1-p-dimethyl aminobenzyl-2-p-dimethylaminophenyl benzimidazoles with cobalt(II), zinc(II) on cadmium(II) salts, *Asian Journal of Chemistry*, 16(4), 2004, 1439-1446.
- [40] M. Singh, V. Tandon, Synthesis and biological activity of novel inhibitors of topo -isomerase I: 2-Aryl-substituted 2-bis-1H-benzimidazoles, *Eur. J. Med. Chem.* 46, 2011, 659-669.

Chapter – 7

Synthesis, Characterization,
DFT and biological studies of
mannich base N-(1H-
benzimidazol-1-ylmethyl)-4-
[(E)-phenyldiazenyl]aniline
and their metal complexes



INTRODUCTION

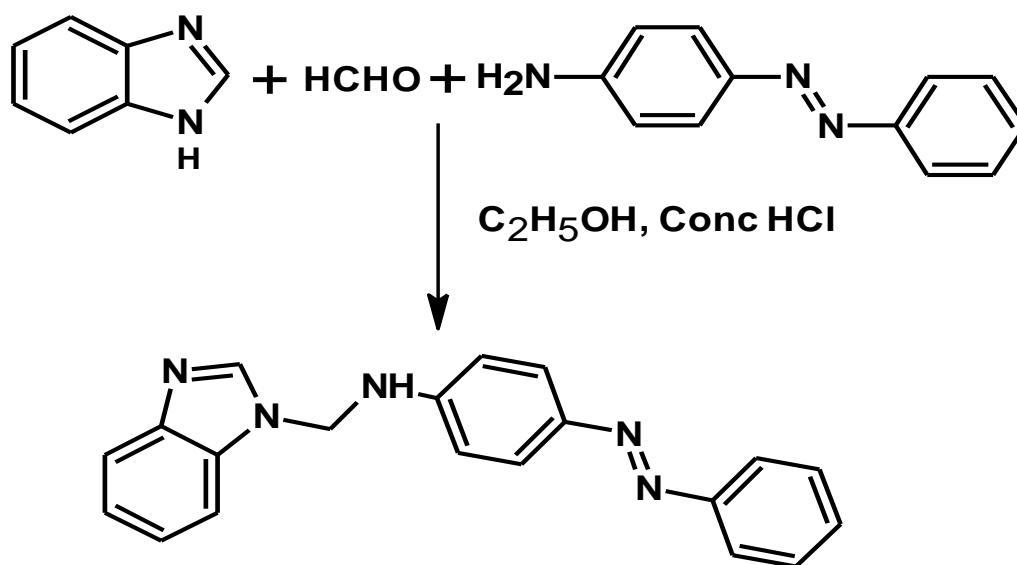
The metal complexes of benzimidazole and its derivatives have been evaluated for medicinal applications such as anticancer agents, antioxidant and enzyme inhibitors [1-5]. The derivative of benzimidazole containing isoniazid moiety has been used as a front-line drug in the treatment of tuberculosis (TB). However resistant TB strains have limited its use. The major route of isoniazid resistance relies on KatG enzyme disruption, which does not promote an electron transfer reaction and the reactivity of isoniazid metal complexes as prototypes for novel self-activating metallo-drugs against TB. It is well known from the literature that benzimidazole compounds containing the amine moiety have a strong ability to form metal complexes [6-10]. Therefore, it was thought worthwhile to synthesize some metal complexes of this type with a ligand containing mannich base and investigate its bonding characteristics. Moreover, heterocyclic mannich bases that are derived from the corresponding heterocyclic intermediates also possess various useful properties. Metal complexes of mannich bases have been studied extensively in recent years due to selectivity and sensitivity of the ligands toward various metal ions [11,12]. In this context, the studies have been extended to determine the binding ability of the ligand to metal ions and evaluate their pharmaceutical activity.

7.1 EXPERIMENTAL

7.1.1 Preparation of ligand N-(1H-benzimidazol-1-yl/methyl)-4-[(E)-phenyldiazenyl]aniline (BPA)

The ligand N-(1H-benzimidazol-1-yl/methyl)-4-[(E)-phenyldiazenyl]aniline [BPA] has been synthesized by reacting the mixture of benzimidazole (0.1mmol), with saturated ethanolic solution and formaldehyde (0.1mmol) and the saturated solution of 4-aminoazobenzene (0.1mmol) in ethanol was stirred for 1h and then refluxed for about 5-6h. The excess solvent was removed under the vacuum, the solid product was obtained, washed with hot ethanol and dried (Scheme 1)

Ligand BPA: Yield: 72%, Mp: 210°C, Anal, C(73.37%) H(5.23%) N(21.39%), Found: C(73.21%) H(4.98%) N(21.54%).MS(LC): 327.38 (328.38).



Scheme 1

7.1.2 Preparation of the metal complexes

The ethanolic solution of BPA (0.1 mol, 20 mL) was mixed with the solution of Co(II), Ni(II), Cu(II) and Zn(II) chlorides (0.2 mol) in ethanol (25 mL) separately with metal–ligand ratio 1:2. The mixture was refluxed for 4 h. The solid product was precipitated on cooling, which was collected by filtration and washed with hot ethanol until the washing becomes colorless. The product was dried in vacuum over anhydrous CaCl_2 .

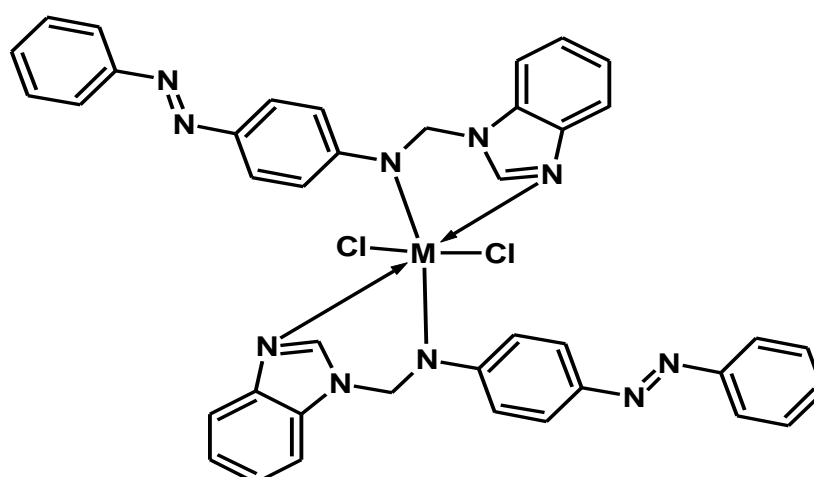


Figure 7.1 Proposed structure of metal complexes [M=Co(II), Ni(II), Cu(II) and Zn(II)]

Table 7.1 Physical properties and analytical data of BPA and their metal complexes

Compounds	Colour	Mol. Wt	Yield (%)	Calcd. (found) (%)				Molar conductance ($\text{ohm}^{-1} \text{cm}^2 \text{mol}^{-1}$)
				C	H	N	M	
$[\text{CoCl}_2(\text{BPA})_2]$	Light green	783.17	65	61.23 (61.11)	4.37 (3.98)	17.85 (18.03)	7.51 (7.22)	18
$[\text{NiCl}_2(\text{BPA})_2]$	Light blue	782.17	62	61.25 (59.97)	4.37 (4.45)	17.86 (17.71)	7.86 (7.92)	28
$[\text{CuCl}_2(\text{BPA})_2]$	Light brown	787.16	60	60.87 (60.57)	4.34 (4.57)	17.75 (17.97)	8.05 (7.88)	23
$[\text{ZnCl}_2(\text{BPA})_2]$	Light cream	788.16	65	60.73 (61.52)	4.33 (4.61)	17.71 (17.81)	8.27 (8.54)	26

7.2 Results and discussion

The physical properties and the analytical data of the ligand BPA and their metal complexes are presented in table 7.1. Most of the complexes are colored and stable. The proposed formula of the complexes was in accordance to the elemental analysis with 1:2 metal ion and ligand ratio [13].

7.2.1. DFT studies

The computational calculations of ligand BPA performed by Becke's three parameter hybrid exchange functional (B3LYP) with support of chemcraft 1.7 software [14] has been used for visualization of optimized structures (Figure 7.2, 7.3), selected bond angles, bond length, dihedral angles (Table 7.2) and HOMO-LUMO of BPH.

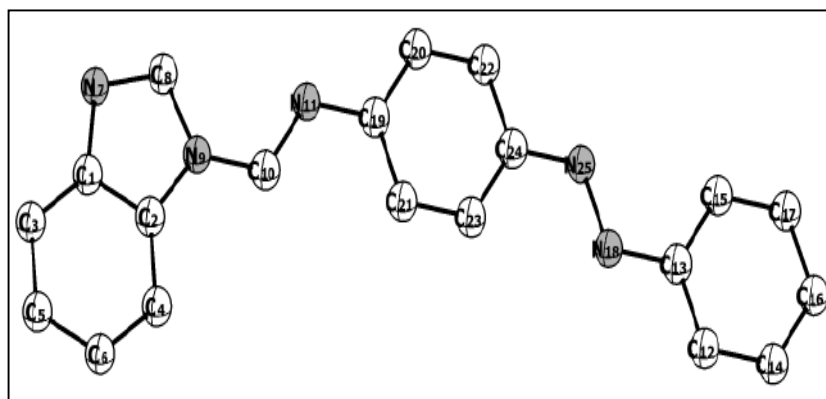


Figure 7.2 optimized geometry of BPA

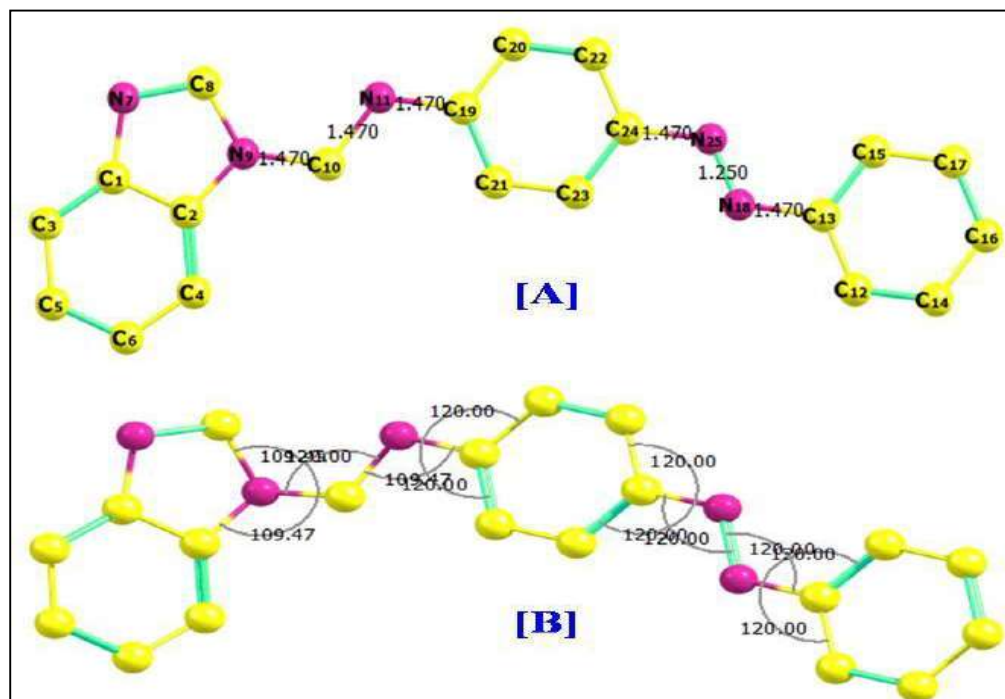


Figure 7.3 Standard bond lengths and bond angles of BPA

Table 7.2 Selected structural parameters of BPA

Bond	Bond length (Å)	Angle	(°)	Dihedral angle	(°)
C(6)-H(31)	1.144	C(1)-N(7)-C(8)	107.555	C(1)-N(7)-C(8)	107.555
N(7)-C(8)	1.352	N(7)-C(8)-N(9)	112.905	N(7)-C(8)-N(9)	112.905
C(8)-N(9)	1.551	N(7)-C(8)-C(10)	123.433	N(7)-C(8)-C(10)	123.433
C(8)-C(10)	1.640	N(9)-C(8)-C(10)	123.656	N(9)-C(8)-C(10)	123.656
N(9)-H(35)	1.054	C(2)-N(9)-C(8)	103.752	C(2)-N(9)-C(8)	103.752
C(10)-N(11)	1.631	C(2)-N(9)-H(35)	120.381	C(2)-N(9)-H(35)	120.381
C(10)-H(33)	1.222	C(8)-N(9)-H(35)	120.506	C(8)-N(9)-H(35)	120.506

Frontier molecular orbital analysis

The HOMO-LUMO gap of organic molecules is important because they transmit to particular movements of electrons and may be most generous for single electron transfer. As seen, the HOMO orbital of the ligands is localized on the benzimidazole rings. But the LUMO orbital is mainly localized on the benzene rings and its substitutions. It has been found that molecules with large HOMO-LUMO gap are highly stable and unreactive; while those with small gaps are generally reactive [15]. By calculating the HOMO-LUMO energy gap, one can easily determine the excitation energy of an organic derivative at its ground state [16].

The frontier molecular orbitals and the energy band gap elucidate the charge transfer interaction within the molecule, i.e., chemical reactivity values as electronegativity ($\chi = (E_{\text{LUMO}} + E_{\text{HOMO}})/2$), chemical potential ($\mu = -\chi = -(E_{\text{LUMO}} + E_{\text{HOMO}})/2$), global hardness ($\eta = (E_{\text{LUMO}} - E_{\text{HOMO}})/2$), global softness ($S = 1/2\eta$) and global electrophilicity index ($\omega = \mu^2/2\eta$) are given in the table 7.3.

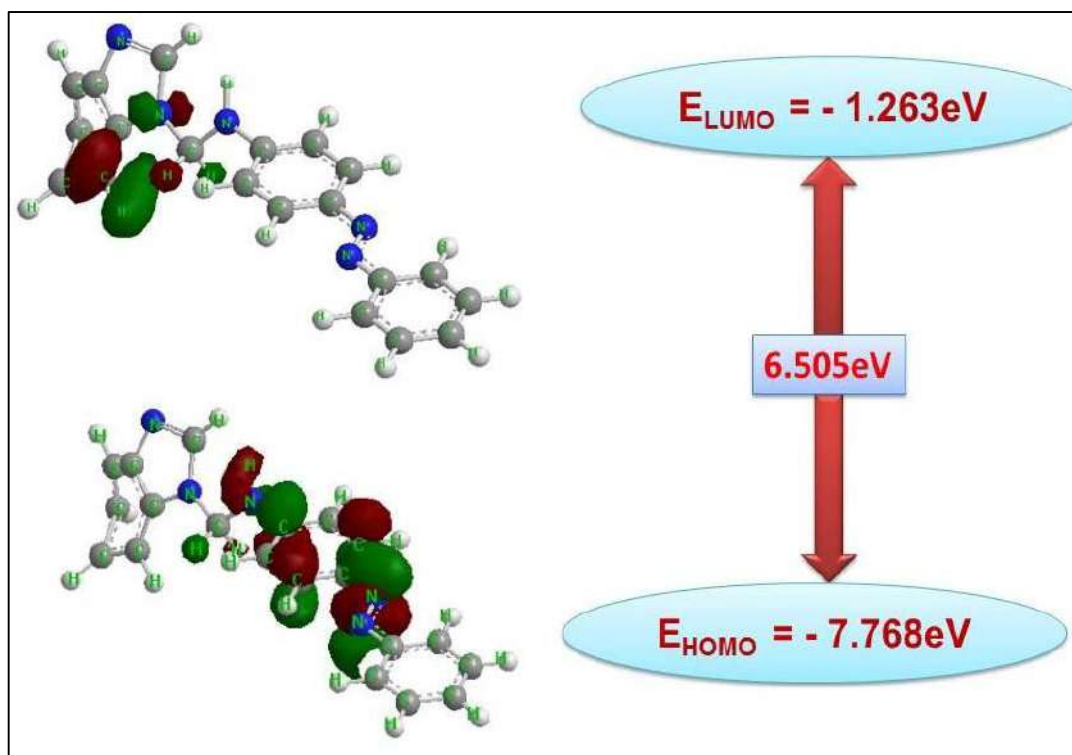


Figure 7.4 HOMO LUMO frontier orbitals of BPA

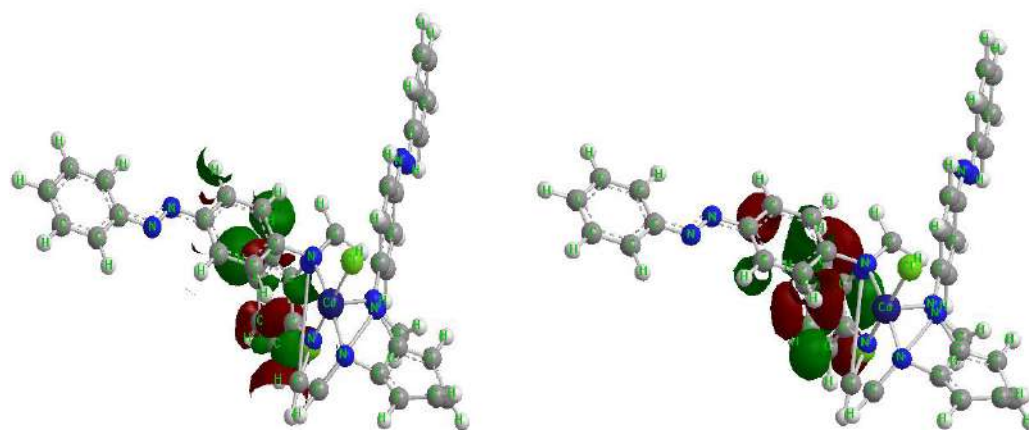


Figure 7.5 HOMO LUMO frontier orbitals of the Co(II) complex

Table 7.3 Calculated quantum chemical parameters for BPA and Co(II) complex

Compound	HOMO in eV	LUMO in eV	ΔE in eV	χ pauling	η in eV	σ	μ in eV	S	ω in eV
BPA	-7.768	-1.263	6.505	-7.125	2.954	0.987	7.125	1.212	3.354
Co(II)	-3.026	-5.639	2.613	-2.961	0.184	1.962	1.852	1.30	5.214

The ^1H NMR spectrum of the BPA showed a singlet at 10.89 ppm due to NH proton. The aromatic protons resonance appeared in range 7.11–7.89 ppm and a doublet obtained at 4.68 ppm is due to $-\text{CH}_2$ protons. In the $[\text{NiCl}_2(\text{BPA})_2]$, the resonance due to the protons of NH shifted towards down field, in which $-\text{NH}$ signal appeared in the spectrum of the uncoordinated ligand at 10.89 ppm disappears due to the coordination with NH proton. The multiple protons also shifted to down field while on complexation and appear at 7.74 ppm and the $-\text{CH}_2$ protons signal obtained at 4.36 ppm indicating the complexation with the ligand and the spectra are represented in the figures 7.6 and 7.7 respectively. The mass spectrum of the ligand and Zn(II) complex is depicted in figure 7.8 and 7.9, which showed a molecular ion peak at m/z 327.38 (328.28) and the Zn(II) complex exhibits a peak at m/z 788.16 (790.1).

^{13}C NMR spectrum also reveal the structure of the ligand, the signal for (C=N) observed at 151.63 ppm and the resonance due to aromatic carbons appeared around

108 to 145.52 ppm and $-\text{CH}_2$ carbon atom signal at 63 ppm, the spectrum is represented in figure 7.10.

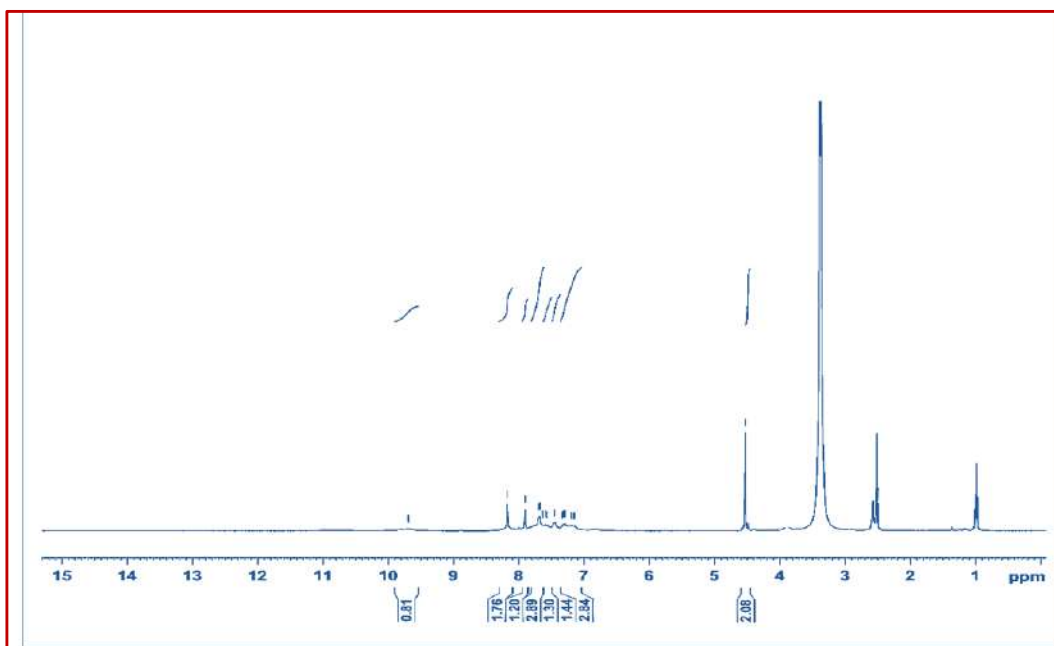


Figure 7.6 ^1H NMR spectrum of BPA

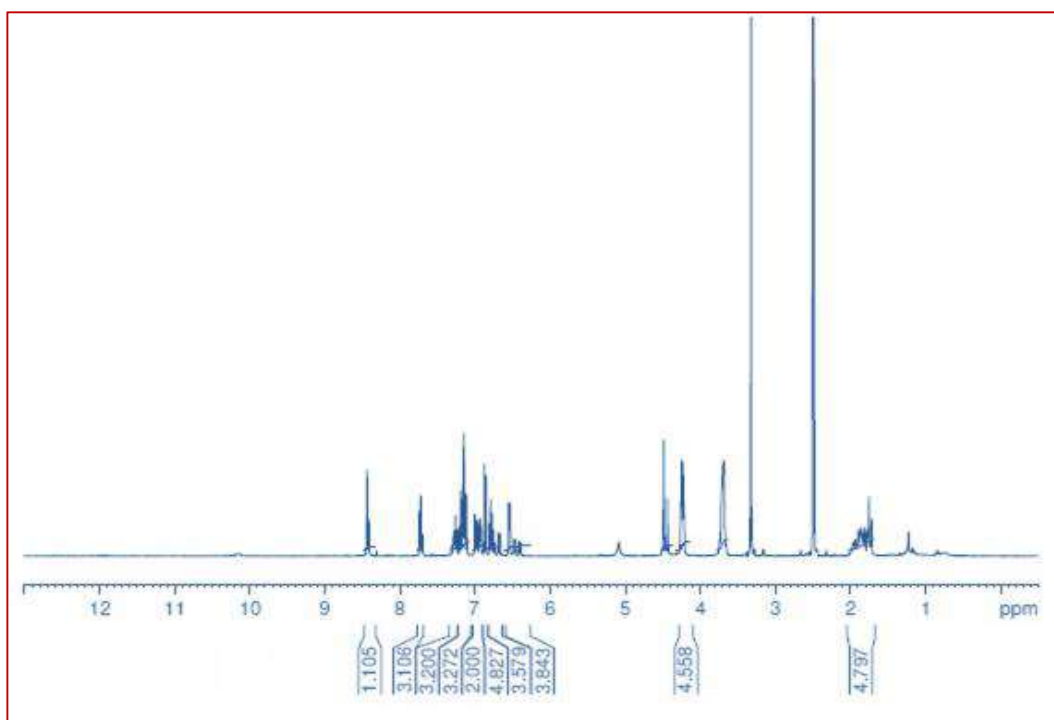


Figure 7.7 ^1H NMR spectrum of $[\text{NiCl}_2(\text{BPA})_2]$

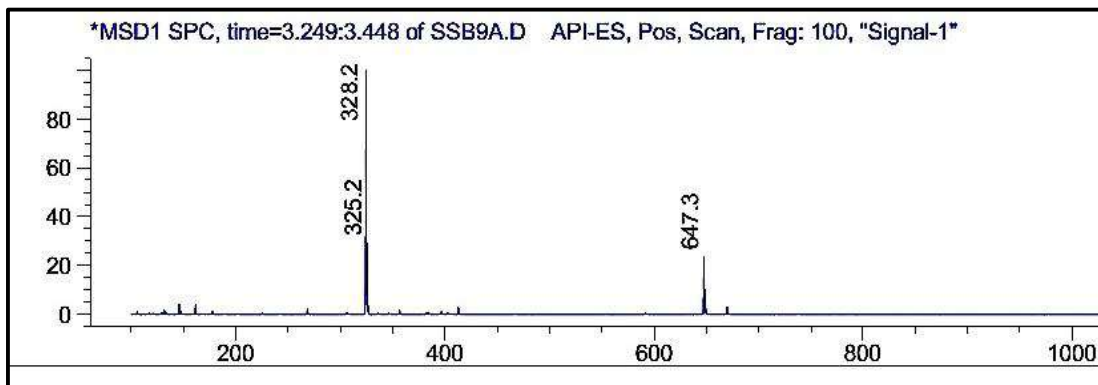
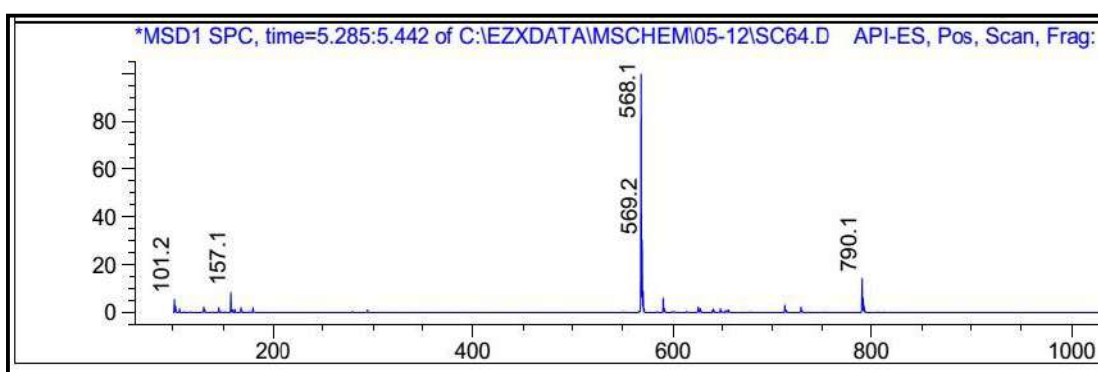
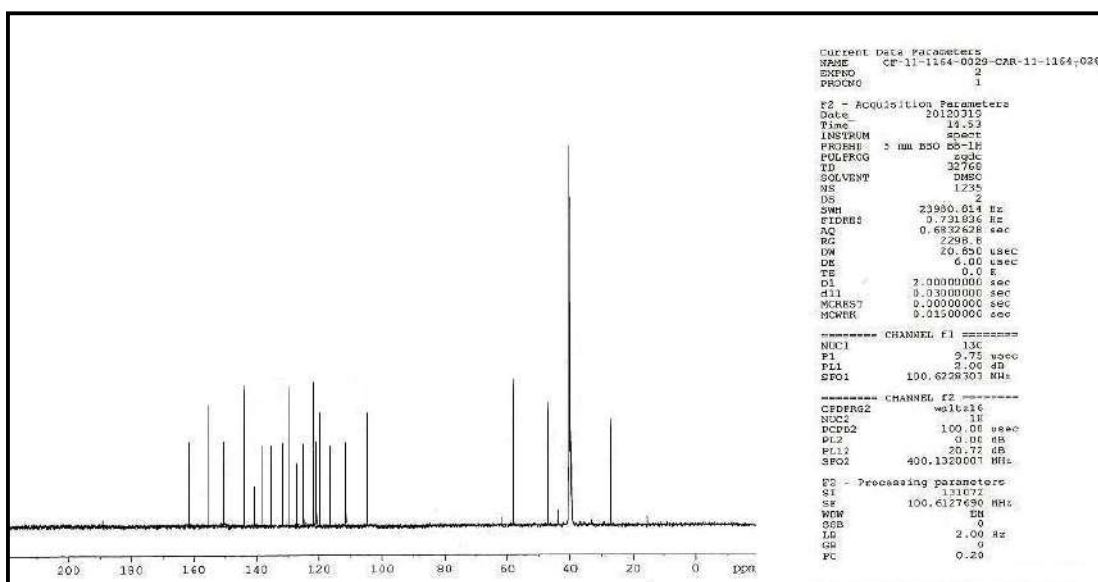


Figure 7.8 Mass spectrum of BPA

Figure 7.9 Mass spectrum of $[\text{ZnCl}_2(\text{BPA})_2]$ Figure 7.10 ^{13}C NMR spectrum of BPA

The most prominent IR spectral features of the ligand and its metal complexes are shown in figure 7.11. The ligand BPA showed that the band at 3354 cm^{-1} , 2914 cm^{-1} and 1655 cm^{-1} attributed for -NH , Ar-CH and C=N respectively [17-19]. In the metal complexes, the -NH band is shifted to lower frequency and appeared at 3251 cm^{-1} and the C=N stretching band also shifted to lower frequency from 1625 to 1640 cm^{-1} indicating the coordination of the ligand to the metal ion and has occurred through (-NH) as well as (C=N) of the BPA. In supports to this, the new bands appeared in the spectra of metal complexes for (M-N) are at 544 , 551 , 532 and 543 cm^{-1} .

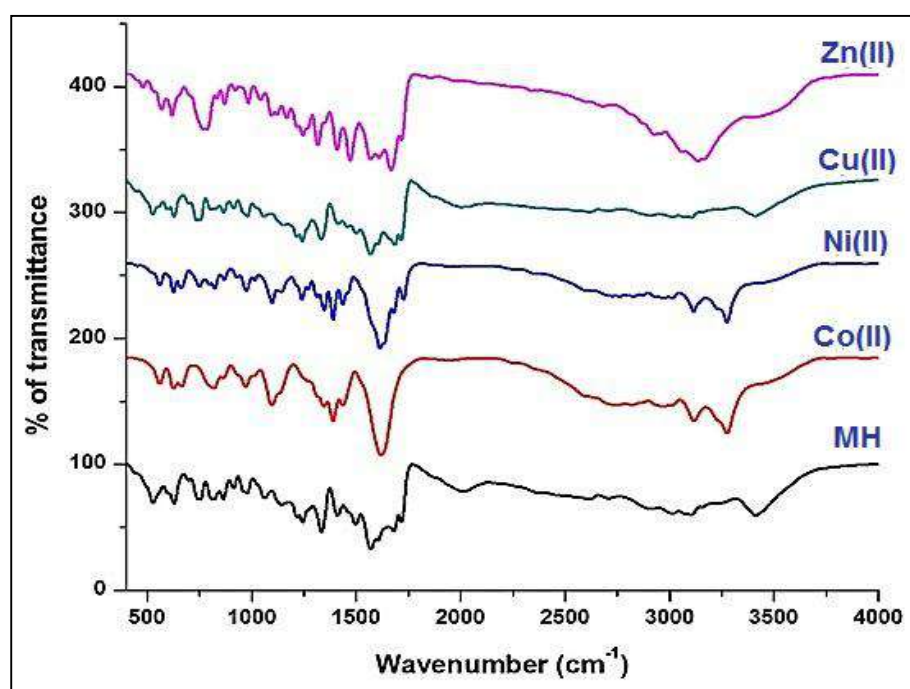


Figure 7.11 IR spectra of BPA and their metal complexes

The Uv-visible spectra of the ligand and its complexes were recorded in DMSO solvent, the Uv-visible spectrum of the ligand showed intense bands at $35,087$ and $31,250\text{ cm}^{-1}$ for $n\rightarrow\pi^*$ and $\pi\rightarrow\pi^*$ transitions in azomethine C=N [20]. The spectra of the metal complexes showed bands at 440 nm to 680 nm due to metal to the ligand charge transfer transitions. The electronic transitions are tabulated in table 7.4.

The magnetic moment value obtained for $[\text{Co}(\text{BPA})_2\text{Cl}_2]\text{H}_2\text{O}$ and their electronic spectrum data represent the octahedral geometry for the complex.

The [Ni(BPA)₂Cl₂]H₂O band at 22,935 cm⁻¹ is assigned to the transition ³A_{2g} (F)→³T_{1g}, (P) and another at 19,305 cm⁻¹ is representing ³A_{2g} (F)→³T_{1g}, (P) transitions. The magnetic moment observed is 3.21 BM also support the complex to have octahedral geometry. The [Cu(BPA)₂Cl₂] complex showed a band at 14,880 cm⁻¹ are due to ²E_g →²T_{2g} transition respectively, and the magnetic moment value 1.92 BM suggest it to have distorted octahedral geometry [21-23].

Table 7.4 Electronic spectral and magnetic moment data of metal complexes

Compounds	Electronic spectral bands (nm)	Assignment	μ _{eff} (BM)	Geometry
[CoCl ₂ (BPA) ₂]	486, 510	⁴ T _{1g} (F)→ ⁴ T _{1g} , (P) ⁴ T _{1g} (F)→ ⁴ T _{2g} , (F)	4.98	Octahedral
[NiCl ₂ (BPA) ₂]	436 518	³ A _{2g} (F)→ ³ T _{1g} , (P) ³ A _{2g} (F)→ ³ T _{1g} , (P)	3.21	Octahedral
[CuCl ₂ (BPA) ₂]	581	² E _g → ² T _{2g}	1.92	Octahedral

The X-ray diffraction analysis of the ligand BPA, Co(II) and Ni(II) metal complexes have carried out, which exhibits sharp peaks. The line boarding of the crystalline diffraction peak in BPA showed minimum crystallinity, while in Co(II) and Ni(II) complexes have higher crystallinity.

The diffractograms and associated data depict the 2θ value for each peak, the relative intensity and inter-planar spacing (d -values) as showed in figure 7.12 to 7.14. This indexing method also yields the Miller indices (hkl), half width full maximum values of all metal complexes. The average crystalline sizes of the complexes dxrd were calculated using Debye Scherrer equation ($D = K\lambda/\beta\cos \theta$) Where D = Particle size, K = Dimensionless shape factor, λ = X-ray wavelength (0.15406Å) β = Line broadening at half the maximum intensity, θ = Diffraction angle. The ligand BPA, Co(II) and Ni(II) complexes crystalline size of 18.21, 28.84 and 32.21 nm respectively, suggesting that the complexes are in a nanocrystalline phase [24, 25]

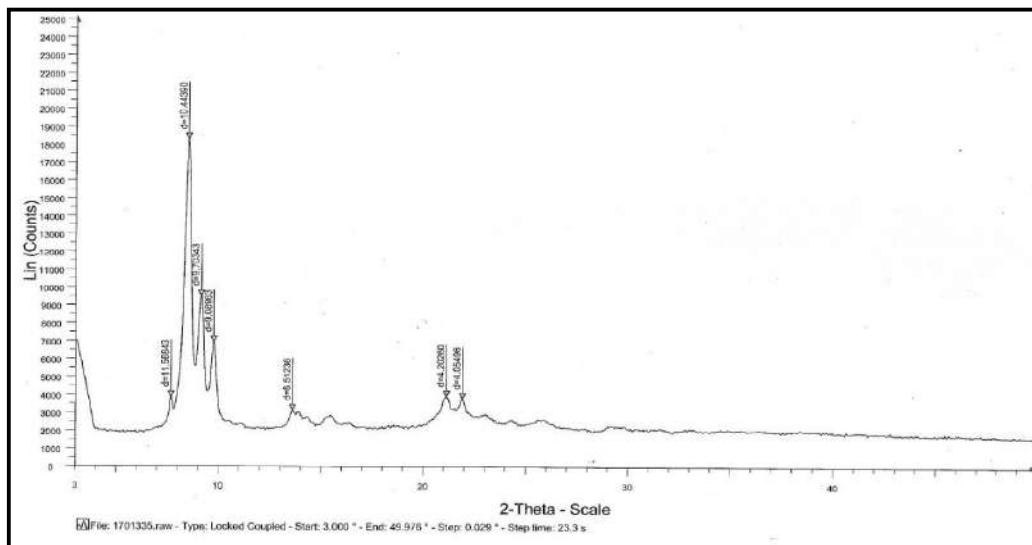


Figure 7.12 XRD pattern of the BPA

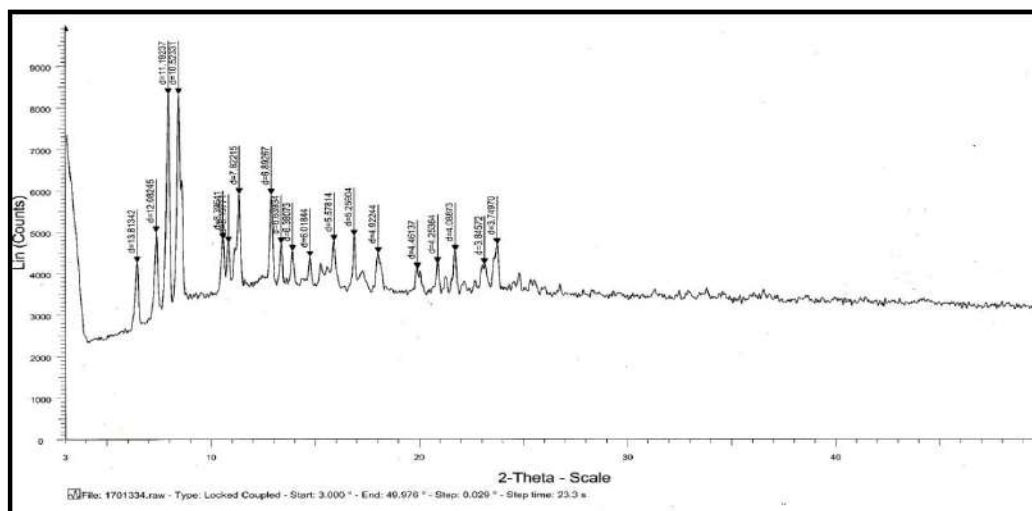


Figure 7.13 XRD pattern of $[CoCl_2(BT)_2]$

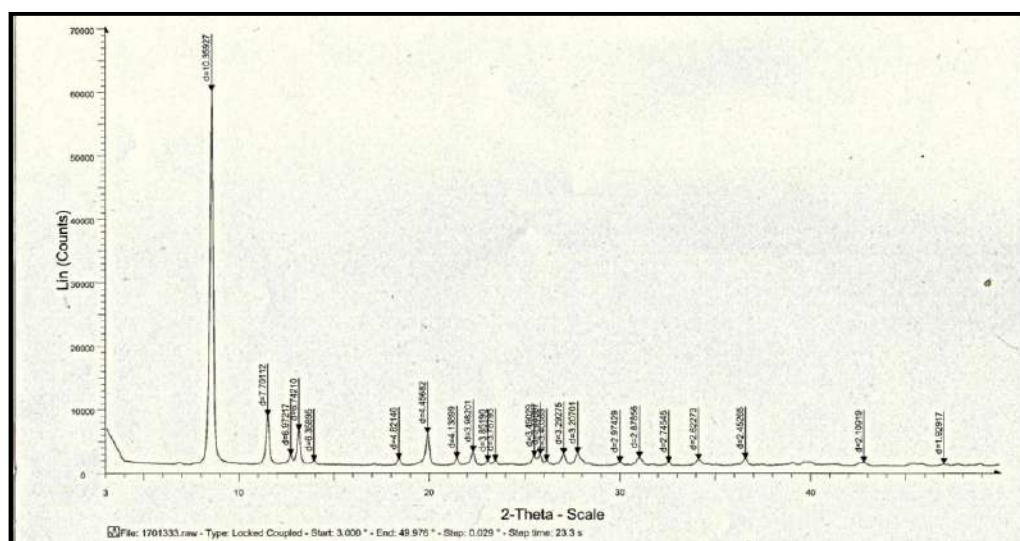


Figure 7.14 XRD pattern of $[CuCl_2(BT)_2]$

7.3 Procedures of biological evaluation

7.3.1 Anti-lipase assay

The procedure for performing anti-lipase activity was described in the previous chapters

7.3.2 Anti-oxidant activity

The procedure for performing both Nitric oxide (NO) scavenging method and DPPH scavenging activity was described in the previous chapters

7.3.4 Molecular docking studies

Molecular docking procedure is same as the procedure given in the previous chapters the human antioxidant enzyme in complex with the competitive inhibitor DTT (PDB ID: 3NMG) by HEX 8.0 and compared with uncoordinated ligand. The receptor was downloaded from RCSB protein data bank.

7.4 Results and discussion

7.4.1 Anti-lipase assay

Lipase inhibitory activity of different concentrations (1mg and 2mg) were carried for BPA and their metal complexes, the BPA showed lesser activity compared to their metal complexes and is represented in figure 7.15. The interaction can be found, such as π - π stacking interaction and σ - π interaction [26].

The results indicate that the Ni(II) and Zn(II) complexes showed potential activity against chicken pancreatic lipase enzyme, due to the presence of heterocyclic moieties of imidazole and azo-benzene, which involves the interactions with metal ions as well as pancreatic enzymes, while ligand, Co(II) and Cu(II) complexes exhibits moderate activity as represented in the figure 7.15.

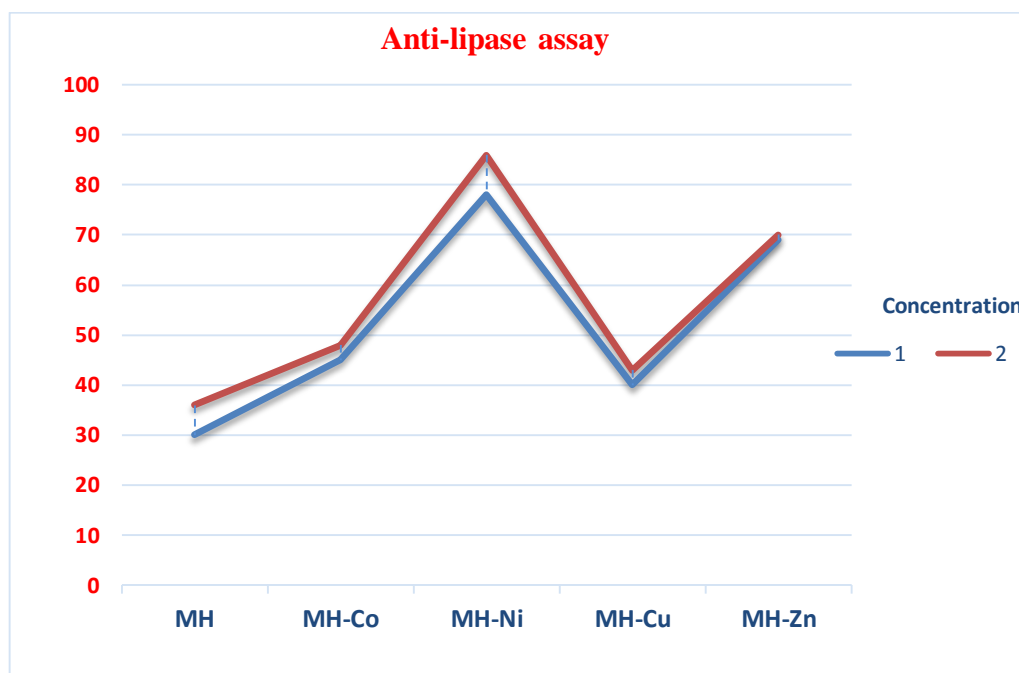


Figure 7.15 Graphical representation of the anti-lipase assay

7.4.2 Nitric oxide (NO) scavenging method

In the Nitric oxide radical scavenging activity, nitric oxide ($\text{NO}\cdot$) was generated from sodium nitroprusside in aqueous solution at the physiological pH, which involves with oxygen to generate nitrate ions that can be predictable by the use of Greiss reagent [27].

Among the tested compounds the Co(II) and Cu(II) complexes showed excellent NO scavenging activity with different concentrations when compared with the standard Butylatedhydroxytoluene (BHT), such enhanced activity could be due to presence of imidazole and the azomethine group. The ligand, Ni(II) and Zn(II) complexes showed moderate activity. Figure 7.16 represents the relative scavenging activity of ligand and their metal complexes.

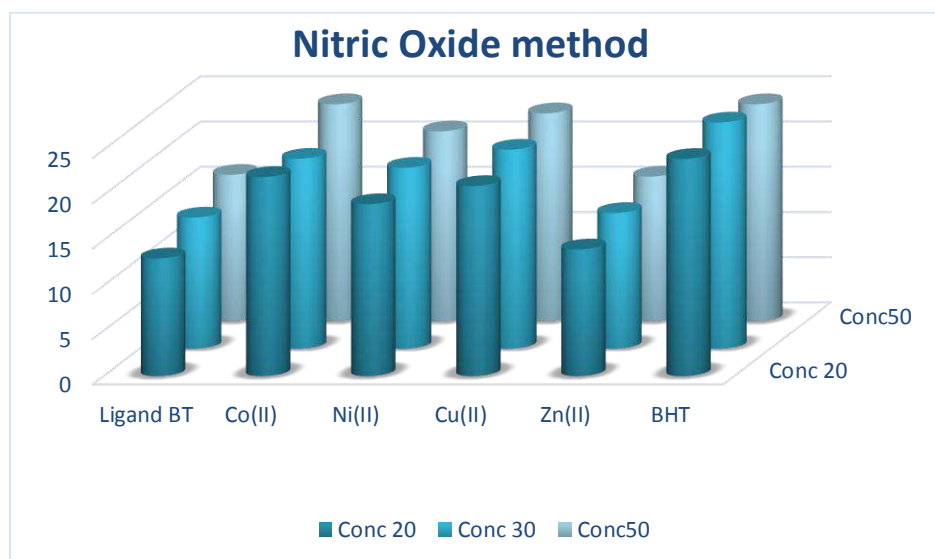


Figure 7.16 Graphical representation of nitric oxide method

7.4.3 DPPH scavenging activity

The DPPH solution exhibits a deep purple colour with an absorption maximum at 517 nm due to DPPH free radical [28-32]. This purple colour normally fades/disappears when an antioxidant is present in the medium. More potent antioxidants are able to reduce the absorbance rapidly. DPPH scavenging activity of the ligand and its complexes have been investigated, the uncoordinated ligand showed least activity, while the Ni(II), Co(II) and Cu(II) complexes showed better scavenging activity in various concentrations (50, 30, 20 mg/mL) when compared with the standard Butylatedhydroxytoluene (BHT).

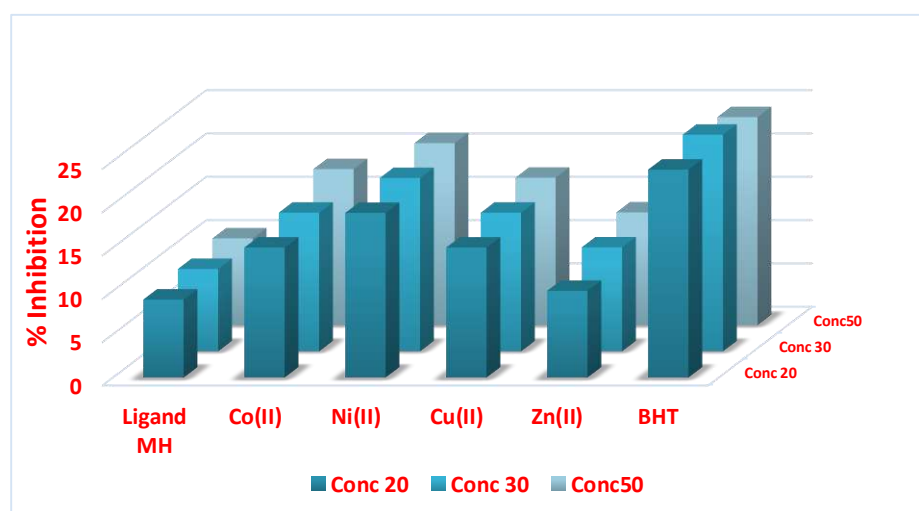


Figure 7.17 Graphical representation of DPPH method

7.4.4 Molecular docking studies

The competitive antioxidant inhibitor 1,2-dithiane-4,5-diol (DTT) with human antioxidant enzyme (3MNG) receptor is used for binding interactions mode of the BPA and their metal complexes [32-35]. The BPA showed lesser amount interactions with active sites of amino acids like Gly 46, Gln 133, Asn 24, with E total value of -244.12 kcal/mol, while the coordinated metal complexes showed prominent binding interaction with enzyme receptor of 311.45, 324.21, 319.14, 309.14 kcal/mol for Co(II), Ni(II), Cu(II) and Zn(II) complexes with amino acid residue of Gly 46, Gln 133, Asn 24, Val 94, Glu 16, Arg 86, and they are represented in figure 7.18 to 7.20.

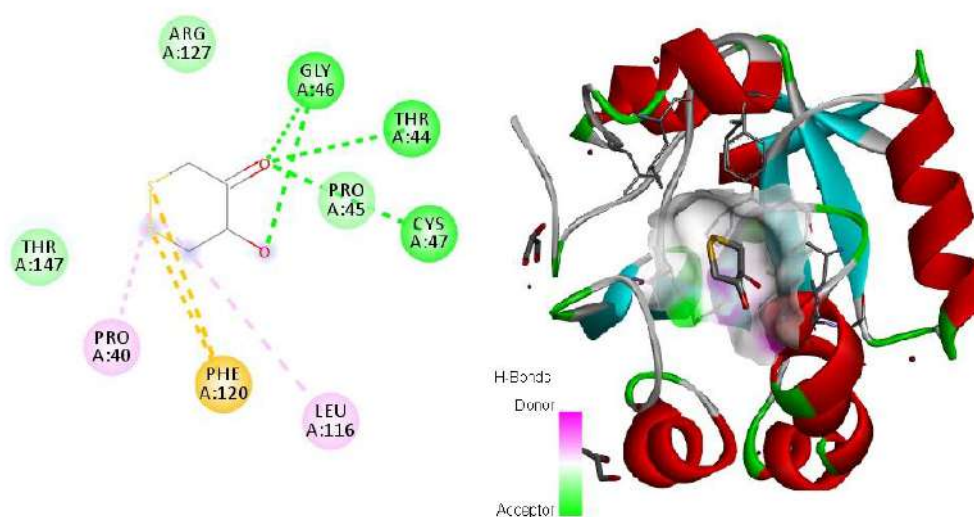


Figure 7.18 3D binding interactions of the ligand BPA

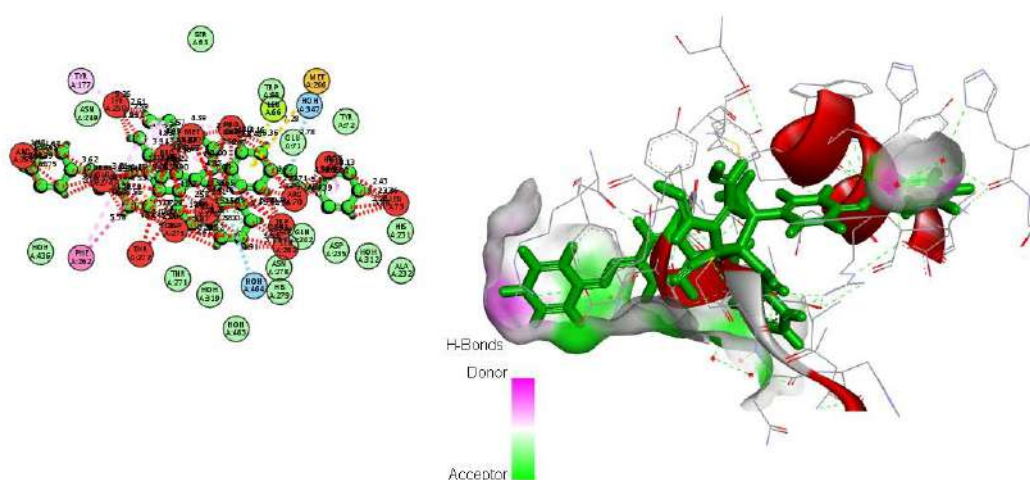


Figure 7.19 3D binding interactions of [CoCl₂(BT)₂]

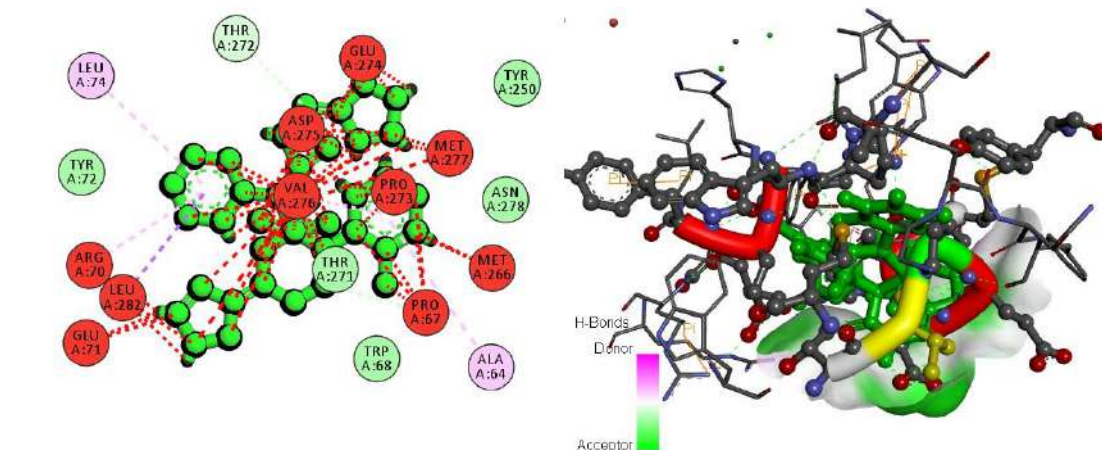


Figure 7.20 3D binding interactions of $[\text{NiCl}_2(\text{BT})_2]$

7.5 Conclusion

The ligand N-(1H-benzimidazol-1-ylmethyl)-4-[(E)-phenyldiazenyl] aniline (BPA) was synthesized *via* mannich base reaction and their Co(II), Ni(II) Cu(II) and Zn(II) metal complexes were prepared. The synthesized compounds were characterized by spectral and analytical data. The spectral data of the ligand indicate bidentate nature by bonding to metal ions through (-NH) and (C=N) groups. The XRD data suggest that the ligand and complexes are in crystalline nature. The theoretical study using DFT/B3LYP supports experimental evidences of the bonding sites of the ligand, geometry and the stability of the complexes. The biological studies reveal that the excellent anti-lipase activity with Ni(II) and Zn(II) complexes, while DPPH and nitric oxide activity also showed enhanced scavenging activity by the metal complexes compared to the uncoordinated ligand. Finally, the molecular docking studies were performed in correlation with both antioxidant assays, in which the ligand showed lesser binding energy and the metal complexes showed promising binding interactions with enzyme receptor.

References

- [1] X. Ma, X. Li, Y.E. Cha, L.P. Jin, Highly thermostable one-dimensional lanthanide(III) coordination polymers constructed from benzimidazole -5,6-dicarboxylic acid and 1,10-Phenanthroline: synthesis, structure, and tunable white-light emission, *Cryst. Growth Des.*, 12, 2012, 5227-5232.
- [2] S. Samai, K. Biradha, Chemical and mechano responsive metal-organic gels of bis (benzimidazole)-based ligands with Cd(II) and Cu(II) halide salts: self sustainability and gas and dye sorptions, *Chem. Mater* 24, 2012, 1165-1173.
- [3] V.C.O. Njar, A.M.H. Brodie, Discovery and development of galeterone (TOK-001 or VN/124-1) for the treatment of all stages of prostate cancer, *J. Med. Chem.* 58, 2015, 2077-2087.
- [4] Y. Bansal, O. Silakari, The therapeutic journey of benzimidazoles: a review, *Bioorgan Med. Chem.* 20, 2012, 6208-6236.
- [5] Y.L. Yao, Y.X. Che, J.M. Zheng, The coordination chemistry of benzimidazole- 5,6-dicarboxylic acid with Mn(II), Ni(II), and Ln(III) complexes (Ln $\frac{1}{4}$ Tb, Ho, Er, Lu), *Cryst. Growth Des.*, 8, 2008, 2299-2306.
- [6] C.H. Chen, W.S. Huang, M.Y. Lai, W.C. Tsao, J.T. Lin, Y.H. Wu, T.H. Ke, L.Y. Chen, C.C. Wu, Versatile, benzimidazole/amine-based am-bipolar compounds for electroluminescent applications: single-layer, blue, fluorescent OLEDs, hosts for single-layer, phosphorescent OLEDs, *Adv. Funct. Mater* 19, 2009, 2661-2670.
- [7] G.G. Mohamed, Z.H. Abd El-Wahab, Salicylidene-2-aminobenzimidazole Schiff base complexes of Fe(III), Co(II), Ni(II), Cu(II), Zn(II) and Cd(II), *J. Therm. Anal. Calorim.* 73, 2003, 347-359.
- [8] M.R. Maurya, A. Kumar, M. Ebel, D. Rehder, Synthesis, characterization, reactivity, and catalytic potential of model vanadium(IV, V) complexes with benzimidazole-derived ONN donor ligands, *Inorg. Chem.* 45, 2006, 5924-5937.

- [9] M.R. Maurya, M. Bisht, A. Kumar, M.L. Kuznetsov, F. Avecilla, J.C. Pessoa, Synthesis, characterization, reactivity and catalytic activity of oxido-vanadium(IV), oxido-vanadium(V) and dioxide-vanadium(V) complexes of benzimidazole modified ligands, Dalton T 40, 2011, 6968-6983.
- [10] O. Dayan, S. Demirmen, N. Ozdemir, Heteroleptic ruthenium(II) complexes of 2-(2-pyridyl) benzimidazoles: a study of catalytic efficiency towards transfer hydrogenation of acetophenone, Polyhedron 85, 2015, 926-932.
- [11] G. Krishnamurthy, Synthesis and thermal degradation kinetics of some Cobalt(II) Complexes with 1,2-disubstituted benzimidazoles, Journal. Teach. Resear, 17(1), 2010, 38-43.
- [12] O. Dayan, N. Ozdemir, Z. Serbetci, M. Dincer, B. Cetinkaya, O. Buyukgungor, Synthesis and catalytic activity of ruthenium(II) complexes containing pyridine-based tridentate triamines ('NNN') and pyridine carboxylate ligands (NO), Inorg. Chim. Acta 392, 2012, 246-253.
- [13] O. Dayan, S. Dayan, I. Kani, B. Cetinkaya, Ruthenium(II) complexes bearing pyridine-based tridentate and bidentate ligands: catalytic activity for transfer hydrogenation of aryl ketones, Appl. Organomet. Chem. 26, 2012, 663-670.
- [14] N.M. Shavaleev, S.V. Eliseeva, R. Scopelliti, J.C.G. Bunzli, Designing simple tridentate ligands for highly luminescent europium complexes, Chem-Eur J. 15, 2009, 10790-10802.
- [15] G. Krishnamurthy, N. Shashikala, Synthesis of Ruthenium(II) Carbonyl Complexes with 2-Monosubstituted and 1,2-Diisubstituted Benzimidazoles, Journal of Serb. Chem. Soc, 74(10), 2009, 1085-1096.
- [16] G. Krishnamurthy Synthesis, molecular modeling and biological activity of zinc(II) salts with 1,4-bis(benzimidazol-2-yl)benzene, Journal of Chemistry, 41, 2013, 54-96.

- [17] Q.Y. Yu, B.X. Lei, J.M. Liu, Y. Shen, L.M. Xiao, R.L. Qiu, D.B. Kuang, C.Y. Su, Ruthenium dyes with heteroleptic tridentate 2,6-bis(benzimidazol-2-yl)-pyridine for dye-sensitized solar cells: enhancement in performance through structural modifications, *Inorg. Chim. Acta* 392, 2012, 388-395.
- [18] A.K. Vannucci, J.F. Hull, Z. Chen, R.A. Binstead, J.J. Concepcion, T.J. Meyer, Water oxidation intermediates applied to catalysis: benzyl alcohol oxidation, *J. Am. Chem. Soc.* 134, 2012, 3972-3975.
- [19] J. Diez, J. Gimeno, A. Lledos, F.J. Suarez, C. Vicent, Imidazole based ruthenium(IV) complexes as highly efficient bifunctional catalysts for the redox isomerization of allylic alcohols in aqueous medium: water as cooperating ligand, *Acs Catal.* 2, 2012, 2087-2099.
- [20] W.J. Ye, M. Zhao, W.M. Du, Q.B. Jiang, K.K. Wu, P. Wu, Z.K. Yu, Highly active ruthenium(II) complex catalysts bearing an unsymmetrical NNN ligand in the (asymmetric) transfer hydrogenation of ketones, *Chem-Eur J.* 17, 2011, 4737-4741.
- [21] G. Krishnamurthy, Shashikala N. Narashimiah, Complexes of zinc(II) with 1,2-disubstituted Benzimidazoles, *Journal of chemical Research*, 12, 2006, 766-768.
- [22] G. Krishnamurthy, Synthesis, Characterization of Ruthenium(III) chloride Complexes with Some 1,2-Disubstituted Benzimidazoles and their Catalytic Activity, Synthesis and Reactivity in Inorganic, Metal-Organic, and Nano-Metal Chemistry, 41(6), 2011, 590-597.
- [23] F. Arjmand, M. Muddassir, Chiral preference of L-tryptophan derived metal based antitumor agent of late 3d-metal ions (Co(II), Cu(II) and Zn(II)) in comparison to d- and dl-tryptophan analogues: their in vitro reactivity towards CT DNA, 50-GMP and 50-TMP, *Eur. J. Med. Chem.* 45, 2010, 3549-3557.

- [24] J.R. Lakowicz, G. Webber, Quenching of fluorescence by oxygen. Probe for structural fluctuations in macromolecules, *Biochemistry* 12, 1973, 4161-4170.
- [25] A. Wolfe, G.H. Shimer, T. Meehan, Polycyclic aromatic hydrocarbons physically intercalate into duplex regions of denatured DNA, *Biochemistry* 26, 1987, 6392-6396.
- [26] H.T.A. Mohsen, F.A.F. Ragab, M.M. Ramla, H.I.E. Diwani, Novel benzimidazole pyrimidine conjugates as potent anti-tumor agents, *Eur. J. Med. Chem.* 45, 2010, 2336-2344.
- [27] S. Demirayak, I. Kayagil, L. Yurttas, Microwave supported synthesis of some novel 13-diarylpyrazino[12-a]benzimidazole derivatives and investigation of their anticancer activities, *Eur. J. Med. Chem.* 46, 2011, 411-416.
- [28] S. Demirayak, A. Usama, A.C. Mohsen, K. Agri, Synthesis and anticancer and anti-HIV testing of some pyrazino[12-a]benzimidazole derivatives, *Eur. J. Med. Chem.* 37, 2002, 255-260.
- [29] A. Kamal, P. Praveen Kumar, K. Sreekanth, B.N. Seshadri, P. Ramulu, Synthesis of new benzimidazole linked pyrrolo [21-c][1,4] benzodiazepine conjugates with efficient DNA-binding affinity and potent cytotoxicity, *Bioorg. Med. Chem. Lett.* 18, 2008, 2594-2598.
- [30] E. Moriarty, M. Carr, S. Bonham, M.P. Carty, F. Aldabbagh, Synthesis and toxicity towards normal and cancer cell lines of benzimidazole quinines containing fused aromatic rings and 2-aromatic ring substituents, *Eur. J. Med. Chem.* 45, 2010, 3762-3769.
- [31] E.J. Hanan, B.K. Chan, A.A. Estrada, D.G. Shore, J.P. Lyssikatos, Mild and general one-pot reduction and cyclization of aromatic and heteroaromatic 2-nitroamines to bicyclic 2H-imidazoles, *Syn-lett* 18, 2010, 2759-2764.

- [32] D. Yang, D. Fokas, J. Li, L. Yu, C.M. Baldino, A versatile method for the synthesis of benzimidazoles from o-nitroanilines and aldehydes in one step via a reductive cyclization, *Synthesis* 1, 2005, 47-56.
- [33] D. Seenaiiah, P. Ramachandra Reddy, G. Mallikarjuna Reddy, A. Padmaja, V. Padmavathi, N. Siva krishna, *Synthesis*, antimicrobial and cytotoxic activities of pyrimidinyl benzoxazole, benzothiazole and benzimidazole, *Eur. J. Med. Chem.* 77, 2014 1-7.
- [34] Subba Poojari, P. Parameswar Naik, G. Krishnamurthy, One-pot synthesis of thieno [2,3-d] pyrimidin-4-ol derivatives mediated by polyphosphonic anhydride, *Tetrahedron Letters*, 53, 2012, 4639-4643.
- [35] R.V. Shingalapur, K.M. Hosamani, R.S. Keri, M.H. Hugar, Derivatives of benzimidazole pharmacophore: synthesis anticonvulsant antidiabetic and DNA cleavage studies, *Eur. J. Med. Chem.* 45, 2010, 1753-1759.

Chapter – 8

Summary and conclusion



SUMMARY AND CONCLUSION

➔ Chapter 1

This chapter presents the overview of introduction on the synthesis of benzimidazoles derivatives with various heterocyclic moieties, medicinal and pharmacological applications. The different types of ligands based on the imidazole derivatives were discussed, the physical parameters like CHN, FT-IR, UV-visible, NMR, Powder XRD, Thermogravimetric analysis, DFT studies and molecular docking studies are included in the section.

➔ Chapter 2

In this chapter, the 5-methoxy-2-mercapto benzimidazole and quinoline based ligand quinolin-8-yl [(5-methoxy-1H-benzimidazol-2-yl)sulfanyl] acetate [QB] and corresponding Co(II), Ni(II), Cu(II) and Zn(II) metal complexes, preparation and their characterization by various physical and analytical techniques like CHN, FT-IR, UV-visible, NMR, Powder XRD, Thermogravimetric analysis and DFT studies have been discussed.

Further, the ligand and their synthesized complexes were screened for cytotoxicity activity, with MCF-7 and HeLa cell lines, in which IC_{50} values of the Cu(II) complex against MCF-7 are closure to standard Tamoxifen, while the Co(II), Ni(II) and Cu(II) complexes are potent against both MCF-7 (estrogen receptor-positive human breast cancer) and HeLa (human cervical cancer cell line). Molecular docking studies were performed to supports evidences of cytotoxicity activity by taking cancer epidermal growth factor receptor (EGFR) tyrosine kinase (PDB ID: 1M17). The synthesized compounds showed prominent anti-lipase inhibitory activity, antioxidant DPPH activity and antimicrobial activity,

➔ Chapter 3

This chapter deals with the synthesis of new mannich base ligand *N'*-(1H-benzimidazol-1-ylmethyl) pyridine-4-carbohydrazide (BI) by condensation of benzimidazole and Isoniazid and their Co(II), Ni(II) and Cu(II) complexes. The synthesized compounds are characterized by elemental analysis, conductivity measurements, 1H NMR, mass, FTIR, UV-Visible, and magnetic susceptibility. The

Powder XRD studies suggested that monoclinic for $[\text{CoCl}_2(\text{BI})_2]$, $[\text{CuCl}_2(\text{BI})_2]$ complexes and orthorhombic for $[\text{Ni}(\text{BI})_2]\text{Cl}_2$ complex.

The results of antioxidant activity indicating that the complexes have excellent modes of DPPH radical scavenging inhibition and the molecular docking studies were performed to evaluate the binding energy interactions by 3MNG human antioxidant protein receptor binds to selective amino acid residues with ligand (BI) and the metal complexes.

➔ Chapter 4

In this chapter, the synthesis of Co(II), Ni(II) and Cu(II) metal complexes with new benzimidazole ligand (BPA) have been discussed. Reaction of 2-methylchloro benzimidazole and Isoniazid produce the BPA which and their complexes were, characterized by using various spectral and analytical techniques, such as ^1H NMR, LCMS followed by IR, UV-visible spectroscopy and thermal studies. The spectral data indicate that the ligand is coordinated through N and S atoms to the central metal ion.

The complexes and ligand were screened DPPH Free radical scavenger activity, the results revealed that, among complexes $[\text{CuCl}_2(\text{L}_2)] \cdot 2\text{H}_2\text{O}$ and $[\text{NiCl}_2(\text{L}_2)(\text{H}_2\text{O})] \cdot \text{H}_2\text{O}$ exhibited good scavenging property followed by $[\text{CoCl}_2(\text{L}_2)(\text{H}_2\text{O})] \cdot \text{H}_2\text{O}$ and the free ligand. Antibacterial and antifungal study reveals that, the ligand and their metal complexes were found to be highly active due to existence of imidazole moiety along with the metal ions. The comparative docking studies were carried out on the synthesized ligand and its complexes compounds exhibited higher binding energy for $[\text{CoCl}_2(\text{L}_2)(\text{H}_2\text{O})] \cdot \text{H}_2\text{O}$ followed by $[\text{NiCl}_2(\text{L}_2)(\text{H}_2\text{O})] \cdot \text{H}_2\text{O}$ and $[\text{CuCl}_2(\text{L}_2)] \cdot 2\text{H}_2\text{O}$ complexes with the tyrosinase enzyme (PDB ID: 3NM8). The anti-lipase activity of Co(II) and Ni(II) ions coordinated to the ligand (BPA) play an important role in the physiological activity, most likely as a result of good conjugation of imidazole and isonicotinic hydrazide ring,

➔ Chapter 5

The Co(II), Ni(II), and Cu(II) complexes with 4- $\{(1Z)\text{-}1\text{-}[2\text{-}(1H\text{-benzimidazol-}2\text{-ylmethyl) hydrazinylidene]ethyl}\}$ phenol (LB) and 4- $\{(1Z)\text{-}1\text{-}[2\text{-}(1H\text{-benzimidazol-}2\text{-ylmethyl) hydra zinylidene]ethyl}\}$ aniline(BN) were synthesized and their characterization by elemental analysis, mass, IR, ^1H NMR electronic

spectra, magnetic studies, molar conductance and other spectral techniques have been discussed in the present chapter. For LB and their metal complexes, the TGA and XRD analysis was carried out. The spectral studies suggest that the ligand is bidentate in nature, For the LB and their metal complexes, the cytotoxic activities were evaluated on two different MCF-7 and HeLa cancerous cell lines in which $[\text{Cu}(\text{LB})_2\text{Cl}_2] \cdot \text{H}_2\text{O}$ showed promising cytotoxic inhibition while the LB, $[\text{Co}(\text{LB})_2\text{Cl}_2] \cdot 2\text{H}_2\text{O}$ and $[\text{Ni}(\text{LB})_2\text{Cl}_2] \cdot 2\text{H}_2\text{O}$ complexes exhibited a moderate activity. The molecular docking studies reveal that the complexes have comparatively good binding scores as compared to the *EGFR tyrosine kinase* receptor may be considered as a potent cytotoxic agent. All the complexes showed significant DPPH antioxidant activity compared to both the uncoordinated ligands also, among the studied complexes, $[\text{Co}(\text{LB})_2\text{Cl}_2] \cdot 2\text{H}_2\text{O}$, $[\text{Cu}(\text{LB})_2\text{Cl}_2] \cdot \text{H}_2\text{O}$, $\text{Ni}(\text{BN})_2\text{Cl}_2] \cdot 2\text{H}_2\text{O}$ and $\text{Co}(\text{BN})_2\text{Cl}_2] \cdot 2\text{H}_2\text{O}$ complexes exhibited promising antioxidant activity. The anti-lipase activity for both the ligands and their respective metal complexes showed best inhibitory activity.

➔ Chapter 6

Chapter-6, deals with the synthesis, characterization and biological activity of two ligands BTC and BT as well as their metal complexes. The results and discussion have been divided into two parts, Part-A, The spectral evidence suggest that the coordination of metal ions with carbonyl oxygen and azomethine nitrogen atom which is having bidentate nature. The XRD studies suggest that the crystalline nature of Co(II), Ni(II) and Cu(II) complexes. The ligand and their metal complexes investigated for *In vitro* α -Amylase activity with porcine pancreatic amylase enzyme, which showed promising activity with metal complexes. Further the DPPH free radical scavenging activity was carried out, which exhibits potential scavenging activity with metal complexes and least activity towards the ligand. In correlation, the docking studies have been done by using human antioxidant enzyme receptor DTT (PDB ID: 3NMG), which supports the wet study data of antioxidant studies. The antifungal activity was performed with *Candida albicans*, *Aspergillus flavus* and *Microspora griseus* by agar well diffusion method.

Part-B, In this section, the synthesis, characterization and biological activity of the ligand 2-[(thiophen-2-ylsulfanyl)methyl]-1H-benzimidazole [BT] and their

metal complexes is presented, which suggest the bidentate nature of the ligand, which coordinate through tertiary nitrogen of imidazole and sulphur atoms to the metal ion. The ligand and metal complexes were tested for the antimicrobial activity, which showed a potential inhibition against different pathogens reveal that the metal complexes are biologically active. The antioxidant activity of metal also showed prominent inhibition against DPPH radical than that of the ligand and it is compared with *in silico* docking with human antioxidant enzyme receptor DTT (PDB ID: 3NMG).

➔ Chapter 7

The ligand N-(1H-benzimidazol-1-ylmethyl)-4-[(E)-phenyldiazenyl] aniline (BPA) was synthesized *via* mannich base reaction and their Co(II), Ni(II) Cu(II) and Zn(II) metal complexes preparation, characterization and biological activity have been described. The spectral data of the ligand indicate bidentate nature by bonding to metal ions through (-NH) and (C=N) groups. The XRD data suggest that the ligand and complexes are in crystalline nature. .

The biological studies reveal that the excellent anti-lipase activity with Ni(II) and Zn(II) complexes, while DPPH and nitric oxide activity also showed enhanced scavenging activity by the metal complexes compared to the uncoordinated ligand. Finally, the molecular docking studies was performed in correlation with both antioxidant assays, in which the ligand showed lesser binding energy and the metal complexes showed promising binding interactions with enzyme receptor.